Structural and energetic characterisation of interactions at the nucleotide-binding site of Hsp90

Eleanor Polly Williams

Department of Structural and Molecular Biology

University College London

A thesis submitted for the degree of Doctor of Philosophy

September 2010

Declaration

The work presented in this thesis was undertaken at University College London. NMR spectra recorded at 800MHz and ^{31}P NMR spectra were undertaken at the National Institute for Medical Research (NIMR). With the exception of the collection of all 3D NMR spectra by Dr John Kirkpatrick and TROSY spectra by Dr. Geoff Kelly, I, Eleanor Williams confirm that the work presented in this thesis is my own. Where information has been derived from other sources, I confirm that this has been indicated in the thesis.

Abstract

Heat Shock Protein 90 (Hsp90) is a ubiquitous molecular chaperone linked to the maturation and activation of a wide range of 'client proteins'. These include steroid hormone receptors, receptor tyrosine kinases and p53. Hsp90 activates ‘clients’ through a series of conformational changes driven by the binding and hydrolysis of ATP in the N-terminal domain. These changes are thought to facilitate the formation of client protein binding sites and aid achieving their functional state.

The aims of this thesis are to investigate the thermodynamics of nucleotide-based ligand binding to the N-terminal domain of Hsp90 and to study the mechanism by which conformational changes are induced by ligand binding.

Thermodynamic characterization of ligand binding using isothermal titration calorimetry was carried out in order to investigate the contribution of the different groups of the nucleotide to the binding affinity and determined the importance of the charge state of the ligand to binding. Measurements of the change in constant pressure heat capacity induced by ligand binding were also performed in order to further investigate previously reported unusual heat capacity changes in this system that may correspond to differences in the conformational changes induced by ADP vs. an ATP analogue (AMPPNP) . Structural studies by NMR of the N-terminal domain reveal a high degree of flexibility and specific conformational changes in response to the binding of different ligands to the N-terminal domain of Hsp90. The thermodynamics of ligand binding to the full length protein and to the isolated N551 (the first 551 amino acids) were also investigated and found to have a significant influence over both the thermodynamics and the heat capacity measurements compared to the isolated N-terminal domain.

Acknowledgements

"The most beautiful emotion we can experience is the mystical. It is the power of all true art and science. He to whom this emotion is a stranger, who can no longer wonder and stand rapt in awe, is as good as dead. To know that what is impenetrable to us really exists, manifesting itself as the highest wisdom and the most radiant beauty, which our dull faculties can comprehend only in their most primitive forms - this knowledge, this feeling, is at the centre of true religiousness." –Albert Einstein

The beauty and complexity of this earth is truly staggering as expressed nicely by Albert Einstein. It has been a privilege over the past four years to have the opportunity to delve deeper into understanding just one small bit of God's creation, to see the complexity He put there and to appreciate its elegance.

This thesis is not only a summary of my work but also a testament to all the many people who helped me along the way. I offer particular thanks to my two supervisors; Prof. John Ladbury who gave me the opportunity to undertake this PhD and who has helped and guided me through my project, allowed me the freedom to pursue the areas that appealed to me and the guidance to understand what I was seeing; and to Dr. Mark Williams for his endlessly patient support, his guidance and advice. His teaching has been invaluable and I am truly grateful for all his efforts and help. I am, I hope, a better scientist now because of him. I am also extremely grateful for the practical help given to me in collecting NMR spectra by Dr. John Kirkpatrick at UCL and Dr. Geoff Kelley at NIMR and for many helpful conversations with Prof. Paul Driscoll and Dr. John Christodoulou.

In the laboratory I have had the privilege to work with many fine scientists and to have had the chance to learn from them. I would like to thank Dr. Roger George, Dr. Zamal Ahmed, Dr. Sunita Sardiwal, Dr. Paul Leonard, Dr. Tjelvar Olssen, Kin Suen, Thomas Lien, David Fallaize, Ragini Ghosh, Dipali Patel and Helene Launay for all their aid and encouragement over the past four years.

I would also like to thank my friends and family for their unwavering confidence in me and in helping me see the top of the mountain even when I thought it was impossible. Their

encouragement through the highs and the lows has been invaluable. I would particularly like to thank Peter, Denise, Tracey, Tris, Ivan, James, Matt, Helen, Chez and Rich. Throughout it all however one person has supported me, kept me pointing in the right direction, helped me reach the end and stopped me giving up- all this despite him likening my data to a sneeze. To my husband Joe I dedicate this thesis. I couldn't have done it without you.

Eleanor Williams

September 2010

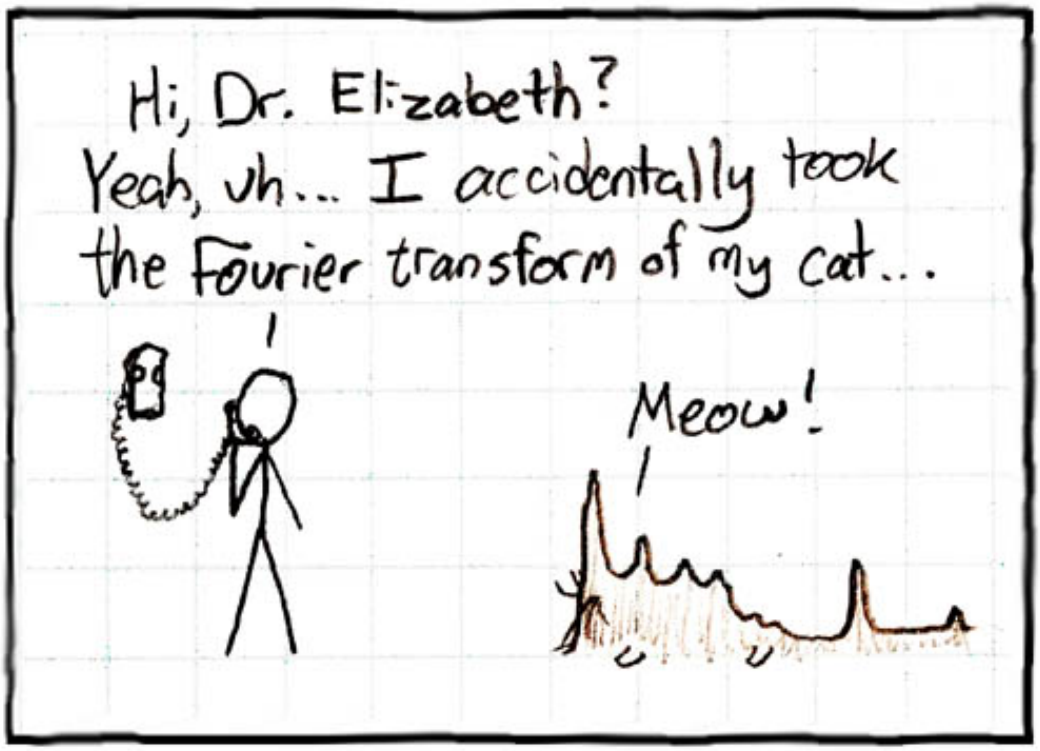

Contents

List of Figures

List of Tables

List of Abbreviations

1D	–	1 dimensional
2D	–	2 dimensional
3D	–	3 dimensional
ACES	–	N-(2-acetamido)-2-aminoethanesulfonic acid
AEBSF	–	4-(2-Aminoethyl) benzenesulfonyl fluoride hydrochloride
A_{np}	–	Surface area of non-polar residues
A_p	–	Surface area of polar residues
ATP	–	Adenosine Tri-Phosphate
AUC	–	Analytical Ultracentrifugation
Bis Tris	–	1,3-Bis(tris(hydroxymethyl)methylamino)propane
CD	–	Circular Dichrosim
^{13}CHSQC	–	Carbon edited Heteronuclear single quantum coherence
DSS	–	4,4-dimethyl-4-silapentane-1-sulfonic acid
E. Coli	–	Escherichia coli
E64	–	L-transepoxysuccinyl-leucylamido-[4-guanidino]butane
EDTA	–	Ethylene-diamine-tetraacetic acid
EM	–	Electron Microscopy
FRET	–	Fluorescence resonance energy transfer
GHKL superfamily	–	Gyrase, Histidine kinase, Mut L superfamily
GndCl	–	Guanidinium Chloride
H/D exchange	–	Hydrogen/Deuterium exchange
HEPES	–	4-(2-hydroxyethyl)-1-piperazineethanesulfonic acid
Hsp90	–	Heat shock protein 90
Hsp90-FL	–	Full length construct of Hsp90
IPTG	–	Isopropyl-β-D-thiogalactopyranoside
ITC	–	Isothermal Titration Calorimetry
kDa	–	kilo Daltons

LB	–	Luria Broth
MES	–	2-(N-morpholino)ethanesulfonic acid
Mg^{2+}	–	Magnesium ions with 2+ charge from MgCl2
N	–	Stoichiometry
N551	–	N-terminal and middle domain construct of Hsp90 consisting of the first 551 amino acids
^{15}NHSQC	–	Nitrogen edited Heteronuclear single quantum coherence
Ni-NTA	–	Nickel-charged nitriloacetic acid
NMR	–	Nuclear Magnetic Resonance
NOE	–	Nuclear overhauser effect
NT	–	N-terminal domain of Hsp90 from amino acids 1 - 207 including a hexa-his tag
PDB	–	Protein data bank
PIPES	–	Piperazine-N,N′-bis(2-ethanesulfonic acid
ppm	–	parts per million
SAXS	–	Small angle x-ray scattering
SDS-PAGE	–	Sodium Dodecyl Sulphate – Polyacrylamide Gel Electrophoresis
T101I	–	N-terminal domain mutant of Hsp90. Residue Thr101 mutated to Ile
T22I	–	N-terminal domain mutant of Hsp90. Residue Thr22 mutated to Ile
TOCSY	–	Total correlation spectroscopy
TPR	–	Tetratricopeptide repeat
Tris	–	Tris(hydroxymethyl)aminomethane
TROSY	–	Transverse relaxation optimized spectroscopy
UV	–	Ultra Violet
UV-Vis	–	Ultra Violet - Visible
v/v	–	volume per volume
w/v	–	weight per volume
WT	–	Wild Type
ΔC_p	–	Change in heat capacity

ΔG	–	Change in Gibbs free energy
ΔH	–	Change in enthalpy
ΔS	–	Change in entropy

1 Introduction

The study of heat shock protein 90 (Hsp90) has been, and continues to be, intensively investigated. Yet despite the accumulated large body of knowledge, there are still many important questions that remain unanswered.

The protein studied in this thesis was the yeast homologue of Hsp90 from *S. cerevisiae*, otherwise known as Hsp82, however the homology between members of the Hsp90 family and the known functional overlap between them is high. Indeed it is known that both yeast and human Hsp90 discriminate in a similar way between Hsp70 and its close homologue Kar2[1]. It has also been observed that introduction of the human Hsp90 homologue can restore viability in yeast when the wild type gene has been knocked out[2]. This establishes the yeast Hsp90 homologue as a suitable reference for the human chaperone protein. Throughout this thesis, and indeed following the example frequently found within the literature, the protein of interest will be referred to as Hsp90.

1.1 The Hsp90 chaperone molecule

The Hsp90 family of proteins are found across all eukaryotic and prokaryotic species, with multiple isoforms involved in tissue and organelle specific functions including those within the endoplasmic reticulum, mitochondria and chloroplasts. Although the presence of Hsp90 is non-essential in bacteria, eukaryotic cell viability requires at least the cytoplasmic version of the chaperone[3]. Hsp90 is present in large quantities (up to 1% of the total yeast cell protein) under normal conditions, although its expression is increased upon heat shock.

Hsp90 is a molecular chaperone involved in the stabilisation and activation of a diverse range of 'client' proteins. Hsp90 does not appear to be involved in *de-novo* folding, instead it is required for the activation of 'clients' to a fully competent state. The details of the process of activation is one of the remaining mysteries of Hsp90 function but it is known to often involve inducing conformational changes within the client or enabling post-translational modification such as phosphorylation or dephosphorylation. The diverse set of client proteins is matched by an equally varying set of co-chaperone molecules that are required for the function of Hsp90

and the specific recruitment of various client proteins. For example the recruitment of the co-chaperone Cdc37 is required for the activation of protein kinase clients[3].

The 'clients' that require Hsp90 for function include telomerase, nitric oxide synthase, a number of both nuclear hormone receptors and transcription factors and a large array of protein kinases. The selectivity for Hsp90 client proteins is such that, although the range of proteins classed as requiring Hsp90 for activity is incredibly diverse, it seems to cover very specific functional areas (for example, cell signalling) [3].

Across the many studies of Hsp90 there are three key features which are consistent. The first is that the chaperone activity is controlled by the binding and hydrolysis of ATP. The second is that this binding and hydrolysis is coupled to a series of conformational changes within the chaperone molecule. The third is that this series of conformational changes is inexorably linked to the function of client proteins.

The link from ligand binding and hydrolysis to conformational changes within the Hsp90 molecule is clear (as described in detail later). These conformational changes are key to the chaperone activity of Hsp90 and a distinct cycle of conformational changes has been observed [4-9]. The Hsp90 chaperone protein functions as a dimer and is comprised of three domains: the N-terminal domain, the middle domain and the C-terminal domain. The role of these domains within the chaperone cycle and the importance of dimerisation will be discussed in detail later. Crystal structures have been solved for the isolated domains [8;10-13] and for the full length protein in a ligand and co-chaperone complex [7]. These structures however, only provide a 'snapshot' of the physical states that correspond to some of the stages in the conformational cycle. The accessibility of the remaining states to crystallography is extremely limited, and so dynamic methods such as nuclear magnetic resonance (NMR)[10;14-19], isothermal titration calorimetry (ITC) [8;17;20;21], fluorescence studies [5;9;22] and mutational analysis [23-27] have all been used to probe conformational changes within the protein.

The use of the isolated N-terminal domain of Hsp90 as a model to study the effects of ligand binding to the chaperone has been adopted by a number of groups. One reason for this is due to the size of the protein while another is the ease with which the N-terminal domain constructs have been crystallised. Size limitations of NMR preclude detailed study of proteins above 50 kDa; the N-terminal domain of Hsp90 has a molecular weight of 24 kDa and thus falls within the working range of NMR spectroscopy while the full length protein in its dimeric state is approximately 160 kDa and thus falls outside this accessible range. Another reason is that the N-terminal domain alone does not dimerise and thus a single binding event and the

corresponding induced conformational changes can be studied in isolation; the complexity of the chaperone cycle is evident [5;6;9;22] and thus simplification of the system in order to de-convolute the events is essential.

1.2 Early studies of the Hsp90 molecular chaperone

For many years it was believed that Hsp90 was involved in the *de-novo* folding of proteins similar to the previously investigated Hsp70 chaperone. Hsp90's ability to prevent the aggregation of GST under heat stress was seen as evidence of its role in general protein stabilisation[28]. It was not until much later that Hsp90's role in inducing the function of proteins rather than *de novo* folding was identified.

For a time the nature of the dimerisation of the Hsp90 chaperone was unknown, with early studies, such as that by Maruya et. al.[29], mistakenly attributing an anti-parallel arrangement to the homodimer. In hindsight, this is understandable as the degree of extension and flexibility actually shown by the dimer is sufficiently large to be mistaken as an anti-parallel arrangement. The parallel nature of the dimerisation was later shown by high resolution techniques such as crystallography [7;11].

Reports of both the existence and the level of ATPase activity of Hsp90 also varied dramatically from group to group. The low level ATPase activity that Hsp90 is now known to possess was often overwhelmed by the background ATPase activity of contaminants including Hsp70, now known to often be present in a chaperone complex with Hsp90. Evidence against the binding of ATP to Hsp90 included the failure to photoaffinity label Hsp90 with 8-azido-ADP or to bind Hsp90 to an ATP-agarose affinity column[30]. Also as evidence against Hsp90 having an intrinsic ATPase activity was its inability to enhance the fluorescence of MABA-ADP in a similar fashion to that observed for Hsp70[30]. Initial crystal structures of the N-terminal domain alone were solved without any nucleotide present, and showed a deep pocket within the molecule. Speculation as to whether this pocket was a binding site for unfolded segments of polypeptide chain continued until 1997 when the work of Prodromou et al.[8] resolved this issue. This structure was solved in the presence of ADP, clearly showing the ligand bound within the N-terminal domain cleft in a 'kinked' conformation. Previous studies such as that by Jakob et al. [30] used C8 adenine-substituted reagents which would not be able to adopt the

'kinked' conformation necessary for binding to Hsp90, thus explaining the erroneous suggestion that the chaperone had no ATPase activity.

Early studies in yeast identified distinct domains comprising the N-terminal and C-terminal ends of Hsp90. These fragments ran from residues 1 – 210 and from residue 262 to the extreme C-terminus. Individually these domains were seen to be insufficient for cell growth in the absence of full length Hsp90 expression. Moreover in cells with a reduced wild type Hsp90 expression these fragments were seen to inhibit Hsp90 function when co-expressed[25]. In light of more recent knowledge this can now be justified by the formation of heterodimers lacking one N-terminal domain. As discussed in detail later, two N-terminal domains are required for the full ATPase activity needed for client protein activation.

1.3 The role of Hsp90 in genetic capacitance

One role proposed for the Hsp90 molecular chaperone is as a 'genetic capacitor' for morphological and phenotypic evolution. A genetic capacitor buffers genetic variation in morphogenic pathways. In the same way that a molecular chaperone buffers potentially disruptive changes within a single cell over a short time, a genetic capacitor buffers changes in a genome across a longer period of time to allow normal development despite destabilising effects upon the organism. Hsp90 is known to associate with already predominantly folded proteins and its function is to allow the maturation and activation of its 'clients'. This ability to stabilise partially unfolded proteins may suggest a role for Hsp90 in buffering mutational variation and promoting evolutionary change. This has been detailed by Lindquist et al. [24-26;31] under a number of different circumstances.

Hsp90 most likely recognises characteristic features common to unstable or unfolding proteins rather than sequence specific motifs, thus allowing it to act upon such a large and diverse range of 'clients'. Under stress conditions, such as heat shock, Hsp90 can be diverted to associate with a more general subset of unstable proteins to prevent their full denaturation.

In a study of Hsp90 mutations in *Drosophila melanogaster* the degree with which the function of Hsp90 was inhibited, either due to mutations within Hsp90 or due to exposure to the Hsp90 inhibitor geldanamycin [26], correlated to the spontaneous appearance of phenotypically visible mutations. Similar results were observed in *A. thaliana* [24].

It was proposed that Hsp90 normally functioned to suppress unstable genetic variation when expressed, and that 'cryptic genetic variation might be expressed to a greater extent' in the case of Hsp90 inhibition [26]. The studies in *A.thaliana* also suggested that[24] the buffering capacity of Hsp90 may allow added stability against stochastic processes. When the buffering capacity of Hsp90 is exceeded by cell stress (increasing the amount of partially unfolded protein requiring stabilisation by Hsp90) or inhibited such as with geldanamycin or radicicol then otherwise silenced polymorphisms can prevail [24;31]. This buffering ability allows the organism to accumulate silent or neutral mutations thus providing a good environment in which beneficial or deleterious mutations can occur and be occasionally tested during times of environmental stress allowing selection pressure to remove unfavourable mutations[24]. Critically a mutation in Hsp90 is not always required, often environmental stress will be sufficient to exceed the buffering capacity of Hsp90 [31]. Hsp90 therefore acts as a capacitor for mutation allowing otherwise unrealised, and potentially useful, mutations to become permanent [26]. In a case where perhaps seven or eight independent determinants, such as mutations, are all required for a particular trait to express, this theory states that a slightly inhibited Hsp90 activity lowers the threshold of how many determinants are required before an altered trait can be expressed by erroneously stabilising the expressed gene product. Thus the chance that the lower number of determinants occurs in one gene increases. Expression of this multiply mutated protein under Hsp90 inhibited conditions allows selection pressure to be placed upon the mutation, which if positive, encourages the gene to gain the remaining determinants that allow it to express independently of impaired Hsp90 [26].

1.4 The substrate molecules of Hsp90

As previously mentioned the chaperone Hsp90 acts upon a diverse but specific set of client proteins. Association with Hsp90 allows the activation of many of these client proteins in a variety of ways. Six proteins that associate with Hsp90, including co-chaperones and substrates, are shown in Figure 1.1. The method by which activation is facilitated however is still unclear despite nearly two decades of intensive study [3;32]. Although the Cdc37 co-chaperone recruits a kinase, which may suggest phosphorylation as an activating mechanism, this does not explain the activation of all clients, as Cdc37 is not associated with all client / chaperone complexes. Some co-chaperone and client associations are shown in Figure 1.1. Even now a full knowledge of which proteins require Hsp90 for maturation is not known and

on-going efforts to discover them are regularly revealing new clients [32]. A full and regularly updated list of client proteins maintained by Didier Picard can be found at:

http://www.picard.ch/downloads/downloads.htm.

The 'clients' of Hsp90 can largely be broken down into three categories. The first is that of the protein kinases, the second is that of transcription factors including nuclear steroid receptors, while the third contains structurally unrelated proteins. This third set can loosely be categorised into intracellular receptors, viral replication proteins and proteins involved in innate immunity[32].

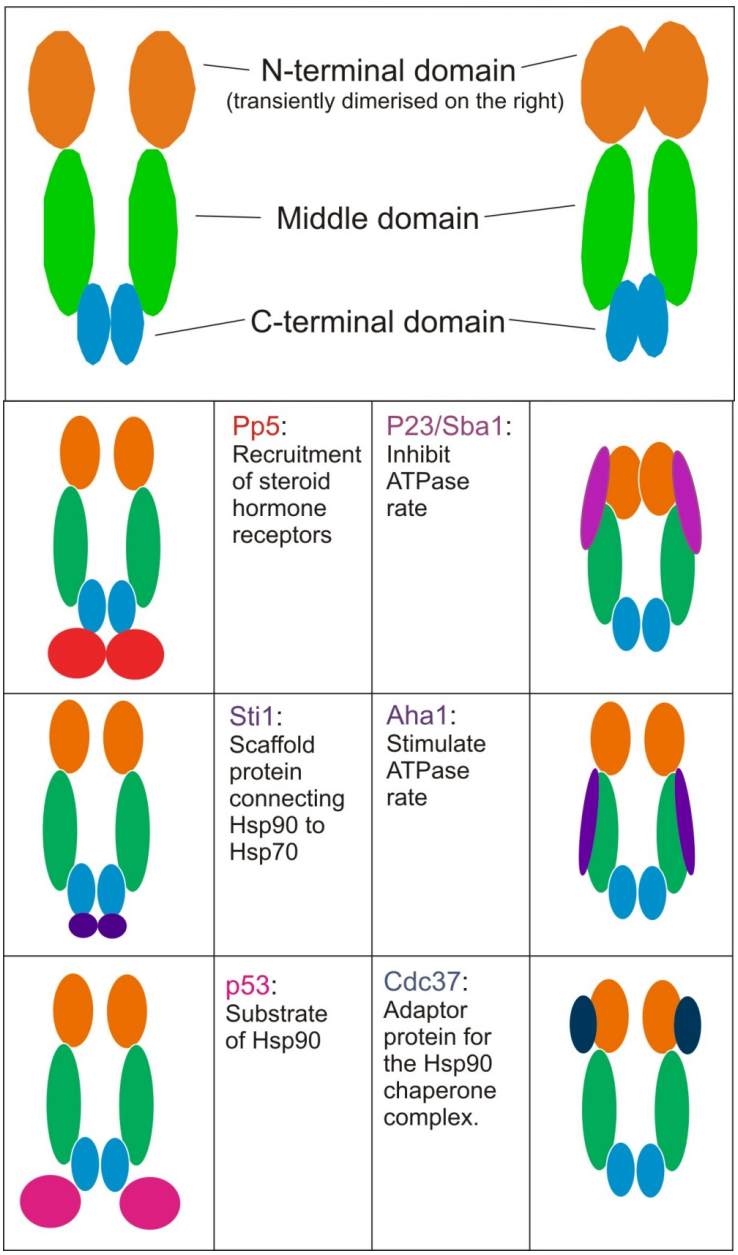

Figure 1.1 Top: A schematic of the full length Hsp90 chaperone in its open (left) and transiently N-terminal dimerised state (right). Bottom: A selection of co-chaperone and substrate proteins to Hsp90 demonstrating the range of binding sites across the chaperone molecule. Co-chaperones and clients not to scale.

The tyrosine kinase $pp60^{v\text{-}src}$ requires Hsp90 for its activation and accumulation[27]. Other kinases that require Hsp90 for activation include ASK1 and Akt/PKB. The glucocorticoid receptor has been shown to require continual association with Hsp90 to maintain it in a hormone-activatable and transcriptionally competent state[27]. Other steroid hormone receptors, (including those for estrogen, progesterone, androgen and mineral corticoids) also require Hsp90 to enable efficient steroid binding to the receptor[33]. Other proteins that require Hsp90 for functionality include eNOS, Bcl-xL and Apaf-1[34].

The tumour suppressor protein p53 is known to associate with Hsp90 only in a mutated form. It is known that oncogenic mutations of p53 have a lower melting point than the wild type p53[16]. This instability leads to partial unfolding of p53 and thus leads to its association with Hsp90. This leads to the stabilisation of p53 allowing its persistence within the cell. It has been observed by NMR that only unfolded or partially unfolded p53 associates with Hsp90 and that the chaperone does not associate with p53 when it is in its native state[16]. Binding of p53 to Hsp90 can therefore only be induced by unfolding of p53 caused by either an increase in temperature or mutations that decrease the protein stability. Some NMR data suggest that p53 binds to Hsp90 in a predominantly flexible but unfolded state. This persistence of an otherwise unstable mutant protein, enabled by Hsp90, can lead to uncontrolled cell proliferation and tumourogenesis [16]. This role in protein stabilisation makes Hsp90 a good target for potential cancer treatment as inhibition of Hsp90 can prevent the stabilisation of otherwise oncogenic proteins. This can lead to the degradation of cancerous proteins or identification of the mutation by the cell and subsequently controlled cell death.

1.5 The chaperone cycle of Hsp90

Over the course of the last decade, the study of the Hsp90 chaperone cycle has advanced dramatically from early work realising that there was a cycle of conformational changes associated with ATP binding and hydrolysis, to recent work that has tracked at least five steps within the cycle, complete with rate constants for each transition [5;9].

Even before the details of the cycle were deduced it was discovered that ADP release was not the rate limiting step in the chaperone cycle [35]. Kinetic studies using displacement of (Pγ)-MABA-ATP, a fluorescent ATP analogue, from the ATP binding site of Hsp90, revealed that

ATP binding can be described as a one-step reversible reaction [35]. The on rate of ATP binding also precluded it from being the limiting step in the chaperone cycle [35]. Early studies using radio-labelled ATP and a 'chase' style experiment with unlabelled ATP revealed that ATP bound to the Hsp90 chaperone was committed to hydrolysis, indicating a likely conformational change trapping the nucleotide in place. This 'trapping' was observed in the full length chaperone and truncation mutants containing the middle domain and the catalytic loop, but not in the isolated N-terminal domain of Hsp90. Although the larger constructs allowed commitment of ATP, none of the truncations regained full ATPase activity [35].

Transient N-terminal dimerisation was confirmed by introduction of a cysteine residue into surface accessible areas of the N-terminal domain and subsequent chemical cross-linking under different ligand bound states. Further experimentation with pyrene molecule labelling showed that N-terminal dimerisation was far more prevalent in the AMPPNP bound form of Hsp90 than the apo or ADP bound states [23] suggesting for the first time that ATP binding promoted N-terminal dimerisation while ADP binding did not.

A series of C-terminal truncation mutations revealed a drastic drop in ATPase activity. The link between constitutive dimerisation and ATPase activity was established. It was also established that in the longer truncated constructs, the presence of AMPPNP bound to the N-terminal domain led to dimerisation from an undimerised apo-state. The degree to which dimerisation in the presence of AMPPNP occurred also correlated with the ATPase activity of the construct [23]. Although the N-terminal domain of Hsp90 alone showed some limited ATPase activity, it was observed to be only 1% of the wild type activity and no dimerisation in any ligand bound state was observed[23;35].

The dramatic decrease in ATPase activity when there is a loss of N-terminal dimerisation suggested that there is a cooperative nature to the reaction, that requires both N-terminal domains within the dimer for efficient hydrolysis [23]. Further mutation studies established that N-terminal domain association between the monomers likely exploited a hydrophobic patch exposed by closure of the ATP 'lid' region. Mutations designed to stabilise the lid 'closed' conformation (such as A107N) led to increased N-terminal dimerisation and increased ATPase activity. When truncation mutations were used and constitutive dimerisation was known to not occur, the presence of the A107N mutation still led to a reduction in ATPase activity [23].

It is relatively clear now that commitment of the ATP molecule requires conformational rearrangement with movement of the ATP 'lid' over the nucleotide binding site. As described in more detail later this allows the middle domain catalytic loop to contact

the γ phosphate. Full ATPase activity requires constitutive dimerisation via the C-terminal domain to, in turn, facilitate transient N-terminal domain dimerisation. In order to understand the significance of these observations it is necessary to know more about the detailed structure of the Hsp90 chaperone and the role of critical key features such as the middle domain catalytic loop and the N-terminal domain ATP 'lid'.

1.6 Structural details of the Hsp90 chaperone

The intact full length Hsp90 molecular chaperone is a constitutive homodimer. It can be subdivided into three domains, the N-terminal domain, the middle domain and the C-terminal domain. Each domain has a distinct function, however there is a large degree of interaction between the domains. The effect of binding and hydrolysis of ATP to the N-terminal domain can be seen to influence the conformation of the entire protein, while binding of co-chaperones can also have a profound influence beyond the domain with which they are associated.

1.6.1 Structure of the N-terminal domain

The N-terminal domain of Hsp90 can be considered to extend from the first amino acid residue to residue 216. It contains the ATP binding site[8] but is also the site of both co-chaperone [7] and client binding. The N-terminal domain of Hsp90 has a high structural similarity to the nucleotide binding domain of DNA Gyrase B, a bacterial type II topoisomerase. This similarity was only recognised during the CASP2 structural prediction competition of 1997, whereupon it was shown that six β strands and five helices had equivalence to the DNA Gyr B structure, thus making it part of a gyrase, histidine kinase, and MutL (GHKL) superfamily of proteins [36].

The N-terminal domain has been crystallised in the presence of ADP and the structure determined to a resolution of 1.85Å[8] and with ATP to a resolution of 2.0Å[8], revealing details of the binding site and some of the contacts formed between the ligand and the protein (Figure 1.2). The nucleotide binding site of Hsp90 also shows many similarities to DNA GyrB and MutL (a DNA mismatch repair protein) [8]. The crystal structure in the presence of nucleotide definitively proved that the Hsp90 chaperone molecule was an ATPase.

Several key features of the N-terminal domain have been identified. The nucleotide binding site has been identified as a deep cleft formed by a β-sheet flanked by α helices. The existence of an ATP 'lid' running from residues 98 to 120 was suggested from homology with DNA GyrB. The role of the first 24 residues in enabling ATPase activity has also been determined[8]. The importance of each of these features will be discussed in detail.

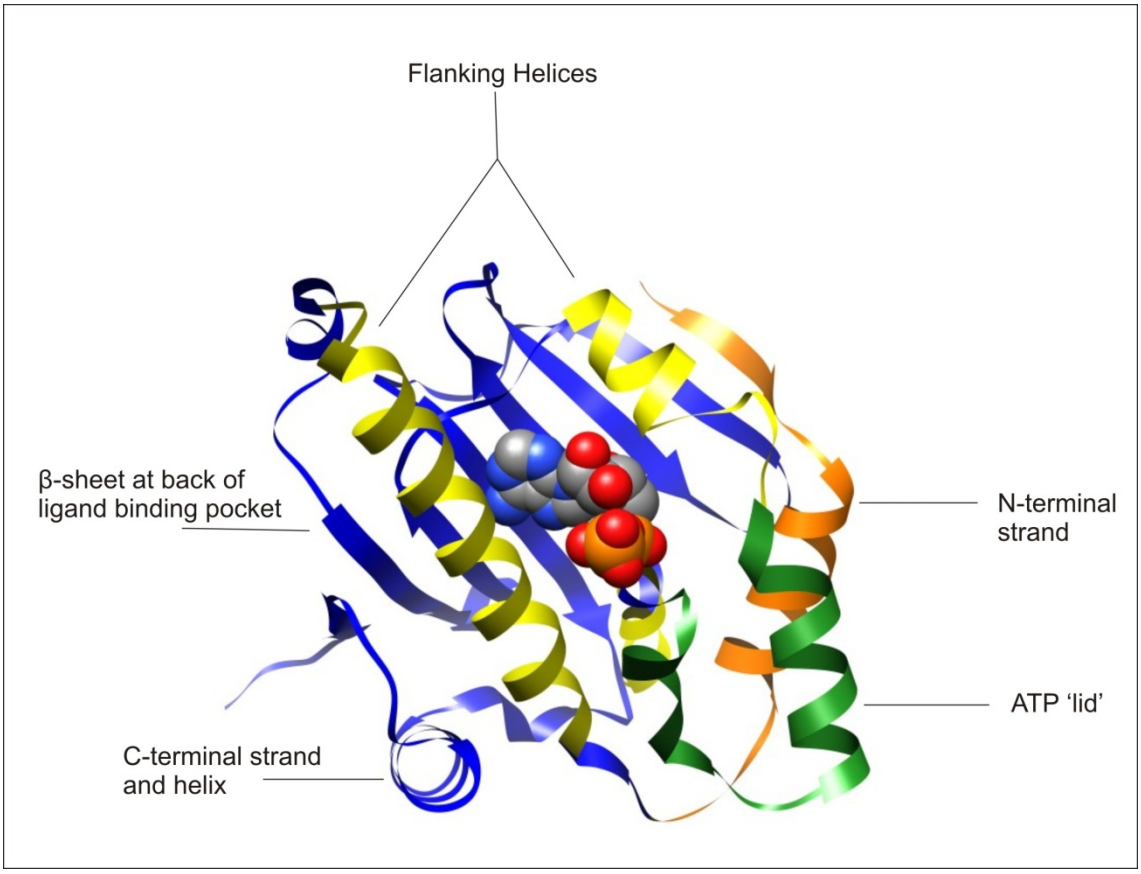

Figure 1.2 Crystal structure of the N-terminal domain of Hsp90 (ribbons) bound to ADP (atoms as space-filled spheres). Structural features are highlighted: the binding pocket is shown in blue (the back of the pocket) and yellow (the flanking helices), the N-terminal helix and strand are shown in orange while the ATP lid is shown in green – in this instance in the 'open' conformation. PDB file 1AMW used for diagram.

The ATP lid

Other members of the GHKL family require the movement of an ATP 'lid' from an 'open' to a 'closed' conformation. This movement results in a covering of the entrance to the nucleotide binding site through the rearrangement of a specific loop region. It is probable that Hsp90 also requires such a lid movement. Crystal structures of the yeast Hsp90 homologue have now identified the lid in two positions – the 'open' state seen in the isolated N-terminal domain[8] and the 'closed' state over the nucleotide binding site in the full length protein in the presence of the co-chaperone p23 [7].

Studies of the lid position of the bacterial Hsp90 molecule suggest that not only does the position of the lid affect the binding and hydrolysis of ATP but that it also has an influence over the binding and release of client proteins [6]. Heterodimers of wild-type yeast Hsp90 and mutants with a lid deletion showed increased ATPase activity on the wild type monomer, suggesting that transient N-terminal dimerisation was still occurring despite the absence of the ATP lid; indeed analytical gel filtration results suggest that in a dimer comprising two lidless mutants the N-terminal dimerisation becomes highly stabilised [10].

Combined EM and crystal data suggests that movement of the lid couples ATP hydrolysis to the client protein binding and release. Crystallographic and EM studies involving the bacterial Hsp90 suggest that in addition to the 'open' and 'closed' states seen in yeast crystal structures [7;8] there may be two further distinct lid conformations. The first of these conformations may be a state where prior to nucleotide binding the lid partially occludes the binding site and a large amount of exposed hydrophobic surface area is presented to encourage client association. This state is observed when the two 'arms' of the Hsp90 chaperone are widely splayed and is incompatible with other known N-terminal and middle domain arrangements due to steric clashes. Movement between the two known arrangements of the two domains would require rearrangement of the lid region (Figure 1.3). The second potential lid state is observed following ATP hydrolysis in the highly compact ADP bound state. In this state the lid may arrange itself to bury hydrophobic surface area newly exposed following the condensation of the chaperone dimer to a more compact form following nucleotide hydrolysis. This may aid in client protein dissociation by reducing accessible hydrophobic surface contacts [6].

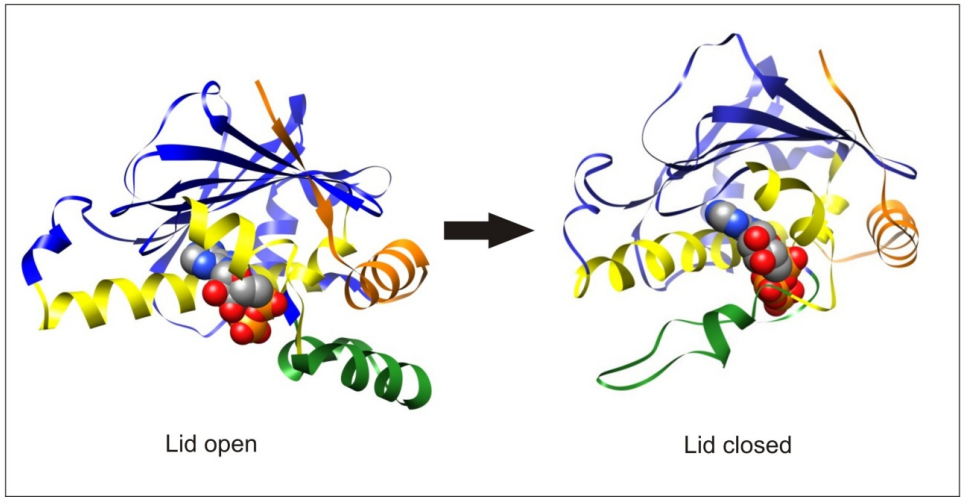

Figure 1.3 Comparison of the ATP 'lid' open and closed forms. The 'open' form is from the crystal structure of the isolated N-terminal domain bound to ADP. The 'closed' form is a proposed model based upon the full length crystal structure of Hsp90 by Ali et al. [7] in the presence of ATP and p23. The same colouring scheme applies as in Figure 1.2. PDB file 1AMW used for 'lid open' form, same file modified and used for 'lid closed' form.

The direct comparisons that can be drawn between the bacterial Hsp90 and the eukaryotic yeast Hsp90 are limited, however the ability of the lid to adopt a varied range of conformations is likely to apply across species even though the details will likely be different. Knowledge that both bacterial and yeast Hsp90 undergo a complex series of conformational changes upon ligand binding and hydrolysis, together with the detail resolved regarding the bacterial chaperone ATP 'lid' conformations, suggests that a similar level of complexity may exist in eukaryotic Hsp90 but is not obviously reflected by the two known crystal structures. Indeed work by Dollins et al. [4] on the mammalian Hsp90 endoplasmic reticulum isoform of Hsp90 (Grp94) suggested the existence of a new 'ground state' form. In this form the binding of ATP did not induce instant conformational change without further input from clients or co-chaperones. This ground state prevented the association of the N-terminal domains and thus did not favour ATP hydrolysis. The existence of this 'ground state' may explain the low ATPase rate seen in the Hsp90 chaperone family compared to other ATPase's in the GHKL family [4], and shows similarity to the pre-ligand bound state observed in the bacterial Hsp90 crystal structure described previously [6].

The nucleotide binding site

The nucleotide binding site of Hsp90 is shown in detail with ADP bound in the crystal structure solved by Prodromou et al. [8]. The binding site described in that paper contains the nucleotide and a number of water molecules with the position of the magnesium ion modelled in. The nucleotide is bound both directly to the protein and indirectly via water molecule contacts that mediate between ligand and chaperone (Figure 1.4). The adenine ring of ADP makes direct contact, via a hydrogen bond, from the N6' atom of the ring to the carboxyl group of Asp79. Interactions between the adenine ring and the side chain of Met84 via van de Waals forces also occur. Indirect links with the adenine ring include contact between the N1' atom and a water molecule that then contacts Asp79, Gly83 and Thr171. Water-mediated contacts are also made between N6' of the ring and the backbone carbonyl of Leu34, N3' of the ring and Asp92 and N7' of the ring and Asn37 [8]. The O2' atom of the ribose of ADP makes a direct contact to Asn92. Other water mediated contacts between the ribose and the protein include from the O2' and O3' atoms to Lys44 and from O2' ribose to Asn92, in addition to the direct contact also made between these two [8].

The phosphate groups are also involved in both direct and indirect binding contacts to the protein. Direct contacts include an oxygen of the α-phosphate to the amide nitrogen of Phe124 and the β-phosphate to Lys98. Indirect contacts include the association of the β-

phosphate to a water molecule at the pocket's mouth. The phosphate groups are also responsible for the contacts to the Mg^{2+} ion known to be essential for ligand binding. Both α- and β-phosphate groups contact the ion which in turn contacts amide oxygen atom of Asn37 and three further water molecules within the binding site [8]. The location and interaction of the terminal phosphate was not present in the ADP bound crystal structures solved by Prodromou et al. [8]. The full length crystal structure later solved by Ali et al. [7] did show the γ phosphate and revealed a contact between it and residue Arg380 from the middle domain. Confirmation of the importance of Arg380 is described later.

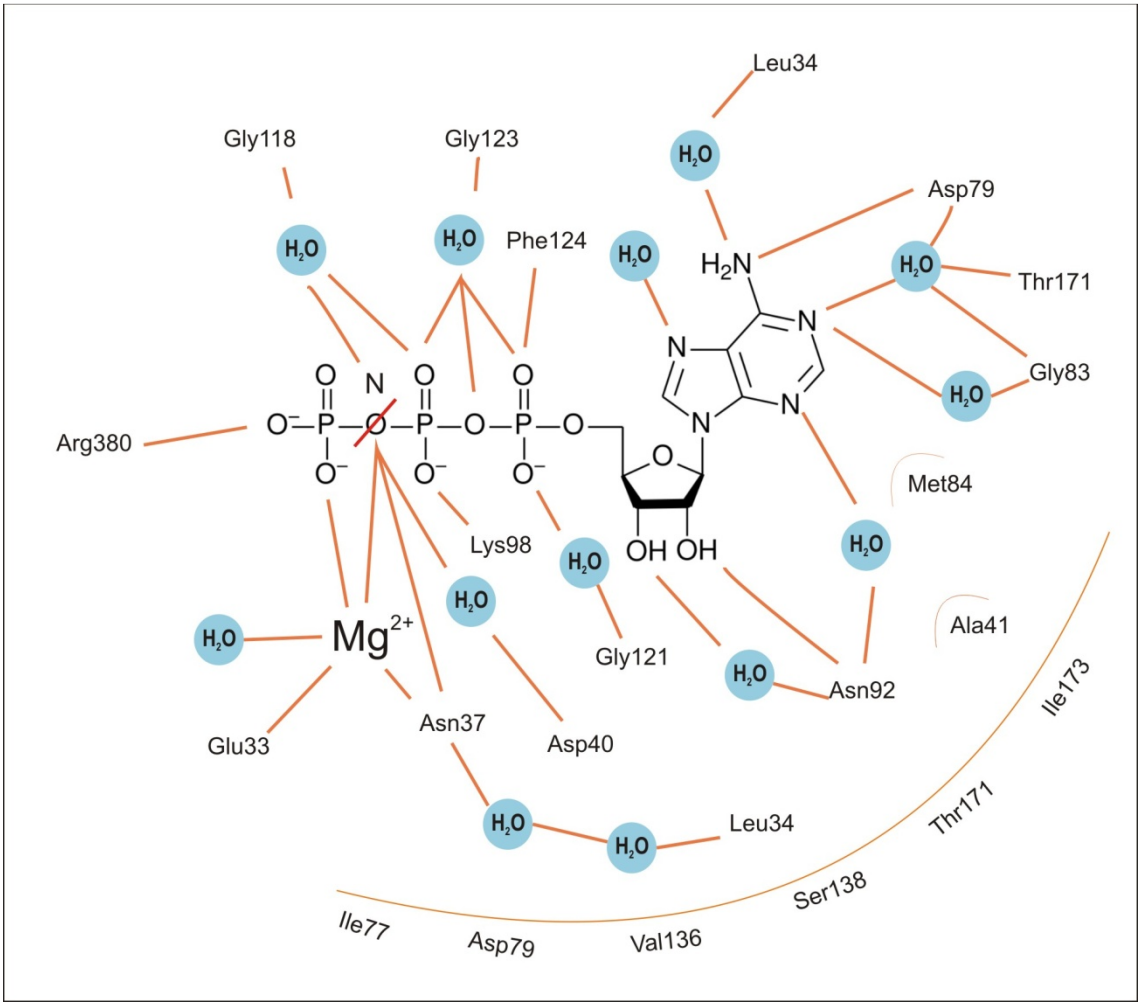

Figure 1.4 Contacts within the ATP binding site of the N-terminal domain of Hsp90. Direct and water mediate contacts are shown with connecting lines. Van de Waals contacts are shown behind curved lines. Based upon data given in Prodoromou et al. (Cell 1997) [8]. The schematic highlights the difference between ADP and AMPPNP ligands, the binding of which will be discussed in depth below.

Ligand binding is known to lead to conformational changes within the intact Hsp90, however H/D exchange mass spectroscopy does not suggest that large structural or dynamic changes occur upon ADP binding compared to the apo-state sufficient to alter the exchange

rate of protons from the molecule. All that is observed is the stabilisation of amide bonds at the back of the binding site pocket [37].

Residues 1 – 24: The N-terminal helix and strand

It soon became apparent that the first 24 amino acids played a critical role in controlling the ATPase activity of the Hsp90 chaperone[38]. Truncation mutants from the N-terminal of the chaperone revealed that binding affinity of ADP was unaffected, as were the on- and off-rates. It was observed, however that removal of the first 8 amino acids led to an increase in ATPase activity above base level, further truncations of 16 and 24 amino acids then severely reduced the ATPase activity of the full length protein [38]. Since it is known that transient N-terminal dimerisation is required for ATPase activity, the contribution of the N-terminal strand to this dimerisation was tested by mixing wild-type Hsp90 with the truncation mutants. This revealed that the first 24 amino acids were key in forming a transient N-terminal dimer to allow efficient ATP hydrolysis. In isolation the crystal structure of the N-terminal domain [8] does not reveal why this might be the case. The full length crystal structure [7] can explain the observations through interactions made by the two N-terminal domains (Figure 1.5). Details of these interactions are discussed later in regard to the whole chaperone molecule.

In the presence of ADP the wild-type crystal structure shows a hydrophobic interaction between the lid and the helix and loop regions formed by residues 10 – 27, suggesting that this 'open' conformation is stable. Crystallisation of a mutant of the N-terminal domain of Hsp90 lacking the residues 1 – 24 showed the ATP 'lid' to be in a more open conformation than previously observed [10]. The association between the lid and residues 10-27 seen in the structure by Ali et al. [7] explains why deletion of the N-terminal strand and helix leads to an increased flexibility in the lid region observed by Richter et al. [10] and implies that the ATPase activity can also be influenced by the lid region as well as the immediate binding site.

The relative influence of the lid and the N-terminal 24 residues can be investigated using deletion mutations. Removal of the lid led to no change in nucleotide binding properties. Removal of the lid and the N-terminal strand, however, did lead to a seven fold increase in dissociation rate of the ligand from the binding site and inhibited the ATPase activity [10]. An absence of transient N-terminal dimerisation in double mutants suggests that the influence of the N-terminal 24 residues over this conformational change is greater than the influence of the lid [10].

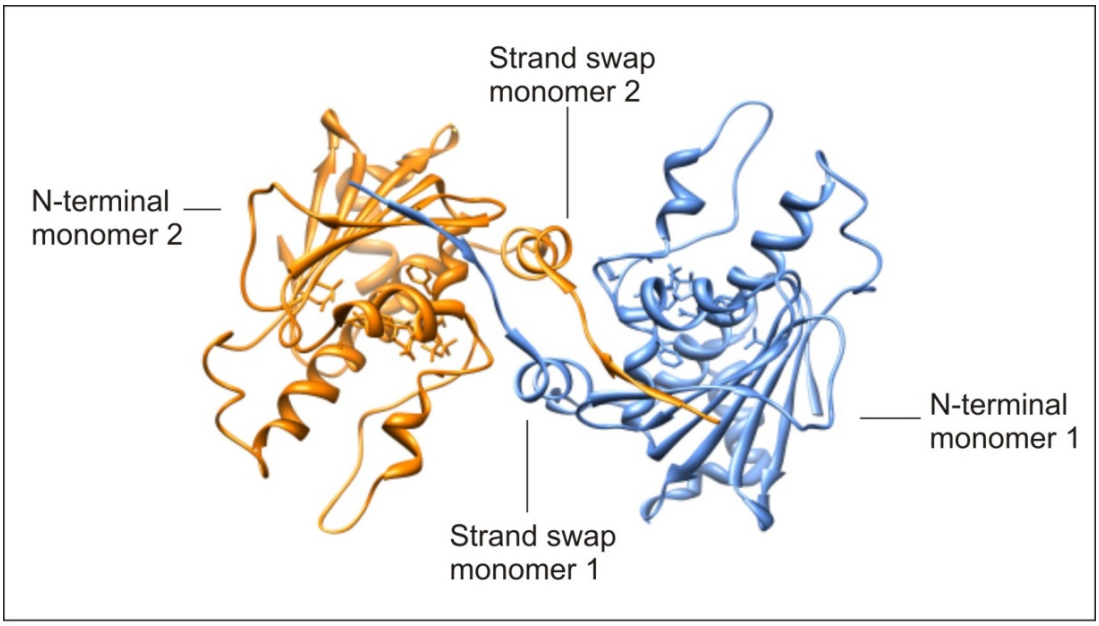

Figure 1.5 Diagram showing the N-terminal 24 residues involved in a strand swap event during transient N-terminal dimerisation from the full length structure by Ali, et. al. [7]. PDB file 2CG9 used for diagram.

1.6.2 Thermodynamics of nucleotide ligand binding

The thermodynamics of ligand binding are important to record in order to understand the nature of ligand binding and how this may influence the conformational changes known to occur in Hsp90. Through the use of ITC the enthalpy (ΔH), entropy (ΔS), binding affinity (K_d) and stoichiometry (N) of the reaction can all be determined from a single experiment. The relationship between these values and how they respond to different conditions (such as a change in temperature) can be used to determine something of the nature of the binding site.

A recent study by Nilapwar et al. [17] demonstrated the need for increased knowledge of the relationship between the thermodynamics of ligand binding and associated conformational changes within Hsp90. By comparing the thermodynamic properties of binding of the adenine based compounds AMPPNP, ADP, cAMP and the Hsp90 inhibitor compound geldanamycin and its analogues 17-AAG and 17-DMAG, various interesting facts emerged. Geldanamycin and its associated compounds bound with a 20-fold higher binding affinity and with a favourable entropy (ΔS) component to the binding. In contrast the adenine based compounds bound less tightly with a less favourable ΔS component, but with a similar enthalpy (ΔH) component suggesting that the difference in ΔS was responsible for the increased affinity.

The change in heat capacity (ΔC_p) of binding represents the change in enthalpy (ΔH) of a reaction with respect to temperature. Contributions towards the ΔC_p can include covalent bond formation, the burial of surface area and the charge state of the atoms. More detail on utilising the recorded ΔC_p values are discussed in Chapter 2. The change in heat capacity (ΔC_p) of binding between the ligands to the N-terminal domain of Hsp90 ranged from positive to negative values– a previously un-encountered situation for a single binding site in response to different ligands. The ansa-ring compounds have a negative ΔC_p, however, in contrast, ADP has a ΔCp close to 0, while AMPPNP shows a positive ΔC_p [17].

A positive contribution to ΔC_p by the binding of water molecules to the complex interface could not be ruled out by mutation studies, as the mutations knocked out the binding capacity of the protein [17]. In predictions, the difference in hydrogen bonding water networks around the adenine- compared to the ansa-ring based compounds should lead to a more negative value of ΔC_p rather than a more positive one. This leads to the conclusion that there must be another process affecting the heat capacity [17]. The differences in ΔC_p between ADP and AMPPNP show that the profiles of each are distinct and that information derived for one bound state cannot automatically be applied to the other bound state. This ties in with the knowledge that structurally the ADP and AMPPNP bound states appear to be distinctly different steps in the chaperone cycle [5;9]. It is therefore important to understand the thermodynamics of each state separately.

The effects of pH on the binding affinity suggested a single protonation event involved in the process of AMPPNP binding. However this appeared to have no effect on the ΔC_p which remained positive throughout the pH range tested (pH 5 – pH 10). The influence of the ionic environment over the ΔC_p was ruled out through experiments conducted over a range of 0 – 200 mM NaCl, which showed no change in ΔC_{pobs}.A full characterisation of the effect of this protonation event has not been undertaken, nor has the effect of pH on any other ligand been investigated.

Having ruled out many of the main possibilities that could contribute towards the positive heat capacity the paper by Nilapwar et al. [17] concluded that conformational changes as the most likely explanation of the positive ΔC_p. Crystals structures show the location of the binding pocket in the apo-form and the position of ADP within the binding pocket [8].

Structural differences between the ligand bound states was confirmed by NMR [17]. That there are differences in structure between the ligand bound states of the N-terminal domain alone is clear from the NMR shifts observed. This ties in with previous studies that also suggest conformational changes within the chaperone protein. The presence of ligand bound

to the N-terminal domain of Hsp90 led to a number of chemical shifts suggesting a change in environment. Figures 1.6 and 1.7 show NMR data collected for this thesis that agree with the data previously reported by Nilapwar et al. [17] and Kessler et al. [19] demonstrating the chemical shifts induced by ADP and AMPPNP binding respectively. Since these shifts extend to beyond the binding site itself, this suggests a more significant range of conformational changes. Overlays of the NMR spectra in the apo and ligand bound states are shown in Figures 1.6 and 1.7. Residues corresponding to the suspected ATP lid are not visible within the spectra.

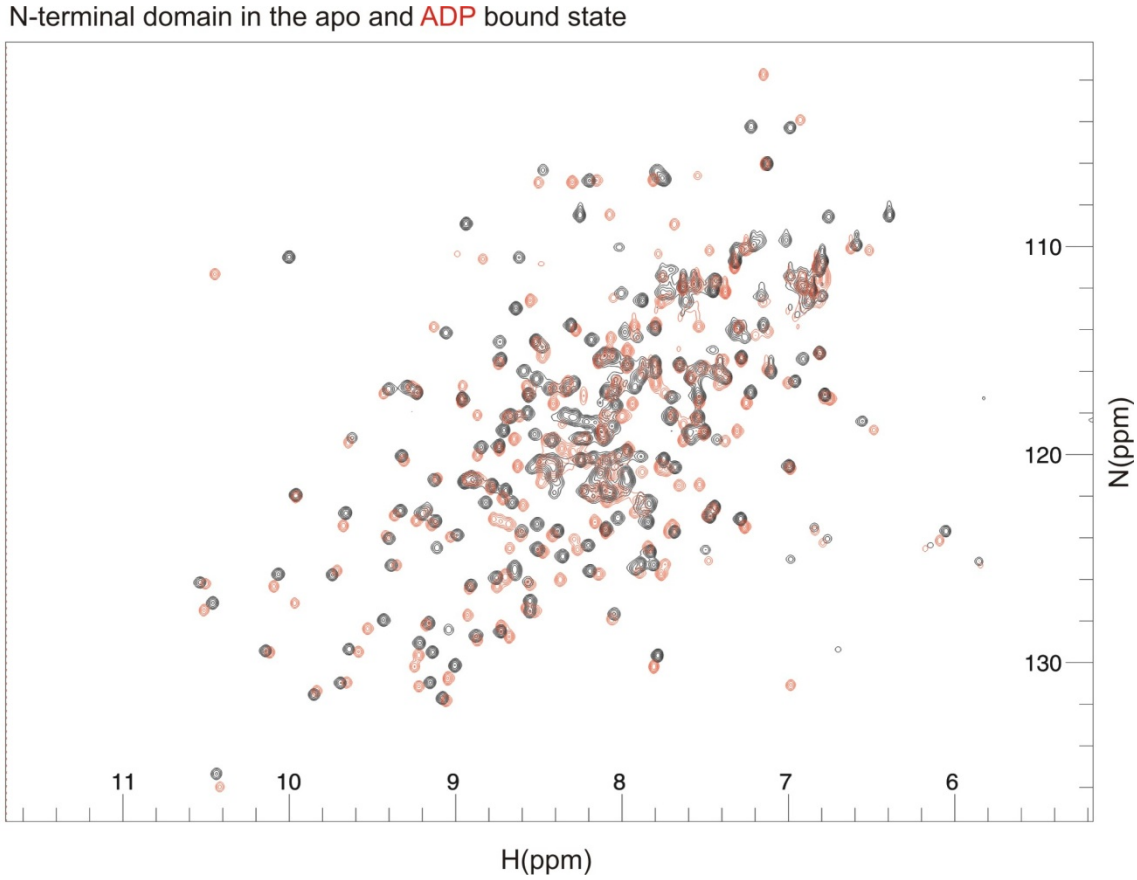

Figure 1.6 Overlay of the HSQC spectra for the apo and the ADP bound state of the N-terminal domain of Hsp90 showing significant differences between the two. Recorded in 20 mM Tris, 5 mM Mg^{2+}, at a concentration of 300 µM N-terminal domain, 5 mM ADP, pH 8, 700 MHz field strength at 25°C.

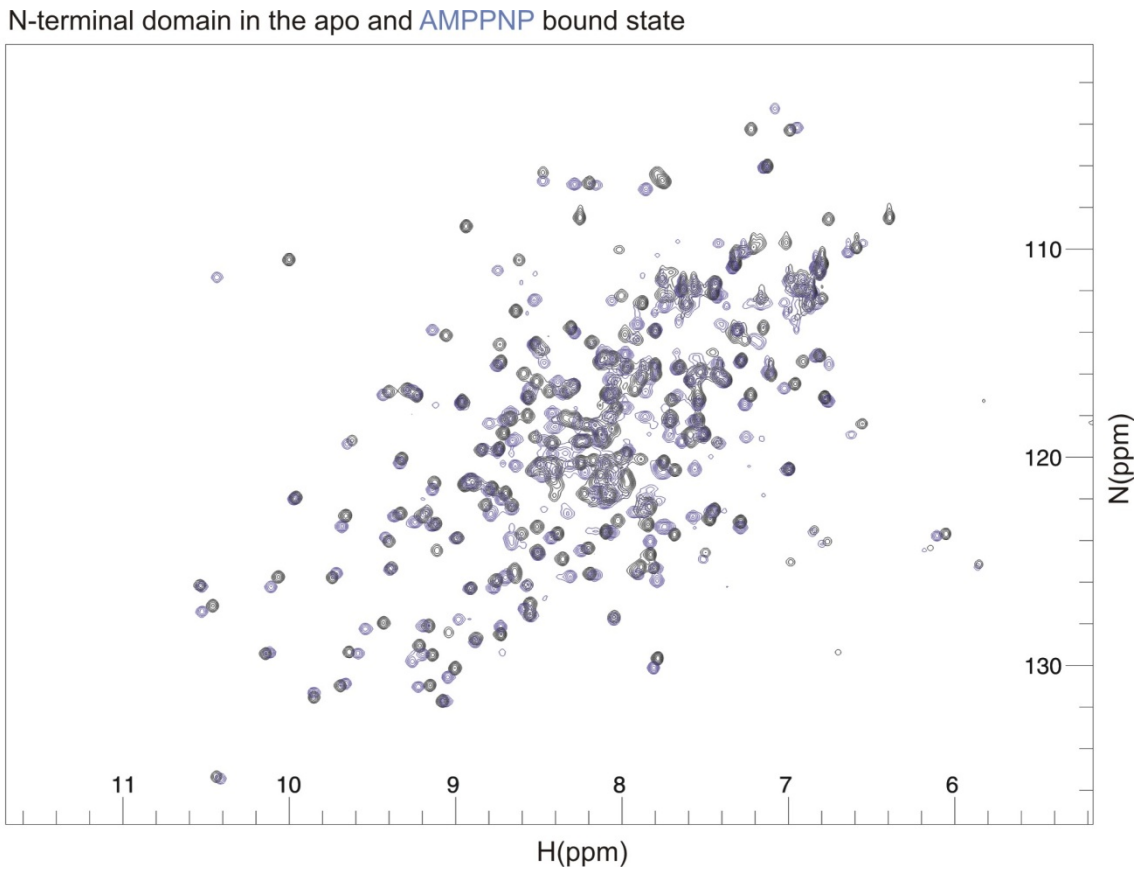

Figure 1.7 Overlay of the HSQC spectra for the apo and the AMPPNP bound state of the N-terminal domain of Hsp90 showing significant differences between the two. Recorded in 20 mM Tris, 5 mM Mg^{2+}, at a concentration of 300 µM N-terminal domain, 5 mM AMPPNP, pH 8, 700 MHz field strength at 25°C.

As discussed below it is known that Hsp90 goes through a series of conformational changes driven by the binding and hydrolysis of ATP, however descriptions of each stage of the cycle lack atomic resolution. It has already been established that the movement of the lid is critical for full Hsp90 activity and that it can influence the overall chaperone cycle [4;6-8;10]. Establishing the exact nature of the movement of the lid during the chaperone cycle is important to the understanding of the overall function/action of Hsp90.

Ligands and inhibitors

There are two very well known inhibitors of Hsp90 activity, both of which bind in the ATP binding pocket in the N-terminal domain. The first is geldanamycin and its relatives such as 17-AAG and DMAG; the second is radicicol which differs in its structure from geldanamycin but acts in a similar fashion. It has been known for a long time that geldanamycin, an ansa-ring based compound, was an inhibitor of Hsp90 activity. However it was not known how it affected the chaperone. With the work of Roe et al.[21] it became apparent that geldanamycin

and radicicol bound to the nucleotide binding site, acting to block ATP binding. Both ligands are shown in Figure 1.8.

The crystal structure of geldanamycin bound to the ATP binding site within the N-terminal domain of Hsp90 shows the ansa-ring of the compound located in the base of the binding pocket close to where the adenosine ring of ATP would normally sit. The benzoquinone ring of geldanamycin then bends towards the opening of the pocket; this is similar to the positioning of the phosphate groups of the native nucleotide when bound. In this state geldanamycin is bent significantly compared to its solution state. This 'bent' conformation is reminiscent of the 'kinked' binding conformation adopted by ATP [21]. Geldanamycin binding to Hsp90 was established by ITC to have a K_d of 1.2μM in a binding interaction that showed an unfavourable entropy. This unfavourable entropic component of association can be explained by the minimal release of ordered water molecules upon binding [21].

The crystal structure of radicicol bound to the N-terminal of Hsp90 shows that the aromatic ring takes the role of the adenosine group and points towards the bottom of the nucleotide binding pocket. The macrocycle and conjugated bond system of radicicol are thus left to point towards the top of the binding pocket, with a similar orientation to the phosphate groups of the native ligand. The folding of radicicol into the pocket is less dramatic than that observed for either geldanamycin or ATP, and is far closer to the free solution structure of radicicol. Radicicol binding to Hsp90 was established by ITC to have a K_d of 19nM in a binding interaction that showed a favourable entropy. The favourable entropic component of the association may well be explained by the displacement of a large number of ordered water molecules from the binding site [21].

Chemical shift perturbation studies rely upon monitoring the change frequency of a given resonance arising from the change in environment of a given group. This change in environment can be due to the proximity of a new chemical group such as when a ligand binds to a protein via direct contacts. More often it is due to a conformational change which alters the environment of the group and thus leads to a shift in the chemical frequency detected for that atom pair.

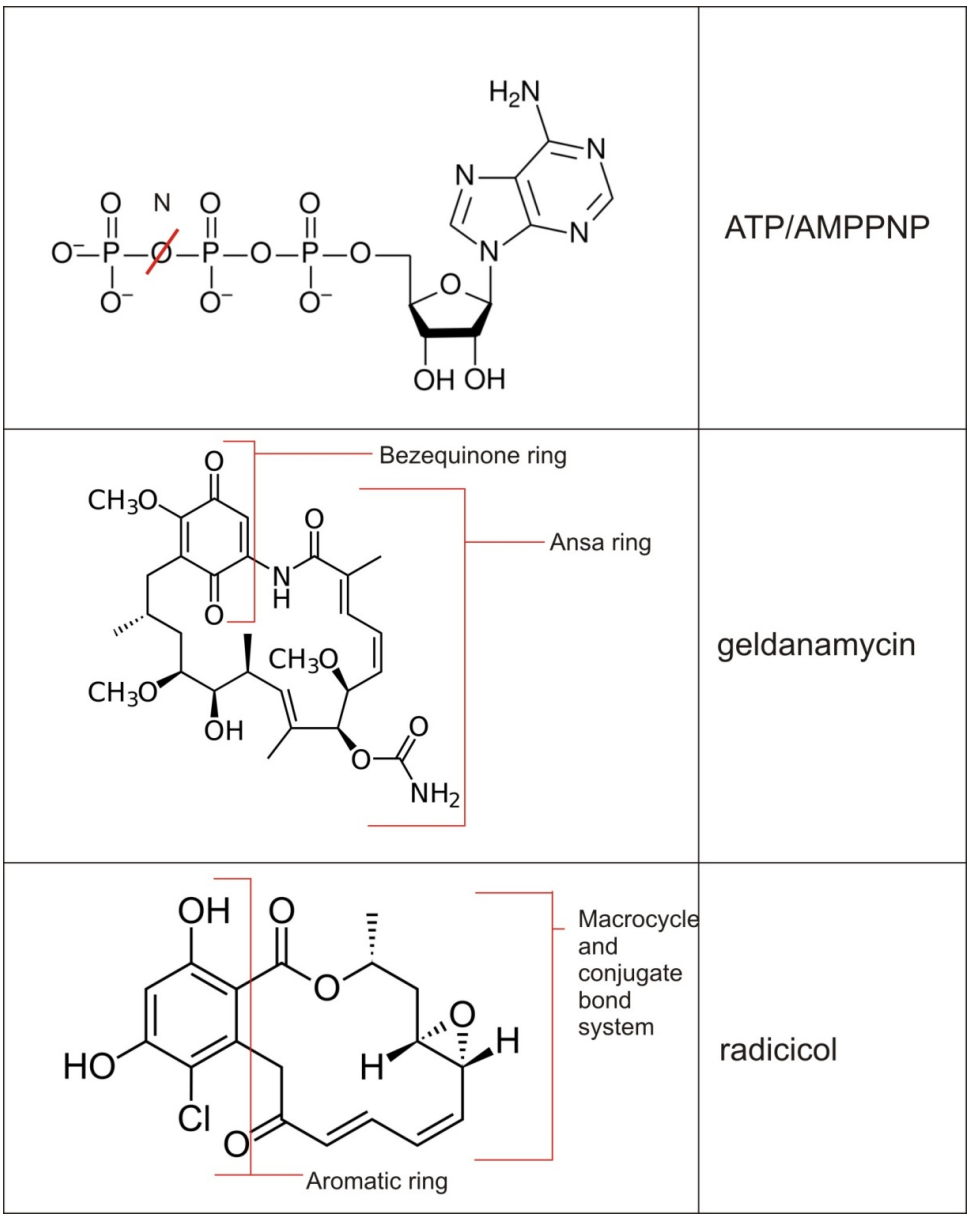

Figure 1.8 Diagram of the chemical structures of the ligands ATP/AMPPNP, geldanamycin and radicicol.

NMR chemical shift perturbation studies revealed distinct shifts for the binding of both geldanamycin and radicicol to the N-terminal domain of Hsp90[17;19]. Shifts observed for geldanamycin binding were large compared to both nucleotide binding and the binding of the inhibitor radicicol. Large shifts were seen at the bottom of the binding pocket in the surrounding two α-helices (residues 10 – 22 and 28 – 50). The shifts in this region were similar to those seen for radicicol and the nucleotide based ligands. Shifts for the long α-helix (residues 28 – 50) show that geldanamycin induces movement similar to the nucleotide based ligands, in contrast to radicicol which shows very few shifts in this region [19] compared to the regions previously described.

The pattern of chemical shifts observed for radicicol binding differs significantly from that seen for the binding of AMPPNP or ADP to the N-terminal domain. The differences can be

explained by consideration of the known crystal structures, where Radicicol is seen to make different contacts with Hsp90 to other known ligands. Some shifts due to Radicicol were smaller while others were larger than shifts induced by nucleotide binding. Larger shifts mapped to the base of the binding pocket [19], which matches the crystal structure observed in which the small radicicol molecule inserts more deeply into the binding pocket than the nucleotides. Decreased shifts matched the observation that fewer contacts are made in the upper region of the binding pocket [21]. When radicicol binding to the full length Hsp90 chaperone was observed via H/D exchange mass spectroscopy, an increased degree of proton protection was observed at the bottom of the binding pocket sufficient to confirm that the ligand had bound but insufficient to suggest large scale structural rearrangements [37]. A small increase in protection from proton exchange in the ligand binding pocket combined with no change in proton exchange rate in the lid region of the N-terminal domain was observed in the radicicol bound state compared to the apo state. This suggests that when bound to the inhibitor, the chaperone adopts an 'open' conformation as is also suggested to be the case in the ADP bound and apo states [37].

1.6.3 Structure of the middle domain

The middle domain extends from residues 262 to 551. Unlike other members of the GHKL family, the connection between the N-terminal and middle domains of Hsp90 is not formed from a continuous element of secondary structure, but is instead linked by a long flexible region of around 50 amino acids. This flexible region varies across species, but includes a positively charged region of between 20 – 30 amino acids that is often subject to hydrolysis. The crystal structure of the isolated 33kDa middle domain was solved to a resolution of 2.5Å by Meyer et al. [12]. From this structure, three main regions can be defined. Initially there is an αβα sandwich domain made up of a five stranded β-sheet flanked by a three turn and a six turn α-helix (see Figure 1.9). This fold is similar to that found in MutL and GyrB, members of the GHKL family to which Hsp90 also belongs [12]. The αβα sandwich is followed by a three helix right handed coil followed by a second αβα sandwich motif [12]. This second novel αβα sandwich fold is distinct from the second αβα sandwich motif observed in MutL and GyrB, although there is still some limited similarity between them [12].

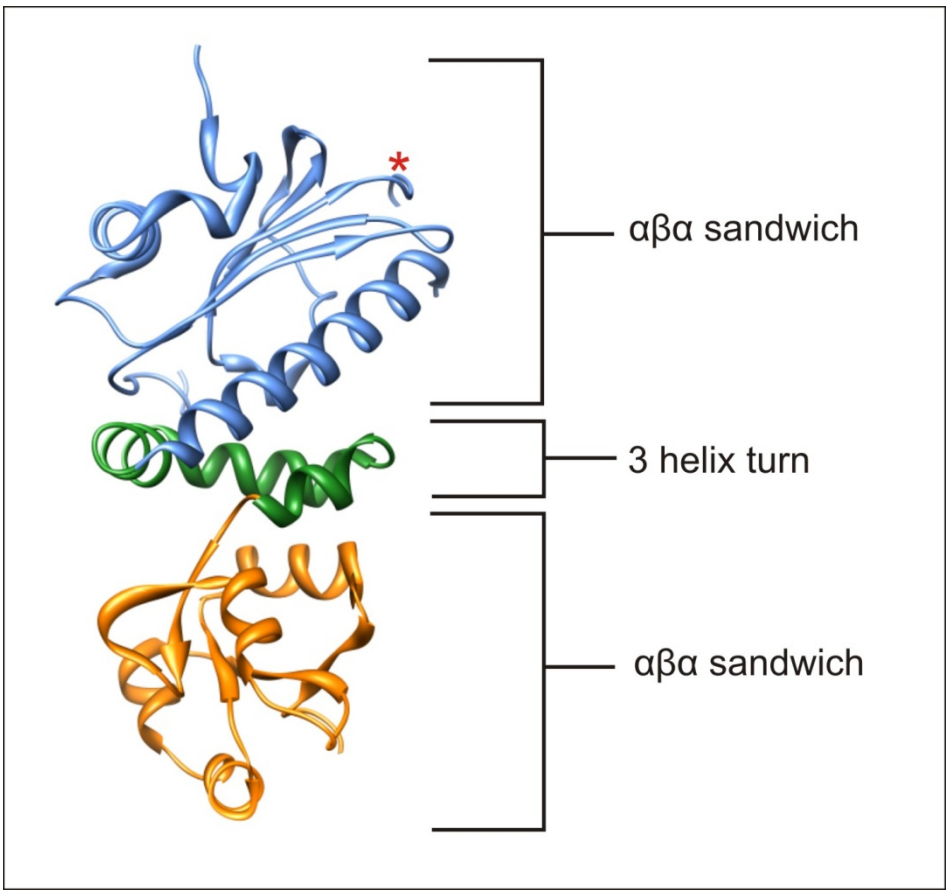

Figure 1.9 Crystal structure of the middle domain of Hsp90 highlighting the key three regions. The αβα sandwich followed by the three helix turn followed by the final αβα sandwich. The catalytic loop (approx. location of start of loop is starred) containing residue Arg380 is too flexible to be resolved in this crystal but is located in the first αβα sandwich. Diagram taken from the PDB file 1HK7.

It is known that in isolation the N-terminal domain of Hsp90 has a very low ATPase activity. Using the homology between MutL, GyrB and Hsp90 it was predicted that a catalytic residue was required from the middle domain to facilitate ATP hydrolysis within Hsp90. Conserved between Hsp90 and MutL and GyrB is a motif found on the tip of the middle domain loop: 377- N(L/I/V)SRExLQ -384. Three residues, Asn377, Arg380 and Gln384, are completely conserved in Hsp90 and capable of interacting with the γ phosphate of ATP. Mutational analysis revealed that two of these residues, (Arg380 and Gln384 – equivalent to Lys337 and Gln335 respectively in GyrB) showed severe retardation of ATPase activity when mutated [12]. The crystal structure shows that both Arg380 and Gln384 are in a position that is able to interact with the N-terminal domain and this interaction was later confirmed by the full-length structure [7] where Arg380 is pointing into the base of the binding pocket. The loop in which Arg380 sits is known as the 'catalytic loop'. H/D mass spectroscopy studies of the middle domain suggest that ligand binding influences the degree of secondary structure in the catalytic loop. The presence of the inhibitor DMAG (an inhibitor based upon geldanamycin) has a destabilising influence over any secondary structural elements within the catalytic loop, thus

leading to more proton exchange in this region. How this compares to a nucleotide bound state is unclear [37].

The long linker connecting the N-terminal and middle domains does not prevent domain association. Since Arg380 from the middle domain is required for hydrolysis, the stability of the interaction must be sufficient to allow this to occur. The surface of the middle domain, close to the N-terminal interaction site, contains a hydrophobic 'patch' centred on Phe349 and close to the catalytic loop already mentioned[12]. H/D exchange mass spectroscopy data also suggests interaction between the N-terminal and middle domains of Hsp90 centred on this hydrophobic patch[37]. This hydrophobic patch interacts with the hydrophobic surface exposed by ATP 'lid' closure on the N-terminal domain [7]. This interaction was disrupted by mutations in the middle domain hydrophobic patch [12]. Both Phe349Ala and Phe349Gln mutants showed a severe retardation of ATPase activity. This confirms that association between the N-terminal and middle domains of Hsp90 is required for full hydrolysis activity, in order to align the catalytic loop of the middle domain correctly with the nucleotide bound to the N-terminal domain [12].

The crystal structure reveals a hydrophobic patch on the inside face of the middle domain of Hsp90 with respect to the dimer arrangement. This region has been suggested as a potential client binding site due to the known association of Hsp90 to partially unfolded 'clients' exposing hydrophobic regions. The middle domain also contains an amphipathic loop with both a positively charged and a hydrophobic face. Mutation studies have established that this region is required for the association of the client PKB/Akt to Hsp90, but does not affect ATPase activity [12]. The co-chaperone Aha1 associates with the catalytic loop of the middle domain and mutations within this loop, such as Glu381Lys, lead to abolition of binding between Aha1 and Hsp90 without inhibition of the ATPase activity of the chaperone [12].

1.6.4 Structure of the C-terminal domain

The role of the C-terminal domain is to both maintain dimerisation and provide binding sites for various co-chaperones and client proteins. The C-terminal domain runs from residues 551 to the end and contains both a coiled-coil region, responsible for dimerisation, and a 'MEEVD' TPR domain binding motif at the extreme C-terminus that is involved in interaction with some co-chaperone and client proteins which contain TPR domains. The structure of the isolated C-terminal domain has been solved for the bacterial HtpG homologue to a resolution of 2.6Å [11], while the structure of the yeast homologue shows most, but not all, of the C-terminal domain in the full length structure already [7].

Both structures agree that the C-terminal domain comprises of a short α-helix followed by a three strand anti-parallel β-sheet, within which is a loop region and a short helix involved in co-chaperone/client interactions. Beyond the β-sheet are three more helices, with the final two forming the dimerisation coiled-coil interface [11]. However, major differences between the two crystal structures can also be observed. The full length crystal shows a helix-strand protrusion from the C-terminal domain that reaches towards the N-terminal domain and which interacts with its equivalent structure from the opposite dimer. In the HtpG structure this protrusion is orientated significantly differently to the yeast homologue.

Constitutive dimerisation via the C-terminal domain of Hsp90 allows the chaperone to maintain a high local concentration of the N-terminal domain since the two N-terminal domains will be tethered close enough to one another to facilitate their interaction. Constitutive dimerisation also provides the correct alignment of each N-terminal domain to facilitate transient dimerisation during the chaperone cycle, despite the low affinity for self-interaction of the N-terminal domain in isolation. As previously mentioned this transient dimerisation is critical for full ATPase activity.

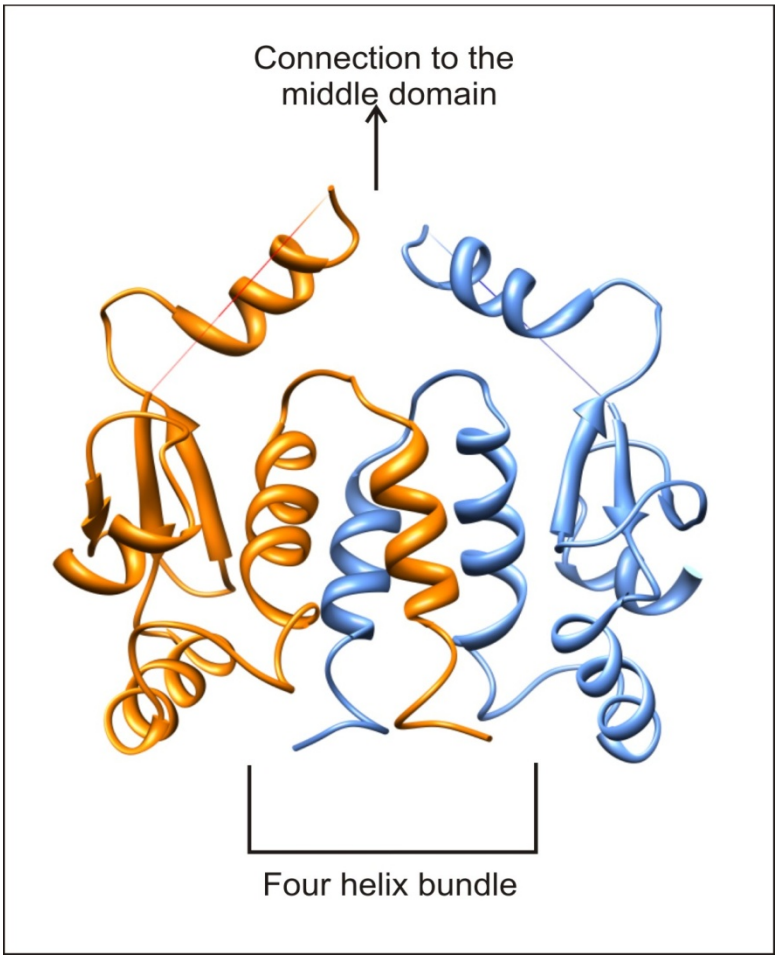

Figure 1.10 Ribbon representation of the crystal structure of the yeast C-terminal domain of Hsp90 showing the four helix bundle dimerisation site [7]. Diagram taken from PDB file 2CG9.

The constitutive dimerisation interface predominantly comprises of two helices from the C-terminal domain of each monomer, these four helices associate in a 4-helix bundle [11] (Figure 1.10). A third terminal helix provides some additional contact through two hydrophobic residues contacting the core four helix bundle (see Figure 1.10). The association of the monomers leads to the burial of a large quantity of hydrophobic surface area and as a result the dimerisation is highly favoured with a K_d of 60nM in the yeast homologue [13] and 24nM in the bacterial HtpG [11]. H/D mass spectroscopy reveals a single amide within the small β-sheet of the C-terminal domain that becomes completely inaccessible when radicicol is bound to the Hsp90 dimer although the identity of the amide is unclear. The interface between the middle domain and the C-terminal domain also becomes more protected in the inhibitor bound state, with three additional amide bonds protected in comparison to the apo-state. This suggests an overall more compact state under some ligand bound conditions [37]. The HtpG homologue of Hsp90 naturally lacks the C-terminal 'MEEVD' motif [11] and the structure of the yeast homologue is disordered in this region [7]. Structural alignment of the bacterial and yeast homologues however suggests that if the MEEVD sequence was present it would extend away from the dimer interface, accessible to the solvent and binding partners [11].

Studies in both human and yeast Hsp90 have suggested that one residue within the C-terminal domain has a significant influence over the chaperone's ATPase activity. This residue is located in the β-sheet of the C-terminal domain; in the human Hsp90 homologue this residue is Cys597, while in the yeast homologue it is Ala577 [39]. The S-nitrosylation of this residue in both homologues leads to a decrease in ATPase activity. Mutations in the yeast homologue of Ala577 to Cys or Ile enhance the inherent ATPase activity of the chaperone, while mutations to Asp or Asn reduce it[39]. Mutations of residues of surrounding Ala577 in both sequence and space had little or no effect on the chaperone ATPase activity[39]. Both mutations and S-nitrosylation of the key residue lead to a decrease in the ATPase activating co-chaperone Aha1 associated with Hsp90. FRET analysis of dimer formation and dissociation revealed that mutations of the key residue led to a change in dimer affinity. Mutations that enhanced the ATPase activity also enhanced the affinity of Hsp90 dimer formation and vice versa[39]. Both *in vivo* and *in vitro* observations showed that mutations that led to tighter C-terminal dimer formation also led to a stronger activation of client proteins. The mutations introduced that enhanced dimerisation, ATPase activity and client activation are also known to stabilise β-sheet structures while the destabilising mutants also destabilise β-sheets. Since it is known that the chaperone cycle of Hsp90 is dynamic and relies upon an equilibrium between states, this mutation may well shift the equilibrium towards the 'open' state within the cycle. As the inhibitory mutations mimic S-nitrosylation, this perhaps indicates a reversible, post-translational regulation mechanism for the Hsp90 chaperone [39].

1.6.5 Inter and intra-molecular domain interactions of the Hsp90 dimer

Although the individual domains of Hsp90 have been studied in some depth, the interaction between the domains is key to understanding the chaperone function. The interplay between the domains and their response to both ligand binding and co-chaperone/client protein interaction is discussed here.

The idea of a 'ground state' has already been discussed, however the molecular details of the transition from this 'ground state' [4] to the first step in the chaperone cycle and from there on to the other known conformations of Hsp90 is still elusive, but clearly involves domain rearrangement. Electron microscopy (EM) data for the apo state full length mammalian Hsp90 show two distinct conformations of the dimer with a distribution of 90% to 10% in each form respectively. The first is an elongated so called 'flying seagull' structure, estimated to be 195 Å x 90 Å using SAXS (small angle x-ray scattering) data where the C-terminal domains are joined and the N-terminal domains point in opposite directions. The second distinct shape is a more compact 'v' shape, not detected in the SAXS experiments [40] but visible in the EM study. This 'v' shape conformer shows a similar C-terminal domain arrangement to the more open 'flying seagull', however the N-terminal domains are orientated differently – both closer to one another and facing in the same direction [40]. A transition between the forms would require two rotations, one of 30° and one of 80° in orthogonal directions around the dimer's symmetry axis [40]. The 'v' shaped structure may represent a transition state from the open to the closed conformation of the Hsp90 chaperone cycle, while the extended 'flying seagull' may show the extended 'ground state' suggested by Dollins et al. [4].

The only crystal of the full length Hsp90 dimer was solved using the yeast homologue by Ali et al. [7] and shows the chaperone with transiently dimerised N-terminal domains facing each other with the remainder of the protein in a non-compact state. Hsp90 was crystallised in the presence of the non-hydrolysable ATP analogue AMPPNP, and the co-chaperone p23/Sba1 which is a known inhibitor of the ATPase activity [20]. The 3.1Å resolution crystal structure [7] shows a dimer of the full length Hsp90 with two copies of p23/Sba1, symmetrically bound on either side of the dimer at the N-terminal end of Hsp90.

The overall architecture of the dimer confirms a parallel arrangement with a left-handed twist about the central longitudinal axis of the chaperone. An amphipathic loop from the middle domain (residues 329 – 339) is observed projecting from the inner face of the monomer towards its dimerisation partner[7]. The C-terminal domain and the middle domain

of each Hsp90 monomer are linked by an extended loop. The MEEVD sequence at the very C-terminal of Hsp90 is disordered in this crystal and cannot be seen, although its importance has already been mentioned [7].

Differing from the middle domain/C-terminal domain crystal structure[4], the interface between the middle and C-terminal domains in full-length Hsp90, shows an additional 'flexing' in the presence of ATP. This 'flexing' of the chaperone results in the middle domains of each dimer moving 10 Å closer together at the C-terminal end and 20 Å closer at the N-terminal end. This movement then leads to a displacement and induction of disorder of the C-terminal protrusion previously described. Several temperature sensitive mutations can be traced back to this region, showing its significance.

The full-length crystal structure [7] also shows important detail concerning the N-terminal /middle domain interface. In the yeast homologue, residues Thr22, Val23 and Tyr24 on the N-terminal domain form a hydrophobic interaction with residues Leu376 and Leu378 from the catalytic loop of the middle domain. The interaction of the leucine residues suggests that the N-terminal and middle domain interactions aid in the positioning of the catalytic residue (Arg380) when ATP, or a suitable analogue, is bound. Another key interaction between the two domains of Hsp90 is the packing of Phe200 from the N-terminal domain into a pocket formed by the middle domain residues Thr273, Pro275, Trp277, Phe292 and Tyr344.

Perhaps the most dramatic change in conformation upon AMPPNP binding is the dimerisation of the two N-terminal domains of Hsp90 (Figure 1.11). The crystal structure provides some explanation for the results of mutational analysis of the N-terminal strand discussed earlier.

The N-terminal β-strand (residues 1 – 9) moves out from the main body of the domain and exchanges with its equivalent structure in the dimer partner. The strand then associates with the β-sheet of the other N-terminal domain. This 'strand swap' is also associated with a movement of the first α-helix from residues 13 – 22 to allow the initial strand movement. This strand swap stabilises the transient N-terminal dimerisation and thus the ATPase competent state. Removal of this helix would destabilise this state and lead to a decrease in the ATPase activity, thus explaining the mutational observations of the same[38].

The other significant conformational change within the N-terminal domain is the closing of the ATP 'lid' region (residues 94 – 125) over the ATP binding pocket. This 'lid' movement results in the exposure of two hydrophobic patches, one around Leu 15 and Leu 18 and the other on the back of the lid involving residues 95-97 and Phe120. These exposed regions form hydrophobic contacts with their partner areas on the other half of the

dimer[7;23]. This association leads to the burial of exposed hydrophobic surface area, which in turn leads to the stabilisation of the transient N-terminal dimerisation of Hsp90.

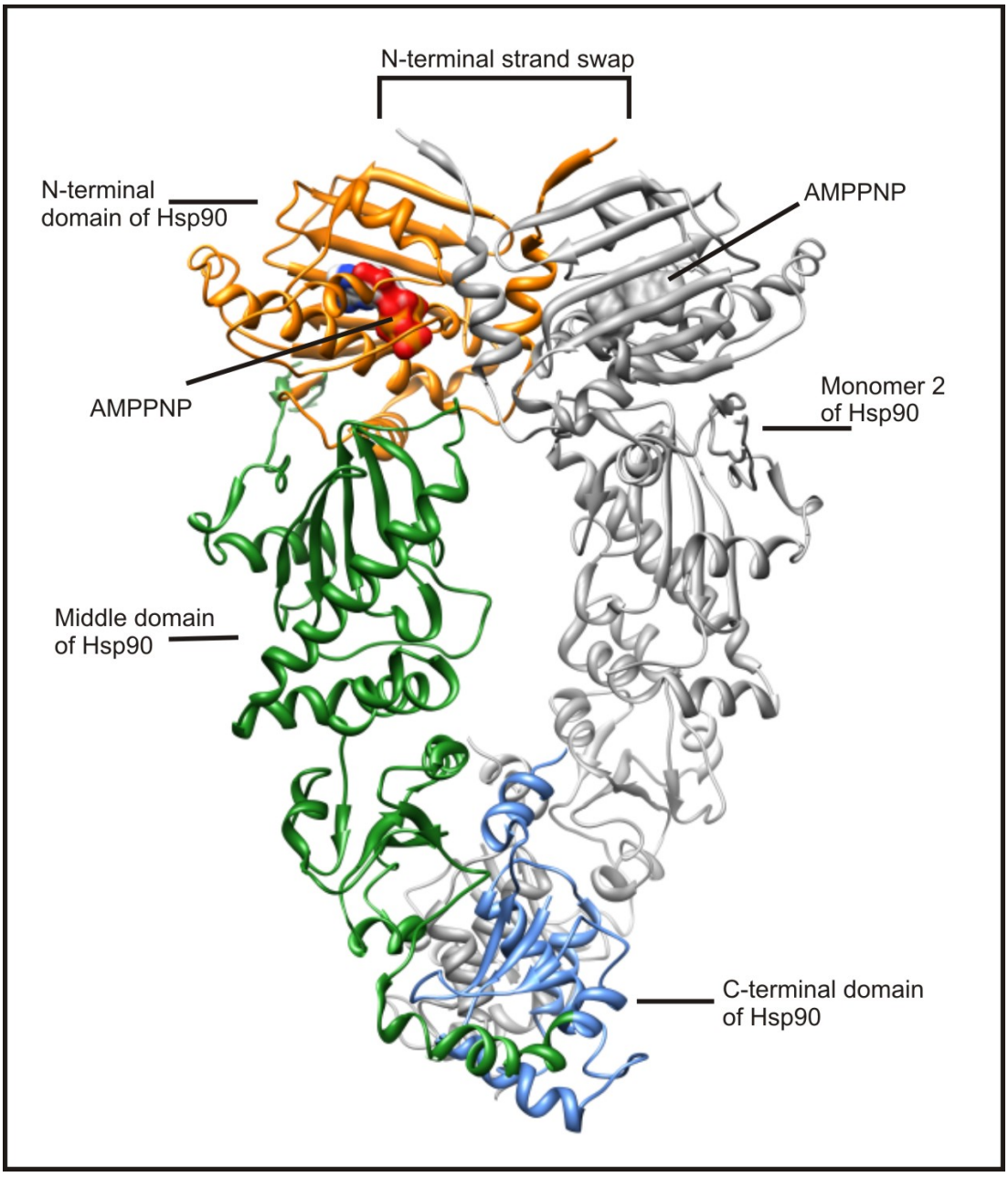

Figure 1.11 Crystal structure of the closed Hsp90 dimer bound to AMPPNP[7]. On one monomer the domains are highlighted in orange (N-terminal domain), green (Middle domain) and blue (C-terminal domain). PDB file 2CG9 was used for this diagram.

The full length crystal structure [7] in the presence of AMPPNP and p23/Sba1 reveals elements of the overall arrangement of the Hsp90 dimer that are not evident from the individual domains alone. Crystal structures such as those mentioned above [4;7;8;12] give some insight into the chaperone cycle under different ligand-bound conditions. The many

subtle differences identified between the structures however highlights the importance of understanding the entire chaperone cycle in order to understand the complex interplay between ligand binding, hydrolysis, co-chaperone influence and ultimately Hsp90's effect on its 'clients'.

1.7 The influence of co-chaperones on Hsp90

Co-chaperones are proteins that associate with the Hsp90 chaperone molecule and either enable the recruitment of client proteins, alter the functionality of Hsp90 or facilitate specific client protein activation. Binding of a co-chaperone to the N-terminal, middle or C-terminal domains of Hsp90 are all possible and the location of the binding site often, but not always, corresponds to the function of the co-chaperone. Those that bind on or close to the N-terminal domain of Hsp90 tend to influence the ATPase activity of the chaperone, while those that bind on or near the C-terminal domain are more likely to be involved in client protein recruitment or activation. Binding of a co-chaperone to the middle domain of Hsp90 may indicate a role in either modification of the ATPase activity or client interaction [3].

One class of Hsp90 co-chaperones are those that contain a TPR (tetratricopeptide repeat) domain that can associate with the TPR binding motif found at the extreme C-terminal end of the C-terminal domain. This short peptide sequence – MEEVD – is found on a highly flexible region in the final 35 amino acids of the protein and is not visible on the crystal structure of the full length Hsp90 [7]. Not all TPR domain-containing proteins are necessarily co-chaperones of Hsp90, nor do all co-chaperones containing TPR domains bind via that domain. For example the co-chaperone Stg1 does not require its TPR domain to associate with Hsp90 [3].

Of those co-chaperones that do associate to Hsp90 via their TPR domains, this is often the only link between them. The protein WISp39 is involved in client recruitment, while Sti1 is involved in recruitment of other co-chaperones. Other TPR domain-containing proteins have an active role such as protein phosphatase 5 (PP5), which is a Ser/Thr protein phosphatase or CHIP, which is an E3/E4-ubiquitin ligase [3].

Another class of Hsp90 co-chaperones are those that influence the ATPase activity of the chaperone. These co-chaperones tend to bind to the N-terminal or N-terminal and middle domains of Hsp90 close to the ATP-binding site, but even here their influence is not always limited to nucleotide binding and hydrolysis. It is known that p23, Sti1 and Cdc37 all inhibit the

ATPase activity of Hsp90, however the latter two proteins are also thought to be involved in client protein recruitment. Sti1 is also different to the other two co-chaperones in that it affects the ATPase activity of the chaperone despite binding to it at the opposite end of the protein to the nucleotide binding site. It is thought that it may stabilise Hsp90 in a conformation that does not support ATPase activity, but this is not fully confirmed [32]. In contrast the co-chaperone Aha1 is known to enhance ATPase activity within Hsp90 [3] binding to the N-terminal and middle domains, while Cpr6 enhances ATPase activity by displacing Sti1 bound to the TPR domain binding motif.

1.7.1 Sba1/p23

The co-chaperone p23 is known to bind preferentially to the N-terminal domain of Hsp90 in the ATP bound state and plays a role in inhibiting ATPase activity [7]. NMR analysis of p23's association with *Gallus gallus* Hsp90 showed significant peak broadening upon the co-chaperone, indicating binding to a larger partner, namely the Hsp90 dimer, but only in the presence of ATP [14] and it was later found that the co-chaperone p23 does bind to the apo-Hsp90 molecule, but with a 70-fold weaker affinity than the AMPPNP bound form [20]. The binding affinity of p23 to Hsp90 is also known to be reduced when mutations that destabilise the transient N-terminal dimerisation of Hsp90 are used. From the binding studies between p23 and Hsp90 it can be observed that association of co-chaperone to chaperone requires the dimerisation of the N-terminal domains of Hsp90, and is not simply due to the binding of ATP. However, since the ATP bound state of Hsp90 favours N-terminal dimerisation, often higher affinity binding of p23 to the chaperone is be seen in the presence of ATP [20].

The full length crystal structure solved by Ali et al. [7] shows two p23 molecules associated with the Hsp90 dimer in a symmetrical fashion [7]. The reason for the decrease in affinity between P23 and Hsp90 in the absence of dimerisation is evident from the structure; p23 binds partially to both N-terminal domains within the Hsp90 dimer (Figure 1.12). Thus any effect that decreases the likelihood of transient N-terminal dimerisation, be that mutation or lack of nucleotide, will lead to a decreased binding affinity for p23.

The crystal structure [7] (see Figure 1.12) also shows contacts between p23 and the middle domain of Hsp90. NMR also reveals chemical shift changes within the middle domain of Hsp90 upon binding of p23 [14]. One possible consequence of this localised association is that the binding of p23 to Hsp90 prevents rearrangement of the middle domain catalytic loop. Thus the catalytic Arg380 residue cannot be aligned with the terminal phosphate of the bound

nucleotide, leading to the inhibition of ATPase activity until p23 dissociates or is displaced by another co-chaperone such as Aha1 [14].

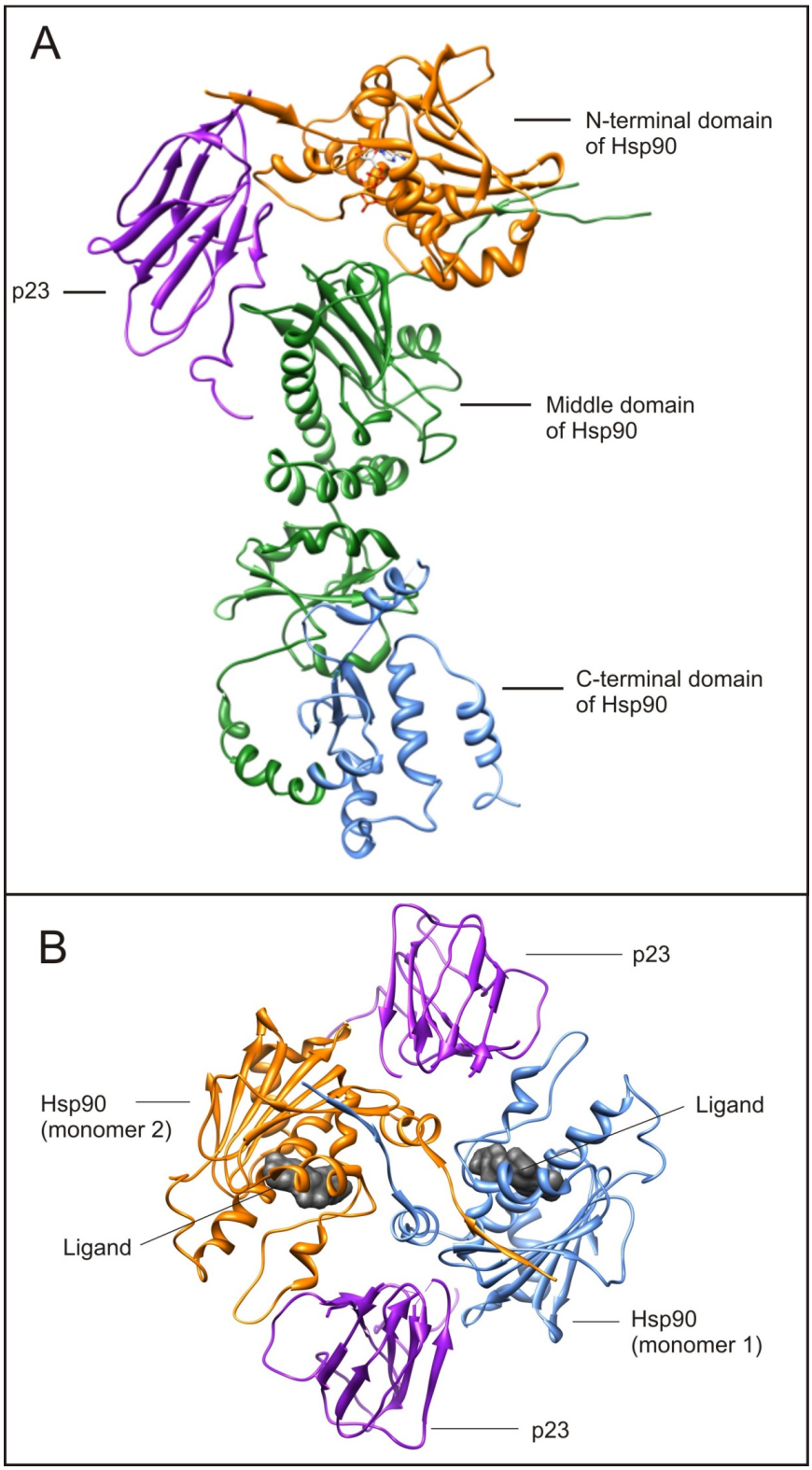

Figure 1.12 The crystal structure of Hsp90 with p23 reveals contacts between p23 and both the N-terminal and middle domains of the chaperone molecule. A: Side view shows contacts to N-terminal and middle domains. B: Top view shows contacts to the N-terminal domains of both monomers of Hsp90 PDB file 2CG9 used for this diagram.

1.7.2 Aha1

In contrast to p23, Aha1 is known to be an activator of Hsp90 ATPase activity [34]. Crystal structures and biochemical studies [41] have shown that Aha1 binds predominantly to the middle domain of Hsp90 (see Figure 1.13), however ITC has revealed that full binding affinity is only achieved in the presence of the full length protein [41]. The crystal structure shows that Aha1 and the middle domain of Hsp90 associate in a parallel fashion [41]. The affinity for Aha1 to the wild type Hsp90 dimer is 0.67µM as determined by ITC [20].

The importance of the ATP 'lid' in the chaperone cycle has already been established [6-8;10]. The position of the ATP 'lid' in Hsp90 can be influenced by particular Hsp90 mutations [23]. These ' lid-altering' mutations of Hsp90 were used in concert with Aha1/Hsp90 studies to ascertain the influence of Aha1 on role of the lid in the chaperone cycle. It was observed that these mutations did not alter the affinity of Aha1 for Hsp90 [20]. The difference in Aha1's influence over the ATPase activity between the wild type Hsp90 and the mutated Hsp90 molecules were minimal, suggesting that Aha1 acts upon the ATPase cycle at a point following closure of the lid, where the mutations no longer influence the cycle [20].

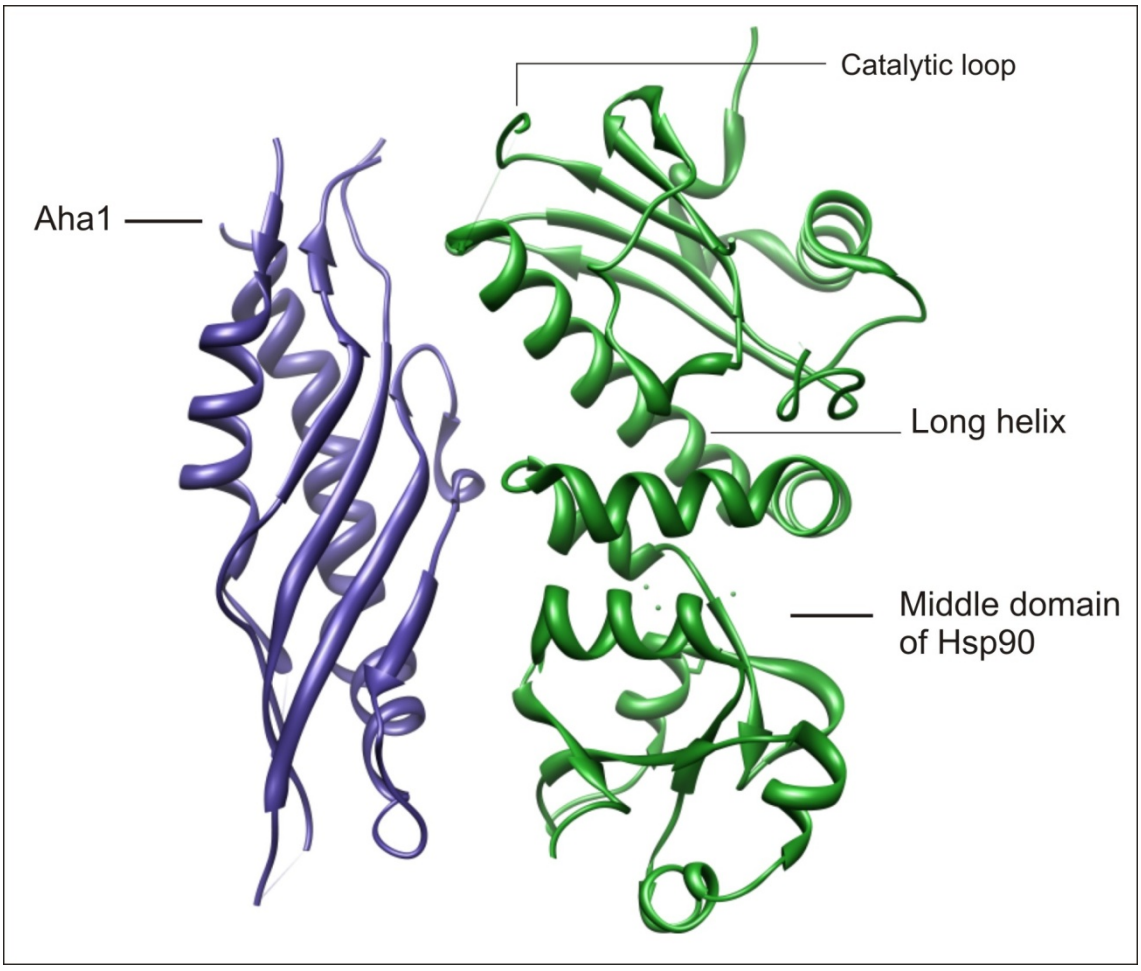

Figure 1.13 Crystal structure showing that association between Aha1 and Hsp90 is limited to the middle domain of Hsp90.

The association of Aha1 with the middle domain of Hsp90 is thought to aid positioning of the catalytic Arg380 residue for efficient hydrolysis of ATP. A reorganisation and extension of the long helix within the middle domain is observed upon binding of Aha1 to Hsp90. This helix extension leads to the movement of the catalytic loop (containing Arg380) away from an interaction with Glu353 and Glu355 of Hsp90 and to instead rotate and orientate it towards the γ phosphate within the ATP binding site in the N-terminal domain [41]. Mutations in Hsp90 which alter the interaction between Aha1 and the catalytic loop of the middle domain affect Aha1's ability to enhance the ATPase activity of Hsp90. The change in activation ability does not always correspond to the binding affinity of Aha1 for Hsp90, showing that association and activation are not coupled [41]. Aha1 has a profound influence on the yeast Hsp90 mutation E381K, designed to interrupt the association of the N-terminal and middle domains of Hsp90. This mutation alone prevents positioning of the catalytic loop of Hsp90 thus inhibiting the ATPase activity. The presence of Aha1 effectively reverses the effect of the mutation allowing ATP hydrolysis, and thus suggesting that Aha1 plays a role in formation of the active conformation involving the positioning of the middle domain catalytic loop [20].

1.7.3 Cdc37

The Hsp90 co-chaperone Cdc37 mediates the interaction between Hsp90 and many protein kinases that are known clients of Hsp90. Cdc37 is known to inhibit the ATPase activity of Hsp90 through direct interaction with the N-terminal domain of the chaperone, preventing ATP lid closure and N-terminal association [42]. NMR chemical shift analysis on the human complex of Hsp90 and Cdc37 confirmed two main areas of contact between the two proteins. Flanking a hydrophobic patch on human Hsp90, two charged regions within two α helices (residues 113-120 and residues 123-134) were identified [18]. The Hsp90/Cdc37 orientations correspond well with the known crystal structure of the complex using the yeast homologue of Hsp90 and the human homologue of Cdc37 [42] although the interface implied by NMR is larger.

H/D exchange mass spectroscopy of the full length Hsp90 chaperone in the presence of Cdc37 showed a degree of protection from proton exchange expected given the crystal structure, where protein/protein interactions lead to the shielding of some regions of the Hsp90 N-terminal domain from the solvent. However, some unexpected results were also seen. Specifically the binding of Cdc37 over the lid region of the N-terminal domain of Hsp90 is reflected by an expected dramatic decrease in exchange at the tip of the lid in the presence of

the co-chaperone [37]. More unexpected is the reduction in exchange across the most C-terminal strand of the β-sheet region of the Hsp90 N-terminal domain [37]. There is also some indication of increased protection in the middle domain/N-terminal domain interface in the presence of Cdc37. The H/D exchange data seen by Phillips et al. [37] matches that observed for the radicicol and DMAG bound states in the absence of Cdc37. Here the domain interface was also stabilised and a more 'compact' dimer form assumed for Hsp90 [37]. The H/D protection and stabilisation at the domain interface observed could represent a rotation of the N-terminal domain with respect to the middle domain to accommodate the co-chaperone binding. The similarity of the exchange data seen for Cdc37 binding, and for the inhibitor bound complex, suggests that ligand binding and Cdc37 binding may be cooperative [37].

1.7.4 Hop/Sti1

The binding of the co-chaperone Sti1 was first identified by Chang et al. [1] in 1994 by affinity purification using immobilised yeast Hsp90. Sti1 is strongly associated with Hsp90 and is known to be an inhibitor of the chaperone ATPase activity, despite it binding away from the nucleotide binding site [1]. It is known to bind to Hsp90 in a 1:1 stoichiometry as determined by ITC and this is likely to represent the binding of a dimer to a dimer with an affinity of approximately 0.24μM [1]. Later studies showed that independently viable mutations in both Sti1 and yeast Hsp90 were lethal when expressed together, confirming a clear connection between the two [43]. Co-precipitation studies and pull down analysis confirms that Sti1 is found in complex with Hsp90, but while a number of other co-chaperones including Hsp70 are seen in these pulldowns , they do not associate directly with Sti1. Sti1 is also not observed in complexes with clients of Hsp90. This suggests that the maturation of Hsp90 chaperone client proteins requires a number of chaperone complexes of which Sti1 is involved in some, but not all, in a transient fashion [43].

Hsp90 has long been associated with the chaperone Hsp70. In these cases Hsp70 is thought to facilitate the folding of client proteins before interaction with Hsp90 leads to their activation [3]. Sti1 is also often found in these complexes and is thought to hold together the Hsp90/Hsp70 chaperone complex. However some studies suggest that the presence of Sti1 is not required for the recruitment of Hsp70, indeed it is seen that Sti1 knock outs do not lead to the unfolding of protein due to a lack of an Hsp90/Hsp70 complex. This may indicate a transient role for Sti1 or may suggest another role entirely.

In addition to inhibiting the ATPase activity of Hs90, Sti1 has also been linked to the activation of known Hsp90 client proteins. When mutations of Sti1 were used *in vivo*, the activation of the glucocorticoid receptor was reduced although accumulation of the receptor was not. Glucocorticoid receptor activity could then be rescued by introduction of active Sti1 protein [43]. A similar effect was seen with respect to other Hsp90 clients such as the v-Src kinase [43]. Over-expression of Sti1 in a yeast strain containing an inactive Hsp90 gene led to the accumulation of the Hsp90 clients, but did not lead to activation of these proteins, showing that Sti1 was necessary but not sufficient for client protein activation [43].

1.8 The chaperone cycle of Hsp90

Understanding the chaperone cycle is vital for understanding the functionality of Hsp90. The chaperone cycle has been studied using three methods – electron microscopy (EM), bulk FRET analysis and single particle FRET analysis. EM allows the direct observation of molecular arrangement albeit at a lower resolution than a crystal structure. The advantage of EM, however, is that a uniform population is not required and thus different conformations of the protein can be observed at the same time. In a system such as Hsp90 where progress through the chaperone cycle is based upon shifting equilibrium, the facility to look at mixed populations is very important.

1.8.1 The chaperone cycle by electron microscopy

The use of negative stain electron microscopy (EM) to monitor the chaperone cycle of bacterial Hsp90 and its response to nucleotide revealed three distinctly different gross conformations of the Hsp90 dimer in the apo-, ADP- and AMPPNP-bound states [6].

In the absence of ligand a flexible 'V' conformation is observed with varying degrees of openness. The EM data can be combined with data from a crystal structure of the full length apo form of bacterial Hsp90 [6]. Using this approach, the three domains of the chaperone can be clearly identified in the EM structure, confirming that the C-terminal domains form the dimerisation region with the N-terminal and middle domains extending out from the C-terminal domain. The degree to which the dimer is 'open' is thought to be attributed to the rigid body movements of the two monomers with a large degree of flexibility at the C-terminal

domain. This variability in openness fits with the 'ground state' described by Dollins et al. [4] and the presence of two 'open' conformations seen by Bron et al. [40] referred to previously as the 'flying seagull' and the 'v' forms. Detail from the apo-state seen by Shaiu et al. [6] also shows residues Phe123 and Gln122 extending into the ligand binding site. This positioning would be displaced by ATP binding and could drive conformational changes of the lid [6].

Distinct 'closed' conformations were observed for ADP and AMPPNP-bound Hsp90. The AMPPNP bound Hsp90 dimer as seen by EM has both a similar size and shape to the yeast Hsp90 crystal structure solved by Ali et al. [7]. This may suggest that the bacterial Hsp90 can achieve the same conformation as the yeast homologue in the absence of co-chaperones.

In the presence of ADP a third conformation of bacterial Hsp90 is seen with a more compact form than observed in the AMPPNP bound state [6]. Dramatic changes in both inter-domain and inter-subunit interactions are observed in both compact forms compared to the apo state. A discrepancy between the EM data and the crystal structure solved by Shiau et al. [6] of the ADP compact state was explained as a crystallographic artefact resulting in a misalignment of the N-terminal domains of the Hsp90 dimer. An *in silico* rearrangement of the N-terminal domains with respect to the arrangement of the middle and C-terminal domains, assuming a flexible linker between them, leads to a form that is consistent with the EM data.

1.8.2 The chaperone cycle by FRET analysis

A study by Hessling et al. [5] used mutations of the yeast Hsp90 molecular chaperone designed to allow the attachment of a fluorescent tag to various specific locations. Subsequent monitoring by Fluorescence Resonance Energy Transfer (FRET) between two labelled molecules could then occur. Two positions, Asp61 in the N-terminal domain and Gln333 in the middle domain, were mutated to Cys residues to allow tag binding. These positions were chosen for their surface accessibility and low probability that they would affect the activity of Hsp90. The neutrality of the mutations was confirmed through the creation of a double mutant which was found to complement the essential function of yeast Hsp90 in a knockout strain [5].

Single mutants were purified and labelled with either donor or acceptor fluorescent tags. The two populations were then mixed to allow the formation of heterodimers. The FRET signal generated by the proximity of the two tags within the heterodimers was then used to monitor the distance between the two monomers under various ligand bound conditions. The

heterodimer combinations possible with two mutants and two tags allowed monitoring of both inter- and intra-monomer distances. The change in FRET intensity across the chaperone cycle allowed the calculation of the number of discrete steps within the cycle as well as the rate constants for the transition between each step (see Figure 1.14).

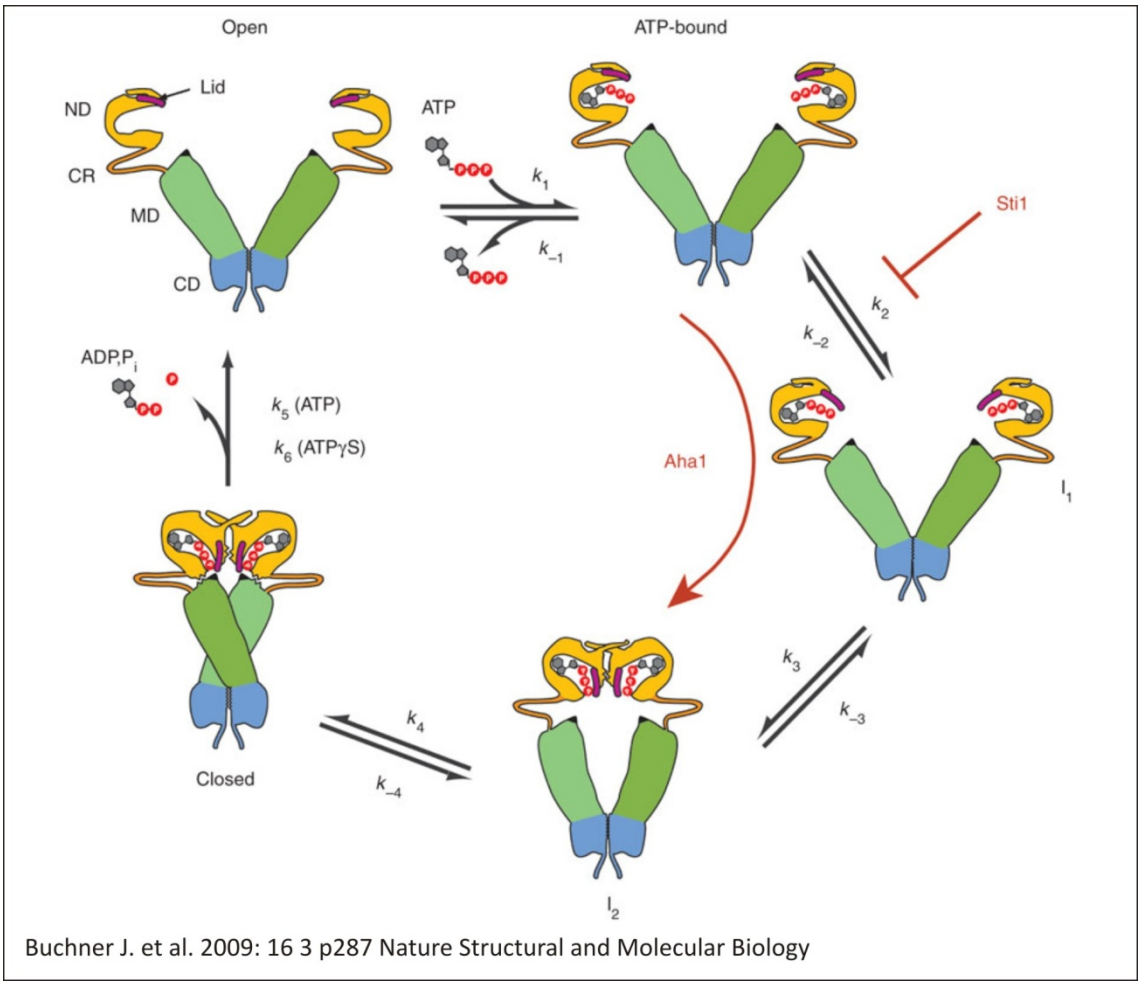

Figure 1.14 The proposed states of the five step chaperone cycle as determined using fluorescence studies by Buchner et al.[5].

The slowest rate detected had a similar k_{cat} to the known ATPase activity of Hsp90, suggesting that hydrolysis is the rate limiting step of the cycle. A five step cycle was shown by global fitting to be in good agreement with the experimental data collected. A global fit to three or four steps did not produce a good fit in comparison. Using a series of truncation mutations of Hsp90, the absence of the lid was seen to enhance the rate of the cycle, while the excision of the entire N-terminal domain from one monomer led to a very different profile where only the initial FRET signal decrease is observed for the first step of the cycle and all subsequent slow changes are not detected. This suggests, in keeping with previous data, that transient N-terminal domain dimerisation is required for the full active cycle, and that part of

that cycle includes the association of the N-terminal and middle domains within a single monomer [5].

The five stages of the cycle begin with the open conformation of Hsp90 with no ligand bound. The first transition is induced by the binding of ATP to the ligand binding site in the N-terminal domain. The second transition is observed by the FRET analysis but there is no evidence for a structural change from other sources. A movement of the ATP lid from the 'open' to the 'closed' state could be the root cause of this detected step. The third transition leads to an association of the two N-terminal domains within the Hsp90 dimer. The fourth transition leads to an association of the N-terminal and middle domains of each monomer, which again can be observed by FRET. The rate constant for the reverse transition is far slower than the rate of ATP hydrolysis, preventing the back reaction from occurring. ATP hydrolysis itself characterises the final transition from the fully closed state to the open state. Within this transition is encompassed the release of ADP and free phosphate. Any further distinct conformations were intractable to the FRET methodology seen by Hessling et al.[5].

ATP hydrolysis is relatively late in the cycle with four previous steps concerning the binding of ATP and the conformational changes associated with that prior to hydrolysis to ADP. The 'closed' state of the Hsp90 dimer does not persist for long, as it occurs following hydrolysis until the dissociation of ADP and the free phosphate very shortly after. It is known, however, that the presence of various co-chaperones can influence the dwell time in certain positions along the cycle. Aha1 is known to accelerate the ATPase activity and from the FRET experiments can also be seen to accelerate the association of the N-terminal domains of Hsp90. This enhancement of this conformational step is observed even in the absence of ligand. In contrast Hop/Sti1 blocks all conformational changes [5].

1.8.3 The chaperone cycle by single particle FRET analysis

Observations of the Hsp90 chaperone cycle by single particle analysis allow the ATP cycle to be studied without the necessity for bulk averaging and synchronization of the system [9]. In the case of Hsp90, where it is clear that there is a complex multi-stage conformational cycle, the ability to de-convolute these steps is vital to the overall understanding of the process.

As was done for the bulk FRET study, single point mutations were made either in the N-terminal (D61C) or middle domain (E385C) of the yeast Hsp90 chaperone. These mutants

were then labelled with either a fluorescent donor or acceptor and dimerisation was measured by increasing FRET signal. The dimers were immobilised onto a surface via either biotinylation or a streptavidin tag [9].

In the absence of any ligand, this single molecule FRET (smFRET) showed an opening and closing of the dimer on a scale far faster than that of the ATPase cycle in the presence of ATP. This was repeated in the presence of the slow hydrolysing ATP analogue ATP-γS, ADP and AMPPNP [9]. By observing the duration of the 'open' and 'closed' states, a minimum kinetic model was calculated. There were no differences in state distribution between the apo- and the ADP-bound states. The introduction of AMPPNP led to an increase in the dwell time within the 'closed' conformation with no conformational fluctuations on a second timescale.

A fit of the data led to the conclusion that there were four detectable stages within the cycle – two in the open and two in the closed state. Of these four states only two crystal structures are known, one in each of the open and closed states. Overall Mickler et al. [9] concluded that occupation of the four states by Hsp90 was not ligand binding-dependent and that there was no strong coupling between hydrolysis and the conformational cycle. The binding and hydrolysis of ATP can increase the rate of transition from one state to another but the transition is itself reversible even though ATP hydrolysis is not [9]. The smFRET study did not reveal an ADP bound state and the authors hypothesise that such a state may be short lived and not highly populated [9].

Overall the single particle study showed similar behaviour to the bulk studies done previously [5]. Most evidence suggests that the nature of the chaperone cycle is one of equilibria between states rather than distinct and irreversible steps. The study of crystal structures or averaged EM images therefore show either a snapshot of one stage in the cycle or an average of the bulk behaviour, as biased by various external factors such as ligand binding and hydrolysis or co-chaperone association. When the action of the Hsp90 chaperone system is considered with regard to understanding client protein activation it is vital to remember that the process is one of equilibrium states and not distinct irreversible steps as understanding and possible future manipulation of an equilibrium system is very different to understanding and manipulation of a cycle of irreversible steps.

1.9 Summary

This thesis primarily focuses on the isolated N-terminal domain of Hsp90, exploring the thermodynamics of nucleotide based ligand binding in detail using ITC and observing the linkage between ligand binding and conformational change using both NMR and ITC. Some investigation into the influence of the full length protein molecule upon the chaperone cycle is also undertaken.

Overall this thesis attempts to provide answers regarding both the structure and the function of Hsp90. What is the nature of the ligand binding site and what are the conformational changes induced by ligand binding? In particular what is the response of the ATP 'lid' to the binding of different ligands? What is the influence of the middle domain and full length protein on this nucleotide binding, and how can this be related to its function as a molecular chaperone?

2 Materials and methods

The protein studied in this thesis is the yeast homologue Hsp82 of the Hsp90 chaperone protein. However throughout the thesis the protein shall be referred to as Hsp90 as is common in the literature.

All chemicals and reagents were purchased from Sigma-Aldrich, VWR or Melford unless otherwise stated. All liquid media were prepared using distilled deionised water. Media was sterilised by autoclaving at 123°C for 15 minutes or through filtration through a 0.22 µM filter.

2.1 Protein Constructs

Five constructs were studied: the N-terminal domain comprising amino acids 1 – 207; the N551 construct (residues 1 – 551) encompassing the N-terminal and middle domains; the full length protein (residues 1 – 667), the T22I mutant of the N-terminal domain (1 – 207) where residue Thr22 was mutated to Ile22; and the T101 mutant of the N-terminal domain (residues 1 – 207) where residue Thr101 was mutated to Ile101. All constructs were cloned into the NheI site of the pRSETA vector under a T7 promoter inducible with Isopropyl β-D-1-thiogalactopyranoside (IPTG). All constructs contained a hexa-histadine Tag. *E. coli* strains were used for all studies; *E. coli* BL21(DE3) cells were used for protein expression while *E. coli* XL1 Blue cells were used for plasmid amplification. All constructs were obtained from Dr. C. Prodromou of the Institute for Cancer Research.

Full Length protein:

The full length protein runs from residue 1 to 709 with the following sequence:

```
HHHHHHG
MASETFEFQAEITQLMSLIINTVYSNKEIFLRELISNASDALDKIRYKSL 50
SDPKQLETEPDLFIRITPKPEQKVLEIRDSGIGMTKAELINNLGTIAKSG 100
TKAFMEALSAGADVSMIGQFGVGFYSLFLVADRVQVISKSNDDEQYIWES 150
NAGGSFTVTLDEVNERIGRGTILRLFLKDDQLEYLEEKRIKEVIKRHSEF 200
VAYPIQLVVTKEVEKEVPIPEEEKKDEEKKDEEKKDEDDKKPKLEEVDEE 250
```

EEKKPKTKKVKEEVQEIEELNKTKPLWTRNPSDITQEEYNAFYKSISNDW 300
EDPLYVKHFSVEGQLEFRAILFIPKRAPFDLFESKKKKNNIKLYVRRVFI 350
TDEAEDLIPEWLSFVKGVVDSEDLPLNLSREMLQQNKIMKVIRKNIVKKL 400
IEAFNEIAEDSEQFEKFYSAFSKNIKLGVHEDTQNRAALAKLLRYNSTKS 450
VDELTSLTDYVTRMPEHQKNIYYITGESLKAVEKSPFLDALKAKNFEVLF 500
LTDPIDEYAFTQLKEFEGKTLVDITKDFELEETDEEKAEREKEIKEYEPL 550
TKALKEILGDQVEKVVVSYKLLDAPAAIRTGQFGWSANMERIMKAQALRD 600
SSMSSYMSSKKTFEISPKSPIIKELKKRVDEGGAQDKTVKDLTKLLYETA 650
LLTSGFSLDEPTSFASRINRLISLGLNIDEDEETETAPEASTAAPVEEVP 700
ADTEMEEVD

N Terminal domain:

The N-terminal domain construct runs from residue 1 to 207 with the following sequence:

HHHHHHG
MASETFEFQAEITQLMSLIINTVYSNKEIFLRELISNASDALDKIRYKSL 50
SDPKQLETEPDLFIRITPKPEQKVLEIRDSGIGMTKAELINNLGTIAKSG 100
TKAFMEALSAGADVSMIGQFGVGFYSLFLVADRVQVISKSNDDEQYIWES 150
NAGGSFTVTLDEVNERIGRGTILRLFLKDDQLEYLEEKRIKEVIKRHSEF 200
VAYPIQL

N551 Construct:

The N551 construct runs from residue 1 to 551 with the following sequence:

HHHHHHG
MASETFEFQAEITQLMSLIINTVYSNKEIFLRELISNASDALDKIRYKSL 50
SDPKQLETEPDLFIRITPKPEQKVLEIRDSGIGMTKAELINNLGTIAKSG 100
TKAFMEALSAGADVSMIGQFGVGFYSLFLVADRVQVISKSNDDEQYIWES 150
NAGGSFTVTLDEVNERIGRGTILRLFLKDDQLEYLEEKRIKEVIKRHSEF 200
VAYPIQLVVTKEVEKEVPIPEEEKKDEEKKDEEKKDEDDKKPKLEEVDEE 250
EEKKPKTKKVKEEVQEIEELNKTKPLWTRNPSDITQEEYNAFYKSISNDW 300
EDPLYVKHFSVEGQLEFRAILFIPKRAPFDLFESKKKKNNIKLYVRRVFI 350
TDEAEDLIPEWLSFVKGVVDSEDLPLNLSREMLQQNKIMKVIRKNIVKKL 400
IEAFNEIAEDSEQFEKFYSAFSKNIKLGVHEDTQNRAALAKLLRYNSTKS 450
VDELTSLTDYVTRMPEHQKNIYYITGESLKAVEKSPFLDALKAKNFEVLF 500
LTDPIDEYAFTQLKEFEGKTLVDITKDFELEETDEEKAEREKEIKEYEPL 550
T

T22I – N Terminal domain mutant:

The T22I N-terminal domain mutant construct runs from residue 1 to 207 with the following sequence:

HHHHHHG
MASETFEFQAEITQLMSLIIN**I**VYSNKEIFLRELISNASDALDKIRYKSL 50
SDPKQLETEPDLFIRITPKPEQKVLEIRDSGIGMTKAELINNLGTIAKSG 100
TKAFMEALSAGADVSMIGQFGVGFYSLFLVADRVQVISKSNDDEQYIWES 150
NAGGSFTVTLDEVNERIGRGTILRLFLKDDQLEYLEEKRIKEVIKRHSEF 200
VAYPIQL

T101I – N Terminal domain mutant:

The T101I N-terminal domain mutant construct runs from residue 1 to 207 with the following sequence:

HHHHHHG
MASETFEFQAEITQLMSLIINTVYSNKEIFLRELISNASDALDKIRYKSL 50
SDPKQLETEPDLFIRITPKPEQKVLEIRDSGIGMTKAELINNLGTIAKSG 100
IKAFMEALSAGADVSMIGQFGVGFYSLFLVADRVQVISKSNDDEQYIWES 150
NAGGSFTVTLDEVNERIGRGTILRLFLKDDQLEYLEEKRIKEVIKRHSEF 200
VAYPIQL

2.2 Competent cells

A single colony of BL21(DE3), DH5α or XL1 Blue cells were introduced into 10 mL of Luria Bertani (LB) media and grown overnight at 37°C while shaking at 200 rpm. No antibiotic was used in the production of competent cells. 1ml of overnight culture was used to inoculate 100mL of LB, which was grown at 37°C while shaking at 200 rpm until an optical density (OD) of 0.45 was recorded at 600 nm.

The cells were then left on ice for 15 minutes before pelleting by centrifugation at 3-5000 rmp at 4°C for 15 minutes. The supernatant was discarded. The pellet was resuspended in 40ml of TFBI buffer (Table 2.1) and kept on ice for a further 30 minutes. The cells were then

pelleted at 3-5000 G at 4°C for 15 minutes and the supernatant again discarded. The pellet was resuspended in 4 mL TFBII buffer (Table 2.1). The cells were then aliquoted into 50 µl samples and frozen immediately at -80°C.

TFBI (filter sterile)	30 mM Potassium acetate, 100 mM Rubidium chloride, 10 mM Calcium chloride, 50 mM Magnesium chloride, 15% (v/v) Glycerol. pH 5.8 adjusted with acetic acid.
TFBII (filter sterile)	10 mM MOPS, 10 mM Rubidium chloride, 75 mM Calcium chloride, 15% (v/v) Glycerol. pH 6.5 adjusted with Sodium hydroxide.
Vitamin Stock x 1000	Per 100 mL distilled H_2O: 0.04 g Acetylcholine chloride, 0.05 g Folic acid, 0.05 g Pantothenic acid, 0.05 g Nicotinamide, 0.1 g Myo-inositol, 0.05 g Pyridoxal HCl, 0.05 g Thiamine HCl, 0.005 g Riboflavin, 0.1 g Biotin.
Mineral Sock x 5000	2 mM Na_2MoO_4, 2 mM H_3BO_3, 2 mM $CoCl_2$, 2 mM $CuCl_2$, 2 mM $NiCl_2$, 10 mM $ZnSO_4$, 10 mM $MnCl_2$, 50 mM $FeCl_3$ (dissolved in 1:100 dilution of conc. HCl)

Table 2.1 Summary of solutions required for making competent cells and for addition to minimal media

2.3 Growth media

All cells were grown using deionised distilled water (Elga), or deuterated water (Cambridge Isotope Laboratories, Cambridge MA). LB liquid media (10 g/L tryptone, 5 g/L yeast extract, 5 g/L NaCl) was sterilized by autoclaving[44]. Solid growth media was made up as LB with 15 g/L agar and sterilized by autoclaving. Solid media was poured into Petri dishes when

cooled but still liquid. If required, filter sterile carbenecillin (250 µg/mL) was added to both liquid and solid media[44].

Minimal media was used to express isotopically enriched proteins for Nuclear Magnetic Resonance (NMR). Growth was carried out in M9 media (11.36 g/L Na_2HPO_4, 2.7 g/L KH_2PO_4, 1 g/L $(NH_4)_2SO_4$, 0.5 g/L NaCl) For expression of ^{15}N labelled proteins $(^{15}NH4)_2SO_4$ (Cambridge Isotope Laboratories) was used in place of $(NH_4)_2SO_4$. The solution was adjusted to pH 7.4 and sterilized by autoclaving.

Sterile M9 media was supplemented with 2 mM $MgCl_2$ (from a 1 M autoclaved stock solution), 1 mL/L filter sterile x1000 vitamin stock (Table 2.1), 200 µL/L filter sterile mineral stock (Table 2.1), 3 g/L D-glucose and carbenecillin. For ^{13}C-labelled protein ^{13}C D-glucose (Cambridge Isotope Laboratories) was used in place of ^{12}C D-glucose. Minimal media was made using deionised distilled water when only nitrogen and/or carbon labelling was required. Minimal media was made using deuterated water when perdeuteration of the protein was also required.

2.4 Plasmid purification

One colony of XL1Blue *E. coli* was picked and used to inoculate 10ml LB with 250µg/ml carbenecillin. The culture was grown overnight at 37°C while shaking at 200rpm. The cells were harvested by centrifugation at 4000rpm for 15min at 4°C. The supernatant was discarded. The plasmid was then extracted from the pelleted cells using a Miniprep kit (Quiagen). The Miniprep kit lyses the cells and causes precipitation of the protein and membrane components of the cells while the nucleotides are solubilised. The precipitated portions are separated from the soluble components by centrifugation and the supernatant is loaded onto a Quiagen spin column. The resin in the column retains DNA while other solubilised components, such as free nucleotides and RNA, are washed through. The DNA is then eluted from the column by centrifugation in 50µl of deionised water. The purified plasmid was stored at -20°C.

2.5 *E. coli* transformations

2 µl of plasmid was incubated on ice with 50 µl of thawed competent cells (BL21(DE3), XL1Blue or DH5α) for 30 minutes. The cells were subjected to 45 s of heat shock at 42°C in a water bath. The cells were then returned to ice for a further 10 minutes. 1 mL of LB was added to the cells which were left at 37°C while shaking at 200 rpm for 1 hour. The cells were then centrifuged at 13,400 rpm for 2 minutes and the supernatant discarded. The pellet was re-suspended in 100 µl of fresh LB and streaked onto a carbenecillin agar plate. The plate was incubated at 37°C overnight[44].

2.6 Glycerol stocks

A single colony was picked from an agar plate and used to inoculate 10 mL of LB culture. The culture was grown overnight at 27°C while shaking at 200 rpm. 500 µl of cell culture was added to 500 µl of glycerol sterilized by autoclaving. The sample was thoroughly mixed in an eppendorf tube and stored at -80°C.

2.7 Protein expression

The same protocols were used for all constructs.

2.7.1 Small scale expression

Small scale expression was carried out in 20 mL of LB media. A single colony from transformed BL21(DE3) or DH5α cells plated on LB agar was used to inoculate a 5 mL culture of LB media containing 250 µg/L carbenecillin. The cells were grown overnight at 37°C shaking at 200 rpm. 200 µl of overnight growth was used to inoculate 20 mL of LB media. The culture was grown at 37°C while shaking at 200 rpm until an OD_{600} of 0.6 - 0.8 was reached. Protein expression was then induced by the addition of isopropyl-[β]-D-thiogalactopyranoside (IPTG) at a final concentration of 1 mM. The cells were left for one hour to allow protein expression before

being harvested by centrifugation at 4000 rpm at 4°C for 20 minutes. The supernatant was discarded and the pellets freeze thawed and resuspended in 250 µL lysis buffer (50 mM Tris, 100 mM NaCl, 10% glycerol, pH 8). The sample was lysed by sonication on ice (3 s burst with a 10 s cooling time repeated three times). The sample was then centrifuged in a 1.5 mL eppendorf at 13,200 rpm for 40 minutes. The supernatant was separated from the pellet and a gel sample was made from each to run on an SDS polyacrylamide gel to test for protein expression.

2.7.2 Large scale expression

A single colony from a plate of transformed BL21(DE3) or DH5α cells or 1 µL from a glycerol stock was used to inoculate 100 mL of LB media. The culture was grown overnight at 37°C with shaking at 200 rpm. 15 mL of the overnight culture was used to inoculate 1 L of LB media. Cells were habitually grown in 5 L batches. 1 L cultures were grown at 37°C at 180 rpm in unbaffled 2 L flasks until an OD_{600} of 0.6-0.9 was recorded. The temperature was reduced to 21°C and protein expression induced with a final concentration of 1 mM IPTG. Expression was allowed to continue overnight before harvesting by centrifugation at 5000 rpm for 15 minutes at 4°C. The pellets were stored at -20°C.

2.7.3 Large scale expression of isotope labelled Hsp90 constructs (1)

A single colony from a plate or 1µl of an appropriate glycerol stock was used to inoculate 10 mL of LB media. The culture was grown for 8 h at 37°C at 200 rpm before being centrifuged at 4000 rpm for 15 min. The supernatant was discarded and the pellet was re-suspended in 100 mL of minimal media. This was incubated overnight at 37°C, shaking at 200 rpm. The 100 mL culture was centrifuged at 4000 rpm for 15 min in two 50 mL falcon tubes and the supernatant discarded. The pellet was re-suspended in 2 mL minimal media and transferred into 1 L of minimal media in a 2 L flask. This was then grown at 37°C shaking at 180 rpm until an OD_{600} of 0.5-0.7 was recorded. Protein expression was then induced with a final concentration of 1 mM IPTG. The temperature was reduced to 21°C and induction allowed to continue overnight. Cells were harvested by centrifugation at 4°C at 5000 rpm for 15 min and the pellets stored at -20°C.

2.7.4 Large scale expression of isotope labelled Hsp90 constructs (2)

A single colony from a plate or 1 µL of an appropriate glycerol stock was used to inoculate 100 mL of LB media. The culture was grown overnight at 37°C with shaking at 200 rpm. 15 mL of the culture was used to inoculate 1 L of LB media with the addition of 3 g/L D-Glucose to suppress 'leaky' expression from the Lac operon. Habitually, 5L of cells were grown in this way at a time.

The culture was grown at 37°C while shaking at 180 rpm in 2L unbaffled flasks until an OD_{600} of 0.8 - 1.1 was reached. The culture was then centrifuged at 5000 rpm for 15 minutes at 4°C and the supernatant discarded. The pellet was re-suspended in 10 mL of minimal media. The re-suspended cells from 5L of LB media were added to a total volume of 1L of minimal media in two baffled 2L flasks. The cells were grown for a further hour at 37°C shaking at 180 rpm prior to induction with 1 mM IPTG. The temperature was then reduced to 21°C and expression allowed to continue overnight [45]. The cells were then harvested by centrifugation at 5000 rpm at 4°C for 15 minutes and the cell pellets stored at -20°C.

2.8 Protein purification

Protein purification was carried out at 4°C or 21°C (room temperature). The pellets were thawed on ice and resuspended in lysis buffer with the protease inhibitors E64 (200 µM), Benzamidine (1 mM) and AESBF (10 µM). the resuspended cells were lysed by sonication on ice (10 s burst followed by a 50 s cooling period repeated 15 times).

The lysed cells were centrifuged at 20,000 rpm for 60 minutes to separate the cell debris from the cytoplasm. Gel samples were taken from both pellet and supernatant and run on a 10% SDS polyacrylamide gel to ensure the presence of the protein in the cytoplasm and absence from inclusion bodies in the pellet. All column purification was done using an AKTA purification system from Amersham. All buffers used are summarised in Table 2.2. The supernatant was loaded onto a pre-equilibrated HisTrap NiNTA column (GE Healthcare, UK) at a rate of between 0.5 mL/min and 1 mL/min to allow coordination of the His Tag in the constructs with the Ni ions on the resin. The column was washed with 5 column volumes (cv) of NiA and 5 cv of 98% NiA with 2% NiB to remove non specifically bound protein. Specifically bound protein was eluted in a step gradient of 2 - 100% NiB and 2.5ml fractions were collected. The column flow through was monitored by UV detection at 280 nm and 254 nm.

NiA – Nickel wash buffer	50 mM Tris Base, 100 mM NaCl, pH 8
NiB – Nickel elution buffer	50 mM Tris Base, 100 mM NaCl, 500 mM Imidazole, pH 8
QA – Anion exchange wash buffer	50 mM Tris Base, 100 mM NaCl, 5 mM EDTA, pH 8
QB – Anion exchange elution buffer	50 mM Tris Base, 2 M NaCl, 5 mM EDTA, pH 8
Gel filtration buffer.	100 mM Tris Base, 200 mM NaCl, 5 mM EDTA pH 8.
Triple buffer	100 mM ACES, 50 mM Tris base, 50 mM Ethanolamine pH 5 – 10, 5 mM Mg^{2+}.
ITC buffer	20 mM Tris pH 8
Heat of ionisation buffers	50 mM NaCl, 5 mM Mg^{2+} 20 mM Tris/Bis-Tris/ACES/HEPES/PIPES

Table 2.2 Buffers used for protein purification and ITC experiments.

The eluted fractions containing protein were concentrated to a volume of no more than 5 mL using a spin concentrator (Vivaspin: molecular weight cut off (mwco) of 10 kDa with a PES membrane; 3800 rpm for 15 minutes at 10°C repeated as necessary with agitation in between runs). The concentrated sample was then loaded onto a pre-equilibrated Superdex 200 gel filtration column (GE Healthcare) and run at a rate of 1 mL/min. Fractions (4 mL) were collected for 1 cv (100 mL) and the protein content of each fraction monitored by UV. For the purification of the N551 construct and the full length Hsp90 molecule, an additional purification step was required between the His-Trap column and the gel filtration column. A Q-sepharose anion exchange column (GE Healthcare) was used for increased purification. The His-trap elution fractions were diluted by a factor of eight to reduce the imidazole concentration to 62 mM, to allow binding to the Q-sepharose column. The sample was loaded on to a pre-equilibrated Q sepharose anion exchange column at a flow rate of 1 mL/min. The column was washed with 5cv of QA buffer before the protein was eluted along a 5cv gradient from 100% QA to 100% QB. Fractions (4ml) were collected along the first 50% of the gradient. Samples were taken at each step for SDS PAGE gel analysis (Figures 2.1 – 2.5).

2.8.1 SDS PAGE Gel analysis

N-terminal

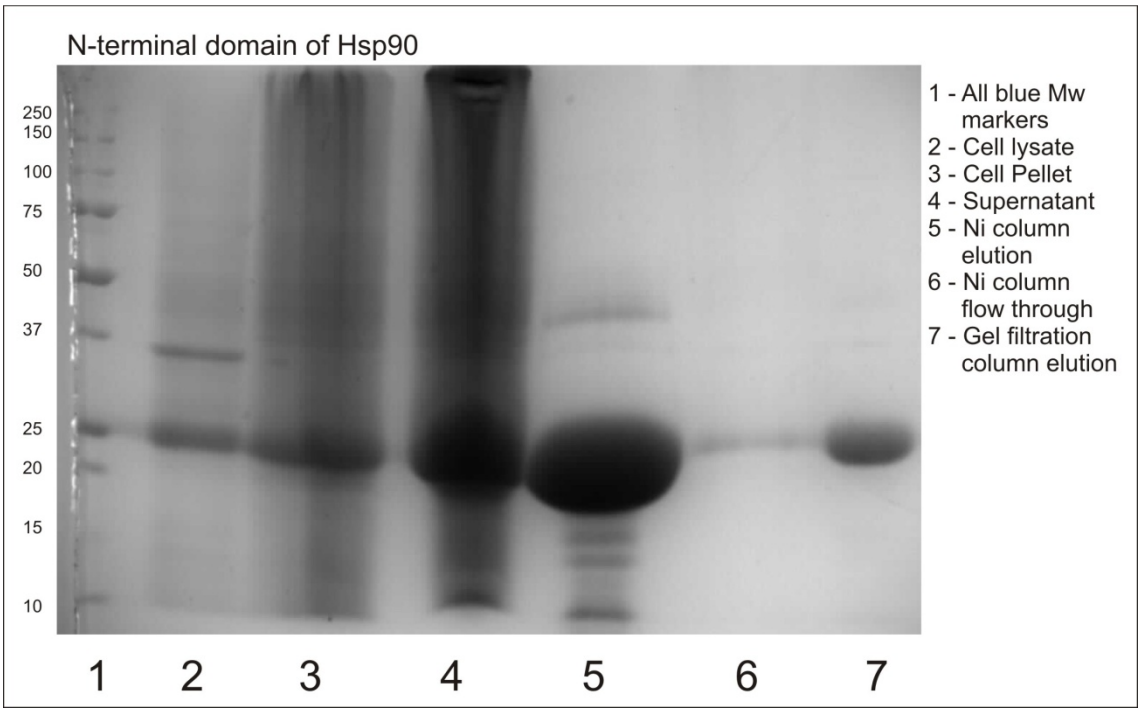

Figure 2.1 SDS PAGE gel analysis of the purification of the N-terminal domain of Hsp90

N551 Construct

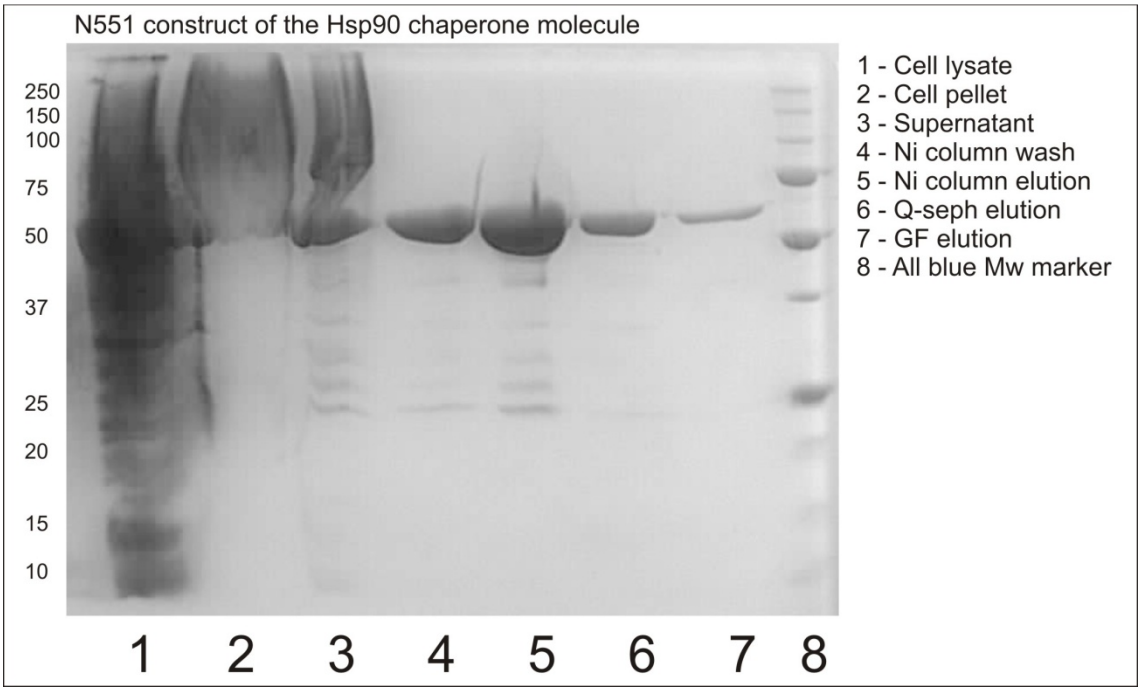

Figure 2.2 SDS PAGE gel analysis of the purification of the N551 construct of Hsp90

T22I N-terminal mutant

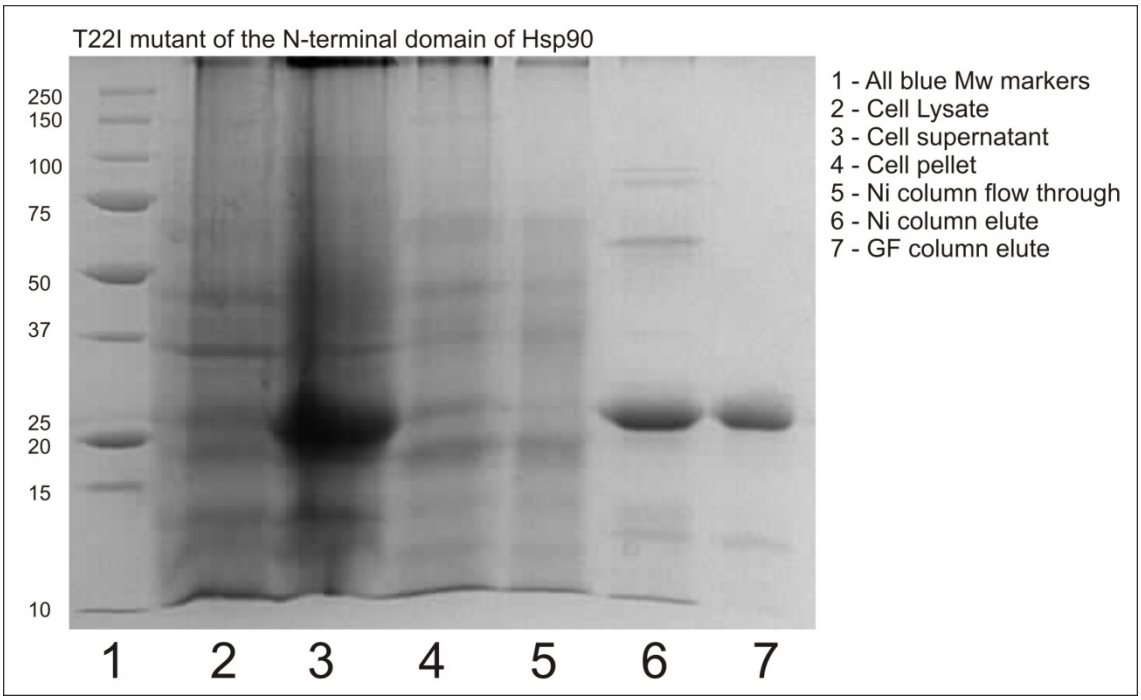

Figure 2.3 SDS PAGE gel analysis of the purification of the T22I mutant of the N-terminal domain of Hsp90

T101I N-terminal mutant

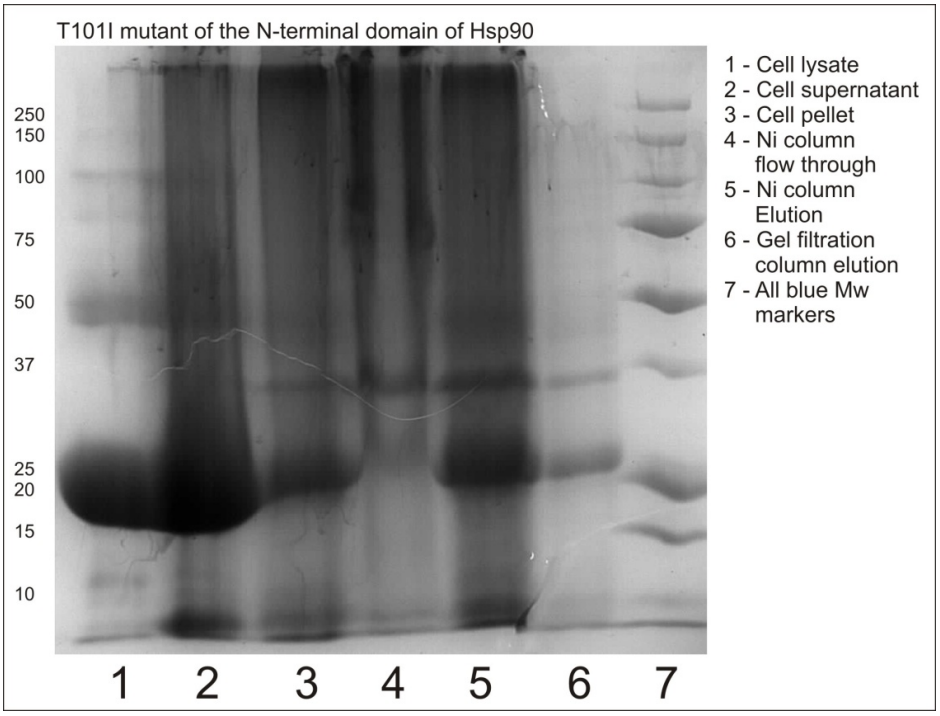

Figure 2.4 SDS PAGE gel analysis of the purification of the T101I mutant of the N-terminal domain of Hsp90

Full length Hsp90

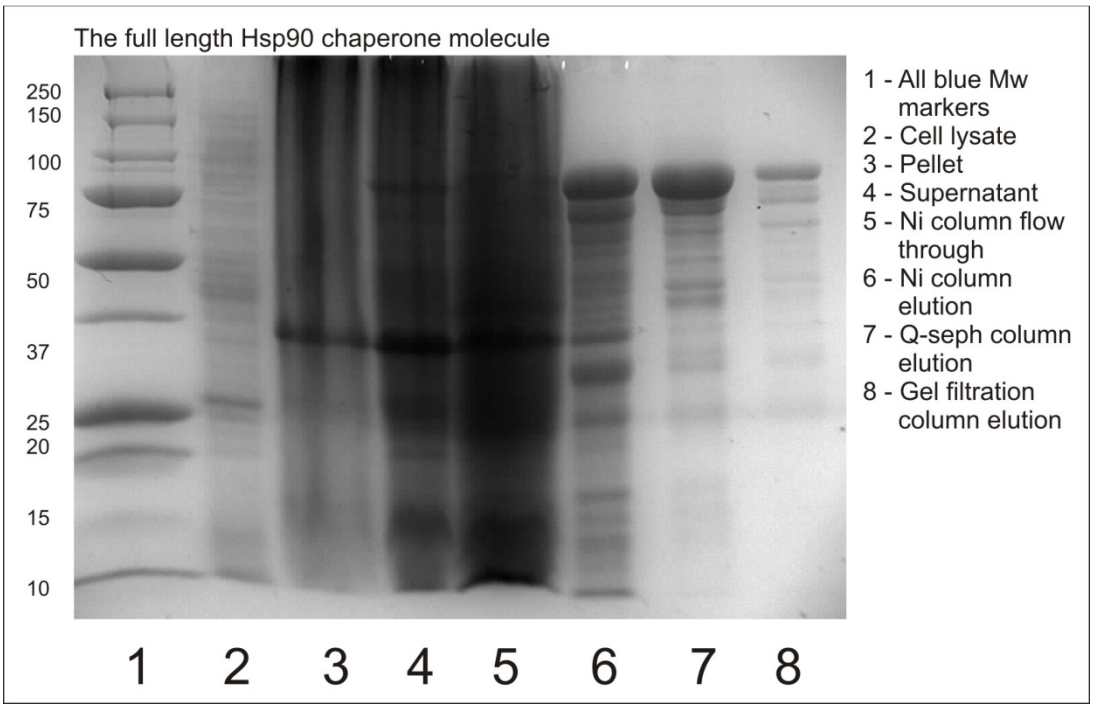

Figure 2.5 SDS PAGE gel analysis of the purification of the full length construct of Hsp90

2.8.2 1D NMR analysis to confirm folding

As described in more detail later, 1D NMR analysis can be used to determine whether a protein contains folded structure. Peaks present above 8.5ppm or below 0ppm are indicative of folded protein and as such 1D NMR can be used as a rapid method for determining the folded state of purified protein. Figure 2.6 shows 1D NMR data for the N-terminal domain, N551 construct and the two N-terminal mutants T101I and T22I. These scans confirm that the expressed protein is folded.

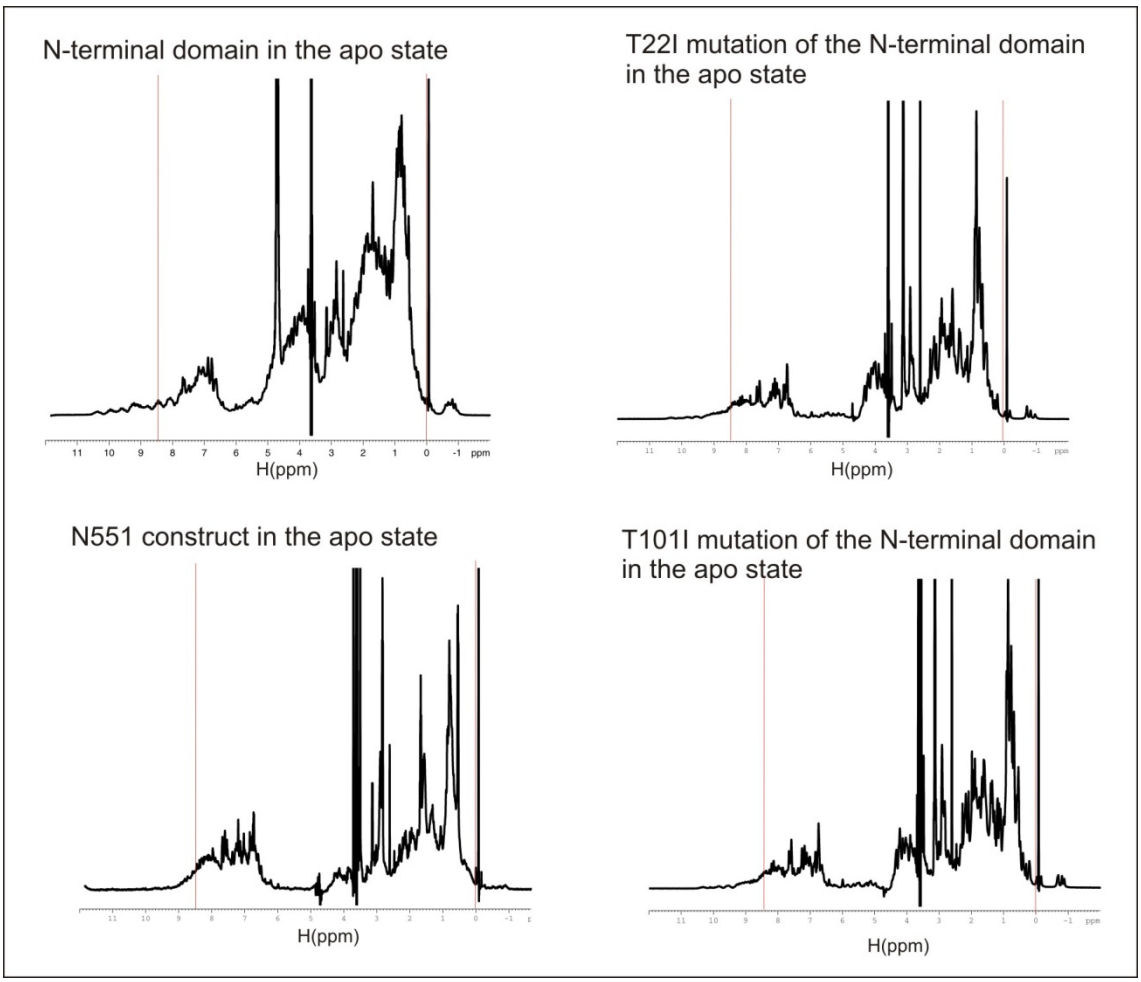

Figure 2.6 1D spectra for the N-terminal domain, N551 construct and T101I and T22I mutants of the N-terminal domain. Peaks above and below the red lines marked are characteristic of a folded protein molecule.

2.9 Concentration determination

2.9.1 Protein Concentration determination

Protein concentration was determined by ultraviolet (UV) spectroscopy. According to the Beer Lambert Law, the absorbance of light at a specific wavelength (for proteins this is at 280nm) is directly proportional to the concentration of the sample.

$$A = \varepsilon c l \qquad (2.1)$$

The extinction coefficient (ε) is specific for each protein construct dependent upon its size and amino acid composition. A is the absorbance, l is the path length in cm and c is the

concentration of the sample in moles. A quartz cuvette was used for all measurements and the relevant buffer was used as a reference to subtract an appropriate baseline from all readings. An absorbance scan was taken across a range of 340 nm to 190 nm of both buffer and the protein solution. If necessary a 1 in 10 or 1 in 20 dilution of protein solution was used so that the absorbance was within the working range of the spectrometer (between 0.1 and 1 absorbance units (AU)). The concentration was then calculated using the appropriate extinction coefficient for each construct (Table 2.3) and allowing for a 1 cm path length (l) and the relevant dilution factor. Equation 2.1 shows the Beer-Lambert Law where A is the absorbance, ε is the specific extinction coefficient, c is the concentration of the sample and l is the path length of the light through the sample.

Molecule	Extinction Coefficient (ε) M^{-1} cm^{-1}
AMP-PNP	14600
ADP	14600
ATP	14600
Adenine	13300
Adenosine	13400
Hsp90 full length	54050
N terminal domain (1 – 220)	14440
Middle domain (245 – 551)	31150
N551 construct (1 – 551)	44520

Table 2.3 Summary of the extinction coefficients of the protein constructs and ligands used. Proteins measured at 280nm. Nucleotide ligands measured at 260nm.

2.9.2 Nucleotide concentration determination

Nucleotide solutions of APMPNP, ADP, adenosine and adenine were used. Nucleotide concentration determination was undertaken in the same way as described for protein concentration determination by UV spectroscopy. The maximum absorbance was monitored at 260 nm instead of 280 nm and dilutions of 1 in 100 or 1 in 200 were used. Extinction coefficients are summarised in Table 2.3.

2.10 SDS Polyacrylamide gel electrophoresis

SDS Polyacrylamide gel electrophoresis (SDS PAGE) allows protein samples to be separated according to size. Proteins are denatured by the presence of negatively charged SDS which binds to the unfolded proteins such that the negative charge from the SDS is proportional to the size of the denatured protein. Movement of protein through the gel matrix is then driven by a voltage applied to it. The concentration of acrylamide used determines the 'percentage' of the gel and proteins meet a greater resistance passing through a higher percentage gel. The 'percentage' used defines the effective resolution for different molecular mass proteins on any given gel. A high percentage gel allows resolution of small proteins, while a low percentage gel gives better resolution for larger proteins. All gels used were 10% SDS PAGE gels unless otherwise specified. 0.75 mm thick gels were cast using frames, flat plates and 10 well combs from Biorad. Stacking and resolving gel mixtures are shown in table 2.4. All gel recipes and protocols adapted from Sambrook and Russell [44]. In all cases TEMED was added last, prior to pouring, to induce crosslinking of the acrylamide. 3.5 mL of resolving gel was used per gel and the top levelled off before setting by the addition of water which, was later removed after the resolving gel had set. The stacking section of the gel was cast and the well comb inserted before it set. The comb was removed immediately prior to running the gel.
Gel samples were prepared with 2:1 ratio of sample to x2 loading dye (Table 2.4) in an eppendorf and heated for 5 minutes at 100°C before loading 10 µL aliquots onto the gel. All gels were run using 'gel running buffer' (Table 2.4) at 120 V for 1 h 15 min. Gels were stained with Coomassie staining dye following 20 s heating in a microwave followed by 1 – 4 h in stain solution while shaking gently. Background dye was removed by immersion in destain solution (Table2.4) after 20 s heating in a microwave. Gels were stored in dH2O and photographed using gel doc’ equipment and 'genesnap' software (both by Syngene, Frederick, MD).

Stacking Gel	500 µL 30% Acrylamide 2 mL H2O 1 mL 3 M Tris pH 8.8 40 µL 10% SDS 100 µL 10% Ammonium persulfate. 5 µL Temed
10% Resolving Gel	1.7 mL 30% Acrylamide 2.55 mL H2O 625 µL 3 M Tris pH 8.8 50 µL 10% SDS 37.5 µL 10% Ammonium persulfate. 10 µL Temed
Coomassie Staining solution	40% Methanol, 10% Acetic acid, 50% dH_20, 0.5 g/L Coomassie brilliant blue.
Coomassie Destaining solution	40% Methanol, 10% Acetic acid, 50% dH_20
X2 Loading Dye	25% SDS, 25% Glycerol, 62.5 mM Tris-HCl (pH 6.8), 0.01% Bromophenol blue.
Running Buffer	14.4 g/L Glycine, 3.03 g/L Tris base, 1 g/L SDS.

Table 2.4 Solutions used in SDS PAGE gel pouring and running.

2.11 Circular dichroism

All spectra were measured using a circular dichroism spectrometer (Aviv Instruments Inc.) and all data was plotted using Microsoft Excel. Circular dichroism (CD) spectroscopy is used to monitor the difference in absorption of a molecule of left-handed and right-handed plane polarized light at wavelengths across the near and far UV range. A difference in absorption results in elliptically polarised light. For there to be a difference the molecule must contain a chiral centre or be within an asymmetric environment. The absorption difference was measured either in units of the difference in molar absorbance $\Delta\varepsilon = \varepsilon l - \varepsilon r \cdot cm^{-1} \cdot dmol^{-1}$, or in terms of the mean residue ellipticity ($[\theta]$mrw. λ) in deg $\cdot cm^2 \cdot dmol^{-1}$. Where mrw = mean residue weight [mass/no. amino acids], θ = observed ellipticity in degrees. d= path length (cm), c = conc. in g/mL. This is calculated by:

$$[\theta]mrw.\ \lambda = mrw[\theta] / 10d.c \quad (2.2)$$

The two units are related by the relationship:

$$[\theta]mrw = 3298\ \Delta\varepsilon. \quad (2.3)$$

The absorption difference of these chiral molecules, such as amino acids, is characteristic at certain wavelengths. The same is also true for distinct chiral structures such as α-helices and β-sheets. These structures, found to varying degrees in folded proteins, display characteristic absorption minima at different wavelengths; α-helices absorb at 222 nm and 208 nm while β-sheets absorb preferentially at 216 nm. The intensity of the signal is dependent upon the amount of each secondary structure in the protein, the concentration of protein and the width of the cuvette used. From the overall signal due to all secondary structure within a protein, and knowing the protein concentration, the proportion of α-helices and β-sheet can be calculated.

Scans were taken across a range of 270 – 195 nm using either a 0.5 or 0.1 mm quartz cuvette. Readings were taken at 3 s intervals, 0.5 nm apart. Each scan was repeated and the average of the two readings was plotted. Identical runs using buffer to provide a blank scan were carried out for each sample. Buffers containing high concentrations of Cl^- ions and Tris base showed high absorbance below 195 nm, thus making accurate readings below 195 nm impossible. Temperature denaturation was measured as a function of disappearance of secondary structure monitored at 222 nm. Melting curves of the change in secondary structure with respect to temperature were created from measurements recorded using a 1 mm quartz cuvette at temperature intervals of 1°C.

For wavelength scans a protein concentration of 50 μM was used. For denaturing curves a lower protein concentration of 10 μM was used in order to reduce the possibility of aggregation of the unfolded protein.

2.12 Isothermal titration calorimetry

All titrations were carried out using a VPITC (Microcal, Northampton, MA) instrument and analysed using origin 5.0 software (OriginLab, Northampton MA). Isothermal titration calorimetry (ITC) can be used to monitor the change in heat of a solution upon injection of a small quantity of another solution, such as a ligand injected into a protein sample (Figure 2.7). The change in enthalpy can correspond to a chemical reaction or a molecular reorganisation. With knowledge of the volume and concentration of both the reactants, the heat measured upon mixing of the two can be related directly to the extent of reaction in the sample cell. In a protein/ligand binding experiment a series of injections leading towards the saturation of the protein in the sample cell can be used to determine the change in enthalpy (ΔH), binding affinity (k_A) and stoichiometry (n) of the binding reaction. From these parameters the change in both entropy (ΔS) and Gibbs free energy (ΔG) can be calculated using the equations 2.4 – 2.7. Over a series of temperatures the change in heat capacity (ΔC_p) can also be calculated as dΔH/dT.

$$\Delta G = \Delta H - T\Delta S \quad (2.4)$$

$$\Delta G = -RT \ln K_a \quad (2.5)$$

$$K_a = \frac{1}{K_d} \quad (2.6)$$

Equations 2.4 to 2.6 show the relationship between the Gibbs free energy and the entropy and enthalpy of a reaction (2.4) and the link this then has to the dissociation constant of a reaction (2.5). Also shown is the inverse relationship between the association and dissociation constants of a reaction (2.6). Shown here, G is the Gibbs free energy, R is the gas constant taken as 8.314 $J.K^{-1}.mol^{-1}$, T is the temperature in Kelvin, S is the entropy, H is the enthalpy, K_a is the association constant of the reaction and K_d is the dissociation constant of the reaction.

The accuracy to which ITC is able to measure the K_a of an interaction is dependent upon the strength of the interaction as measured by a value called 'c', a unit-less parameter that is the product of the total concentration of the sample (P_{tot}) and the K_a. Values of c that are between 1-1000 allow accurate determination of the thermodynamic parameters described above by ITC. Values of c lying outside of this range are not readily accurately measured by ITC.

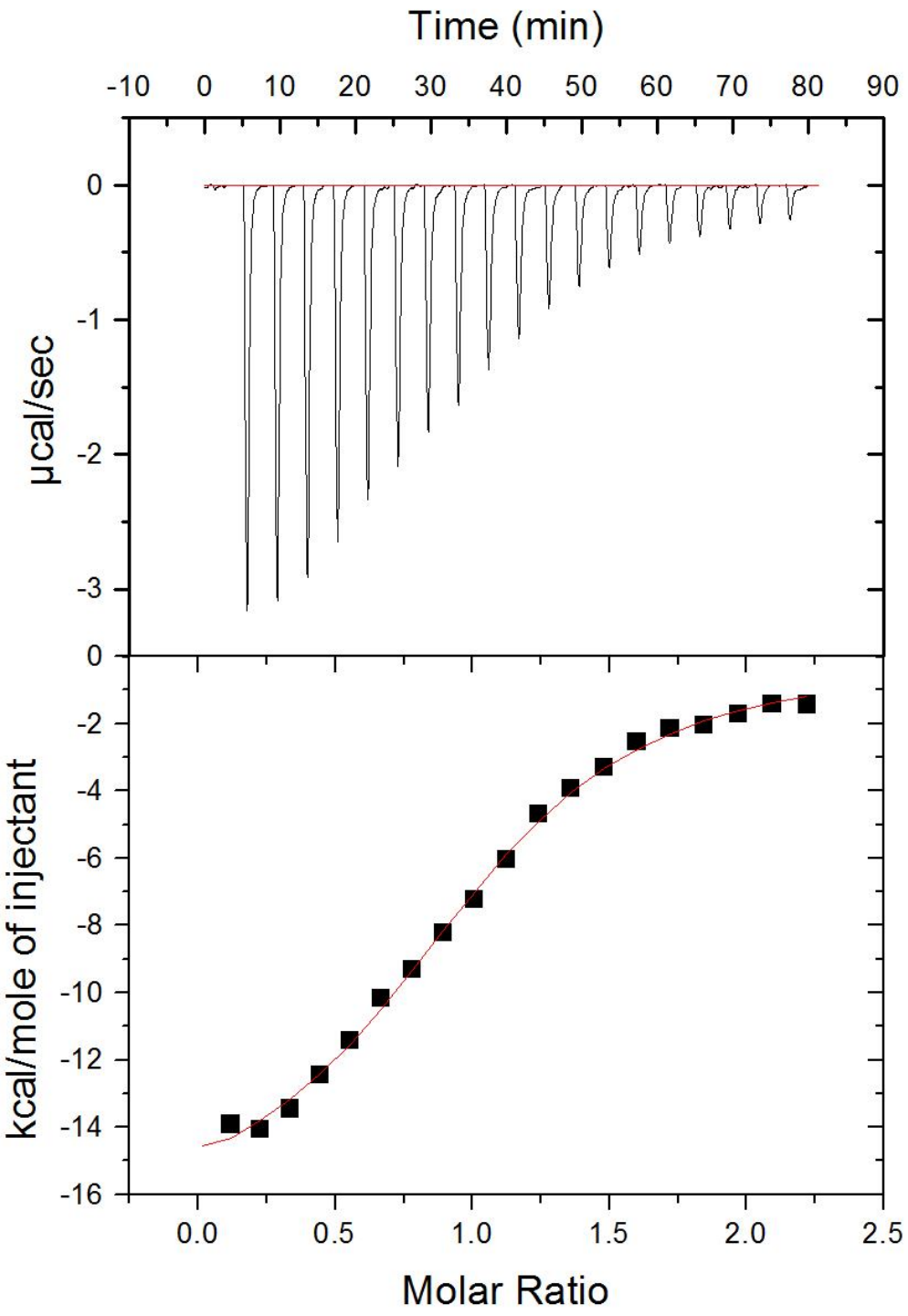

Figure 2.7 ITC trace showing the raw heats (top) and the integrated heats (bottom) of the reaction of the N-terminal domain of Hsp90 (100 µM) with ADP (1 mM). 20 mM Tris, pH 8 15°C.

For a single site binding interaction, titrations are fitted to a curve by Origin software following the equation:

$$Q = \frac{nM_t\Delta HV_o}{2}\left[1 + \frac{X_t}{nM_t} + \frac{1}{nKM_t} - \sqrt{\left(1 + \frac{X_t}{nM_t} + \frac{1}{nKM_t}\right)^2 - \frac{4X_t}{nM_t}}\right] \quad (2.7)$$

Where Q is the total heat, V_0 is the active cell volume, M_t is the bulk concentration of the protein, X_t is the bulk concentration of the ligand. Over a series of injections this equation can be fitted and the value of Q adjusted for the increased volume due to the injection of ligand into the cell, from this n (the number of binding sites), ΔH (the enthalpy of the reaction) and K (the binding constant) can be determined[46].

All experiments were carried out under a constant temperature and pressure to measure the enthalpy and binding affinity of a variety of ligands and binding partners to all or part of Hsp90. A purified protein sample was transferred into an appropriate ITC buffer by serial dilution; Triple buffer (Table 2.2) at every half pH unit from pH 5 - 10, 20 mM Tris pH 8, 50 mM Tris 50 mM NaCl pH 7.5 were all used. All buffers contained 5 mM $MgCl_2$. Titrations were done every 5°C from 10°C to 30°C.

1.5 mL Hsp90 full length, N terminal or N551 was loaded into a clean sample cell using a 2 mL syringe (Hamilton, Nevada) according to microcal instructions. The sample cell was allowed to equilibrate with the reference cell at the relevant temperature before the titration was started.

The ligand used (AMPPNP, ADP, adenosine or adenine) was dissolved in the same buffer as the protein at a 10 fold higher concentration than the protein. The ligand solution was adjusted for pH if necessary to match the protein. 300 µL from a reservoir of 500 µL ligand was loaded into a clean ITC syringe according to microcal instructions. The contents of the syringe was purged and refilled twice to remove air bubbles. Residual ligand was removed from the syringe tip with a kimwipe prior to inserting the syringe into the cell. All experiments were carried out at reference power of 15 µcal/s with a series of 20 injections. The first injection had a volume of 2 µL with a delay of 120 s before the second injection. All subsequent injections had a volume of 15 µL with a delay of 240 s between each. A constant stirring speed of 300 rpm was used in all

cases. For each set of experimental conditions a heat of dilution experiment was run with ligand injected into buffer in the cell without protein. This was then used to adjust the final results so only heats of interaction were used in the final calculations.

2.12.1 Heat capacity

What is a heat capacity change?

The change in constant pressure heat capacity, or ΔC_p, of a protein can be simply defined as the change in the enthalpy (ΔH) of a process (ligand binding or protein unfolding for example) with respect to temperature. However this simplistic definition does not describe the many processes that contribute to the ΔC_p value. A change in heat capacity results from a change in the degrees of freedom within a system from the transition from the free to the bound state. This change in freedom can be induced by either the unfolding or folding of a protein [47], by the binding of another molecule to the protein, a change in hydration of a protein[48] and displacement of water molecules, or a conformational change[49]. A change in the degrees of freedom will in turn alter the energy required to raise the temperature of the system. Gomez et al. [47] described three main contributions to the ΔC_p; the first arises from the covalent structure of the protein including contributions from vibrational motions due to bond stretching and internal rotations; the second is due to non-covalent interactions due to secondary and tertiary structure; the third is due to the hydration of the molecule including the overall buried surface area and the solvent accessible polar and non-polar surface area. These three factors can be further classified as being either intrinsic to the molecule (such as the first two) or extrinsic involving the surrounding solute (the third) and the total heat capacity classified below:

$$C_p = C_{p,bond} + C_{p,nonbond} + C_{p,hydration} + C_{p,protonation} \quad (2.8)$$

$$\Delta C_p = \Delta C_{p,nonbond} + \Delta C_{p,hydration} + \Delta C_{p,protonation} \quad (2.9)$$

Equations (2.8, 2.9) show contributions to the heat capacity from various sources[47], where $C_{p,bond}$ is the heat capacity due to the atomic and covalent interactions, $C_{p,nonbond}$ is the heat capacity due to non-covalent interactions, $C_{p,hydration}$ is the heat capacity due to the hydration of the protein molecule and $C_{p,protonation}$ is the heat capacity due to the protonation state of the side chains within the protein. When a process involving a single protein is considered then the

term $C_{p,bond}$ remains the same both before and after the event and so the equations is simplified to equation (2.9).

Hydration changes of protein surface groups and non-covalent interactions, however, have a small influence on the total heat capacity of a protein compared to the primary heat capacity ($C_{p,a,}$ equation 2.8)[47]. However, when changes in heat capacity on going from one state to another with respect to a single protein are considered, the primary heat capacity contributions are identical, and as such small influences from hydration change and non-covalent interactions account for most of the ΔC_p associated with any given process[47] and thus the simplified equation (2.9) can be used.

This summation towards the overall heat capacity allows for a varied and unequal contribution from each source. The exact relative influence over the overall ΔC_p from each of these sources is widely contested however the agreement is that the influence is small[47;50].

What contributes to the heat capacity and what can these tell us about a physiological process?

The C_p of an unfolded protein over a physiological temperature range of 0°C – 50°C is known to change linearly with respect to temperature [48]. The ΔC_p of a protein actively unfolding over a physiological temperature range of 0°C – 50°C is not linear, but instead fits to a second order polynomial equation [47]. The exposure and hydration of non-polar surface area during protein unfolding is known to lead to a positive ΔC_p [47], while the hydration polar groups lead to an opposing ΔC_p change. The non-linear change in the ΔC_p of unfolding is due to hydration exposure of polar and non-polar groups responding differently to a change in temperature, and thus the sum of the two contributions changes in a non-linear fashion with a maximum to the curve at around 50°C [48].

However as previously mentioned a change in heat capacity is not only associated with protein unfolding but also with ligand binding. Indeed, a large negative ΔC_p is thought to be characteristic of site-specific binding between two molecules due to the associated removal of exposed non-polar surface area and the restriction of freedom of the associated polar surface area.[49;51;52].

The influence over the heat capacity of a protein due to a change in non-covalent interactions is small compared to the change in solvation due to surface area burial. It is well known that a good approximation of the heat capacity change due to hydration can be

calculated from changes in polar and non-polar solvent accessible surface area[47;51;53]. From experimental data this contribution has been quantitatively assessed[51;54].

$$\Delta C_p = (1.34 \pm 0.04)\Delta A_{np} - (0.59 \pm 0.04)\Delta A_p \; J\, mol^{-1}K^{-1} \quad (2.10)$$

$$\Delta C_p = 1.874\Delta A_{np} + 0.711\Delta A_{oh} - 1.097\Delta A_p \; J\, mol^{-1}K^{-1} \quad (2.11)$$

Equation 2.10 calculates the change in heat capacity (ΔC_p) from the change in non polar (ΔA_{np}) and polar (ΔA_p) surface area[51]. Equation 2.11 also calculates the change in heat capacity but includes a term allowing for the change in hydration of the protein (ΔA_{oh}). Both equations are valid depending on the number of variables under consideration. For most purposes equation 2.10 is sufficient while equation 2.11 allows for the small influence the change in hydration will have over the heat capacity.

Conformational changes will often lead to a change in exposed surface area and so one might expect them to also contribute to the ΔC_p of a process. Observations of ΔC_p associated with a protein complex formation, frequently cannot be accounted for by models which assume 'rigid body' association. This discrepancy is only resolved if a conformational change is also assumed to result from binding[49;51]. A variety of examples have confirmed the idea that an 'anomalous' ΔC_p can be used to investigate conformational changes induced by binding. Using the measured ΔC_p of a binding interaction and the calculated change in surface area associated with rigid body binding, it is therefore possible to assess whether a conformational change is likely to be coupled to the binding[51;55]. If conformational changes are expected or hypothesised to occur then predictions of the ΔC_p based upon the expected change in surface area can be compared to the recorded ΔC_p. This can then be used to confirm the predicted conformational changes or look for other effects influencing the ΔC_p.

Positive heat capacity changes are anticipated within cooperative systems where 'order to disorder' transitions occur, such as during protein unfolding or subunit dissociation and water network disruption. The decrease in the water molecules 'soft' vibrational modes through the formation of H-bond networks can lead to a more negative ΔC_p, thus the disruption of such a network would mitigate the heat capacity effect due to H-bond networks[52;55]. Sometimes disruptions can lead to the reduction for freedom of water molecules within a binding interface and the associated negative ΔC_p change[52].

2.12.2 Proton linkage

The measured enthalpy of a binding event can be used to determine the proton linkage of the binding if the experiment is repeated across a pH range. The following explanation is based upon Bradshaw et al. 1998 [56].

If a protonation is required for binding then the linkage scheme can be described as shown in figure 2.8.

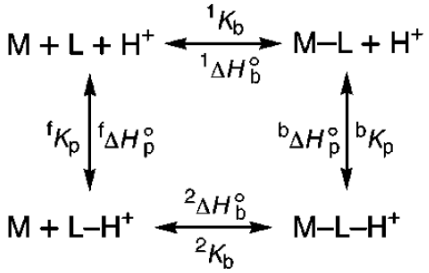

Figure 2.8 Interaction profile for a single proton linkage binding between a ligand and a macromolecule. L = ligand. M = macromolecule. H = proton. Subscripts: p = protonation, b = binding. Superscripts 1 = binding deprotonated, 2 = binding protonated ligand. Superscripts f = protonation of free ligand, b = protonation of bound ligand.

The relationship between the binding constant of the macromolecule for both the protonated (^2K_b) and deprotonated (^1K_a) and the proton binding constants of the free (^fK_b) and bound (^bK_p) ligand can be expressed thus:

$$(^1K_b)(^bK_p) = (^2K_b)(^fK_p) \quad (2.12)$$

The proton binding constants can be related to the proton acid dissociation constants by a simple inverse relationship:

$$^fK_p = {}^1/_{fK_a} \quad (2.13)$$

$$^bK_p = {}^1/_{bK_a} \quad (2.14)$$

Linkage theory then shows that the association constant of the interaction (K_{obs}) as a function of pH is equal to the product of a reference equilibrium constant (^1K_b) and the quotient of the subpartition functions for binding of protons to the bound and free forms of the ligand (Z_b and Z_f).

$$K_{obs} = {}^1K_b \frac{Z_b}{Z_f} \quad (2.15)$$

For a single protonation event Z_b and Z_f can be described thus:

$$Z_b = 1 + 10^{(pK_a)_{b-pH}} \quad (2.16)$$

$$Z_f = 1 + 10^{(pK_a)_{f-pH}} \quad (2.17)$$

This is derived using the relationship:

$$(pK_a)_b = \log {}^bK_p \quad (2.18)$$

$$(pK_a)_f = \log {}^fK_p \quad (2.19)$$

Therefore for a single protonation event K_{obs} as a function of pH can be described as:

$$K_{obs} = {}^1K_b \frac{1+10^{(pKa)_{b-pH}}}{1+10^{(pKa)_{f-pH}}} \quad (2.20)$$

Experimental data fit to this equation can then be used to determine the binding constants of the proton in both the bound and free state and the binding constant of the unprotonated ligand to the macromolecule.

The enthalpy of binding can also be used to assess the proton linkage of an interaction between a ligand and a macromolecule. The ΔH_{obs} recorded by ITC comprises of both the intrinsic enthalpy of a binding event ($\Delta H°_b$) and the enthalpy associated with the ionization enthalpy of the buffer used. These relate to each other in the following manner[57]:

$$\Delta H_{Obs} = \Delta H_b + (n)\Delta H_{ion} \quad (2.21)$$

Where ΔH_b is the intrinsic enthalpy of the interaction accounting for buffer effects, ΔH_{ion} is the enthalpy of ionisation of the buffer used and n is the number of protons absorbed upon ligand binding to the macromolecule. Thus at any given pH the number of protons taken up in an interaction can be determined if the enthalpy is recorded under different buffer conditions with different heats of ionisation. The gradient of a plot of ΔH_{obs} vs. ΔH_{ion} should reveal the number of protons taken up. If ligand binding is dependent upon protonation of the ligand then n can be described thus:

$$n = {}^{b}f - {}^{f}f \tag{2.22}$$

Where ${}^{b}f$ and ${}^{f}f$ refer to the fractional saturation of protons at a given pH for the bound and free ligand respectively. These fractions can then be expressed in terms of the pKa of the ligand and the solution of the pH.

$${}^{b}f = \frac{10^{(pKa)_b - pH}}{1 + 10^{(pKa)_b - pH}} \tag{2.23}$$

$${}^{f}f = \frac{10^{(pKa)_f - pH}}{1 + 10^{(pKa)_f - pH}} \tag{2.24}$$

The enthalpy of the binding process (ΔH_b) can then be determined using equation 2.20 and the following expression where T is the temperature and R is the gas constant:

$$\frac{\delta \ln K}{\delta (1/T)} = -\frac{\Delta H}{R} \tag{2.25}$$

This then gives:

$$\Delta H_b = {}^{1}\Delta H_b + ({}^{b}f)^{b}\Delta H_p - ({}^{f}f)^{f}\Delta H_p \tag{2.26}$$

Where ΔH_b is described in terms of the enthalpy of the deprotonated ligand (${}^{1}\Delta H_b$) and the enthalpies of the bound (${}^{b}\Delta H_p$) and free (${}^{f}\Delta H_p$) ligand and the proton saturation fraction of the bound (${}^{b}f$) and free (${}^{f}f$) ligand.

As also described by Baker et al. [57] the ΔH_{obs}, ΔH_{ion} and the pH can all be related to one another through the following expression combining equations 2.26 and 2.21:

$$\Delta H_{obs} = {}^{1}\Delta H_b + ({}^{b}f)^{b}\Delta H_p - ({}^{f}f)^{f}\Delta H_p + (n)\Delta H_{ion} \tag{2.27}$$

This expression describes all the single proton linkage parameters in terms of the solution pH and the ΔH_{ion} of the buffer used allowing these parameters to be derrived by experimentation

at different pH values and different ΔH_{ion} values. This can be globally fit to determine the pKa values in the bound and the free states.

2.13 Nuclear Magnetic Resonance

2.13.1 Facilities

Nuclear magnetic resonance (NMR) spectrometers at the UCL Biomolecular NMR facility and at the MRC Centre for biomedical NMR at Mill Hill were used for this study.

UCL Biomolecular NMR facility: Three spectrometers were used during this study; a Varian Inova operating at a Lamour frequency of 600 MHz with a 5 mm ^{1}H, ^{13}C, ^{15}N cryoprobe and cooled ^{1}H pre-amplifier; a Bruker Advance III operating at a Lamour frequency of 700 MHz with a 5 mm ^{1}H, ^{13}C, ^{15}N cryoprobe with cooled ^{1}H and ^{13}C preamplifiers; and a Bruker Advance III operating at a Lamour frequency of 500 MHz with a 5 mm ^{1}H, ^{13}C, ^{15}N room temperature probe.

MRC Centre: Three spectrometers were used during this study; A Varian Inova operating at a Lamour frequency of 800 MHz with a 5 mm ^{1}H, ^{13}C, ^{15}N cryoprobe; a Bruker Advance III operating at a Lamour frequency of 700 MHz with a 5 mm ^{1}H, ^{13}C, ^{15}N cryoprobe; and a Varian Inova operating at a Lamour frequency of 600 MHz with a 5 mm ^{1}H, ^{13}C, ^{15}N cold probe and a ^{31}P X-detect probe.

2.13.2 Acquisition of data

Varian spectrometers were controlled using VNMR software, Bruker spectrometers were controlled using Topspin software. All experiments were performed at 25°C unless otherwise stated. Each sample contained between 5% - 10% (v/v) D2O to allow a frequency lock to adjust for drift in the magnetic field over the time course of the experiments. All samples contained 0.02% sodium 2,2-dimethyl-2-silane-pentane-5-sulphonate (DSS) (v/v) to allow for referencing recorded spectra to one another. Most experiments were run using 5mm Shigemi tubes (Shigemi co. Ltd.) with exceptions noted using 5mm standard NMR tubes (Wilmad Glass co. Inc.). Water signals were suppressed using the 'watergate' or 'presaturation' methods. The details used for each experiment are noted in Table 2.5, including the spectral width and the number of points.

2.13.3 Processing and analysis of NMR data

Processing of the free induction decay (FID) data from both Varian and Bruker spectrometers was carried out using NMRPipe spectral processing and analysis system [58] and viewed using NMRDraw. The direct proton time-dimension data were treated with a solvent suppression function (SOL) followed by a squared sine-bell apodisation function (SP) and zero filled. The treated data was then Fourier transformed and phased as required. This process was repeated for the second and third dimensions if applicable. The last dimension, either the second for 2D datasets or the third for 3D datasets was linear predicted before being processed in a similar way to the first proton dimension. Baseline correction (POLY) was applied following phase correction to all dimensions, using either first or second order polynomial correction as required.

Processed data were then converted to AZARA format and analysed using the Collaborative Computing Project for NMR (CCPNMR) Analysis software v.2.1.3 [59]. Chemical shifts were referenced to DSS. Peaks were picked either automatically using CCPN software and subsequently edited by hand or picked by hand entirely.

2.13.4 NMR experiments

	1H			D2			D3			Mix (ms)
Experiment	SF	SW (Hz)	NP	Nuc	SW (Hz)	NP	Nuc	SW (Hz)	NP	
^{1}H-1D	500	8012.82	32768							
^{1}H-1D	600	10000	8192							
^{1}H-1D	700	8012.82	32768							
^{31}P-1D	600			^{31}P	20000.0	10000				
^{15}N-HSQC (wt apo and H/D exchange)	500	2652.774	815	^{15}N	1750.01	512				
^{15}N-HSQC (wt AMPPNP and H/D exchange)	700	9455.00	1024	^{15}N	4525.000	128				
^{15}N-HSQC (wt ADP and H/D exchange)	700	3860.044	1805	^{15}N	2150.019	256				
^{15}N-HSQC (mutants)	700	3830.178	512	^{15}N	2100.565	903				
^{15}N-HSQC	800	10999.6	4096	^{15}N	3243.98	512				
^{15}N-TROSY	700	12626.263	2048	^{15}N						
CT-^{13}C-HSQC	700	8741.259	2084	^{13}C	12437.15	1024				
^{13}C-HSQC (folded)	800	10999.58	1100	^{13}C	8000.00	160				
HCCH-TOCSY (apo)	700	8741.258	2048	^{1}H	5952.38	256	^{13}C	12437.15	256	100
HCCH-TOCSY (ADP/AMPPNP)	700	5606.192	1364	^{1}H	7002.801	256	^{13}C	12333.46	256	100
CCH-TOCSY (all)	700	5605.469	1148	^{13}C	12435.45	256	^{13}C	12435.45	256	100

Table 2.5 Summary of NMR parameters used for all experiments.

One Dimensional NMR

One dimensional (1D) scans of the protein constructs were recorded prior to all other experiments on each sample. This was done to ensure consistent nature of the sample as peaks below 0ppm are characteristic of the folded protein in each state. It also allowed referencing and calibration of the water suppression using the Watergate method.

Two Dimensional NMR

Various different two dimensional (2D) experiments were undertaken on the protein constructs. Heteronuclear Single Quantum Correlation (HSQC) experiments were performed in order to detect resonances from H-N and NH_2 groups from both the protein backbone and amino acid side chains (Figure 2.9). A ^{15}N-HSQC observes one proton from a one bond correlation between ^{15}N - ^{1}H and requires a sample of ^{15}N-labelled protein. Magnetisation from the proton can be transferred to the nitrogen and the spin allowed to evolve during a t1 relaxation period, where it acquires a frequency label according to the offset of the nitrogen atom. The magnetisation is then transferred back onto the proton where it is observed but retains the frequency label from the nitrogen atom in addition to the frequency of the proton itself.

Signals from protons which are unconnected to a nitrogen atom can be suppressed, using a 90° pulse to invert all magnetisation on the nitrogen atom that will only affect the spins in antiphase. This means only spins in the ^{15}N – ^{1}H situation are inverted. If this experiment is repeated in the inverse dimension then again only the ^{15}N – ^{1}H spins will be inverted. If these two signals are subtracted from one another, then any resultant signal will be due to the correct ^{15}N-^{1}H correlations with all other proton signals cancelled out[60-62].

A TROSY experiment is designed to observe the resonances between ^{1}H-^{15}N pairs on protein backbones (side chain ^{1}H-^{15}N are not observed with this experiment). The signals detected from the ^{1}H-^{15}N pair are subject to two methods of relaxation: dipole-dipole interactions and chemical shift anisotropy (CSA). These two methods of relation affect the four peaks of the multiplet (^{1}H-^{15}N) differently with one generally being an intense narrow peak and the others being shallower, broader, peaks. The local magnetic fields generated – one from the CSA and the other from the dipole – either reinforce one another or cancel one another out, depending on whether the spins are in the same, or opposite, states. Also unlike an HSQC experiment where the multiplet peak splitting is collapsed to a single peak, the asymmetrical nature of the peaks is exploited in a TROSY to detect just the intense narrow peak, thus increasing the signal to noise ratio when the peak narrowing outweighs the loss of ¾ of the

peaks, i.e. for large proteins. Compared to the HSQC pulse sequence, the TROSY pulse sequence lacks a 180° pulse applied to the proton during the t1 phase and lacks decoupling of the ^{15}N nucleus. This leads to detection of a multiplet separated by J_{HN}. The degree of splitting is dependent upon the degree of peak asymmetry due to the cross correlation. Detection of all the peaks would lead to a crowded spectrum however spectra are simplified by suppression of all but the wanted peak.

The different peaks arise from transitions between the different energy levels associated with the cross correlation effects being either in phase or anti-phase with respect to each nuclei. Different transitions can be suppressed with a specific low radiofrequency 180° pulse that will select only for the unwanted transitions but will not affect the wanted peak [60-62].

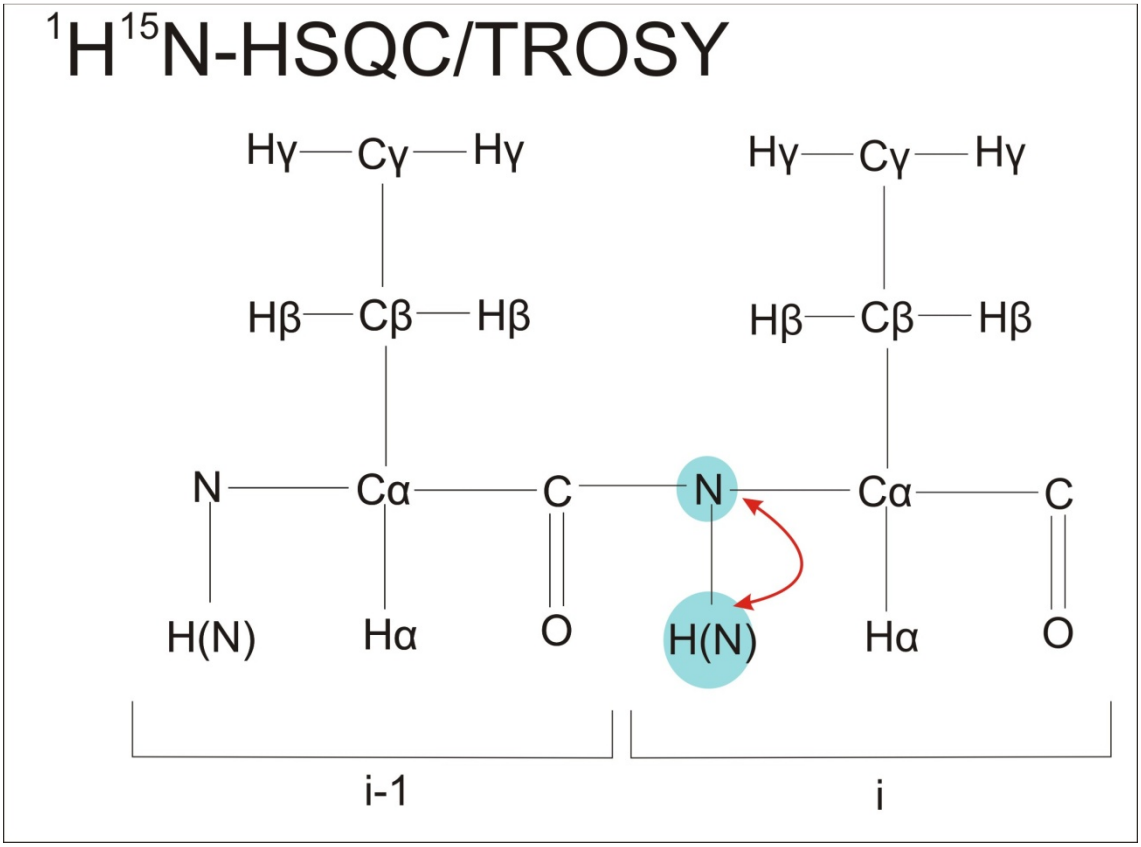

Figure 2.9 Transfer of magnetisation that occurs during a ^{15}N-HSQC and a ^{15}N-TROSY experiment. All transfers are within a single amino acid.

A ^{13}C-HSQC observes one proton from a one bond correlation between ^{13}C - ^{1}H and usually requires a ^{13}C labelled sample of protein (Figure 2.10). Magnetisation from the proton can be transferred to the carbon and the spin allowed to evolve during a t1 relaxation period where it acquires a frequency label according to the offset of the carbon atom. The

magnetisation is then transferred back onto the proton where it is observed but retains the frequency label from the carbon atom in addition to the frequency of the proton itself. This will allow the detection of protons involved in ^{13}C - ^{1}H bonds on the backbone from Cα to Hα and from all ^{13}C - ^{1}H bonds along the side chains. When multiple protons are attached to a carbon atom each ^{13}C - ^{1}H bond will generate a separate signal however signals may be degenerate. In the case of CH_2 groups, each proton may be in a different environment and so two ^{13}C - ^{1}H bonds will be recorded. In the case of a methyl group the rotation of the group is sufficiently fast that each ^{13}C - ^{1}H bond is in an equivalent environment to the others and so a single averaged peak will be detected for the three ^{13}C bonded protons [60].

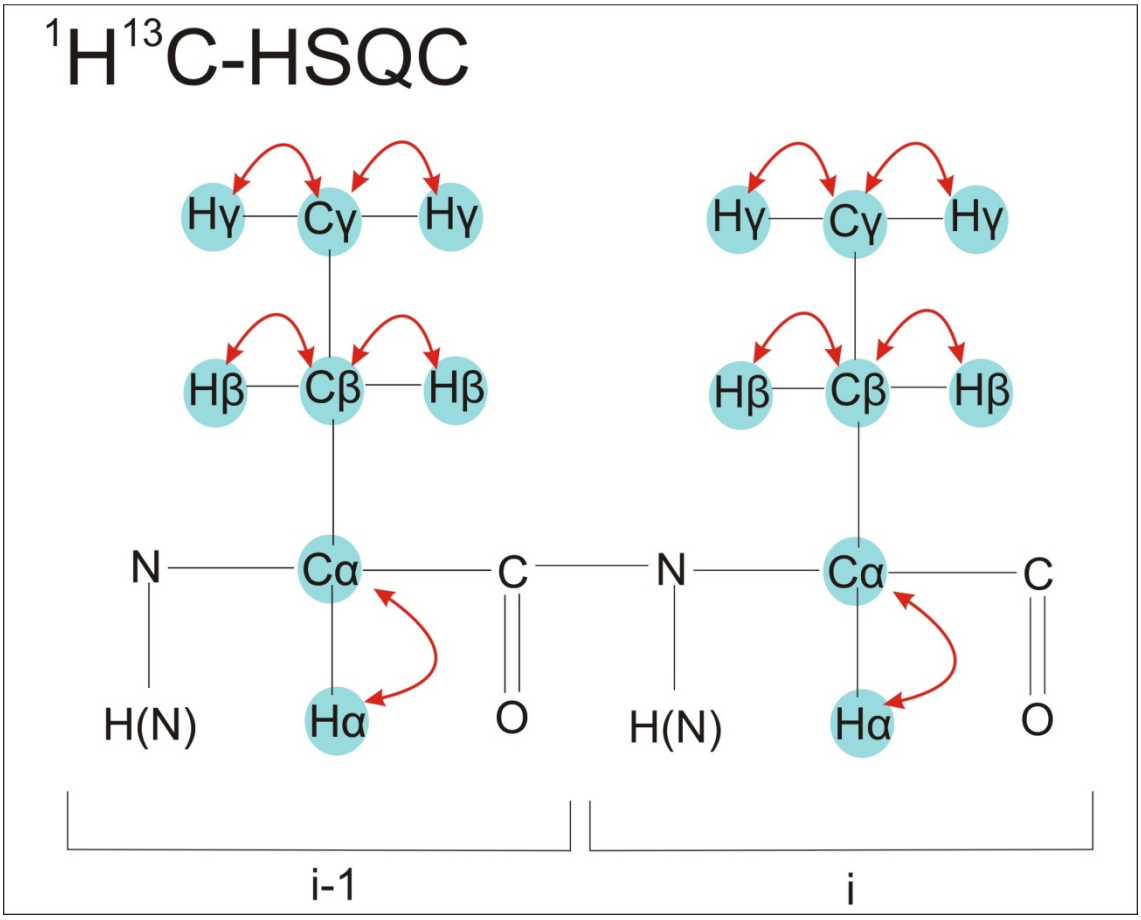

Figure 2.10 Transfer of magnetisation that occurs during a ^{13}C-HSQC. All transfers are within a single amino acid.

Two experiments were recorded to aid in the assignment of the ^{13}C - ^{1}H resonances from the side chains, both require a ^{13}C labelled sample of protein and the experiment is best undertaken in deuterated buffer to minimise the water solvent signal in the spectrum. The H(C)CH and (H)CCH TOCSY experiments work in a very similar way to one another (Figure 2.11). The TOCSY experiment generates cross-peaks between spins that are either directly

connected or that are connected by an unbroken chain of couplings. This allows the detection of couplings across an extended network such as an amino acid side chain by coherence transfer of magnetisation. The transfer of magnetisation along the network is dependent upon the mixing time of the experiment and the coupling constant between the two nuclei. The magnetisation transfer reaches maximum intensity in a time roughly equal to 1/(2J) where J is the largest coupling constant between the two spins in the system being observed. Thus when the system extends to beyond one coupling, the time required for magnetisation transfer is increased. This necessitates using a longer mixing time in the experiment. The experiment can be set up to label the magnetisation with the frequency of the detected proton, the carbon directly connected to it and a second carbon that is connected to it through an unbroken chain of couplings; this is a (H)CCH-TOCSY experiment. Alternatively the experiment can be set up to label the magnetisation with the frequency of the detected proton, the carbon directly connected to it and a second proton connected to a carbon that is connected to the first carbon through an unbroken chain of couplings. The second carbon does not label the magnetisation but merely provides a connection to the second proton. This is known as a H(C)CH-TOCSY experiment [60].

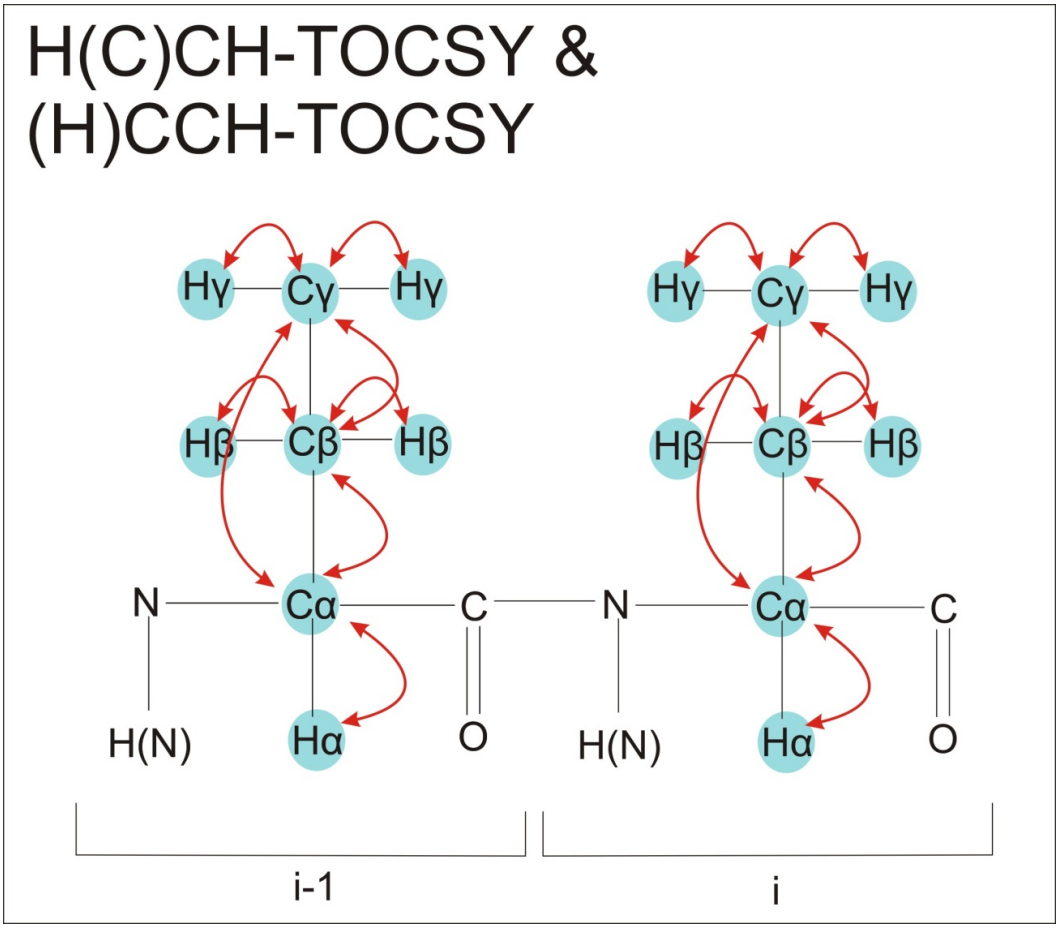

Figure 2.11 Transfer of magnetisation occurring in an (H)CCH or H(C)CH TOCSY experiment within a single amino acid.

2.13.5 Hydrogen/Deuterium exchange experiments

NMR samples of the N-terminal domain of Hsp90 labelled with ^{15}N were prepared as previously described in this chapter. A 300 µL sample of 600 µM protein was prepared in 20 mM Tris, 5 mM $MgCl_2$, Ph 8 using protonated distilled water. A sample of matching buffer (20 mM Tris, 5 mM $MgCl_2$, pH 8) was made using deuterated distilled water.

Initial NMR calibration for the experiment was undertaken using a 600 µL sample consisting of a 1:1 ratio of deuterated and protonated buffer without protein to act as a 'blank' sample. Immediately prior to the experimental start, the 300 µl protein sample was quenched with 300 µl of the matched deuterated buffer used for the blank calibration. Rapid calibration was undertaken using the previous 'blank' calibration to minimise the duration of this step. Subsequently HSQC spectra were recorded every 15 minutes for the first 10 h 30 min. The number of scans was then doubled and 30 min spectra were recorded for 11 h 30 min. The number of scans was then doubled again and 1 h spectra were recorded for 25 h. This experiment was repeated in the presence of a final concentration of 3 mM AMPPNP or 3 mM ADP. The spectra were processed as detailed in section 2.13.3 and the change in peak height intensity analysed using NMRPipe software[58].

3 The thermodynamics of N-terminal ligand binding and conformational flexibility

As has previously been detailed (see Chapter 1) the binding and hydrolysis of ATP to the N-terminal domain of Hsp90 is required for the function of the protein. The conformational changes induced by the ligand extend not only to the N-terminal domain but are observed across the entire protein. The control of the Hsp90 chaperone cycle therefore rests in interaction with the ligand, and thus a full understanding of the nature of the binding site is important for any future inhibitor design of the Hsp90 chaperone function. Once the binding of the isolated N-terminal domain is understood then its potential influence on the rest of the protein can be investigated.

In order to fully understand the binding of a ligand to the N-terminal domain it is important to know the thermodynamic parameters and any conformational changes associated with binding. The affinity (K_d), enthalpy (ΔH) and entropy (ΔS) of a binding event can all provide important information on the nature of the binding process as described in Chapter 1. Crystal structures of the N-terminal domain of Hsp90 in complex with ADP [8] and for the full length protein bound to p23 and AMPPNP[7] have been solved. This reveals two potential structures of the molecule, in the product (analogue)- and substrate-bound states respectively. Other studies, using fluorescence resonance energy transfer (FRET) to monitor the rate of conformational change induced by binding and hydrolysis of ATP, determined five distinct rate constants associated with the cycle of reactant binding, hydrolysis and product release[5]. It is clear that there is structural information missing between the five rate constants detected and the two known conformations. Such a dynamic process of binding, hydrolysis and induced conformational changes requires more information to fully understand than that provided by static crystal structures alone.

The nature of the binding site has been investigated using both ITC and NMR. The work falls into two main categories. First, binding of different nucleotide-based ligands was investigated using ITC. All errors shown for the ITC are taken from the fit of the titration determined by the Origin software. Following this the influence of pH on the binding of AMPPNP and ADP was investigated and revealed a significant difference in behaviour between the two ligands. This change was believed to be due to a protonation event which was then further investigated using both $^{1}H/^{15}N$ NMR and ^{31}P NMR.

The remainder of the chapter concerns the change in heat capacity (ΔC_p) upon ligand binding to the N-terminal domain of Hsp90. The different ligands binding to the same site within the N-terminal domain of Hsp90 have ΔC_p values of opposite signs (positive ΔC_p for AMPPNP binding compared to a negative ΔC_p for ADP binding). One of the many factors that can have a significant influence over the ΔC_p of binding is conformational change and consequent change in solvent exposed surface area. The ΔC_p was used to investigate possible changes in conformation of the 'ATP lid' region of the N-terminal domain of Hsp90 (residues 98 – 120). Mutations of the N-terminal domain of Hsp90 designed to stabilise the lid in either an open or closed conformation were used to investigate the influence on the binding constants and the ΔC_p associated with ligand binding.

3.1 The binding of ADP to the N-terminal of Hsp90 shows significant differences to the binding of AMPPNP to the same domain

3.1.1 Dissection of the thermodynamics of binding of AMPPNP to the N-terminal domain of Hsp90 reveals a destabilising effect of the γ-phosphate group on binding affinity

In order to understand the binding of AMPPNP to the N-terminal domain of Hsp90 the ligands ADP, adenosine and adenine were used to dissect the contributions of the chemical components of AMPPNP to its binding thermodynamics. The relationships of these molecules to each other are shown in Figure 3.1. By observing the thermodynamic profile of these substructures it begins to be possible to look at the contributions to binding of the different structural regions.

ITC titrations were performed for the interactions between the N-terminal domain and ADP, AMPPNP, adenine and adenosine across a temperature range from 10°C – 30°C. Additionally experiments were also performed with ADP and AMPPNP across a pH range of pH 10 – 5.

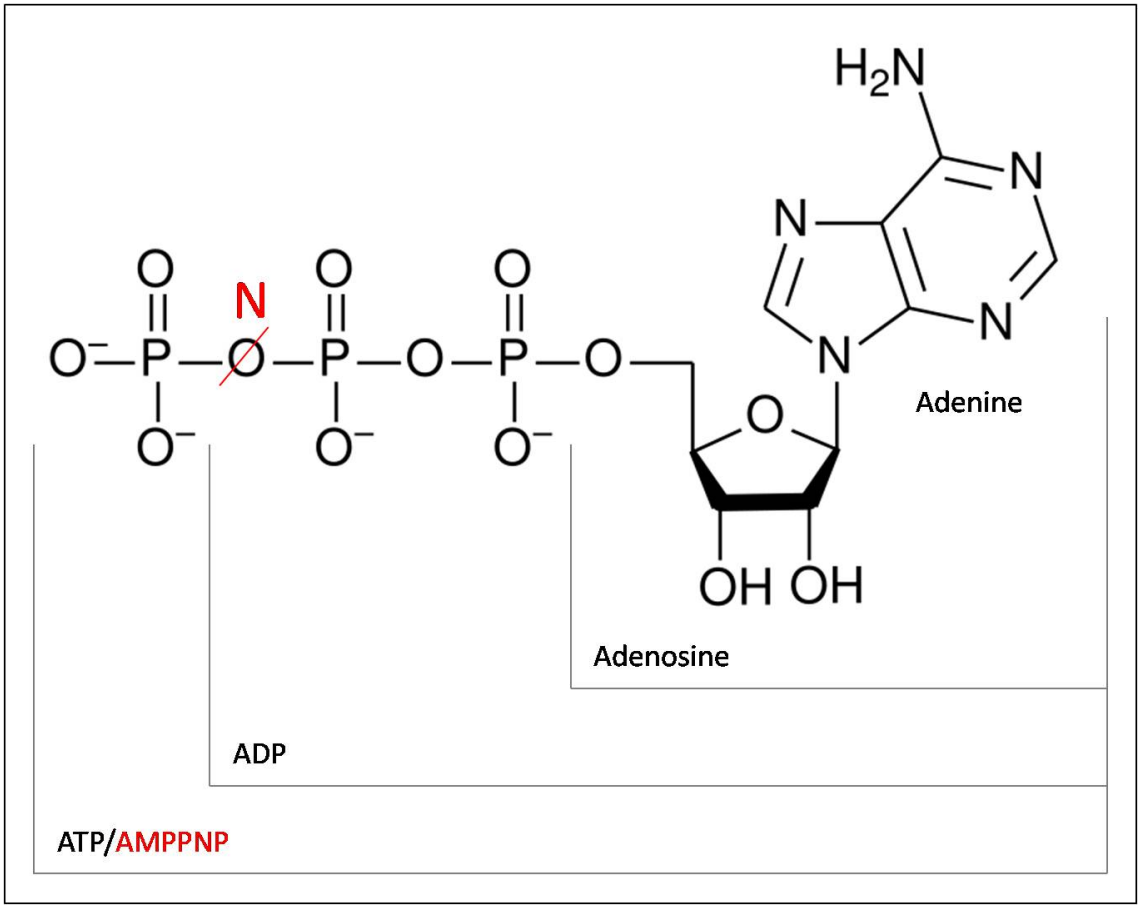

Figure 3.1 The ATP molecule (analogous to AMPPNP shown in red) highlighting the smaller ligands adenine, adenosine and ADP within the ATP structure.

Results for the nucleotide-based ligands are summarised in Table 3.1. ITC titrations initially undertaken in 20 mM Tris with ADP showed a binding affinity (K_d) of 19.6 µM at 15°C. Both entropy and enthalpy were negative with the process of binding being enthalpically driven with a favourable ΔG value of around -26 kJ·mol^{-1}. The binding of ADP is enthalpically driven similar to many other natural ligand binding situations[63]. While this binding is relatively weak, ADP has three times greater affinity than the binding of AMPPNP to the NT domain whose K_d is 74.6 µM at 15°C. Results are shown at 15°C due to very small enthalpy values at 25°C making the ITC data for adenine too difficult to fit.

N-terminal w/	K_d (μM)	Error (K_d)	ΔH (kJ mol^{-1})	Error (ΔH)	TΔS (kJ mol^{-1})	ΔG (kJ mol^{-1})
Adenine	101.5	±18.0	-10.1	±0.8	+12.3	-22.4
Adenosine	67.2	±1.7	-45.9	±1.3	-22.9	-23.0
ADP	19.6	±0.9	-74.7	±1.0	-48.8	-25.9
AMPPNP	74.6	-	-35.9	±0.3	-13.1	-22.8

Table 3.1 Thermodynamic parameters of binding of ligands adenine, adenosine, ADP and AMPPNP as determined by ITC at 15°C in 20 mM Tris, 5 mM Mg^{2+} pH 8. (AMPPNP data from Nilapwar et al. 2009[17]).

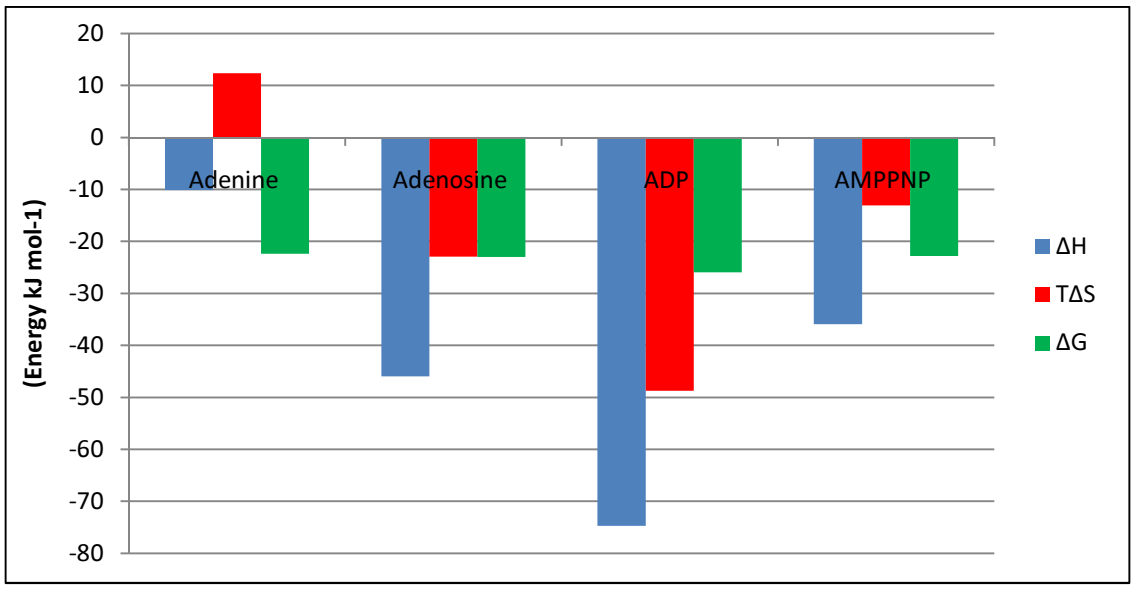

Figure 3.2 The ΔH TΔS and ΔG values for the four ligands adenine, adenosine, ADP and AMPPNP binding to the N-terminal of Hsp90 as determined by ITC at 15°C in 20 mM Tris, 5 mM Mg^{2+} pH 8.

The binding of adenosine shows a similar affinity to that of AMPPNP at around 70 μM with a free energy of -23.0 kJ·mol^{-1}. It also shows a similarly enthalpically driven thermodynamic profile. The adenine moiety contributes most of the binding affinity of the nucleotide based ligand with a K_d of around 100 μM. Adenine also shows an entropically driven profile very different to that seen by the other ligands. The binding of AMPPNP is less favourable than the binding of the product ADP. The binding of the product more tightly than the substrate is unusual given the need for removal of the product from the binding site. This may indicated that the remainder of the protein plays a role in ATP turnover.

A paper by Nilapwar et al. [17] showed that the binding of AMPPNP to the N-terminal of Hsp90 changed dramatically with respect to pH. Although this effect was noted it was not fully explored within the paper. This response could indicate presence of a protonation event upon binding. As has already been stated, one way to investigate the nature of the binding site is to look at the binding of the chemical components of ATP to the N-terminal domain of Hsp90. Given that there is a significant difference between the binding affinities of ADP and AMPPNP to the N-terminal domain of Hsp90 at pH8, the next logical step would be to investigate whether the binding of ADP responded to a change in pH in a similar way to that of AMPPNP. Then confirmation of whether the effect is the result of a protonation event or not can be investigated.

3.1.2 Nucleotide based ligand binding to the N-terminal of Hsp90

The thermodynamics of ligand binding to the N-terminal domain of Hsp90 can be considered with respect to the binding of increasingly extending ligand molecules, from adenine to AMPPNP. In this context it is possible to see some interesting features emerging. The dissociation constant of adenine is within the μM range suggesting that the adenine moiety contributes most to the binding affinity. This is a view supported by the packing of the adenine ring against the β-sheet of the NT binding domain as seen in the crystal structure. The binding of adenosine is comparable to the binding of AMPPNP. This suggests that the addition of the ribose ring leads to a stabilisation of the binding as seen by the lower dissociation constant. The contacts made by the ribose ring include one direct contact with Asn92[8] and a number of contacts made with the water molecules within the binding site. It is interesting to note that despite the presumable trapping of water molecules within the binding site upon the binding of adenine the entropy is still favourable. This favourable entropy is probably caused by the displacement by adenine of additional water molecules within the binding site that counteracts the trapping of water. In contrast the addition of the ribose group then leads to an unfavourable entropy. This may indicate that additional water molecules are trapped by the ribose moiety that cannot be fully counteracted by the initial displacement of water.

The addition of the two phosphate groups in ADP has the most stabilising effect beyond the initial adenine ring, reducing the K_d to 19.6 μM. These two phosphate groups are thought to mediate contacts between the ligand and several residues via a water molecule network and one direct contact with Lys98 [8]. It is also thought that it mediates several contacts to a magnesium ion known to be essential for ATP, AMPPNP and ADP binding. The

thermodynamic profile also changes quite dramatically with both increased entropy and enthalpy values compared to adenosine.

The addition of the third phosphate group with AMPPNP appears to have a destabilising effect upon the binding affinity as it is reduced from 19.6 µM to 74.6 µM, close to that of the base adenosine molecule. The values of ΔH and TΔS are slightly less negative than those recorded for adenosine. These subtle changes in enthalpy and entropy may well be due to the trapping and release of additional water molecules within the binding site by the terminal phosphate group as well as any direct contacts between the γ-phosphate and the closed lid seen in crystal structure of the full length protein [7]. The degree of change of the binding affinity suggests that the number of water molecules affected by the γ-phosphate is roughly equal to the number of water molecules affected by the α and β-phosphates but with opposing influence. It is known that ATP (and presumably thus AMPPNP) must adopt a kinked conformation within the binding site – the presence of the terminal phosphate may well allow the final structural rearrangements of the ligand that is likely to put it under strain that might make binding less favourable. This combined with any stabilisation of the 'lid closed' state may put the remainder of the domain under strain not seen under other ligand bound states.

3.1.3 ITC reveals distinctly different pH dependencies of binding affinity for ADP and AMPPNP

A comparison set of data looking at the binding of ADP with respect to pH was collected at 15°C in the same triple buffer conditions (See Table 3.2 and Figure 3.2).

From Table 3.1 and Figure 3.2 it can be seen that although there is some variation in the binding affinity of ADP to the N-terminal domain of Hsp90, the changes are negligible compared to those observed for AMPPNP where the K_d varied by a factor of 10 from ≈20 µM to ≈200 µM across the entire pH range (Figure 3.3).

pH	N Stoichiometry	K_d (μM)	Error (K_d)	ΔH (kJ mol^{-1})	Error (ΔH)	TΔS (kJ mol^{-1} K^{-1})	ΔG (ΔH-TΔS)
pH10	1.05	18.8	±1.1	-71.8	±1.0	-43.7	-28.1
pH9.5	1.01	24.0	±1.5	-76.7	±1.4	-50.9	-25.8
pH9	1.05	14.5	±0.8	-84.6	±1.3	-57.9	-26.7
pH8.5	0.95	15.6	±1.3	-82.3	±2.1	-55.9	-26.4
pH8	1.00	19.6	±0.9	-74.7	±1.0	-48.7	-26.0
pH7.5	1.06	6.4	±0.3	-70.3	±1.8	-41.7	-28.6
pH7	1.00	8.6	±0.6	-70.6	±1.3	-42.7	-27.9
pH6.5	0.98	9.9	±0.9	-69.4	±1.8	-41.8	-27.6
pH6	1.10	11.1	±1.2	-73.2	±2.7	-45.8	-27.4
pH5.5	1.04	10.5	±0.7	-55.7	±1.3	-28.2	-27.5
pH5	1.09	15.9	±1.8	-75.4	±3.6	-49.0	-26.4

Table 3.2 pH dependence of ADP binding to the N-terminal domain of Hsp90 by ITC at 15°C in 20 mM Tris 5 mM Mg^{2+}.

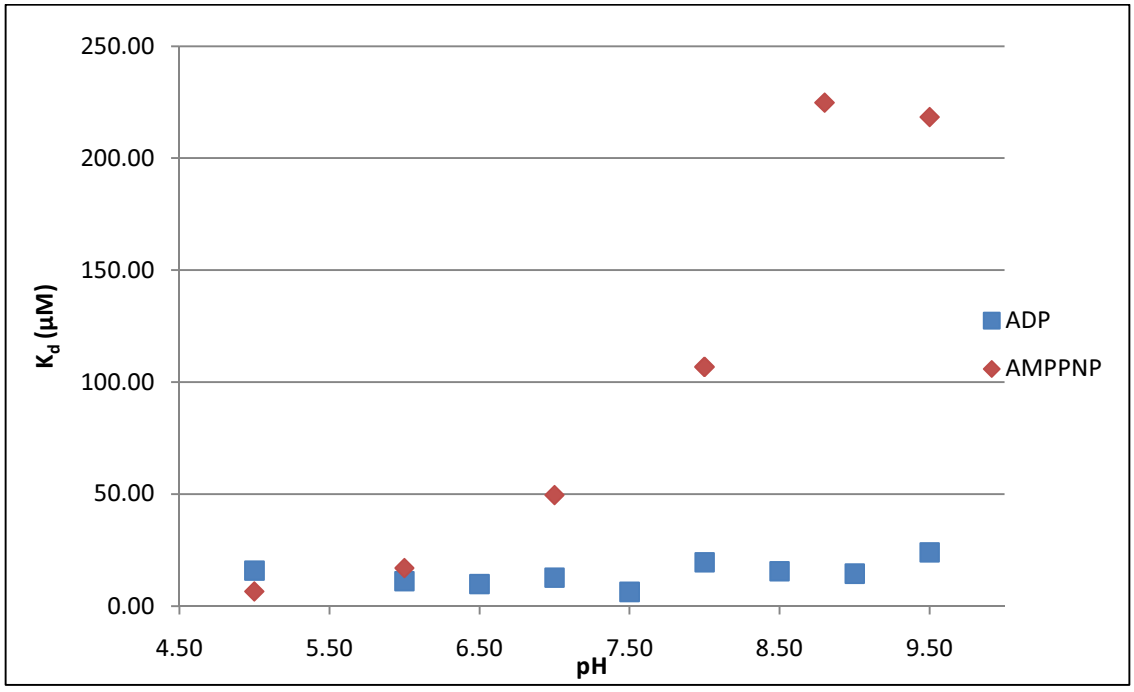

Figure 3.3 The pH dependence of AMPPNP and ADP binding to the N-terminal domain of Hsp90 binding determined by ITC at 15°C in 50 mM Ethanolamine, 100 mM ACES, 50 mM Tris Base, 5 mM Mg^{2+} (AMPPNP values were taken from Nilapwar et al. [17]).

A fit of the K_d to equation 3.1 describing one event upon ligand binding across a range of pH9.5 - pH5 gave pKa values for the protonation of the free (pH 6.5) and bound states (pH8.0) [64] (See Figure 3.4).

$$K_{obs} = K_b \frac{1+10^{(pKa)_b - pH}}{1+10^{(pKa)_f - pH}} \quad (3.1)$$

Equation 3.1 Single proton linkage (K_{obs}) as a function of the bound and the free pK_a values for the protonation event as described by Bradshaw et at.[65]

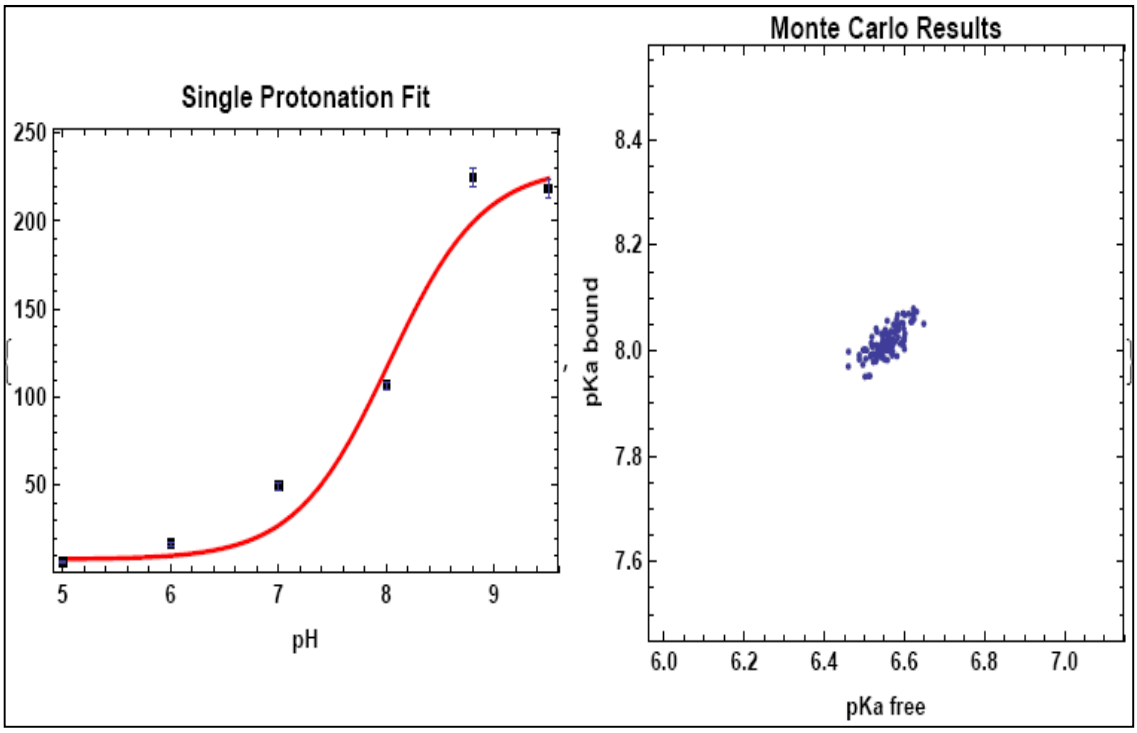

Figure 3.4 A single protonation fit of the K_d data of the binding between AMPPNP and the N-terminal domain of Hsp90 by ITC across a pH range. The corresponding Monte Carlo results show the range of values possible for both the bound and free pK_a of the protonation event. Single protonation fitting and Monte Carlo analysis undertaken by Dr. Mark Williams – Birkbeck College London.

3.1.4 Uncovering the number of protonation events associated with binding of ADP and AMPPNP to the N-terminal of Hsp90 using the heats of ionisation of different of buffer solutions

ITC has been used to probe the binding affinity of ADP and AMPPNP with respect to pH and has identified a potential protonation event at pH7. A single protonation event associated

with binding has been assumed, however data fitting alone cannot exclude the possibility of multiple protonation events. Further characterisation of this protonation event is possible exploiting the differing heats of ionisation of a variety of buffers as described in the Introduction chapter.

The heats of ionisation can be used to confirm the number of protons involved in a binding event [64-66] as previously only a single protonation event was assumed. A series of ITC experiments were carried out in five different buffers with both ADP and AMPPNP at pH7.5. This pH is approximately midway between the bound and free pK_a's and should give the maximum change in enthalpy arising from the change of protonation state. The results are summarised in Tables 3.3 and 3.4. A plot of the specific enthalpy of ionisation of each buffer against the ΔH value can be used to determine the number of protons involved in a protonation event as described by Baker et al. [64] and detailed in chapter 2 (also see Figures 3.5 and 3.6).

Buffer	Stoichiometry (N)	K_d (μM)	Error (K_d)	ΔH (kJ mol^{-1})	Error (ΔH)	TΔS (kJ mol^{-1})	ΔG (kJ mol^{-1})	Heat of ionization (kJ mol^{-1})
Hepes	1.1	35.9	±0.7	-95.7	±0.8	-70.4	-25.4	21.0
Hepes	1.0	21.9	±0.8	-59.7	±0.6	-33.1	-26.6	21.0
Pipes	0.9	34.7	±1.1	-95.1	±1.3	-69.7	-25.5	11.5
Pipes	0.9	34.2	±1.1	-93.8	±1.4	-68.3	-25.5	11.5
Tris	1.1	35.7	±1.8	-91.2	±2.2	-65.8	-25.4	47.3
Tris	1.1	44.5	±6.0	-92.3	±6.7	-67.4	-24.8	47.3
Bis Tris	1.1	43.5	±2.6	-77.5	±2.3	-52.5	-24.9	28.2
Bis Tris	1.1	39.8	±2.2	-72.6	±1.8	-47.5	-25.1	28.2
ACES	1.0	33.6	±1.6	-75.0	±1.5	-49.5	-25.5	31.3
ACES	1.0	53.0	±8.2	-72.8	±4.7	-48.3	-24.4	31.3

Table 3.3 The binding of the N-terminal domain of Hsp90 to ADP by ITC at 25°C, pH 7.5 in 50 mM buffer, 20 mM NaCl, 5 mM Mg^2. The heats of ionisation for each buffer are shown.

Buffer	Stoichiometry (N)	K_d (μM)	Error (K_d)	ΔH (kJ mol^{-1})	Error (+/-)	TΔS (kJ mol^{-1})	ΔG (kJ mol^{-1})	Heat of ionization (kJ mol^{-1})
ACES	1.0	60.4	±3.4	-29.5	±1.6	-5.4	-24.1	31.3
ACES	1.0	61.8	±4.3	-31.0	±2.2	-7.0	-24.0	31.3
Pipes	1.0	80.5	±4.7	-47.5	±3.7	-24.2	-23.4	11.5
Pipes	1.0	76.2	±2.2	-41.8	±1.4	-18.4	-23.5	11.5
BisTris	1.1	70.3	±2.8	-39.7	±1.8	-15.9	-23.2	28.2
Hepes	1.0	87.5	±2.3	-54.6	±1.4	-31.5	-23.1	21.0
Hepes	1.0	90.3	±1.4	-56.3	±2.4	-33.2	-23.7	21.0

Table 3.4 The binding of the N-terminal domain of Hsp90 to AMPPNP by ITC at 25°C, pH 7.5 in 50 mM buffer, 20 mM NaCl, 5 mM Mg^{2+}. The heats of ionisation for each buffer are shown.

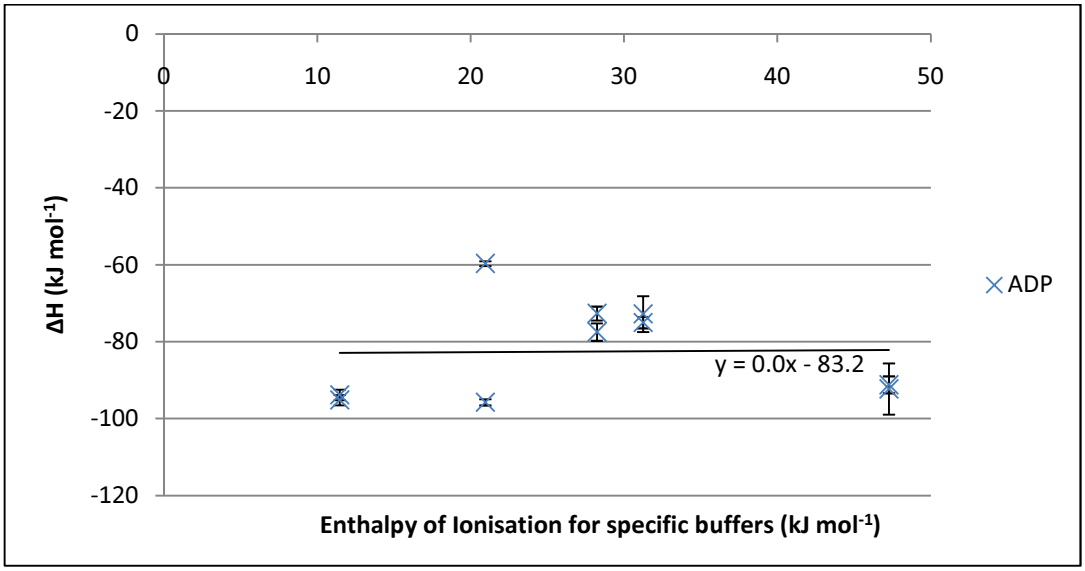

Figure 3.5 The enthalpy of the binding of ADP to the N-terminal domain of Hsp90 determined by ITC plotted against the ionisation enthalpy constants of the buffers the titrations were performed under. ITC was carried out at 25°C, pH 7.5 in 50 mM buffer, 20 mM NaCl, 5 mM Mg^{2+}.

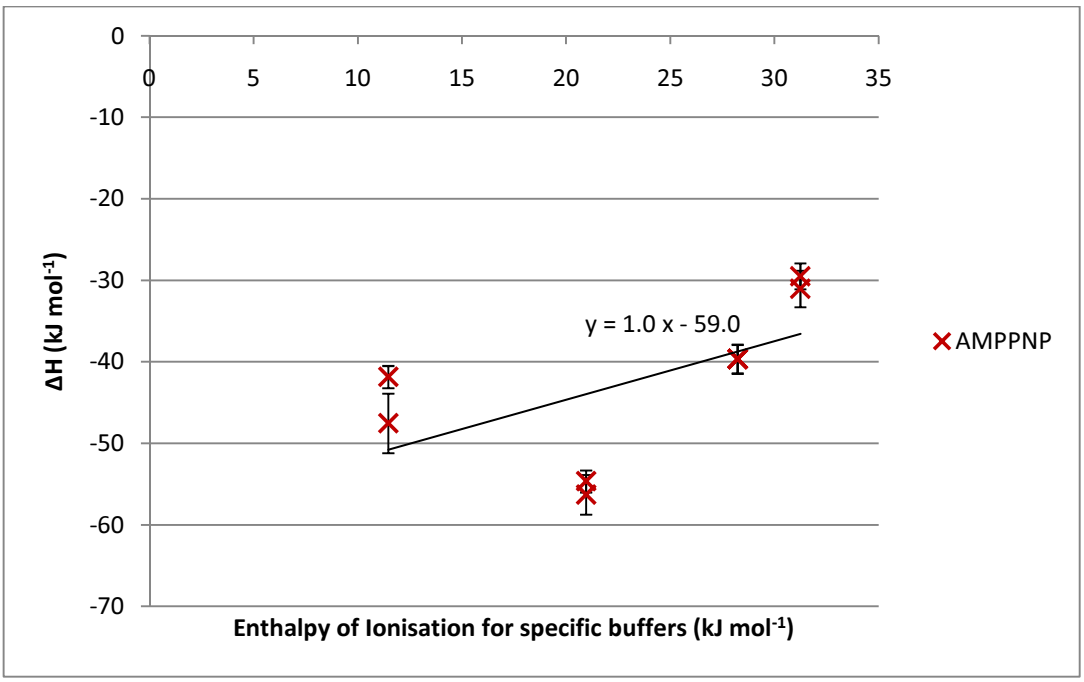

Figure 3.6 The enthalpy of the binding of AMPPNP to the N-terminal domain of Hsp90 determined by ITC plotted against the ionisation enthalpy constants of the buffers the titrations were performed under. ITC was carried out at 25°C, pH 7.5 in 50 mM buffer, 20 mM NaCl, 5 mM Mg^{2+}.

Figures 3.5 and 3.6 show a clear difference in the proton linkage of the two ligands ADP and AMPPNP in their binding to Hsp90 at pH 7.5. ADP shows close to 0 (1 d.p.) protons taken up/released upon binding in comparison to 1 (1 d.p) proton taken up/released upon binding to AMPPNP thus confirming a single protonation event associated with the binding to the N-terminal domain of Hsp90 at pH7.5. This is consistent with the fit of the binding affinities as described previously to a single protonation event. However the information this provided still does not reveal whether the protonation event is on the protein or the ligand.

3.1.5 Variation in the K_d of AMPPNP binding to the N-terminal of Hsp90 compared to the binding of ADP to the same with respect to a change in pH

The strong pH dependence of binding AMPPNP but not ADP, to the N-terminal domain of Hsp90 suggests that the sensitivity to pH originates in the interaction of the terminal γ-phosphate of the molecule. The destabilising effect of the γ-phosphate is only apparent at pH values of 7 and above which suggests that a protonation event may be occurring that affects binding, i.e. in the physiological range. Although the most likely source of this protonation is the γ-phosphate itself this cannot be verified by ITC alone.

From what is known about the properties of the isolated ligands ADP and ATP, the fitted pK_a value for the free state in the AMPPNP/Hsp90 interaction coincides with the transition of ATP from an $ATP^{-3}.Mg^{2+}$ state to an $ATP^{-4}.Mg^{2+}$state [67]. The assumption is made that AMPPNP behaves in a similar way to ATP. At low pH values both ADP and ATP are in a -3 charge state and both show similar binding affinities to the N-terminal of Hsp90 of around 19µM. As the pH increases the binding affinity of AMPPNP decreases however the affinity of ADP does not change. Co-incident with this as the pH increases the charge state of AMPPNP changes to -4 through deprotonation of the γ-phosphate while ADP remains in a -3 charge state. This implies that the -3 charge state is the preferred state for binding.

3.2 pH dependence of NMR spectra of the apo and AMPPNP bound states of the Hsp90 N-terminal domain

NMR can be used to observe the behaviour of individual amino acids directly in response to changes in environmental conditions. If a change in the protonation state of an amino acid residue occurs this will not only induce changes in chemical shift for that amino acid but also to others nearby due to a local environmental change.

A series of HSQC spectra were collected at each half pH unit from 5 to 9.5 for both the apo and the AMPPNP bound state of the NT domain. Peak shifts induced by the pH change were used to identify whether or not a protonation event occurred on the protein.

In addition, in order to directly observe the phosphorus groups on the AMPPNP molecule by NMR, a series of 1D spectra were collected using a ^{31}P phosphorus probe. Spectra across the pH range 5 – 10 were recorded to observe the ligand directly to identify a protonation event occurring across this range.

3.2.1 Observation of change in chemical shifts by 2D protein NMR identified residues affected by the protonation event across the pH5 – 10 in the apo state.

Initially ^{15}N NMR HSQC spectra of the NT domain in the apo-state were collected across the pH range 5 – 10 at every half pH unit. Peaks where changes in chemical shift (hereafter referred to as 'chemical shifts' or 'shifts') were induced by a change in pH were identified using the backbone assignments [15]. Shift differences between pH5.5 and 6.5, 6.5 and 7.5, 7.5 and 8.5 and 8.5 and 9.5 were identified and quantified. The magnitude of the overall shift for each pH unit interval was calculated based upon the relationship between proton and nitrogen shifts given by:

Combined H/N shift = Proton shift + (nitrogen shift/6.4) (3.2)

(Taylor J. PhD Thesis UCL. 2006 – Internal lab results.)

Equation 3.2. Calculation of the combined proton and nitrogen shift used to compare peak shifts.

This equation allows for direct comparison of the range of shifts in the proton and nitrogen dimensions. It accounts for the greater scale over which the nitrogen shifts are observed compared to the proton shifts. Thus the contribution of the proton shift is equal to the contribution of the nitrogen shift in the calculated values for the overall shift.

Residues with shifts < 0.01 (combined H/N ppm) in at least one pH unit range were considered to be unaffected and not analysed further. No significant shifts were observed between pH 5 and pH 5.5. From the analysis of the peaks significant shifts can be identified across each pH range (Figures 3.7 and 3.8) and each shift compared between residues and across the pH range (see Figure 3.9).

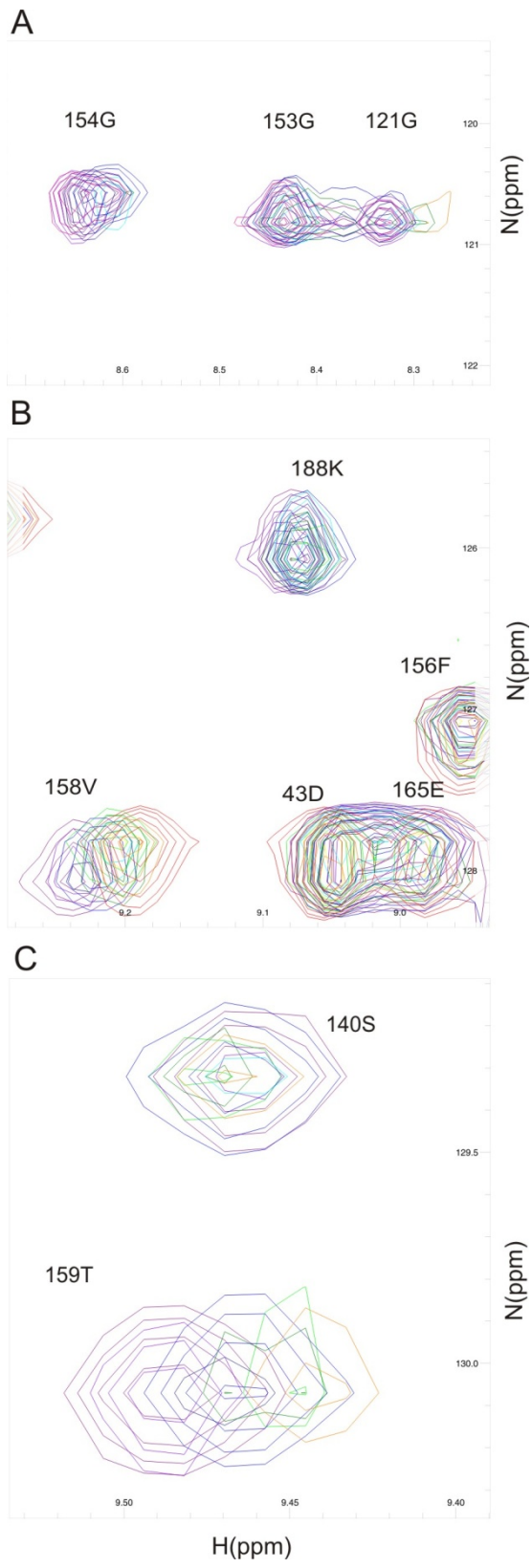

Figure 3.7 pH dependent peak shifts of selected peaks from the N-terminal domain of Hsp90 in the apo state. ^{15}N labelled sample at 300 µM in triple buffer. Colouring of peaks runs from high pH (red) to low pH (purple) through the spectrum.

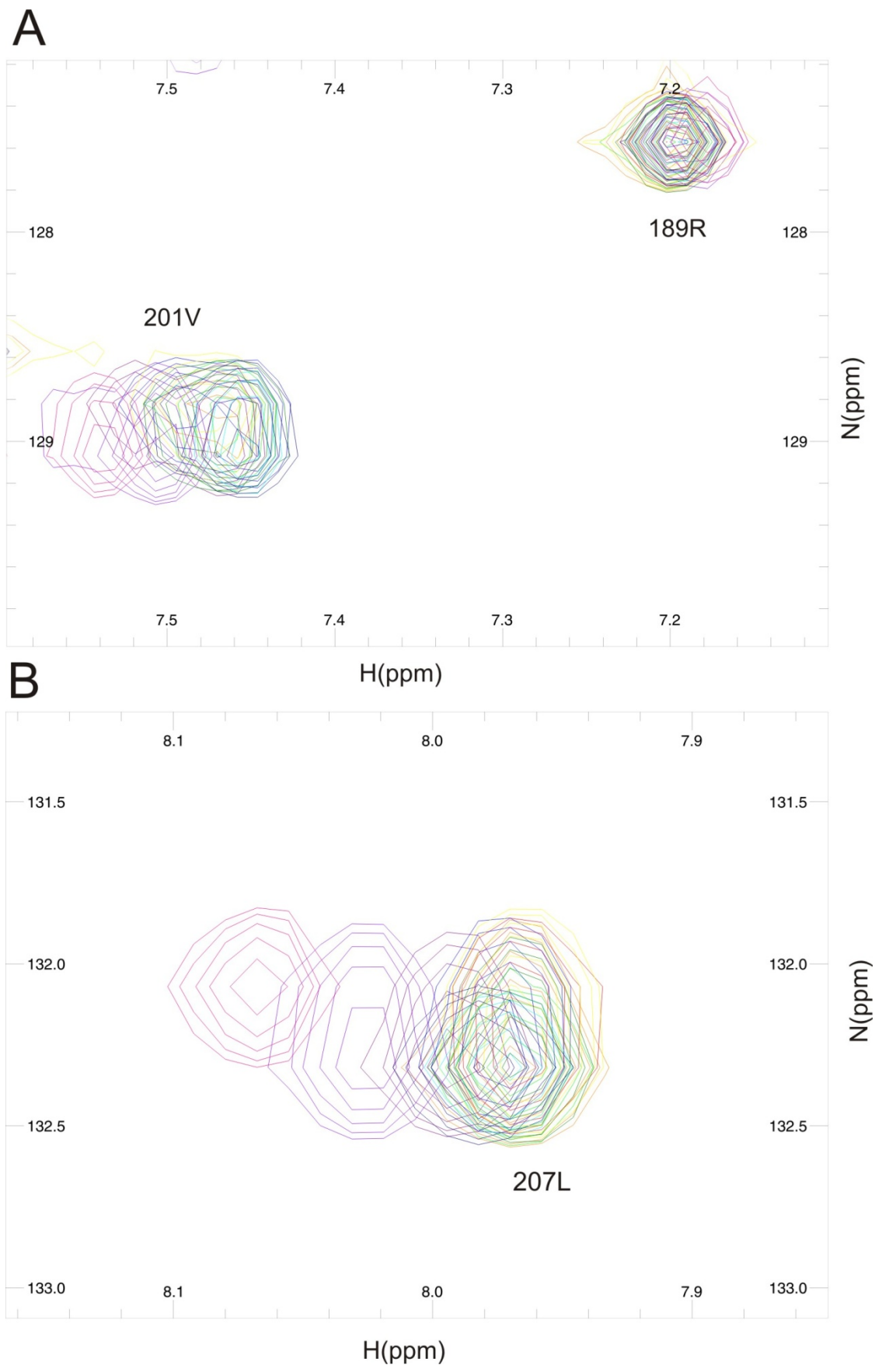

Figure 3.8 pH-dependent peak shifts of selected peaks from the N-terminal domain of Hsp90 bound to AMPPNP. ^{15}N labelled sample at 300 µM in triple buffer. Colouring of peaks runs from high pH (red) to low pH (purple) through the spectrum.

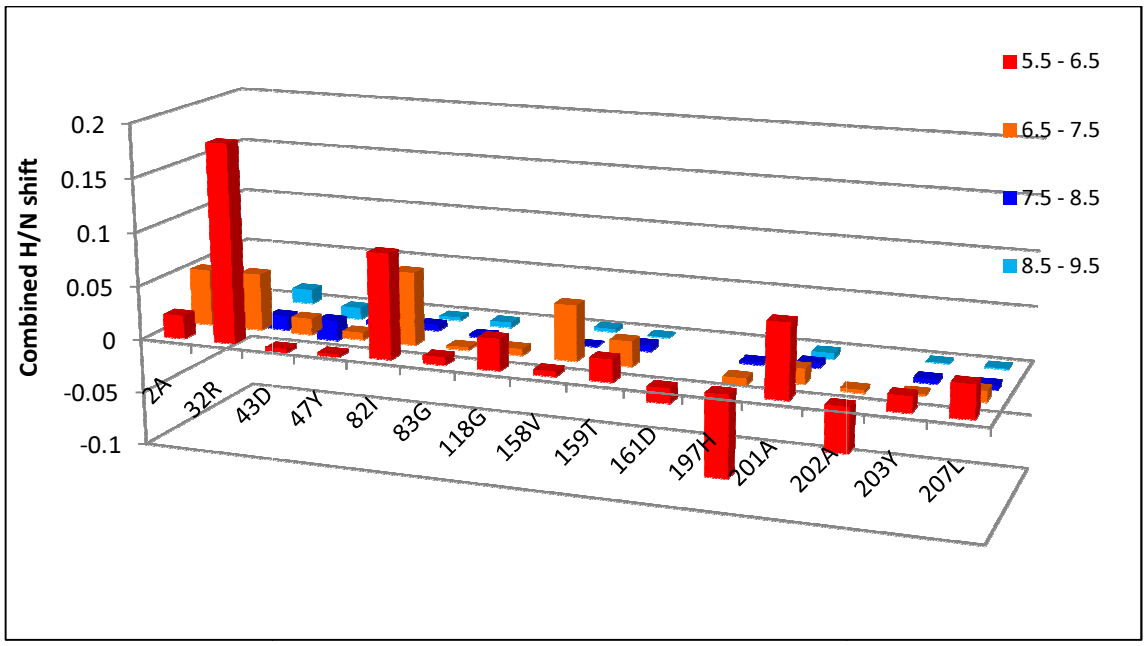

Figure 3.9 Combined $^{15}N/^{1}H$ chemical shifts for the apo state N-terminal domain of Hsp90 in response to a change in pH. Shifts are shown across the range 5.5-6.5, 6.5-7.5, 7.5-8.5 and 8.5-9.5.

From figure 3.9 it is clear that in the apo state there are two events which occur. The first is in the low pH range between pH5.5 and pH6.5 with residues Arg32, Ile82, Gly83, Gly118, Asp161, His197, Ala201, Ala202, Tyr203 and Leu207. The second event that occurs is in the slightly higher pH range at pH 6.5 – 7.5 involving residues Ala2, Asp43, Tyr27, Val158 and Thr159. The residues with these shifts have been mapped onto the crystal structure for the N-terminal domain of Hsp90[8] with low pH shifts (pH 5.5 – 6.5) in red and those at the higher pH (pH 6.5 – 7.5) in orange (see Figure 3.10).

The shifts observed for the apo-N-terminal domain of Hsp90 can be divided into two groups based upon the pH range at which the greatest shift is detected. These are shown in Figure 3.10 in red for the lower pH and orange for the higher pH. Two of the most prominent shifts at the lower pH are residues Arg32 and His197. The histidine imidazole side chain has a pKa value of around 6 which is within the pH range (5.5 – 6.5) described. His197 is the only histidine in the N-terminal domain and also the only residue with a side chain titratable at this pH value. The close proximity of the side chains of Arg32 and His197 is such that a protonation event on His197 may well influence the environment of Arg32 sufficiently to explain the large chemical shift detected by NMR. In the same pH range shifts are also observed for Gly118, Val201, Ala202, Tyr203 and Leu207 as well as Ile82, Gly83 and Asp161. The shifts on the first five residues listed could be explained by propagation of any change to the His197 side chain upon protonation. The later three are somewhat distant from His197 and so their shift is less easily explained by changes to the His residue. The pKa of the Asp side chain is around 4 which

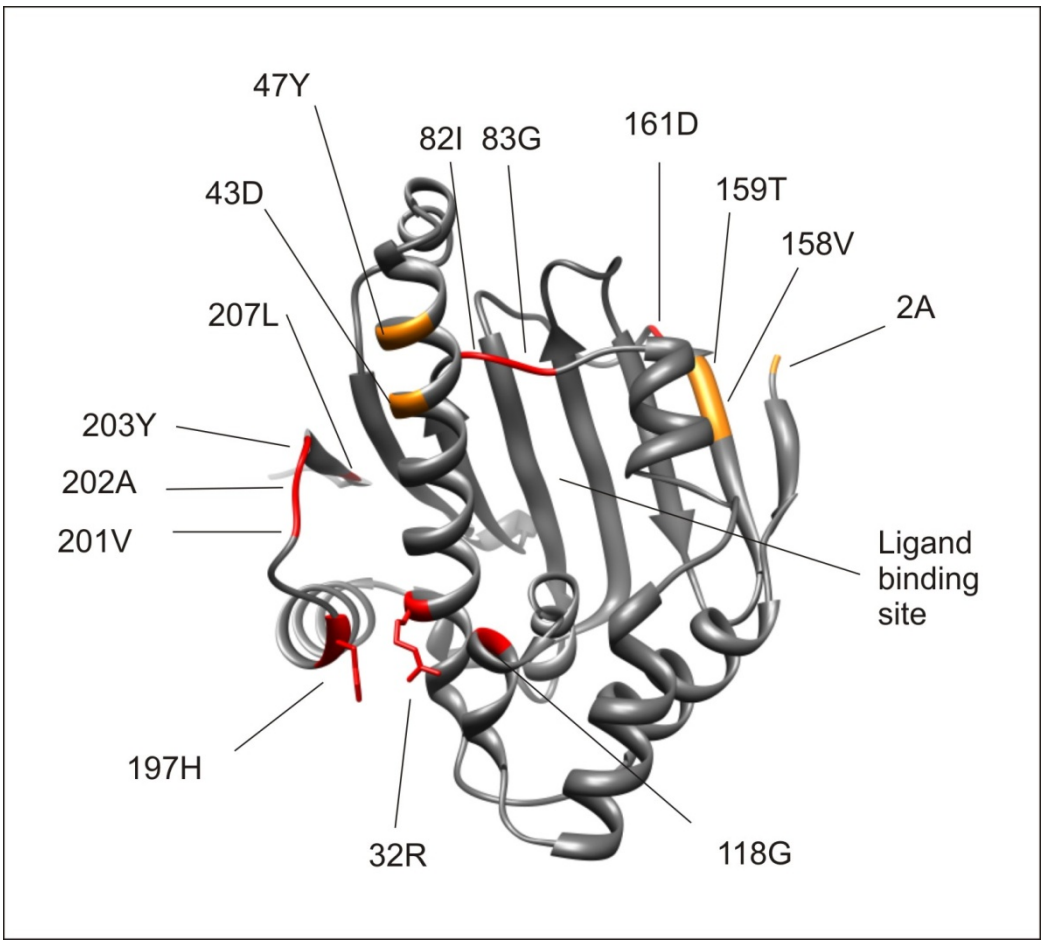

Figure 3.10 Chemical shifts of the apo N-terminal domain of Hsp90 induced by a change in pH are shown here on the crystal structure taken from PDB file 1AMW of the ADP bound domain. It is assumed that the apo state and the ADP state are structurally similar. Residues highlighted in red indicate large shifts while residues highlighted in orange indicate smaller shifts.

is fairly distant from the pH5.5-6.5 range observed however it is possible that the location of Asp161 within the folded protein might alter the pKa value to closer to the range being observed however this cannot be easily confirmed here as observations are not directly of the side-chain but of the backbone. The shifts observed for Ile82 and Gly83 may be influenced by Asp161 as they are relatively close however this is unconfirmed.

The second set of observed shifts is at a slightly higher pH within the range 6.5 – 7.5. These residues include Asp43, Tyr47, Thr159, Val158 and Ala2. On the structure these five residue fall into two groups – The first includes Thr159, Val158 and Ala2 are all in close proximity and may be linked to the same cause. The involvement of the N-terminal strand in this set may suggest that flexibility of this strand in the apo state may be somewhat pH dependent. The second set includes Asp43 and Tyr47 which are at one end of the long helix and fairly exposed to the solvent.

3.2.2 Observation of chemical shifts by 2D protein NMR identified residues affected by the protonation event across the pH5 – 10 in the AMPPNP bound state.

A second set of NMR spectra were obtained across the same pH range however these were done in the presence of AMPPNP. Shifts were detected and analysed in the same way to the apo-dataset with the following shifts identified (see Figure 3.11). Again shift differences across the range of pH5 to 6.5 and then every unit from 6.5 to 7.5, 7.5 to 8.5 and 8.5 to 9.5 were identified and the same selection criteria as for the apo dataset were applied. The magnitude of the overall shift for each pH unit interval was calculated in the same way as for the apo-data (equation 3.2). In this case pH5 data were included, since in the presence of ligand shifts were observed between pH5 and pH5.5.

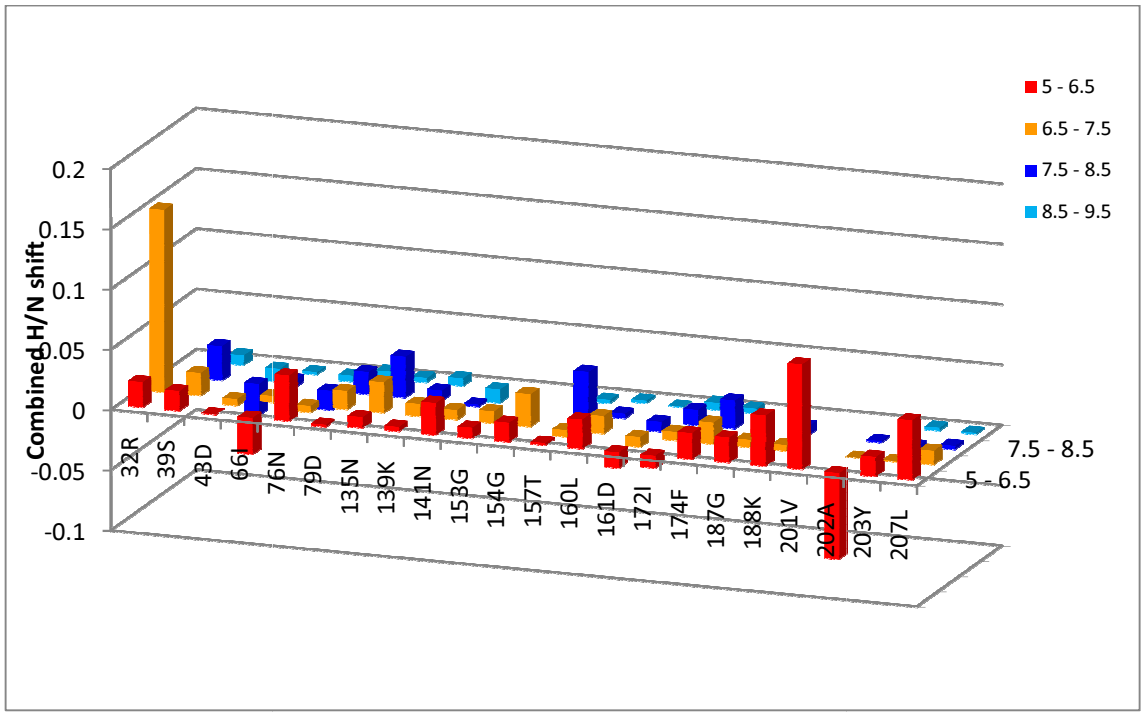

Figure 3.11 Combined $^{15}N/^{1}H$ chemical shifts for the AMPPNP bound N-terminal domain of Hsp90 in response to a change in pH. Shifts are shown across the range 5.0-6.5, 6.5-7.5, 7.5-8.5 and 8.5-9.5

From Figure 3.11 it can be seen that in the AMPPNP bound state of the N-terminal of Hsp90 there are three events caused by a change in pH: one in the low pH range between pH 5 and pH 6.5 involving residues Ile66, Asn76, Asn141, Leu160 Asp161, Gly187, Lys188, Val201, Ala202, Tyr203, and Leu207: the second between the pH values of 6.5 – 7.5 involving residues Arg32, Gly153 and Gly154: the third in the mid/high pH range from pH 7.5 to pH 9.5 involving residues Ser39, Asp43, Asp79, Asn135, Lys139, Thr157, Ile172 and Phe174. These shifts have

been mapped onto the crystal structure for the N-terminal domain of Hsp90[8] with shifts between pH 5 – 6.5 in red, shifts between pH 6.5 – 7.5 in orange and shifts from pH 7.5 – 9.5 in blue (see Figure 3.12).

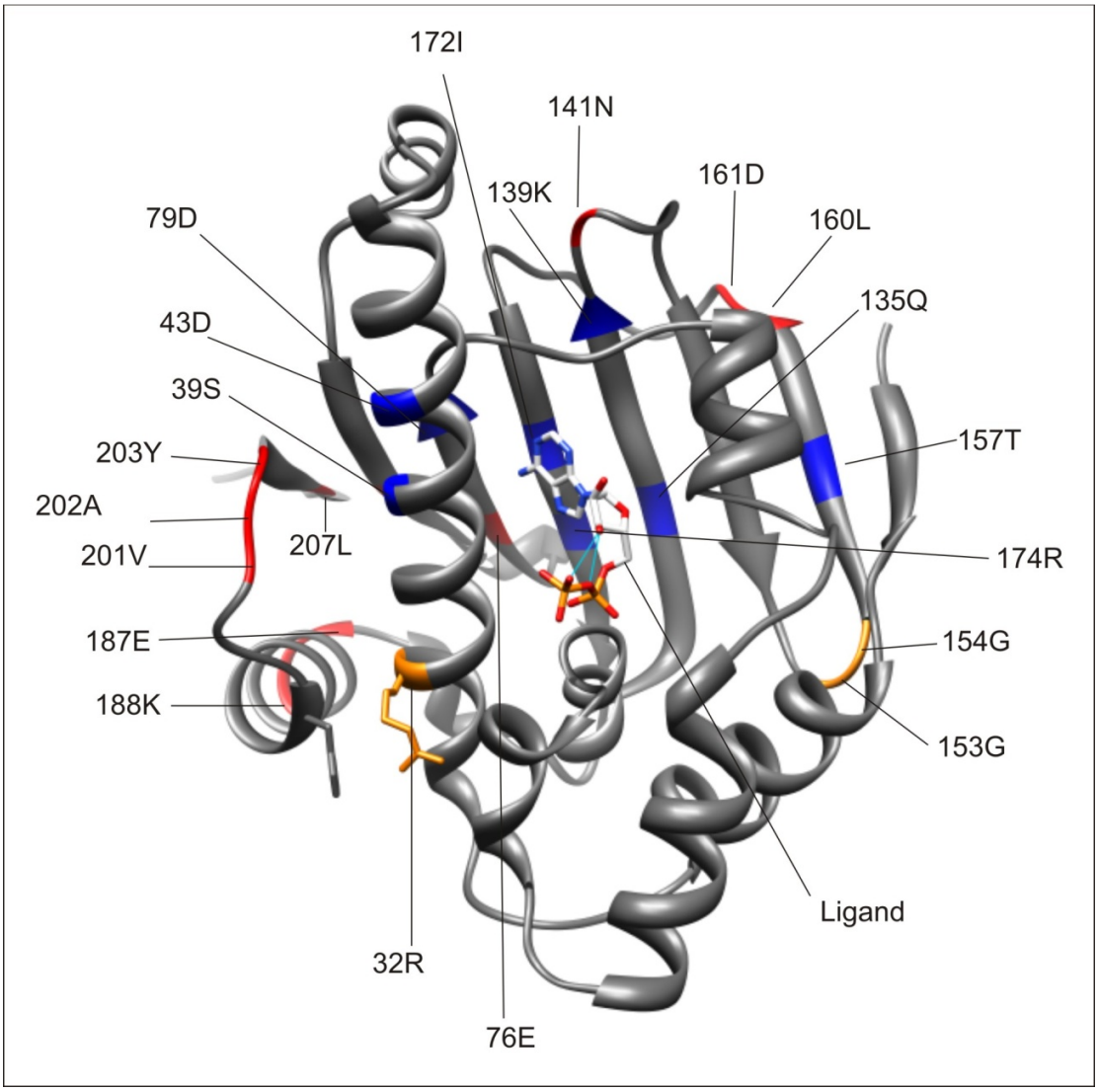

Figure 3.12 Chemical shifts on the AMPPNP bound N-terminal domain of Hsp90 induced by a change in pH are shown here on the crystal structure taken from the PDB file 1AMW. Residues highlighted in red indicate shifts observed in the low pH range (pH5 – 6.5). Residues highlighted in orange indicate shifts observed between pH6.5 – 7.5. Residues highlighted in dark blue indicate shifts observed between pH7.5 – 9.

In the AMPPNP bound state, three events occur at distinct pH ranges. The first low pH event involves Asp161, Leu207, Tyr203, Ala202, Val201, Glu187 and Lys188. The first four residues were also implicated in the apo state as changing with respect to pH however this was previously thought to be due to the protonation of His197. In this case Arg32 (acting as a reporter for His197) does not show a shift until pH 6.5 – 7.5. This may suggest that the set of residues that move at the C-terminal end of the N-terminal domain move independently of

His197. Residues Glu187 and Lys188 were not implicated previously in the apo state however their proximity to the other residues of the C-terminal end of the N-terminal domain may explain the shifts. The presence of AMPPNP may alter the conformation such that they are now subject to the influence of the C-terminal tail of the N-terminal domain.

As mentioned the shift observed in Arg32 has moved to a higher pH. In this construct a backbone resonance cannot be observed for His197 however the response of Arg32 may suggest that the presence of AMPPNP bound to the N-terminal domain has led to an increase in the pKa of the His197 side chain. This shift however still does not fall at the correct range for that predicted for the pKa of the bound protonation event detected by ITC. It was also observed in the apo state albeit at a lower pH. This suggests that His197 is not the protonation event detected by ITC. The two other shifts observed at this pH range are Gly153 and Gly154.

The final set of shifts observed are Ser39, Asp43, Asp79, Asn135, Lys139, Thr157, Ile172 and Phe174. With the exception of Asp43, all these shifts are unique to the AMPPNP bound state. These shifts are also the only significant shifts observed in the pH7.5 – 9 range which is where the expected protonation event detected by ITC is predicted to occur. All of these higher range shifts are also located on the back of the binding site in the β-sheet or on the long helix that flanks the binding site, suggesting that the binding of AMPPNP may exert an influence over them at this pH range. None of the shifts identified belong to residues that have titratable groups in this region, nor do any of the peaks look significant enough to suggest a protonation event on it. Although this does not confirm that the protonation event is on the ligand it strongly suggests that it is not on the protein.

The protonation of the γ-phosphate of AMPPNP would change the charge state and significantly affect the electrostatic interactions of the phosphate with the surrounding protein environment. This change could force the rearrangement of the ligand within the binding site, inducing movement and displacement of water within the binding site to accommodate the newly positioned ligand and thus changing the overall environment of the binding site. An alternative would be a change in the ring currents on the Adenosine moiety of the AMPPNP molecule causing shifts at this pH range upon their interaction with the amino acids in the binding pocket. Protonation on the ligand however cannot be confirmed by protein NMR.

Both sets of low pH shifts observed in both the apo state and the AMPPNP bound state are located at the periphery of the protein and are some distance from the nucleotide binding domain. The binding of AMPPNP appears to influence the number of residues that shift with respect to pH, however, it is already known that the binding of nucleotide ligand causes some structural rearrangement to the N-terminal domain of hsp90. The differences between the apo

and bound state suggest that these rearrangements reach to the periphery of the protein. The lack of shifts seen in Thr159, Val158 and Ala2 may suggest that AMPPNP binding stabilises the N-terminal strand thus reducing the influence of pH over it. The binding of AMPPNP also influences residue His197 leading to a change in its pKa value as reflected by the change in shift of Arg32.

3.2.3 Investigation of the protonation of the γ-phosphate of AMPPNP by 31 phosphorous NMR

Direct observation of the phosphate groups of the ligand is possible using ^{31}P NMR 1D spectra. Due to the simplicity of the molecules involved, i.e. each has only two or three phosphate groups, 1D NMR can be used to monitor each group and detect any shift induced by pH in both free AMPPNP and when bound to the N-terminal domain of Hsp90.

^{31}P NMR studies of ADP and ATP have been undertaken in the past and the assignments of these spectra will be of use in assigning those of AMPPNP, the effect of the protein upon the NMR signals of the bound ligand are unknown.

Spectra were recorded for ADP, ATP and AMPPNP at both high (pH9) and low (pH5) pH values, with and without magnesium (Figure 3.14). A comparison of the spectra and the data in papers by Cohn et al. [68;69] allowed peak assignment of ADP, ATP and AMPPNP. Subsequent experiments were then recorded for AMPPNP with Mg^{2+} both in the absence and presence of the N-terminal domain of Hsp90 (Figures 3.15 and 3.16). 1D spectra were recorded at each half pH unit in each case. All experiments were done in triple buffer with ligand concentrations at 400μM.

3.2.3.1 Assignment of the ^{31}P phosphate peaks of AMPPNP

Previous studies [68;69] of ^{31}P spectra with ATP and ADP under various pH and magnesium bound conditions identified the resonances of ATP by the characteristic splitting patterns arising from spin-spin interactions as described above. The γ-peak showed a doublet due to its interaction with the neighbouring β-phosphate. The β-phosphate showed a triplet pattern due to its interaction with both γ- and α-phosphate groups both across oxygen atoms. The α-phosphate showed a less distinct splitting pattern due to its interaction with both the β-

phosphate and the influence of the neighbouring ribose ring. Cohn[69] also demonstrated that as pH decreased, the peak due to the terminal phosphate shifted towards the α-phosphate peak. The apparent pK_a of this shift corresponds with the pK_a of the transition to either the ADP^{3-} or ATP^{4-} state respectively[68]. The β-peak of ATP showed limited movement over this range. The addition of Mg^{2+} to ATP was seen to cause a shift in the β- and γ-phosphate peaks however no shift was observed on the α-phosphate. This suggests that the Mg^{2+} ion contacts predominantly the terminal two phosphates in ATP. With ADP shifts were observed with both the β-phosphate and α-phosphate peaks suggesting that Mg^{2+} contacts both phosphate groups in the smaller ligand.

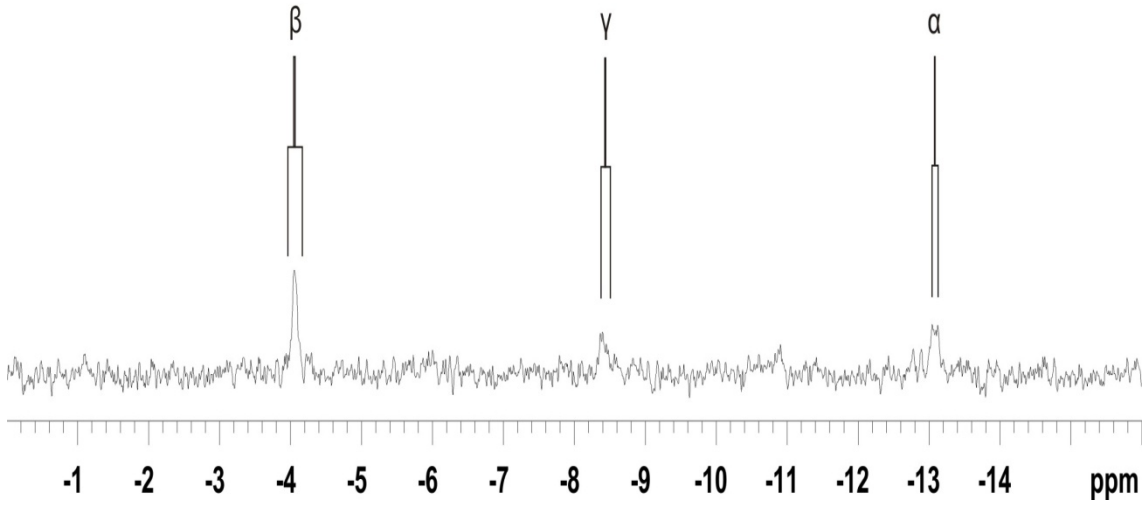

Figure 3.13 Assignment of the phosphate peaks of AMPPNP using the peak splitting patterns identified in the 1D spectrum.

Turning to the AMPPNP spectra, the peak splitting pattern observed for each of the three phosphate groups is distinct and allows for their initial identification. The α-peak shows a symmetrical doublet splitting pattern caused by the presence of two phosphorus atoms linked by one oxygen atom. The β-peak should show a four peak split as it is bound on one side through an oxygen to another phosphorus atom and on the other side by a nitrogen to the third phosphate. Due to this asymmetrical structure the splitting pattern is not as predictable and here results in the superposition of the split peaks leading to a more intense peak with a broad shouldered base. The γ-peak should show a doublet pattern but the splitting across a nitrogen atom, while symmetrical, will not be identical to the α-phosphate. This is shown in Figure 3.13 with a slightly broader peak suggesting less significant separation between the split peaks but with a similar intensity to the α peak. Further confirmation of the peak identification was undertaken by monitoring the peak behaviour with respect to pH in the unbound state using the known behaviour of the peaks of ATP as a guide.

The AMPPNP spectra recorded across the pH range shows clearly that at pH9 the terminal phosphate has moved away from the α-phosphate as anticipated compared to the spectra recorded at pH5. In this way AMPPNP behaves like ATP. When AMPPNP is observed without Mg^{2+} at low pH one large peak is seen corresponding to the α- and γ-phosphates with a second peak which can be attributed to the β-peak. At pH 9 three peaks are seen – the α- and γ- peaks as previously described and the β-peak which has shifted slightly in response to a change in pH as anticipated. At both high and low pH this β-peak is very far distant from the β peaks observed for ATP but can be explained when considered in relation to the modification made to AMPPNP to negate hydrolysis of the terminal phosphate. Instead of being linked by an oxygen atom, the β- and γ-phosphates are linked by a nitrogen atom which appears to have profoundly affected the position of the β peak, yet its behaviour under changing pH and the behaviour of the other peaks confirms their identities. The β peak of ADP behaves in a similar fashion to the terminal phosphate of ATP and AMPPNP.

The effect of the magnesium, again as expected, has caused a shift in both the β- and γ-phosphates in all cases (Figures 3.14). At low pH the peaks are very much broader causing the β to disappear completely when magnesium is added with both ADP and ATP. As with ATP, an increase in pH caused the movement of the γ peak away from the α peak with a small effect on the β-peak. Addition of Mg^{2+} (see Figure 3.14) shows a small movement of the β- and γ-peaks from their positions without Mg^{2+} however the gross differences between ATP and AMPPNP are maintained.

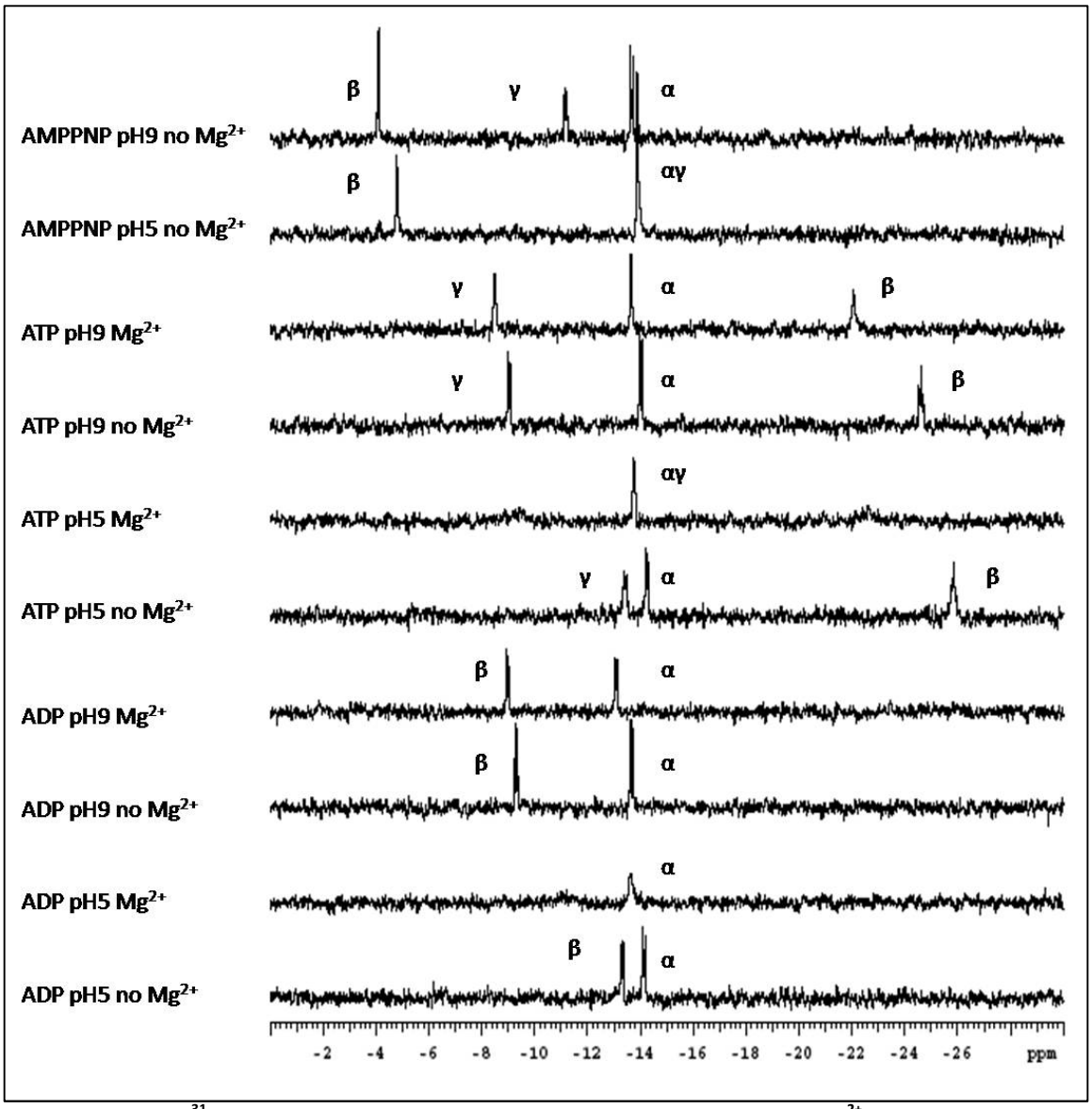

Figure 3.14 Control ^{31}P 1D spectra collected for ADP and ATP, with and without 5 mM $Mg^{2+,}$ and at pH 5 and pH 9 in each case. ^{31}P 1D spectra collected for AMPPNP without Mg2+ at pH 5 and pH 9. Spectra in 50 mM Ethanolamine, 100 mM ACES, 50 mM Tris Base. Ligands at 400 µM concentration. 600 MHz field used.

3.2.4 Titration data for both free and bound AMPPNP reveals a chemical shift transition as pH changes.

Using free AMPPNP 1D NMR spectra were recorded using a ^{31}P probe in the triple buffer across the pH range used for previous ITC and NMR experiments. The ligand was used at 400µM concentration. A Mg^{2+} concentration of 5 mM was used. Protonation of any phosphate group will introduce an extra electron thus increasing the shielding of the nucleus and leading to a reduction in chemical shift.

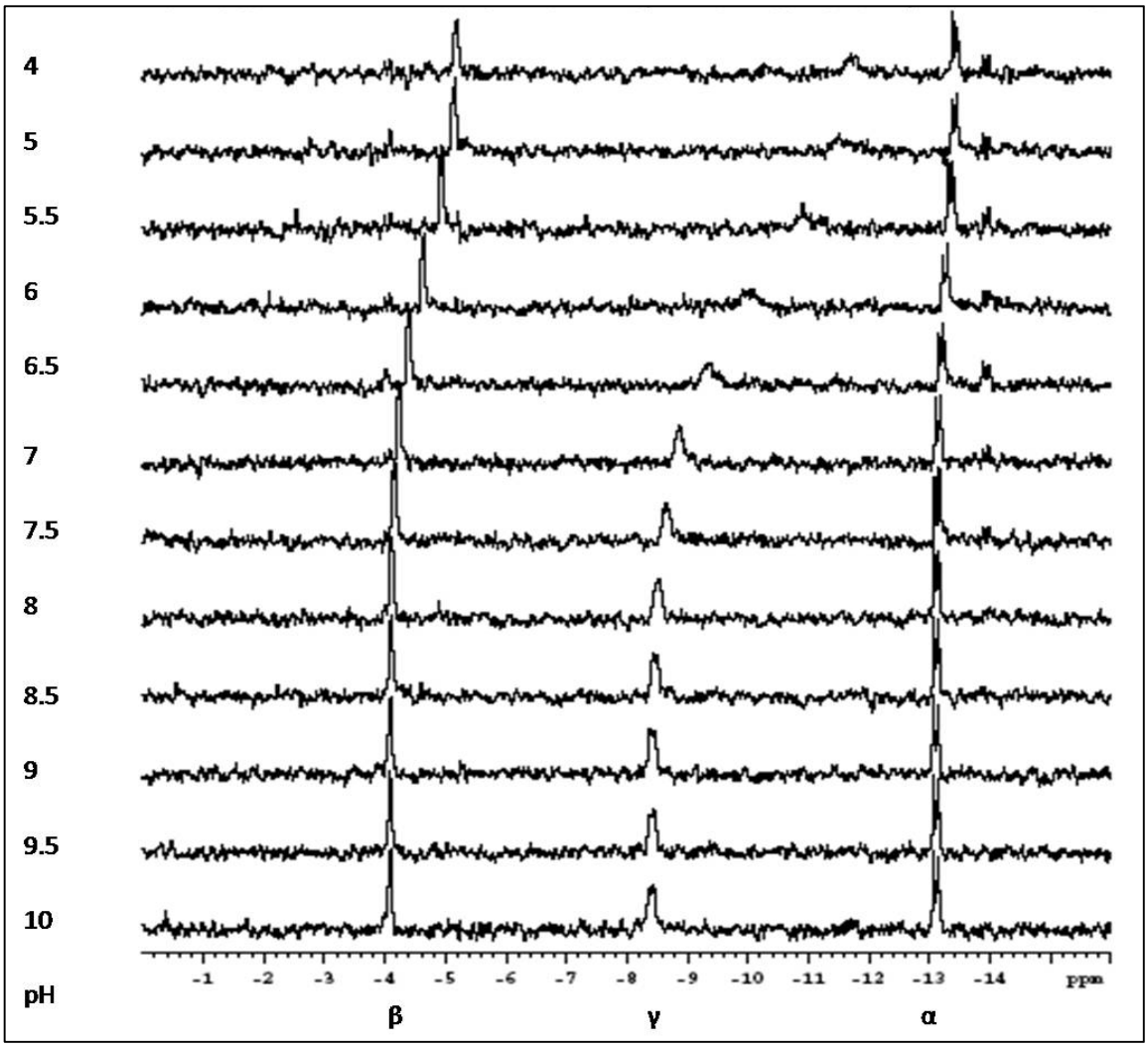

Figure 3.15 The pH dependence of ^{31}P 1D spectra of free AMPPNP at a concentration of 400 µM. Buffer conditions 50 mM ethanolamine, 100 mM ACES, 50 mM Tris Base, 5 mM Mg^{2+}. 600 MHz field used.

Observations of the ligand while bound to the N-terminal domain of Hsp90 are important to understand how the ligand interacts with the protein. The binding of a small fast tumbling ligand to a larger slower tumbling protein may act to slow the tumbling time of the ligand thus leading to faster relaxation of the phosphorus signal from the ligand phosphates and peak broadening of any signals detected. This may reduce the intensity of the overall signal.

1D NMR spectra were recorded using a ^{31}P probe in triple buffer across the pH range used for previous ITC and NMR experiments (Figure 3.15). The ligand was used at 400 µM concentration with equimolar N-terminal Hsp90. A Mg^{2+} concentration of 5 mM was used. Titrations were conducted from pH 6 – pH 10 for the protein bound scans as at the concentrations used the N-terminal domain of Hsp90 precipitated.

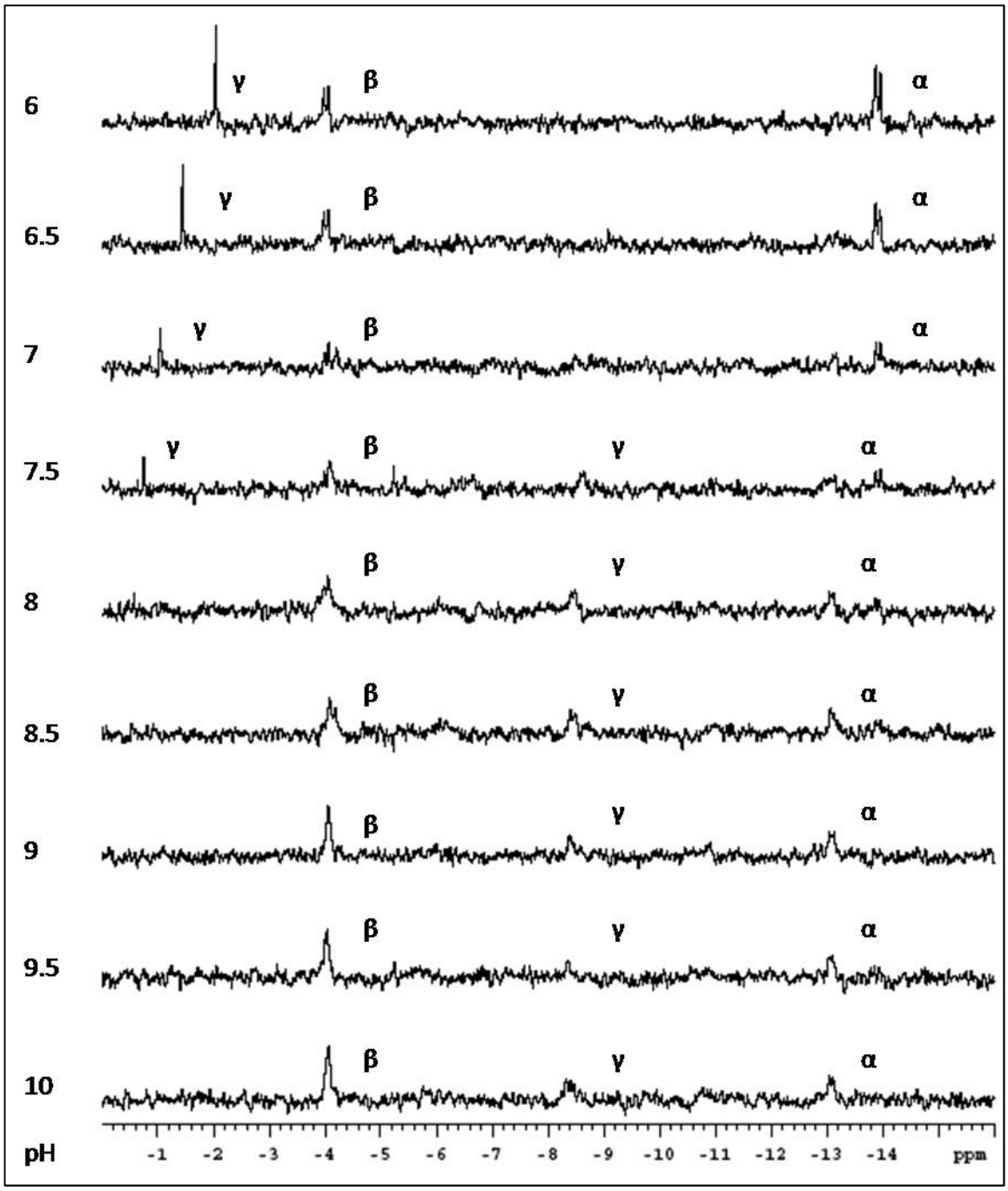

Figure 3.16 ^{31}P 1D spectra of a pH dependent titration of AMPPNP bound to equimolar concentrations of the N-terminal domain of Hsp90 at concentration of 400 µM. Buffer conditions: 50 mM ethanolamine, 100 mM ACES, 50 mM Tris Base, 5 mM Mg^{2+}. 600 MHz field used.

Assignment of all three peaks for AMPPNP bound to the N-terminal domain of Hsp90 is as seen in the free AMPPNP spectra from pH 10 – 8, (see Figure 3.16) During the transition from pH 8 - 7 both the α- and β-peaks are visible and show a clear movement from one pH to the next with some slight movement. The γ-peak over this range however decreases in intensity before disappearing completely. The appearance of a fourth peak at pH 7.5 at -0.9

ppm however and its subsequent increasing intensity from pH 7.5 to pH 6 correlates to the disappearance of the γ peak. This suggests that this is indeed the γ-phosphate peak having undergone a radical chemical shift upon an event, possibly protonation, at pH 7.5. The presence of both peaks, both at a low intensity, suggest a mixed population of both the protonated and un-protonated γ-phosphate of AMPPNP at this pH. The intensity increase as pH decreases would then be as the population moved away from a mixed population to a single charge state.

3.2.5 Analysis of titration data for both the free AMPPNP ligand and AMPPNP bound to the N-terminal domain of Hsp90

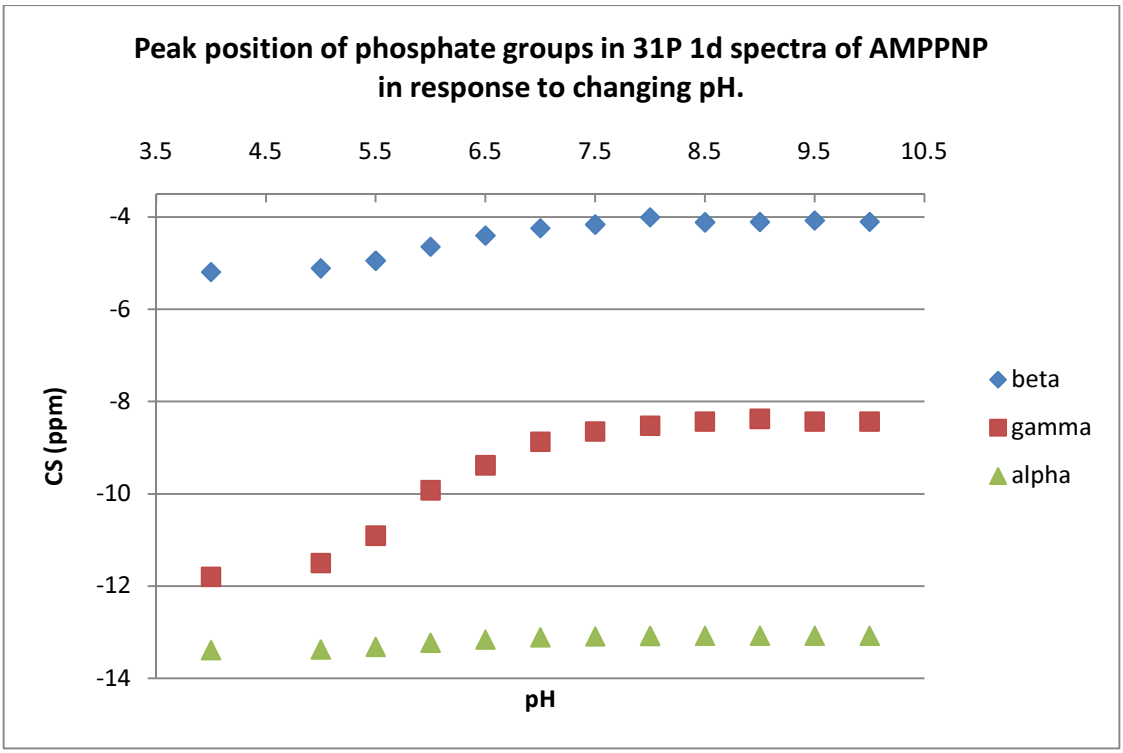

Figure 3.17 Chemical shift changes with respect to pH of the three phosphate groups of free AMPPNP as determined by ^{31}P NMR.

The shifts for AMPPNP in the presence of the N-terminal domain of Hsp90 are summarised in Figure 3.18.

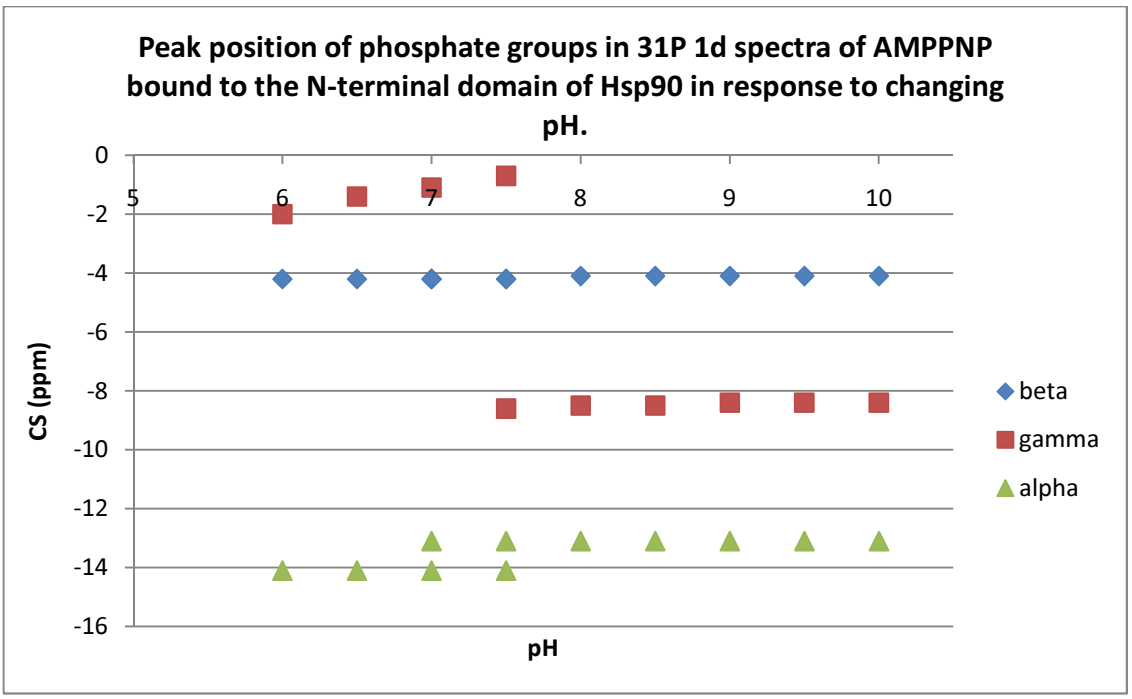

Figure 3.18 Chemical shift changes with respect to pH of the three phosphate groups of AMPPNP bound to the N-terminal domain of Hsp90 as determined by ^{31}P NMR.

A plot of the shifts for the free AMPPNP ligand (Figure 3.17) shows clearly that both the γ and β peaks are both responding to a protonation event between pH 6.5 – 7. The effect on the γ peak shift is of a greater magnitude than that observed on the β-peak suggesting that a protonation event is occurring on the γ-phosphate. When this is compared to the results of the ^{1}H/^{15}N NMR pH titration (Figure 3.11) and the ITC data (Figure 3.3) it can be seen that this corresponds to the pKa value calculated for the 'free' event.

A plot of the shifts for the bound AMPPNP ligand (Figure 3.18) shows different results to that of the free ligand. Unlike in the free ligand the β-peak shows a very slight shift in response to pH change suggesting that being bound to the protein acts to stabilise the β-phosphate group. In contrast the effect on the γ-phosphate is very pronounced. A slight shift is seen between pH 10 – 8 however at pH 7.5 the intensity of the peak decreases and as previously mentioned a new peak appears and increases in intensity. A possible interpretation is that as pH decreases, the terminal phosphate becomes protonated and that this protonation profoundly changes its chemical shift. This transition occurs at a higher pH than in the free ligand corresponding to the 'bound pKa' calculated by the ITC data shown previously. This suggests that the presence of the protein acts to alter the pKa of the terminal phosphate to between pH 7 – 8. Unlike the free ligand, a transition is observed for the α-phosphate however the transition is small compared to the γ phosphate suggesting that, like the β-phosphate in the free ligand, the chemical shift change is due to neighbouring groups rather than any direct effect. It is already known that the protonation event described leads to a wide spread range

of chemical shifts across the N-terminal domain of Hsp90 (Figure 3.12), this may well explain why protonation of the γ-phosphate leads to a change in the environment of the α phosphate and subsequent chemical shifts, due to effects transferred via the ligand binding site.

When the transition for the γ-phosphate in the bound state is compared to the previous protein NMR titration data and the ITC data it can be seen that the shift in peak position occurs in the same pH range as shifts observed previously. It can be concluded that the protonation event observed on the γ-phosphate of bound AMPPNP is the same as the protonation event observed by protein NMR and ITC. Therefore when combined with the knowledge of ATP protonation [68;69] linking the γ peak movement to the formation of an ATP^{-4} form, this suggests that the protonation of AMPPNP on the γ peak is as AMPPNP moves from a -3 to -4 charge state. This transition corresponds to a change in binding affinity as previously seen. This, combined with the knowledge that ADP remains in a -3 charge state across the pH range without altering its binding affinity, suggests that binding in the -3 charge state is more favourable than the -4 charge state.

3.2.6 Summary of NMR pH titration data

The ITC studies of the N-terminal domain of Hsp90 binding to AMPPNP in triple buffer at different pH values are consistent with a single protonation event with a free pKa of 6.5 and a bound pKa of 8. A single protonation event is confirmed by a value of 0.7 protons released at pH7.5 i.e. between the free and bound pKa values. No protonation event is associated with ADP binding to the N-terminal domain of Hsp90.

With the combination of the 2D ^{15}N-HSQC pH titration data and the ^{31}P 1D pH titration data it can be confirmed that there is a protonation event that occurs at pH7 and that this is limited to the terminal γ-phosphate of the AMPPNP ligand and does not map to the protonation of any amino acid within the NT domain. This pH range corresponds to the transition of AMPPNP from the $AMPPNP^{-3}$ to the $AMPPNP^{-4}$ state, assuming similar behaviour to ATP [67] as the pH increases.

As previously described the binding affinity dramatically decreases at around pH7 with AMPPNP but not ADP. At low pH when both ligands bind with a similar affinity both ligands are in the -3 charge state. The weakening in binding of AMPPNP coincides with the pH of the known transition of ATP from the -3 to the -4 charge state. Assuming a similar behaviour for AMPPNP this may indicate a de-protonation of the AMPPNP γ-phosphate as observed by ^{31}P

NMR. In contrast the ADP binding affinity does not vary with pH, nor does the charge state of the ligand [67]. This reveals that the -3 charge state of both ligands is preferable for binding to the NT domain of Hsp90. Additionally the spread of the shifts observed on the protein associated with this change in charge state across the binding site suggests that it is not one functional group responsible for an increased binding affinity but a less specific effect influencing the entire binding site.

This knowledge has important ramifications for future drug molecule design as it is clear that the charge state of the ligand has a profound effect upon the binding affinity while not clearly corresponding to any one specific side chain or functional group.

3.3 The ΔC_p values found by ITC upon binding of ligands ADP, AMPPNP, adenine and adenosine to the N-terminal of Hsp90 suggest conformational changes are occurring

It is known that Hsp90 goes through a series of conformational changes in response to the binding to and hydrolysis of ATP at the NT domain [5;10;20;22;23;35;38;70]. Many of these conformational changes are not limited to the NT domain but have long ranging effects throughout the chaperone. The crystal structures of the N-terminal domain alone and of the full length Hsp90 protein bound to AMPPNP and the co-chaperone p23, [7;8] suggest that a key conformational change is the movement of the ATP lid over the ligand binding site upon complex formation. This conformational change appears to be very important in the overall nucleotide hydrolysis cycle, however detailed information on how hydrolysis is linked to this conformational change is not clear.

3.3.1 ΔC_p data was collected for the binding of ADP and AMPPNP to the N-terminal domain of Hsp90 across a pH range from pH 5 – 10

As has been previously described in Chapter 1, the change in heat capacity of a reaction can be used to identify large changes in conformation because it is a measure of the change in degrees of freedom of a system on going from a free to bound state, which is often largely dictated by the displacement of water molecules from protein surfaces and changes in

the rotational and vibrational degrees of freedom. Thus if a conformational change results from the binding of the N-terminal of Hsp90 to ADP and/or AMPPNP then this may be reflected in the change in heat capacity of the binding reaction.

ITC can be used to determine the change in heat capacity of a protein/ligand interaction by recording the ΔH values of binding at different temperatures. These experiments have been undertaken from 10°C to 25°C, across the pH range 10 – 5 every half pH unit for ligands binding to NT. These data are summarised in Tables 3.5 and 3.6.

Protein:	N-Terminal	**Ligand:**	ADP	**pH:**	10	**ΔC_p:**	-1.72	kJ mol^{-1} K^{-1}
Temp (C)	Stoichiometry (N)	Error ±	K_d (µM)	Error (µM) ±	ΔH (kJ mol^{-1})	Error (±)	TΔS (kJ mol^{-1})	ΔG (kJ mol^{-1})
10	0.99	0.01	10.66	0.92	-68.03	1.17	-41.11	-26.92
15	1.05	0.01	18.76	1.07	-71.76	1.02	-45.69	-26.06
20	1.06	0.01	33.11	1.50	-77.95	1.19	-52.86	-25.08
25	1.00	0.02	62.11	3.30	-94.56	2.58	-69.11	-25.45

Protein:	N-Terminal	**Ligand:**	ADP	**pH:**	9.5	**ΔC_p:**	-3.21	kJ mol^{-1} K^{-1}
Temp (C)	Stoichiometry (N)	Error ±	K_d (µM)	Error (µM)	ΔH (kJ mol^{-1})	Error (+/-)	TΔS (kJ mol^{-1})	ΔG (kJ mol^{-1})
10	0.95	0.02	10.72	0.73	-69.37	1.16	-42.41	-26.96
15	1.01	0.01	23.98	1.46	-76.65	1.43	-50.85	-25.80
20	1.05	0.02	43.80	2.86	-91.80	3.14	-67.29	-24.51
25	0.97	0.02	81.50	3.18	-117.74	3.93	-94.37	-23.37

Protein:	N-Terminal	**Ligand:**	ADP	**pH:**	9.0	**ΔC_p:**	-1.33	kJ mol^{-1} K^{-1}
Temp (C)	Stoichiometry (N)	Error ±	K_d (µM)	Error (µM)	ΔH (KJ mol-1)	Error (+/-)	TΔS (KJ mol-1)	ΔG (kJ mol^{-1})
10	0.99	0.01	6.94	0.57	-78.70	1.23	-50.74	-27.96
15	1.05	0.01	14.49	0.79	-84.60	1.25	-57.92	-26.68
20	1.11	0.01	24.49	1.17	-90.08	1.51	-64.15	-25.93
25	1.13	0.01	41.81	1.51	-98.78	1.70	-73.78	-25.01

Protein:	N-Terminal	**Ligand:**	ADP	**pH:**	8.5	**ΔC_p:**	-2.44	kJ mol^{-1} K^{-1}
Temp (C)	Stoichiometry (N)	Error ±	K_d (µM)	Error (µM)	ΔH (KJ mol-1)	Error (+/-)	TΔS (KJ mol-1)	ΔG (kJ mol^{-1})
10	0.91	0.01	7.75	0.70	-73.64	1.37	-45.94	-27.70
15	0.95	0.02	15.57	1.30	-82.34	2.09	-55.88	-26.46
20	0.99	0.02	30.01	1.71	-93.01	2.20	-67.61	-25.40
25	0.98	0.02	75.30	6.17	-110.71	3.72	-86.27	-24.43

Protein:	N-Terminal	**Ligand:**	ADP	**pH:**	8.0	**ΔC_p:**	-0.95	kJ mol^{-1} K^{-1}
Temp (C)	Stoichiometry (N)	error	K_d (µM)	Error (µM)	ΔH (KJ mol-1)	Error (+/-)	TΔS (KJ mol-1)	ΔG (kJ mol^{-1})
10	1.00	0.01	8.76	0.80	-68.57	1.22	-41.15	-27.43
15	1.00	0.01	19.60	0.93	-74.73	1.04	-48.73	-26.00
20	1.06	0.02	35.93	2.01	-80.42	1.78	-55.48	-24.94
25	1.15	0.02	42.88	3.12	-82.51	2.42	-57.58	-24.93

Protein:	N-Terminal	**Ligand:**	ADP	**pH:**	7.5	**ΔC_p:**	-0.95	kJ mol^{-1} K^{-1}
Temp (C)	Stoichiometry (N)	error	K_d (µM)	Error (µM)	ΔH (KJ mol-1)	Error (+/-)	TΔS (KJ mol-1)	ΔG (kJ mol^{-1})
10	1.01	0.01	3.85	0.13	-67.74	0.49	-38.38	-29.36
15	1.06	0.01	6.37	0.27	-70.33	0.80	-41.71	-28.62
20	1.05	0.01	10.68	0.50	-76.23	1.29	-48.33	-27.91
25	1.04	0.02	19.78	1.19	-81.55	2.24	-54.51	-27.03

Protein:	N-Terminal	**Ligand:**	ADP	**pH:**	7.0	**ΔC_p:**	-0.84	kJ mol^{-1} K^{-1}
Temp (C)	Stoichiometry (N)	error	K_d (μM)	error	ΔH (KJ mol-1)	Error (+/-)	TΔS (KJ mol-1)	ΔG (kJ mol^{-1})
10	1.01	0.01	6.21	0.29	-50.88	0.45	-22.63	-28.25
15	1.00	0.01	8.62	0.62	-70.58	1.34	-42.68	-27.91
20	1.01	0.01	12.76	0.60	-73.43	1.10	-46.00	-27.44
25	1.01	0.01	20.45	1.05	-78.95	1.73	-52.14	-26.81

Protein:	N-Terminal	**Ligand:**	ADP	**pH:**	6.5	**ΔC_p:**	-0.69	kJ mol^{-1} K^{-1}
Temp (C)	Stoichiometry (N)	error	K_d (μM)	error	ΔH (KJ mol-1)	Error (+/-)	TΔS (KJ mol-1)	ΔG (kJ mol^{-1})
10	1.01	0.01	5.50	0.53	-63.85	1.26	-35.30	-28.54
15	0.98	0.02	9.90	0.88	-69.41	1.76	-41.84	-27.58
20	1.01	0.02	13.23	0.93	-71.30	1.64	-43.91	-27.39
25	1.05	0.02	21.83	1.75	-74.73	2.55	-48.15	-26.57
30	1.03	0.09	59.52	0.53	-98.74	12.78	-74.20	-24.54

Protein:	N-Terminal	**Ligand:**	ADP	**pH:**	6.0	**ΔC_p:**	-0.81	kJ mol^{-1} K^{-1}
Temp (C)	Stoichiometry (N)	error	K_d (µM)	error	ΔH (KJ mol-1)	Error (+/-)	TΔS (KJ mol-1)	ΔG (kJ mol^{-1})
10	1.05	0.01	6.33	0.40	-68.58	1.10	-40.40	-28.18
15	1.10	0.03	11.12	1.24	-73.22	2.66	-45.81	-27.41
20	1.09	0.03	12.89	1.38	-76.07	2.81	-48.57	-27.49
25	1.09	0.05	27.55	3.42	-81.09	5.61	-55.01	-26.07

Protein:	N-Terminal	**Ligand:**	ADP	**pH:**	5.5	**ΔC_p:**	-0.83	kJ mol^{-1} K^{-1}
Temp (C)	Stoichiometry (N)	error	K_d (µM)	Error	ΔH (KJ mol-1)	Error (+/-)	TΔS (KJ mol-1)	ΔG (kJ mol^{-1})
10	1.00	0.01	6.17	0.38	-53.76	0.88	-25.47	-28.29
15	1.04	0.02	10.52	0.66	-55.69	1.25	-28.21	-27.48
20	1.01	0.04	20.33	2.05	-60.71	3.18	-34.34	-26.37
25	1.02	0.08	40.10	5.66	-65.94	7.37	-40.82	-25.12

Protein:	N-Terminal	**Ligand:**	ADP	**pH:**	5.0	**ΔC_p:**	-0.23	kJ mol^{-1} K^{-1}
Temp (C)	Stoichiometry (N)	error	K_d (μM)	Error	ΔH (KJ mol-1)	Error (+/-)	TΔS (KJ mol-1)	ΔG (kJ mol^{-1})
10	1.10	0.01	10.88	0.57	-70.88	1.19	-43.95	-26.93
15	1.09	0.03	15.87	1.84	-75.44	3.58	-48.95	-26.49
20	1.28	0.08	19.34	4.86	-67.32	6.73	-40.84	-26.48
25	1.15	0.08	40.32	6.42	-77.45	8.63	-52.39	-25.05

Table 3.5 Summary of binding data including errors of the binding of the N-terminal of Hsp90 to ADP across the pH range pH10 - 5 across a temperature range of 10°C to 25°C.

A summary of the calculated ΔC_p values for the N-terminal of Hsp90 binding to ADP is shown in Table 3.6.

pH	ΔC_p (kJ mol^{-1} K^{-1})	Error (+/-) (kJ mol^{-1} K^{-1})
10	-1.72	0.01
9.5	-3.20	0.16
9	-1.33	0.1
8.5	-2.44	0.16
8	-0.95	0.11
7.5	-0.95	0.08
7	-0.84	0.08
6.5	-0.69	0.12
6	-0.81	0.20
5.5	-0.83	0.21
5	-0.23	0.34

Table 3.6 The pH dependence of the ΔC_p values for the binding of ADP to the N-terminal domain of Hsp90 as determined by ITC. A temperature range of 10°C - 25°C was used. Buffer conditions: 50mM ethanolamine, 100mM ACES, 50mM Tris Base, 5mM Mg^{2+}.

The ΔC_p of the binding of AMPPNP was determined by Nilapwar et al.[17] and is summarised in Table 3.7.

pH	ΔC_p (kJ·mol^{-1}·K^{-1})	Error (+/-) (kJ·mol^{-1}·K^{-1})
10	0.28	0.04
9.5	0.50	0.10
8.7	0.24	0.08
8	0.15	0.08
7	0.23	0.02
6	-0.01	0.02
5	0.03	0.03

Table 3.7 The pH dependence of the ΔC_p values for the binding of AMPPNP to the N-terminal domain of Hsp90 as determined by ITC by Nilapwar et al. *[17]* Buffer conditions: 50mM ethanolamine, 100mM ACES, 50mM Tris Base, 5mM Mg^{2+}.

A comparison of the ΔC_p data for both ADP and AMPNP binding to the N-terminal of Hsp90 across a physiological pH range is summarised in Figure 3.19.

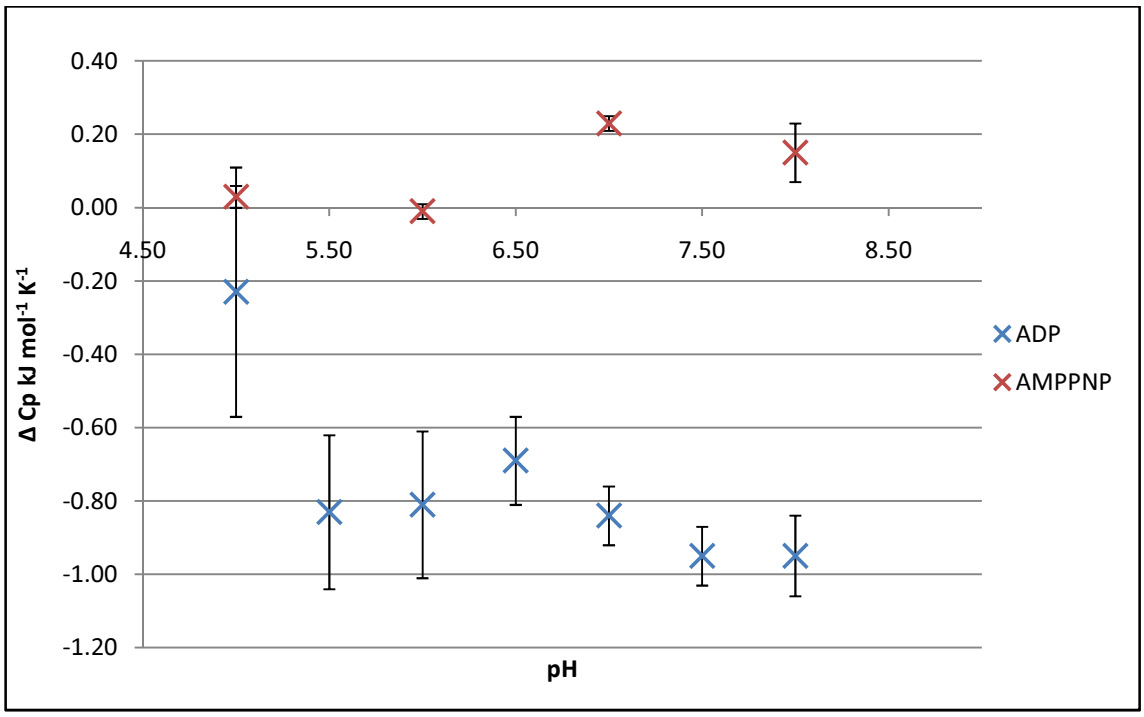

Figure 3.19 The pH dependence of ΔC_p of the binding of ADP and AMPPNP to the N-terminal domain of Hsp90.

3.3.2 The ΔC_p values for ADP and AMPPNP binding to the N-terminal domain of Hsp90 show a significant variation to each other

A cursory glance at the numbers in Table 3.6 shows that the ΔC_p for ADP binding to the N-terminal of Hsp90 is predominantly negative with a more negative value at the higher pH values gradually decreasing towards zero as the pH decreases. This effect must be independent of the K_d since no change in K_d is observed with the change in pH with ADP. A negative heat capacity in relation to the binding of a protein is not unexpected since this usually represents the burial of hydrophobic/apolar surface area caused by the binding of ligand to the protein binding site. However contributions towards this heat capacity can come from many other sources [66;71].

It is also clear to see that the ΔC_p values previously reported for AMPPNP differ significantly to those recorded for ADP, i.e. the ΔC_p's for AMPPNP are predominantly positive and decrease to zero as pH decreases.

This large variety in ΔC_p values involving similar ligands at the same binding site is an unusual phenomenon suggesting that the binding must involve a complex series of events as has been suggested previously in this chapter. It is also noteworthy that the magnitude of the ΔC_p values between ADP and AMPPNP differ significantly.

The effect of pH on the ΔC_p alone has been described by Baker and Murphy.[64] and under constant buffer conditions the ΔC_p across a pH range should reveal minima and maxima at both the pK_a of the free and bound state as well as showing the ΔC_p for the protonation of free protein upon ligand binding described as $\Delta C_{p.p}$. From plots of the ΔC_p values against pH for ADP and AMPPNP (Figure 3.19) it is clear to see that this simple pattern is not evident suggesting other factors are affecting the ΔC_p.

3.3.3 The ΔC_p values for the binding of ADP and AMPPNP to the N-terminal of Hsp90 can be used to predict conformational changes

Large negative ΔC_p values are often associated with site specific ligand/protein binding events[71] as ligand binding often results in the burial of surface area and the displacement of water molecules. Conformational changes caused by ligand binding may also displace water molecules and contribute to the ΔC_p. The ΔC_p value is comprised of several components including both polar and apolar surface area burial, atomic and covalent bond contributions and the protonation state of the side chain. Some of these factors, such as surface area burial, have a greater influence over the ΔC_p value than others such as atomic bond contributions[71]. The result of this dominance is that changes in the surface area burial and conformational changes are reflected in the ΔC_p and thus the ΔC_p can be used as an indication that these events are occurring. From the ΔC_p a rough estimate of the surface area burial can be calculated. Should this differ from that expected by structural modelling then a conformational change associated with binding may be inferred[51]. Due to the many factors contributing to ΔC_p the calculations only take surface area burial under consideration and are therefore no more than an indication as to the existence and rough scale of any changes. However since the dominant contribution to the ΔC_p value is the burial of surface area the equation is still a valid indicator of structural rearrangement. Using the crystal structures [7;8] as a starting reference the anticipated ΔC_p was calculated by Nilapwar et al.[17] (Table 3.8) as described below [71;72]. Although there is no crystal structure of the AMPPNP bound state of the NT domain alone, a prediction of this state was made from the full length crystal bound to p23[7].

There was a difference between the calculated ΔC_p based upon the crystal structure and models and the actual observed ΔC_p for both AMPPNP and ADP.

NT Hsp90 ligand	$\Delta C_{p\ obs}$ (J mol^{-1} K^{-1})	$\Delta C_{p\ calc}$ (J mol^{-1} K^{-1}) (eq. 3.3)	$\Delta C_{p\ calc}$(J mol^{-1} K^{-1}) (eq 3.4)
ADP	-840	-140	-190
AMPPNP (open)	+230	-150	-170
AMPPNP (closed)	+230	+600	+680

Table 3.8 Comparison of the observed and calculated ΔC_p for ADP and AMPPNP binding to the N-terminal domain of Hsp90 at pH7. Predictions for the ADP bound protein are based on the N-terminal crystal structure while predictions for the AMPPNP bound protein are based from the ADP bound N-terminal structure (assuming a 'lid open' conformation as in ADP binding) or modelled assuming a 'lid closed' position using information from the full length AMPPNP bound Hsp90 in complex with p23. AMPPNP data from Nilapwar et al. *[17]*

The two equations used were taken from Bergqvist et al.[54] and derived from work by Freire et al. [47] and Luque et al.[72]. They are summarised in Equations 3.3 and 3.4.

$$\Delta C_p = 1.34\Delta A_{np} - (0.59 \pm 0.04)\Delta A_p \text{ J mol}^{-1} \text{ K}^{-1} \quad (3.3)$$

$$\Delta C_p = 1.874\Delta A_{np} + 0.711\Delta A_{oh} - 1.097\Delta A_p \text{ J mol}^{-1} \text{ K}^{-1} \quad (3.4)$$

Above are the equations used to calculate the predicted ΔC_p for the binding of ADP and AMPPNP to the N-terminal of Hsp90 and applied to the N-terminal crystal structure bound to ADP and the predicted model for the N-terminal of Hsp90 bound to AMPPNP based on the full length crystal structure and the N-terminal crystal structure as previously detailed. Both equations are valid with the first taking just polar and non-polar surface area under consideration while the second adds in the influence of change in hydration. For the work presented here the first equation only was used.

This difference between observed and predicted results is most likely attributed to the differential movement of the ATP lid upon binding of the different ligands. The conformational change associated with the lid-closed conformation exposes a large amount of hydrophobic surface area on the back of the lid thus providing a major contribution to the ΔC_p. It is possible that disruption of the extensive hydrogen bond network within the binding site might also influence the ΔC_p as binding would displace water within the binding site and reduce the water trapped between the binding interfaces. It was also theorised by Nilapwar et al. that replacement of the flexible hydrogen bonding network with a more rigid ligand within the binding site might weaken the stability of the overall protein domain structure *'creating additional vibrational modes within the protein both locally and globally'*[17]. Although this is rather speculative it is somewhat supported by the NMR titration data where binding is seen to influence a large number of residues even far from the binding site.

The expanded results for the ΔC_p of ADP show that the ΔC_p value is more negative than previously thought. The ΔC_p calculated at low pH is close to that predicted in the absence of conformational change (around -100 $J \cdot mol^{-1} \cdot K^{-1}$) however as pH increases the ΔC_p decreases dramatically to around -1000 $J \cdot mol^{-1} \cdot K^{-1}$.

3.3.4 Explaining the heat capacity observed in reference to movement of the ATP lid upon ligand binding

It is clear that there is a significant difference between the predicted and observed values for the ΔC_p associated with both ADP and AMPPNP binding to the N-terminal of Hsp90. The difference between the predicted values and the observed values for ADP could be explained by considering the position of the ATP lid (residues 98 – 120) at various points within the nucleotide binding and hydrolysis cycle. The various positions of the lid are shown in Figure 3.20.

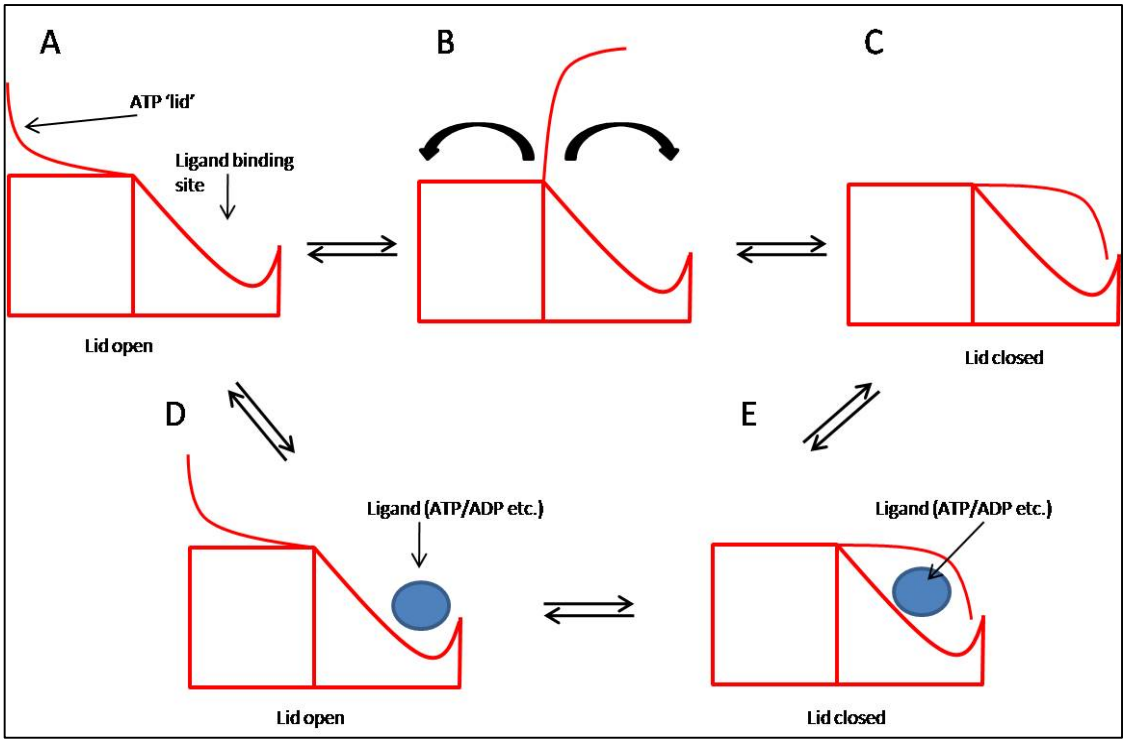

Figure 3.20 The various possible lid positions of the N-terminal domain of Hsp90 during ligand binding are shown. A: Shows the apo state with the lid in an open conformation. B: Shows the apo state with the lid neither in the fully open or fully closed state. B: Shows the apo state with the lid in a closed conformation. D: Shows a ligand bound state with the lid in the open conformation. E: Shows a ligand bound state with the lid in the closed conformation.

ADP binding to the N-terminal domain of Hsp90 is thought to favour an 'open' position[8] for the ATP lid as shown in Figure 3.20D. If we assume movement of the lid from a position of not being fully open (Figure 3.20B) to a fully open position (Figure 3.20D) upon ligand binding, the ΔC_p is therefore based upon the change in exposed non-polar surface area as the back of the lid contacts the main body of the protein. Table 3.9 shows a ΔC_p value of -840 $J \cdot mol^{-1} \cdot K^{-1}$ for ADP binding which can be interpreted as arising from the burial of a large amount of non-polar surface area that was not anticipated in the prediction. If ADP binds when the lid is already in the open position (from A to D) then binding will not induce any further conformational changes, only the displacement of water molecules from within the binding site. There will be no change in surface area burial and as such no major contribution to a change in ΔC_p. If however the lid does not start in the fully 'open' position then the binding of ADP may induce full opening of the lid leading to the burial of surface area along the back of the lid.

However as pH increases the ΔC_p value observed for the binding of ADP becomes more negative until it is greater than that predicted from any model involving ADP. If an increase in pH caused the starting position of the apo protein to resemble Figure 3.20B more than Figure 3.20A, then upon ADP binding opening of the lid would now result in the burial of surface area between the back of the lid and the main body of the protein. This suggests that in the apo state at higher pH, the ATP 'lid' of the protein is not in the fully open position but is more likely to be in an equilibrium between open and closed as shown in Figure 3.20B.

AMPPNP binding to the N-terminal domain of Hsp90 is thought to favour a 'closed' position of the lid as shown in Figure 3.20E. Calculations were made assuming induction of either a 'closed' or 'open' conformation of the lid. Predictions for the ΔC_p of an 'open' lid while bound to AMPPNP were close to that predicted for ADP. Predictions for the 'closed' lid conformation give a large positive ΔC_p. Closure of the lid results in the occlusion of some exposed surface area on the inside of the lid but also the exposure of a large area of non-polar surface area on the back of the lid and the main body of the protein. This exposure of surface area has led to a prediction of a large positive ΔC_p for the binding of AMPPNP to the N-terminal domain of Hsp90.

The experimental results show a positive ΔC_p favouring AMPPNP inducing a lid closed conformation however the results show a far less positive ΔC_p than expected. This suggests that the difference in surface area exposed between the free and bound states is less than anticipated. This again supports the idea that in the apo state the lid of the N-terminal of Hsp90 is closer to Figure 3.20B than Figure 3.20A.

The calculated figures give a difference between the predicted fully 'open' state (ADP bound) and the fully 'closed' state (AMPPNP bound) of the lid as being 850 $J \cdot mol^{-1} \cdot K^{-1}$. The experimentally determined figures give the difference between the ADP and the AMPPNP bound states as being 1100 $J \cdot mol^{-1} \cdot K^{-1}$. This shows a discrepancy of 250 $J \cdot mol^{-1} \cdot K^{-1}$ between the prediction and the experimental data. This may suggest an additional influence, such as a conformational change, on the ΔC_p that is independent of the lid but dependent upon ligand binding.

As the pH increases the discrepancy increases while at lower pH the ΔC_p difference between the two ligand bound states is reduced. At pH five there is a difference of only 260 $J \cdot mol^{-1} \cdot K^{-1}$ however at pH10 there is a difference of closer to 2700 $J \cdot mol^{-1} \cdot K^{-1}$. This suggests a pH dependence to the conformational changes induced by ligand binding that extend beyond the lid region alone. The NMR results from the pH titration with AMPPNP show a series of subtle yet extensive chemical shift changes predominantly across the binding site as described earlier as well as a number of pH dependent but ligand independent chemical shifts. This may indicate an overall shift in the domain as theorised in Nilapwar et al. [17].

3.3.5 Binding of adenosine and adenine to the N-terminal domain of Hsp90 and associated ΔC_p values

As has already been established the binding of adenine-based ligands to NT Hsp90 reflects something of the nature of the binding site. Adenine binds more weakly than adenosine and in turn adenosine binds less tightly than ADP. AMPPNP is then seen to bind less tightly again than ADP, with a similar affinity to adenosine. Previously in this chapter it has been detailed why this might be the case based on the influence of the protonation state of the ligand in relation to the binding of the ligand. Now we consider the ΔC_p of the binding of adenine and adenosine to the NT Hsp90 domain and what information this provides.

From previous NMR experiments [17] it is known that the shifts induced by the adenosine or adenine binding are far fewer than those observed for ADP or AMPPNP suggesting that there is less rearrangement and conformational change associated with binding even accounting for the reduction in contacts due to the smaller molecule. The titration data is shown in Table 3.9. The heat capacity for binding of both adenosine and adenine were calculated at pH8 in 20mM Tris as shown in Figures 3.21 and 3.22.

Protein: N-Terminal		**Ligand:** Adenosine		**pH:** 8.0		**ΔC_p:** 0.65 kJ mol^{-1} K^{-1}		
Temp (C)	Stoichiometry (N)	error	K_d (µM)	Error	ΔH (KJ mol^{-1})	Error (+/-)	TΔS (KJ mol^{-1})	ΔG (KJ mol^{-1})
10	0.96	0.11	79.9	11.8	-69.0	10.2	-46.8	-22.2
10	1.04	0.03	49.9	1.5	-57.4	2.1	-34.1	-23.3
15	0.98	0.01	67.2	1.7	-45.9	0.8	-22.9	-23.0
15	1.03	0.04	82.3	2.1	-60.3	2.7	-37.7	-22.6
20	1.06	0.01	111.6	1.6	-50.4	0.7	-28.1	-22.3
20	0.97	0.04	116.1	2.0	-56.4	2.1	-34.3	-22.1
25	0.84	0.03	174.3	5.6	-46.3	1.7	-24.8	-21.5
25	1.10	0.22	169.2	17.1	-46.6	10.6	-25.0	-21.6
Protein: N-Terminal		**Ligand:** Adenine		**pH:** 8.0		**ΔC_p:** -0.23 kJ mol^{-1} K^{-1}		
Temp (C)	Stoichiometry (N)	error	K_d (µM)	Error	ΔH (KJ mol^{-1})	Error (+/-)	TΔS (KJ mol^{-1})	ΔG (KJ mol^{-1})
10	1.00	0.04	202.9	13.8	-15.7	0.9	4.3	-20.0
15	1.02	0.07	101.5	17.5	-10.1	1.3	12.3	-22.4
20	1.05	0.05	124.1	18.2	-7.2	0.6	14.7	-21.9
25	1.06	0.09	243.7	32.4	-16.5	2.0	4.1	-20.6
30	0.97	0.04	161.4	16.4	-8.4	0.5	13.6	-22.0

Table 3.9 Summary of binding data including errors of the binding of the N-terminal of Hsp90 to adenosine and adenine at pH 8, 20 mM Tris, 5 mM Mg^{2+} across a temperature range of 10°C to 25°C or 30°C.

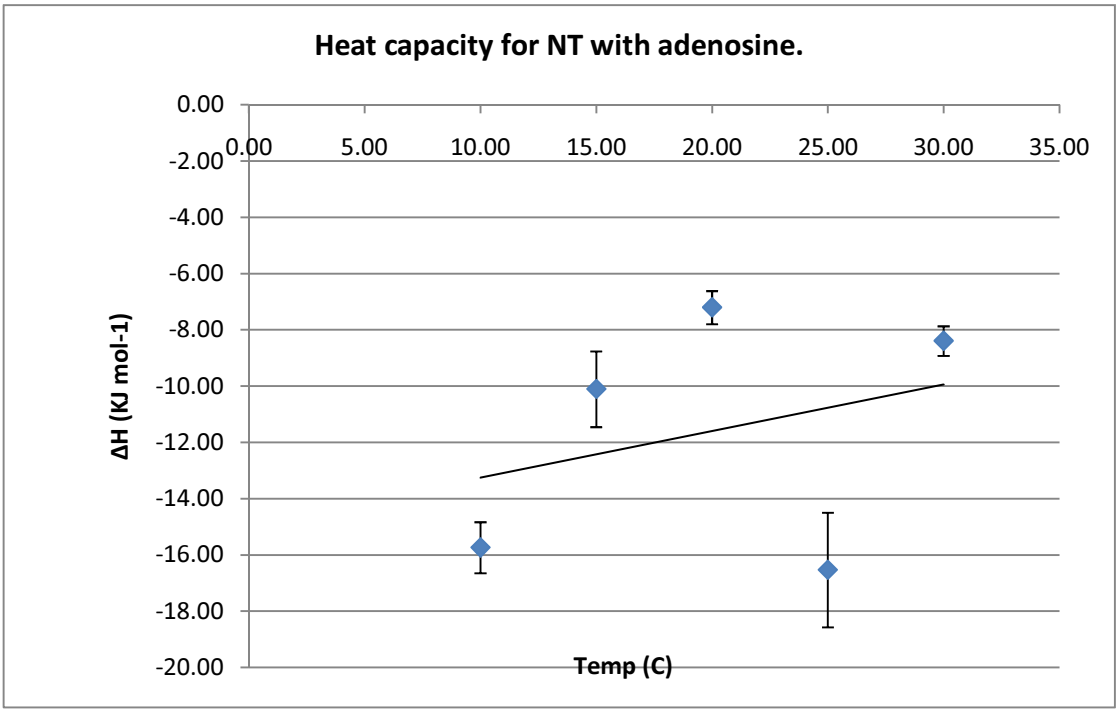

Figure 3.21 The ΔC_p associated with the binding of adenine to the N-terminal domain of Hsp90 showing a slight positive heat capacity as determined by ITC; 20 mM Tris, pH 8. The calculated $\Delta C_p \approx 160$ J·mol^{-1}·K^{-1}.

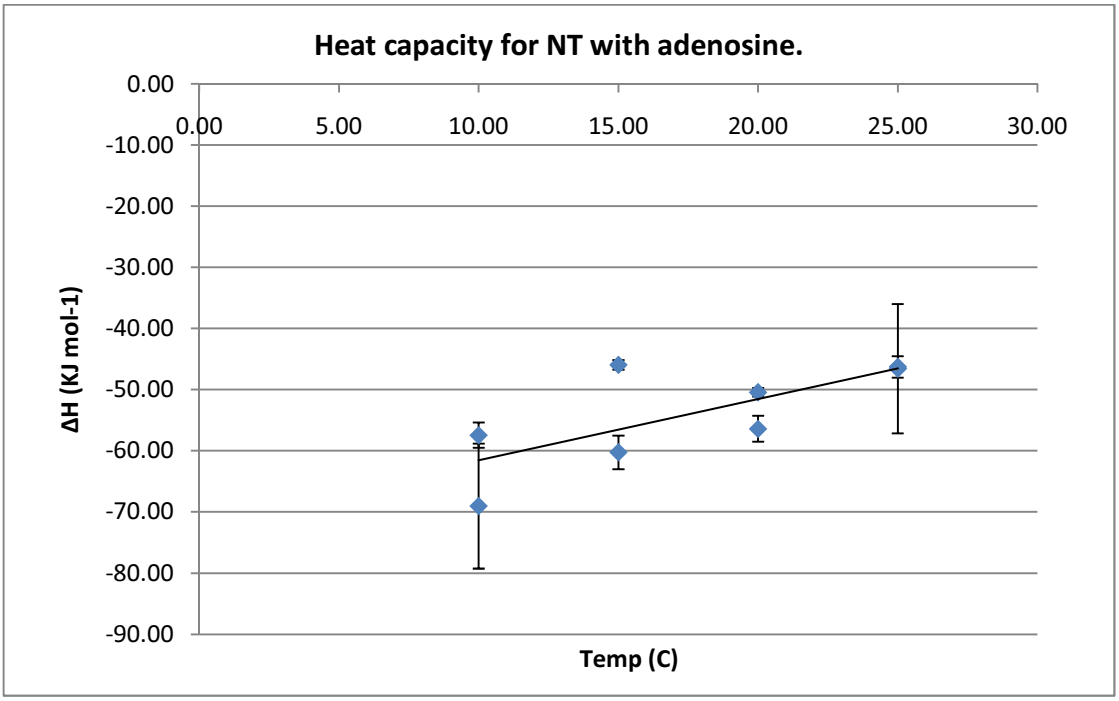

Figure 3.22 The ΔC_p associated with the binding of adenosine to the N-terminal domain of Hsp90 showing a positive heat capacity as determined by ITC; 20 mM Tris, 5 mM Mg^{2+}, pH 8. The calculated $\Delta C_p \approx 650$ J·mol^{-1}·K^{-1}.

From the calculated ΔC_p values (+1000 ±220 $J \cdot mol^{-1} \cdot K^{-1}$ for adenosine and +160 ±80 $J \cdot mol^{-1} \cdot K^{-1}$ for adenine) we can see that both adenosine and adenine have positive heat capacities however the ΔC_p for adenosine is greater than that of adenine and AMPPNP at pH8. The value of +1000 $J \cdot mol^{-1} \cdot K^{-1}$ exceeds the calculated value for the closing of the lid suggesting that there is an additional effect occurring to explain the increased positive heat capacity change. This could include an interaction with water molecules that would be displaced using any large chemical compound. Earlier in the chapter, the binding of the adenosine ring has already been shown to be one of the major contributors to the binding affinity of the nucleotide based ligands. Since the adenosine ring is common to both ADP and AMPPNP it is likely that any changes induced solely by adenosine will not include any movement where ADP and AMPPNP show opposing effects, such as in the movement of the ATP lid. The positive ΔC_p indicates however that there are additional processes occurring to the movement of the 'lid' that may contribute to the discrepancy in differences between the ΔC_p values described previously. The exact nature of these processes however cannot be easily determined by the methods described here and may be the culmination of a number of complex events.

3.3.6 Mutations in the N-terminal of Hsp90 stabilise the 'lid open' and 'lid closed' conformations of the domain

From the experiments described above it is clear that the response of the N-terminal domain to the binding of nucleotide is more complex than a simple lid open/lid closed situation. It may include a number of intermediate positions in equilibrium. Two mutant constructs of Hsp90 were used to probe the binding of ligands to the NT domain with the lid region stabilised or destabilised in each case to explore the equilibrium by attempting to bias the position of the lid to either open or closed. Both mutants were obtained from C. Prodromou from Imperial College London.

Two mutant proteins were made. The T101I mutant is close to the base of the lid region and mutation of this residue to an isoleucine strengthens the contacts between the back of the lid and the domain, thus favouring the open conformation and hence stabilising the open state. In contrast the T22I mutant is on the main body of the NT domain facing out towards the end of the back of the lid (see Figure 3.23). The mutation of residues 22 from Threonine to Isoleucine interferes with hydrophobic contacts between it and the back of the lid with residues such as Val114, thus destabilising the 'open' conformation and favouring the closed form.

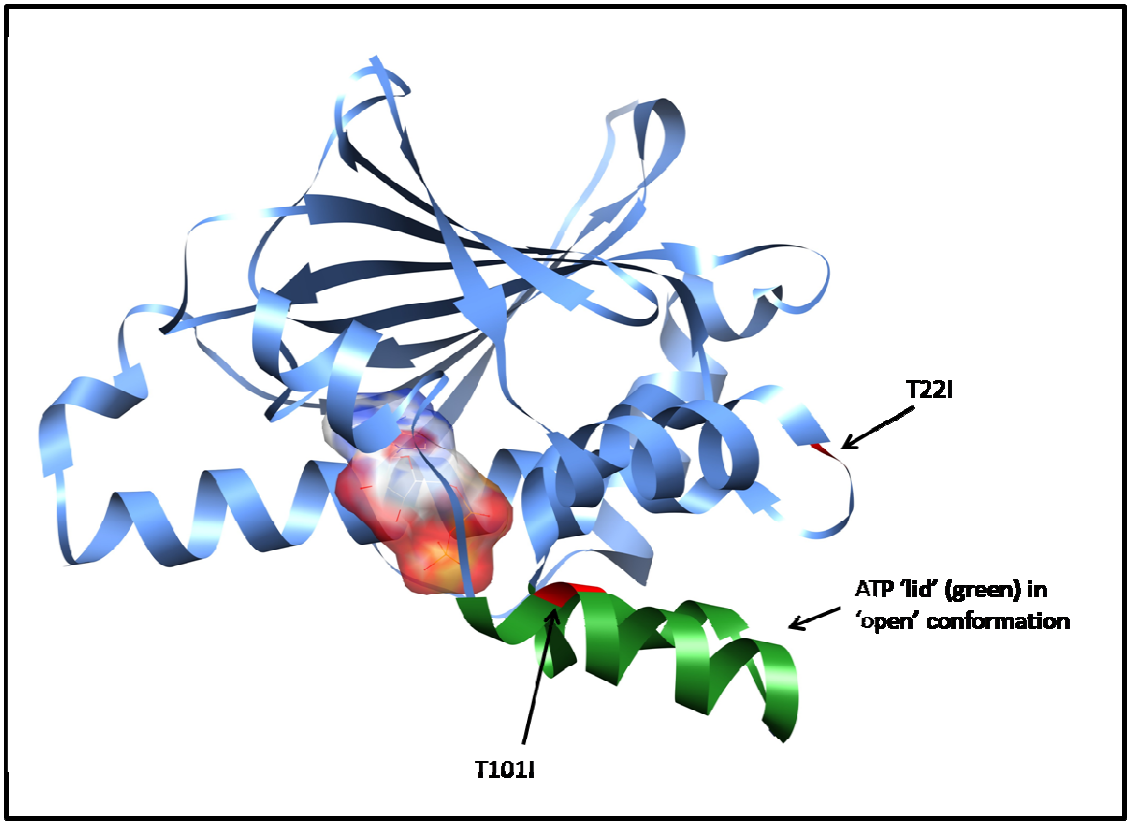

Figure 3.23 The position of the T101I and T22I mutants (red) shown on the crystal structure of the N-terminal domain of Hsp90. The ATP 'lid' region is highlighted (green). Diagram taken from PDB file 1AMW.

Tables 3.10 and 3.11 show a summary of the binding data for the ligand ADP, AMPPNP and adenosine to both the T22I and T101I mutants of the N-terminal domain of Hsp90. Differences between the binding parameters of the wild type and the mutants can be interpreted using the knowledge of how the mutants affect the ATP lid region.

A							ΔC_p -2.05	kJ·mol^{-1}·K^{-1}
Temp (C)	Stoichiometry (N)	Error (N)	K_d (μM)	Error (K_d)	ΔH (kJ mol^{-1})	Error (ΔH)	TΔS (kJ mol^{-1})	ΔG (kJ mol^{-1})
10.00	1.00	±0.02	15.90	±1.18	-73.51	±2.28	-47.51	-26.01
10.00	1.00	±0.01	4.39	±1.18	-67.36	±2.28	-38.27	-29.10
15.00	1.03	±0.02	8.33	±0.48	-71.13	±1.42	-43.04	-28.09
20.00	0.99	±0.04	18.08	±4.18	-85.31	±8.80	-58.63	-26.68
20.00	0.91	±0.06	50.76	±4.18	-101.0	±8.80	-76.90	-24.14
25.00	0.82	±0.09	60.24	±6.72	-97.61	±14.34	-73.48	-24.14
B							ΔC_p -0.79	kJ mol^{-1} K^{-1}
Temp (C)	Stoichiometry (N)	error	K_d (μM)	Error (K_d)	ΔH (kJ mol^{-1})	Error (ΔH)	TΔS (kJ mol^{-1})	ΔG (kJ mol^{-1})
10.00	1.01	±0.04	102.44	±2.29	-57.36	±2.80	-35.72	-21.64
15.00	0.95	±0.13	143.47	±8.16	-50.71	±7.48	-29.53	-21.18
20.00	1.04	±0.21	188.22	±10.57	-59.75	±13.00	-38.83	-20.92
25.00	0.90	±0.62	252.27	±40.63	-67.57	±50.21	-47.05	-20.52
C						ΔC_p -5.9	kJ mol^{-1} K^{-1}	
Temp (C)	Stoichiometry (N)	error	K_d (μM)	Error (K_d)	ΔH (kJ mol^{-1})	Error (+/-)	TΔS (kJ mol^{-1})	ΔG (kJ mol^{-1})
10.00	0.98	±0.02	72.93	±2.96	-55.73	±1.71	-33.29	-22.44
10.00	0.97	±0.22	48.31	±8.79	-63.64	±1.65	-40.28	-23.36
15.00	1.02	±0.03	110.62	±3.72	-58.62	±1.89	-36.77	-21.85
20.00	1.06	±0.15	258.40	±15.08	-124.9	±20.41	-104.87	-20.07

Table 3.10 Binding data for the mutant T22I to the ligands ADP (A) AMPPNP (B) and adenosine (C) as determined by ITC in 20 mM Tris, 5 mM Mg^{2+} at pH 8.

A						ΔC_p -610	J mol^{-1} K^{-1}	
Temp (C)	Stoichiometry (N)	error	K_d (µM)	Error (K_d)	ΔH (kJ mol^{-1})	Error (+/-)	TΔS (kJ mol^{-1})	ΔG (kJ mol^{-1})
10.00	1.01	0.01	3.47	±0.17	-69.12	±0.43	-39.55	-29.57
15.00	1.06	0.01	6.53	±0.26	-72.26	±0.45	-43.64	-28.61
20.00	1.04	0.01	12.30	±0.80	-75.31	±1.05	-47.75	-27.56
25.00	1.07	0.01	20.24	±1.59	-78.32	±1.63	-51.53	-26.79
B						ΔC_p -1290	J mol^{-1} K^{-1}	
Temp (C)	Stoichiometry (N)	error	K_d (µM)	Error (K_d)	ΔH (kJ mol^{-1})	Error (+/-)	TΔS (kJ mol^{-1})	ΔG (kJ mol^{-1})
10.00	1.04	0.02	45.03	±2.64	-35.43	±0.79	-11.66	-23.77
15.00	1.04	0.02	74.85	±3.67	-38.17	±0.97	-15.41	-22.76
20.00	1.00	0.04	165.87	±9.91	-48.33	±2.66	-27.13	-21.19
C						ΔC_p -1360	J mol^{-1} K^{-1}	
Temp (C)	Stoichiometry (N)	error	K_d (µM)	Error (K_d)	ΔH (kJ mol^{-1})	Error (+/-)	TΔS (kJ mol^{-1})	ΔG (kJ mol^{-1})
10.00	0.99	0.02	53.76	±2.39	-53.22	±1.55	-30.09	-23.14
15.00	1.06	0.03	72.46	±3.15	-51.00	±1.69	-28.09	-22.84
20.00	1.08	0.02	116.60	±2.88	-54.43	±1.41	-32.38	-22.07
25.00	1.00	0.14	194.20	±16.86	-74.68	±12.51	-53.52	-21.19

Table 3.11 Binding data for the mutant T101I to the ligands ADP (A) AMPPNP (B) and adenosine (C) as determined by ITC in 20 mM Tris, 5 mM Mg^{2+} at pH 8.

The data in Tables 3.10 and 3.11 can be used to calculate the ΔC_p values for the binding of ADP, AMPPNP and adenosine to both the T22I and T101I mutants of the N-terminal domain of Hsp90. The graphs for the ΔC_p values are shown in Figures 3.24 - 3.26 and summarised in Table 3.9.

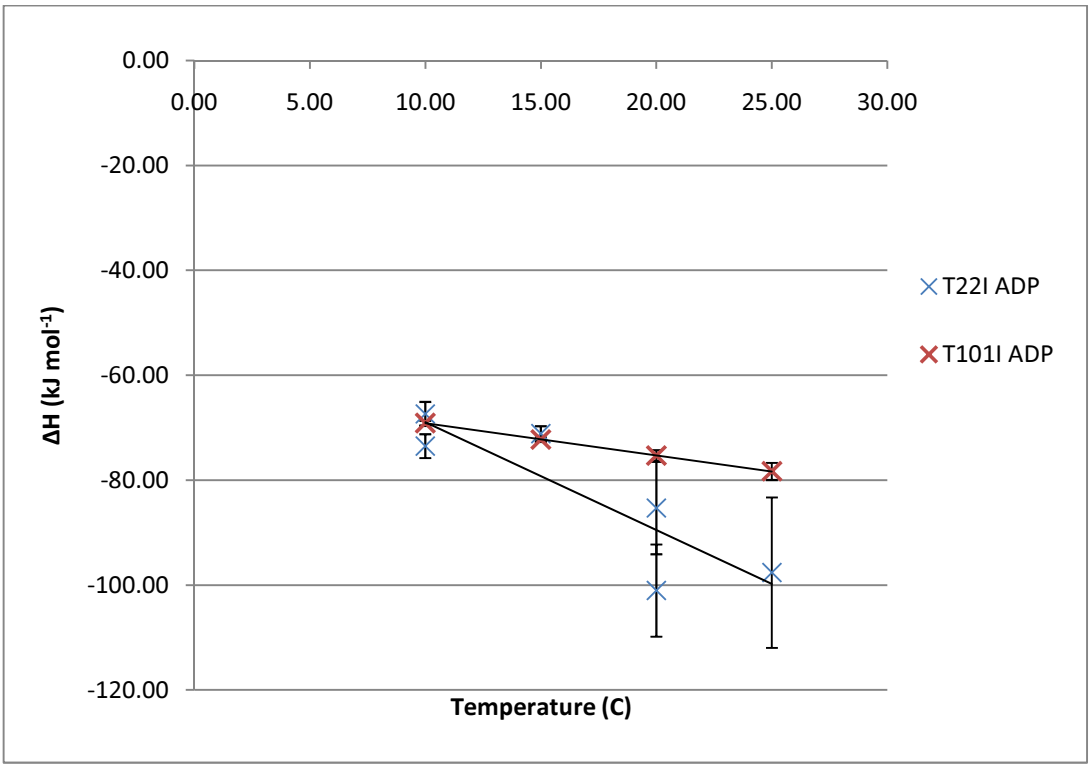

Figure 3.24 The ΔC_p associated with the binding of ADP to the mutants T101I and T22I of the N-terminal domain of Hsp90 as determined by ITC at pH 8, 20 mM Tris, 5 mM Mg^{2+}.

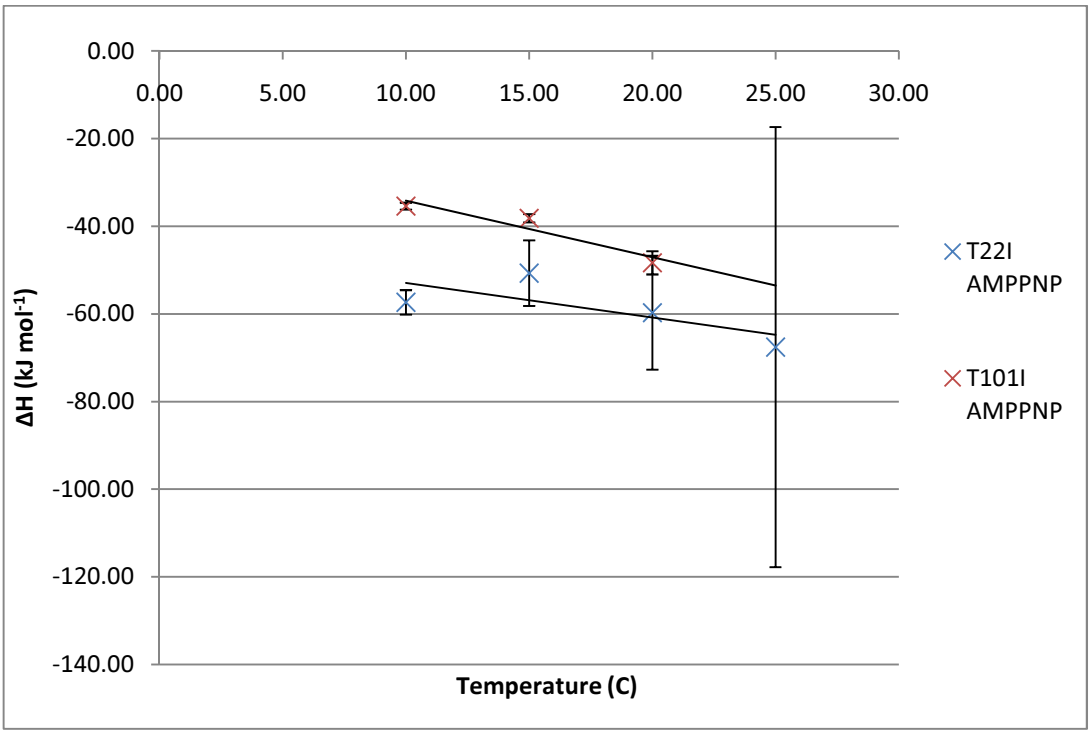

Figure 3.25 The ΔC_p associated with the binding of AMPPNP to the mutants T101I and T22I of the N-terminal domain of Hsp90 as determined by ITC at pH 8, 20 mM Tris, 5 mM Mg^{2+}.

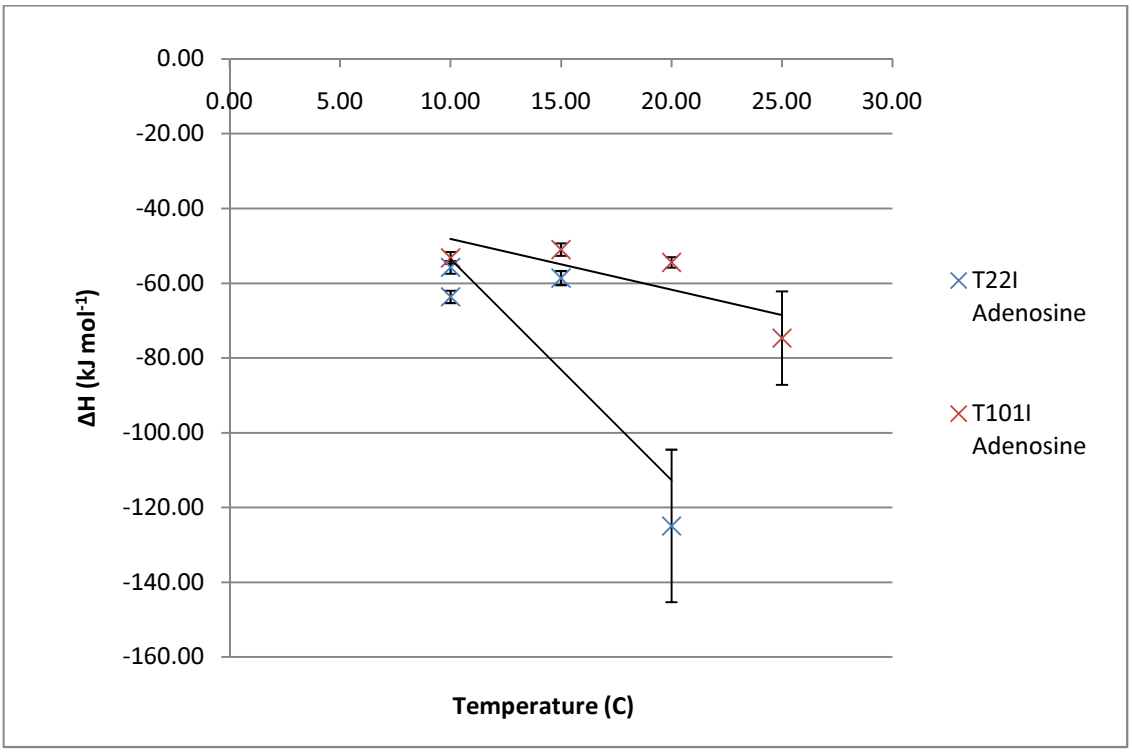

Figure 3.26 The ΔC_p associated with the binding of adenosine to the mutants T101I and T22I of the N-terminal domain of Hsp90 as determined by ITC at pH 8, 20 mM Tris, 5 mM Mg^{2+}.

3.3.7 Analysis of the binding of ADP, AMPPNP and adenosine to the mutants T22I and T101I of the N-terminal of Hsp90 can be used to inform upon the position of the ATP lid region and its response to the binding of different ligands

Table 3.12 summaries the binding constants as determined by ITC for each mutant and the wild type of the N-terminal domain of Hsp90 with ADP, AMPPNP and adenosine. The binding affinity differences between the mutant forms can be explained with the knowledge of how the mutants affect the ATP lid region.

Construct and ligand used.	K_d (μM)	ΔH (kJ mol^{-1})	TΔS (kJ mol^{-1})	ΔG (kJ mol^{-1})
WT w/ ADP	35.93	-80.42	-55.48	-24.94
T22I w/ ADP	18.08	-85.31	-58.63	-26.68
T101I w/ ADP	12.30	-75.31	-47.75	-27.56
WT w/ AMPPNP [17]	105.00	-39.70	-17.40	-22.30
T22I w/ AMPPPNP	188.22	-59.75	-38.83	-20.91
T101I w/ AMPPPNP	165.86	-48.33	-27.13	-21.19
WT w/ adenosine	111.63	-50.42	-28.15	-22.27
T22I w/ adenosine	258.40	-124.93	-104.87	-20.07
T101I w/ adenosine	116.60	-54.43	-32.38	-22.07

Table 3.12 A summary of the binding parameters associated with binding of ADP, AMPPNP and adenosine to the wild type and T22I and T101I mutants of the N-terminal domain of Hsp90. Data shown from ITC titrations at 20°C, pH 8.

3.3.8 ADP binding in both the T22I and T101I mutants of the N-terminal domain of Hsp90

The T22I mutant stabilises the 'lid closed' conformation. This is the conformation that is favoured upon AMPPNP binding to the N-terminal domain of Hsp90. The binding of ADP to the T22I mutant appears to be more favourable than the wild type (Table 3.12). It can be seen that the K_d is lower for binding of ADP to the T22I mutant than the wild type and that both the ΔH and TΔS are slightly more negative however the ΔG value is very close for the two.

The T101I mutant stabilises the 'lid open' conformation. The ΔH and TΔS value are slightly less negative than in the wild type however not by much. It is interesting to note then that binding of ADP both mutants is tighter than the wild type. The T101 'lid open' mutant mimics the ADP bound form and so this is not surprising however it is also the case for the 'lid closed' T22I mutant that should be closer to the AMPPNP bound state.

This suggests that although binding of ADP induces an opening of the ATP lid this is not the only route leading to an increase in affinity. If the ATP binding and hydrolysis cycle of Hsp90 is considered then ATP binds, induces a lid closure and is then hydrolysed to ADP. There is then a conformational change induced by this hydrolysis that leads to lid opening, other conformational changes across the protein, and release of ADP and the free phosphate. Thus initially ADP and free phosphate are present in the lid closed position. It is possible that the lid closed conformation is more stable for the binding of ADP with free phosphate than the lid open conformation and that the conformational change leads to a destabilisation of the bound ADP ligand allowing it to dissociate. Normally however ADP binding causes the lid to open so that ADP binding to the lid closed state is never observed. It is also impossible to observe the ADP with free phosphate as there is no way to mimic the presence of both ADP and the free phosphate in the immediately post hydrolysis state. The T22I mutant may have allowed the conformational changes induced by ADP to be overcome by the destabilisation of the open lid conformation and has allowed the domain to retain elements of the 'lid closed' state (Figure 3.27).

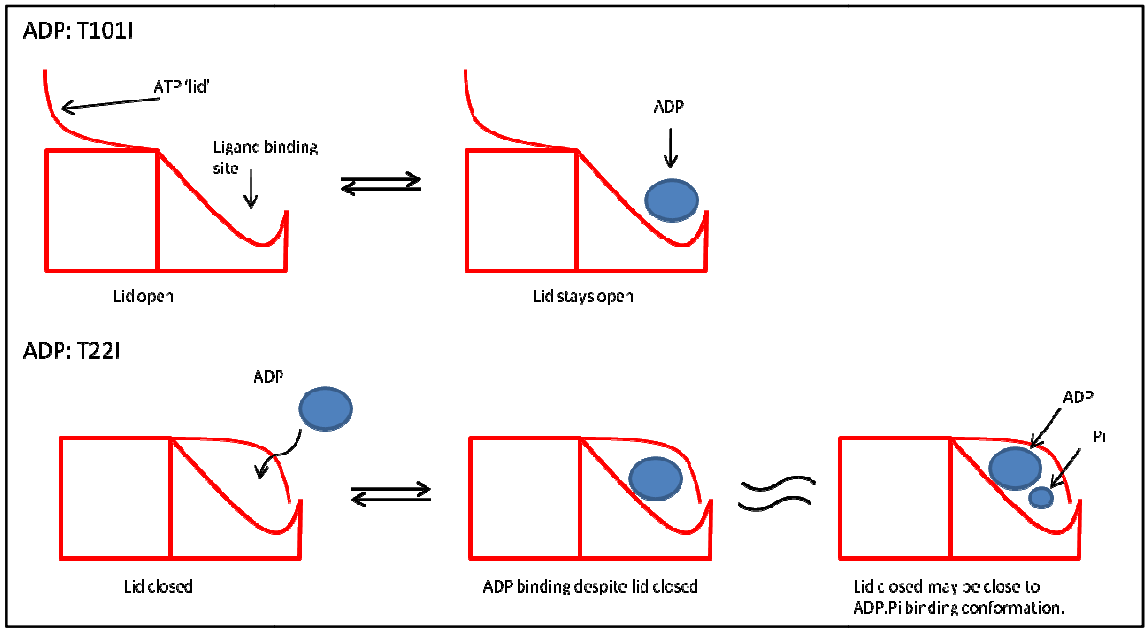

Figure 3.27 Schematic representation of the binding of ADP to both T22I and T101I mutants of the N-terminal of Hsp90 showing the possible conformational changes induced by ligand binding.

3.3.9 AMPPNP binding in both the T22I and T101I mutants of the N-terminal domain of Hsp90

The T22I mutant stabilises the 'lid closed' conformation. It is thought that AMPPNP binding induces movement towards the 'lid closed' state. The binding of AMPPNP to the T22I mutant shows a greatly decreased binding affinity compared to the wild type (Table 3.12). This result suggests that this state is highly unfavourable for the binding of AMPPNP despite mimicking the structure of the AMPPNP bound state. A far more negative ΔH and TΔS are observed. When binding of AMPPNP to the T22I mutant is considered then accessibility of the binding site must be considered (Figure 3.28) as well as the affinity of the binding site. If the lid is in a closed position without any ligand bound then it will occlude the binding site and thus it will be less favourable for the lid to move away to allow ligand to bind thus leading to a less favourable binding constant.

The T101I mutant stabilises the 'lid open' conformation which is thought to be opposing the structure favoured by the binding of AMPPNP. The titration results reveal that the binding affinity is far less favourable than the wild type but more favourable than the T101I mutation. If the 'lid open' state favours ADP and not ATP binding then this will lead to a decrease in binding affinity for AMPPNP despite the accessibility.

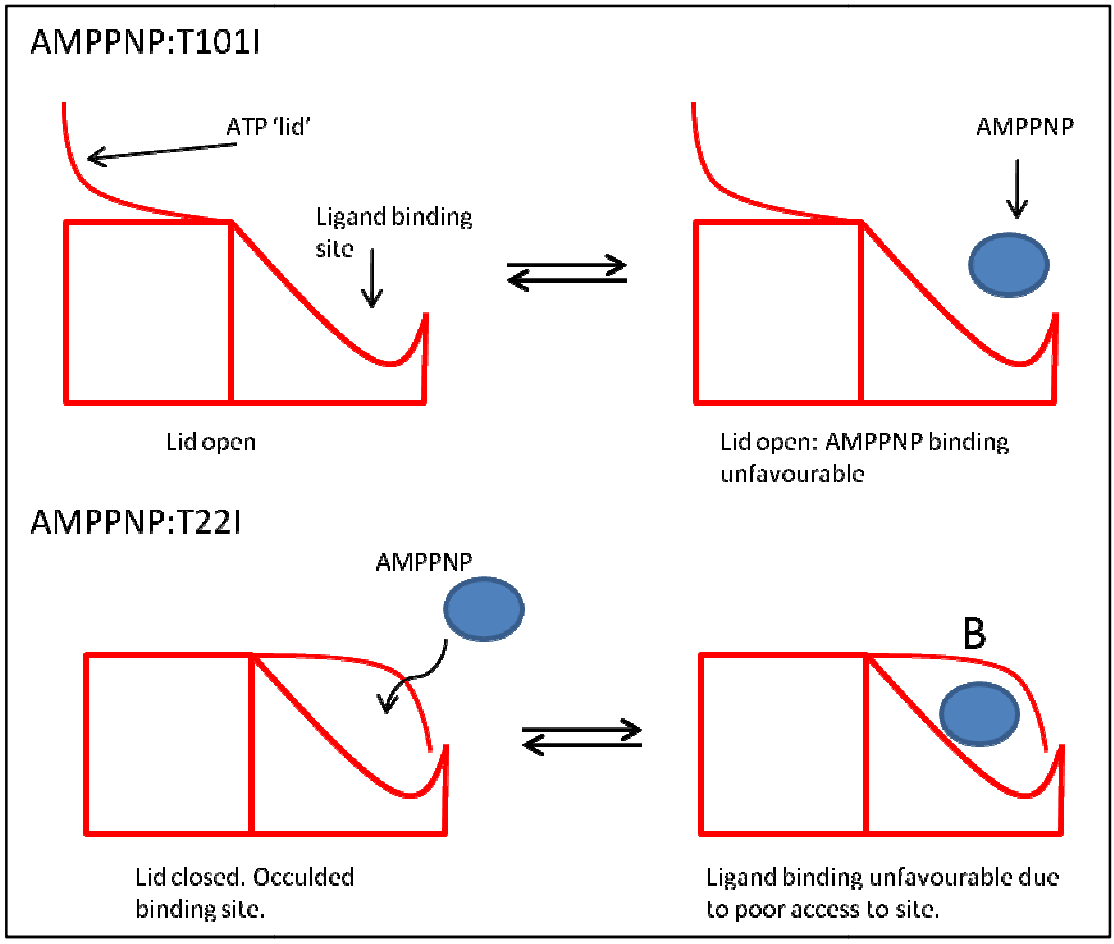

Figure 3.28 Schematic representation of the binding of AMPPNP to both T22I and T101I mutants of the N-terminal of Hsp90 showing the possible conformational changes induced by ligand binding.

3.3.10 Adenosine binding in both the T22I and T101I mutants of the N-terminal domain of Hsp90

Binding of adenosine to the T22I mutant shows a dramatic decrease in binding affinity with both ΔH and TΔS becoming more negative. If the 'lid closed' conformation favoured by the T22I mutant is causing the occlusion of the binding site this may explain the less favourable binding affinity.

Binding of adenosine to the T101I mutant shows little change in binding affinity or ΔH and TΔS compared to the wild type. This suggests that the 'lid open' state does not destabilise the binding of adenosine to the protein and thus the adenosine base binds to the protein when it is in the same conformation as that induced by AMPPNP binding.

3.3.11 Analysis of the ΔC_p of the mutant NT Hsp90 domains

The ΔC_p was determined for both mutants with both ADP and AMPPPNP at pH8. These are shown in Figures 3.24 – 3.26 and summarised in Table 3.13.

Construct of NT Hsp90	ΔC_p with ADP ($kJ \cdot mol^{-1} \cdot K^{-1}$)	ΔC_p with AMPPNP ($kJ \cdot mol^{-1} \cdot K^{-1}$)	ΔC_p with adenosine ($kJ \cdot mol^{-1} \cdot K^{-1}$)
WT	-0.95	+0.15 ref:[17]	+0.65
T22I mutant (lid 'closed')	-2.05	-0.79	-5.90
T101I mutant (lid 'open')	-0.61	-1.29	-1.36

Table 3.13 A summary of the ΔC_p data for ADP, AMPPNP and adenosine comparing the wild type, T22I and T101I mutants of the N-terminal of Hsp90 at pH 8.

The ΔC_p obtained for the T101I mutant with ADP is smaller and less negative than that determined for the WT although the binding constants are very different. In contrast the ΔC_p value for the T22I mutant is 1.0 $kJ \cdot mol^{-1} \cdot K^{-1}$ more negative than the wild type with ADP. This suggests that the mutations alter the equilibrium position of the lid between open and closed. The T22I mutation favours lid closing while ADP induces a 'lid open' state thus when the overall the lid equilibrium shifts towards the 'fully open' state it does so from closer to the 'closed state' thus leading to more burial of surface area upon binding. In contrast the T101I mutant is working with the influence of ADP binding and thus the lid equilibrium shifts more towards the 'lid open' state upon ligand binding, but since it is already closer to being 'open' to begin with there is less burial of surface area and thus a smaller heat capacity change. This also suggests that the influence of the nucleotide is stronger than the influence of the T22I mutation over the lid conformation since the lid does appear to still close in the presence of ligand.

The ΔC_p obtained for the T101I and T22I mutants with AMPPNP are both more negative than for the wild type binding to AMPPNP. The negative ΔC_p value determined for the binding of AMPPNP to the T101I mutant suggests that the ligand is less able to overcome the influence of the mutation and thus the lid does not shut in response to AMPPNP binding. The binding of AMPPNP to the T22I mutant does not appear to be sufficient to give a positive ΔC_p that would be expected if the lid were closed. This suggests that the destabilising of the lid open conformation and the addition of the AMPPNP ligand does not lead simply to the 'lid closed' conformation. The destabilisation of the 'lid open' conformation may lead to more wide ranging conformational effects beyond the lid its self that influence the ΔC_p values observed.

The ΔC_p values associated with adenosine binding to the mutant constructs of Hsp90 are both very negative in contrast to the positive ΔC_p displayed by the wild type. As has already been discussed it is likely that the ΔC_p due to adenosine binding to the wild type N-terminal domain is not solely due to the lid movement. In combination with the effects the mutations have on the protein, it is likely that the disruption causing the large negative ΔC_p values is, in addition to any movement of the lid region, also due to numerous other conformational changes.

3.3.12 NMR of the mutants T22I and T101I of NT Hsp90

In order to look at the mutant NT domains in more detail ^{15}N-HSQC spectra were collected in the apo state and when bound to AMPPNP and ADP (Figures 3.29, 3.30 and 3.31). These spectra were then compared to the wild type ^{15}N-HSQC spectra obtained previously for the three states described and shifts due to the mutations identified for each state. The complete list of shifts for each mutant and the shifts common to each mutant are shown plotted onto the crystal structure in Figure 3.32. Shifts unique to each mutant were identified and plotted onto the known crystal structure of the ADP bound form (PDB file 1AMW) [8] as shown in Figure 3.33.

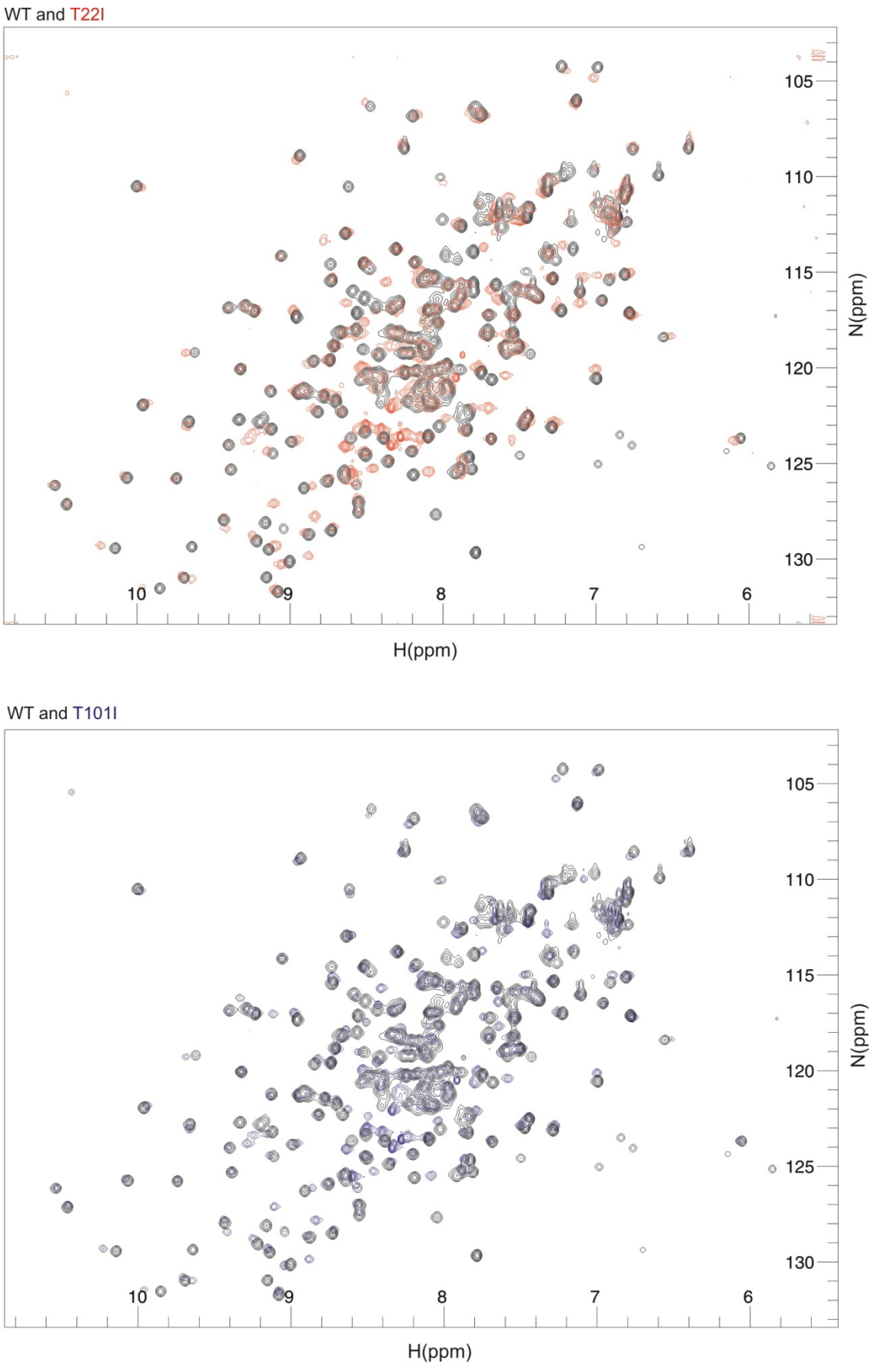

Figure 3.29 Overlays of the wild type (black) and mutant forms of Hsp90 (T22I – top red, T101I – bottom blue) in the apo state. Spectra recorded in 20 mM Tris, 5 mM Mg^{2+}, pH 8 at 700 MHz field strength.

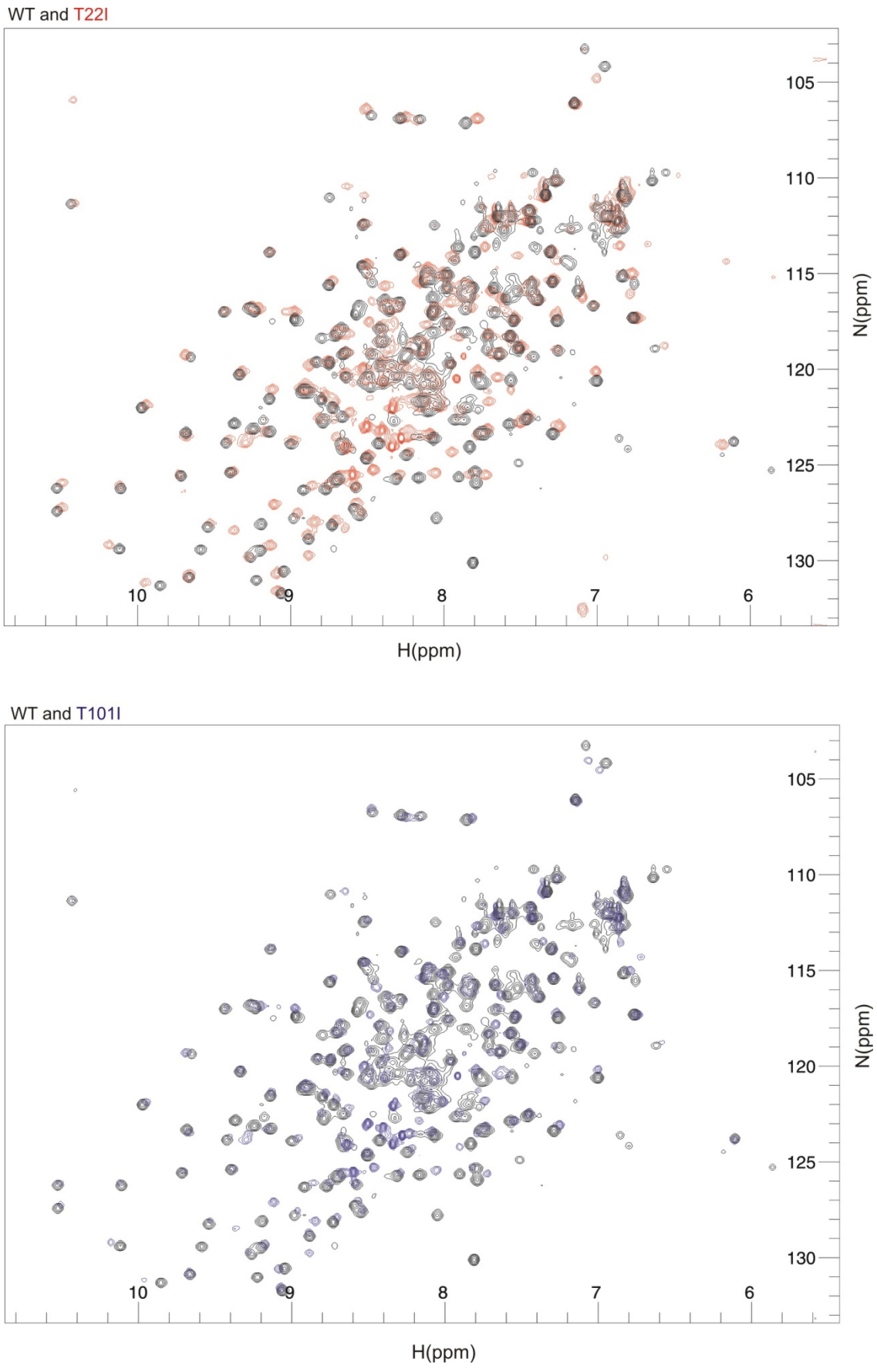

Figure 3.30 Overlays of the wild type (black) and mutant forms of Hsp90 (T22I – top red, T101I – bottom blue) in the AMPPNP bound state. Spectra recorded in 20 mM Tris, 5 mM Mg^{2+}, pH 8 at 700 MHz field strength.

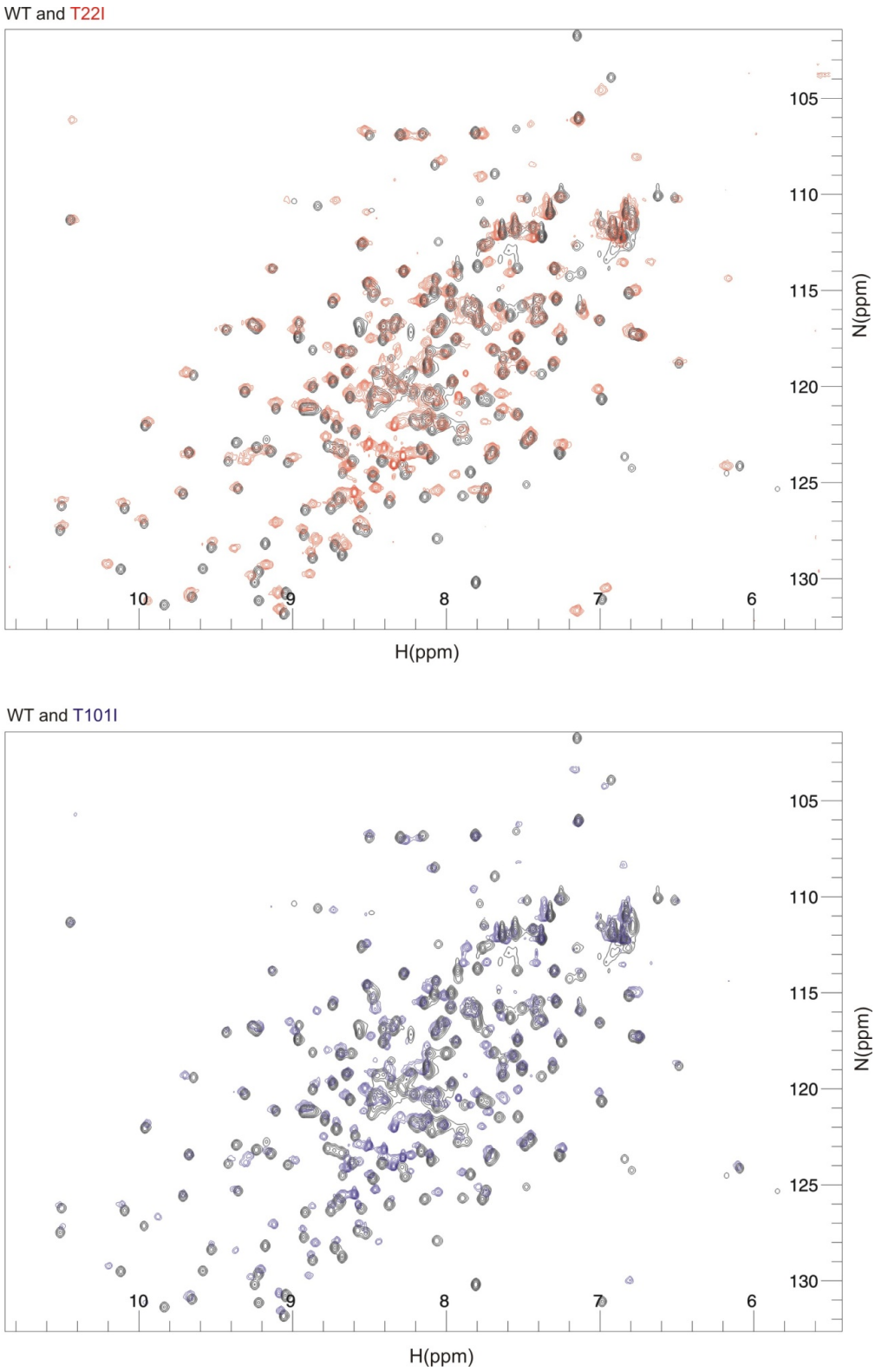

Figure 3.31 Overlays of the wild type (black) and mutant forms of Hsp90 (T22I – top red, T101I – bottom blue) in the ADP bound state. Spectra recorded in 20 mM Tris, 5 mM Mg^{2+}, pH 8 at 700 MHz field strength.

There are a number of distinctive differences both between the mutants and the wild type and between the mutants themselves in each state. The shifts associated with each mutant in the apo state can be seen to map to one side of the protein with subtle differences between the two constructs (See fig. 3.32).

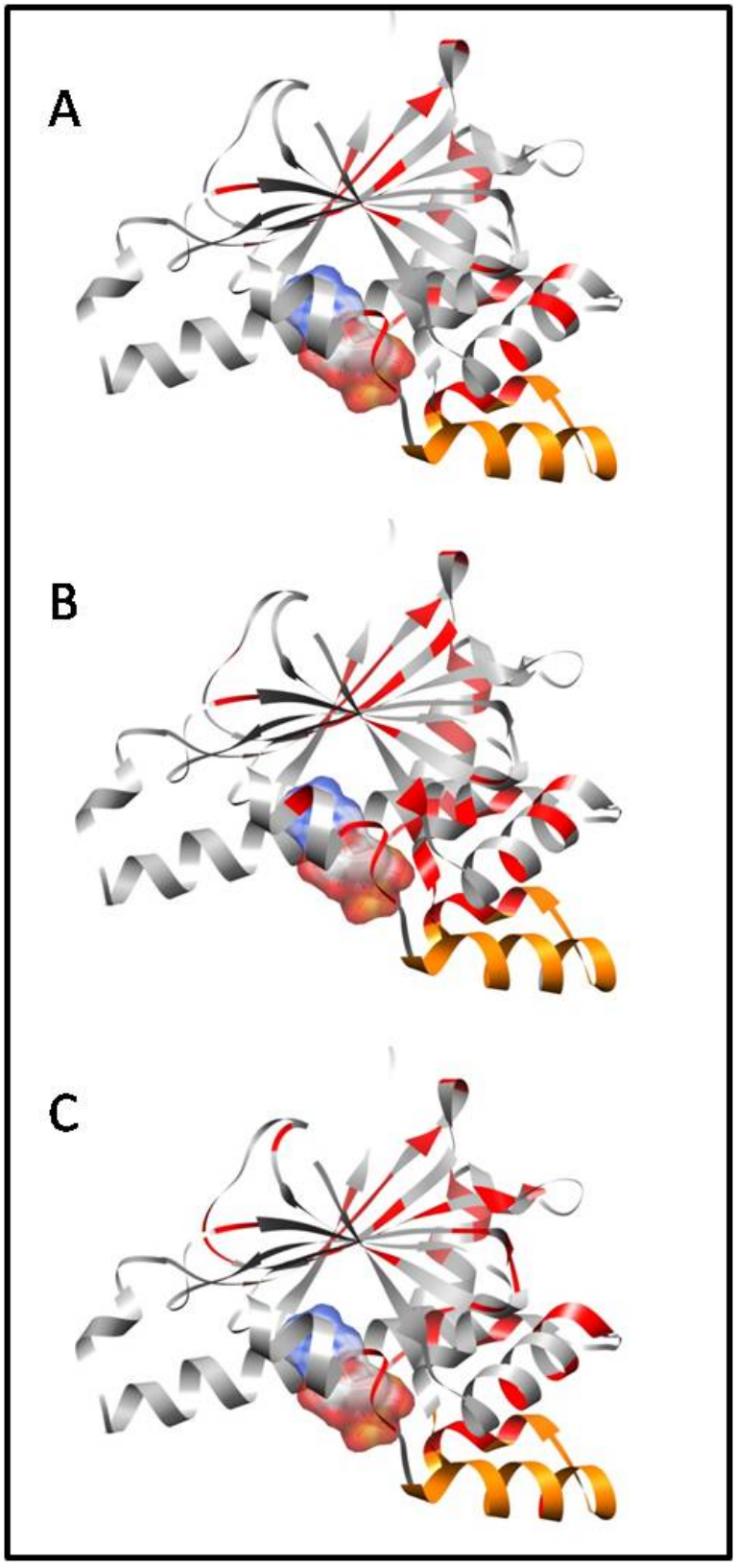

Figure 3.32 Diagrams for the shifts of the T22I and T101I mutants of the N-terminal domain of Hsp90 in the apo state. ATP lid is shown in orange. A: Shows the shifts associated with both mutant constructs. B: shows all shifts associated with the T101I construct. C: shows all shifts associated with the T22I. Position of the ligand ADP shown only for the purpose of comparison with other figures. Diagram taken from PDB file 1AMW.

The shifts common to both mutants of the N-terminal of Hsp90 (Figure 3.32A) map to the lid region, the β-sheet which forms the back of the binding pocket and the two α helices that contact the back of the lid. Shifts that are unique to each mutant are highlighted in Figure 3.33.

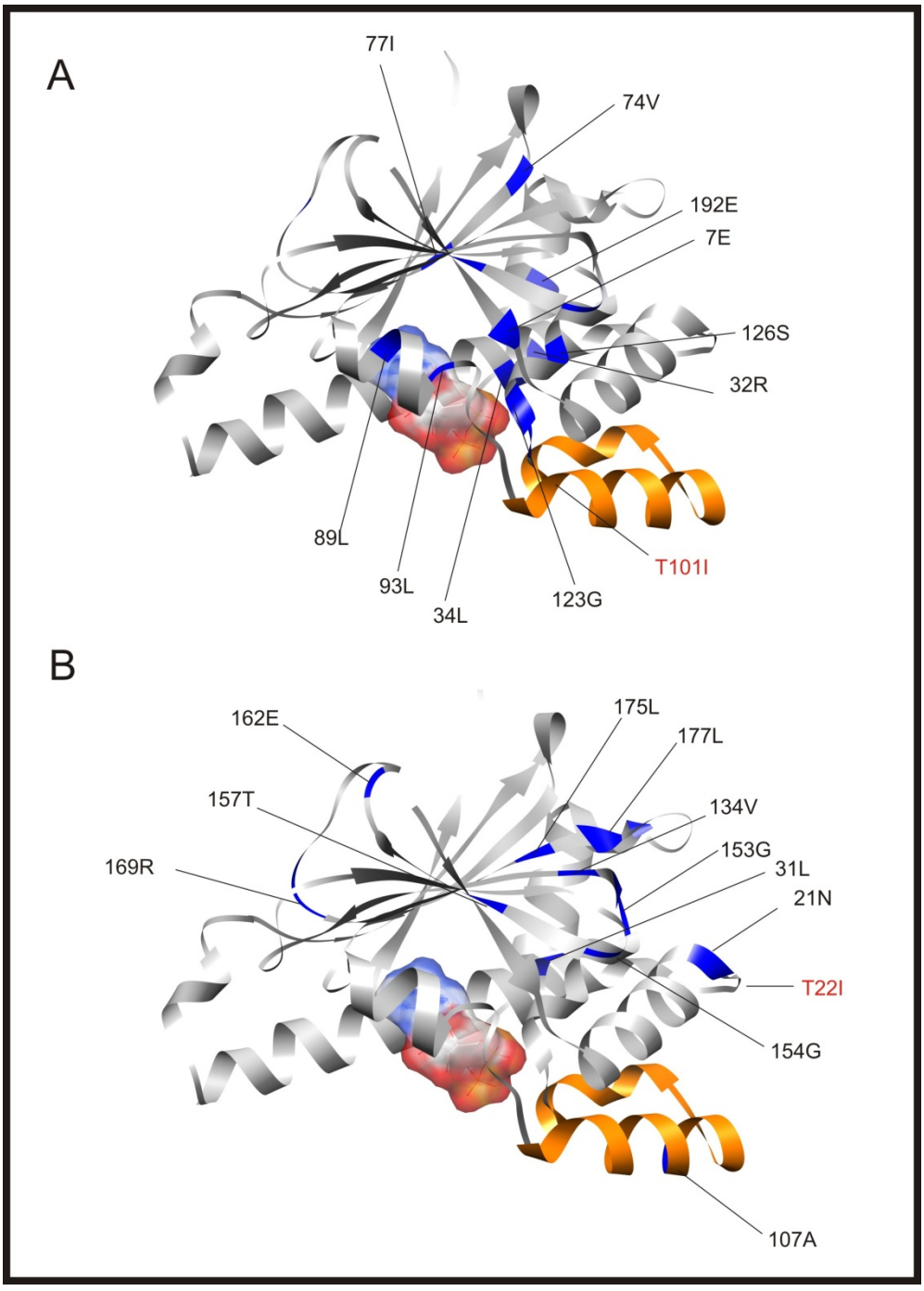

Figure 3.33 Diagrams for the unique shifts of the T22I and T101I mutants of the N-terminal of Hsp90 in the apo state. ATP lid is shown in orange. A: Shows the shifts only associated with the T101I mutant construct only. B: Shows shifts associated with the T22I mutant construct only. Diagram taken from PDB file 1AMW. Locations of mutant residues labelled in red.

The T22I mutant (Figure 3.32 C all shifts and Figure 3.33 B unique shifts) shows a number of shifts unique to it at the base of the binding pocket on the β-sheet structure that forms the back of the binding pocket. The only shifts that are not located within this region are Glu162, Gly168 and Arg169 which are located on a loop at the top of the β-sheet. Two shifts are observed within the lid region itself, these are Ala107 and Gly118 while two shifts are seen close to the mutation site but also close to the two shifts observed in the lid – these also are the only two shifts not observed within the β-sheet. Ala107 is opposite a shift in Asn21 which is also directly next to the mutation T22I itself. Gly118 is opposite a shift in Leu31 which is also close to the original mutation. The collection of shifts around the base of the binding pocket (Val130, Ala131, Arg133, Gly154, Thr157, Leu175, Lue177 and Leu182) is likely to alter the nature of the binding site significantly around the region where the adenine ring system sits. As has already been established, it is the adenine ring that provides much of the binding affinity and disruptions to these contacts is likely to affect the binding affinity of the ligands. This is supported by the reduced binding affinities observed for both ADP and AMPPNP.

The T101I mutant (Figure 3.32 B showing all shifts and Figure 3.33 A showing unique shifts) shows a number of shifts on the periphery of the binding site on the edges of the β-sheet and the long helix with few shifts observed in the lid itself and in close proximity to it. The β-sheet shifts (Ile64, Val74, Ile77 on one side and Gly153, Gly 154, Thr157 and Glu7 on the other) flank the bound nucleotide and may well represent an overall movement in the domain as suggested by the ΔC_p values discussed previously. Within the lid itself residues Gly118 and Val122 show shifts although why this should be in a 'lid open' conformation is unclear. Shifts seen in Glu33, Leu89 and Leu93 are at the mouth of the ligand binding site. The former is on the long helix while the later two are part of a smaller helix, both regions however would be impacted by closure of the lid. Shifts observed in Gly123 and Ser126 are close to the terminal phosphate of the ligand thus showing additional alteration of the binding site which will contribute to the altered binding constants as previously seen.

The large number of residues seen to show chemical shifts upon mutating either T22I or T101I suggests that each has a significant effect upon the protein beyond the region of the mutation (either the lid or the helix adjoining the lid). Although shifts are observed in this region, shifts are also observed across the base of the binding pocket in the β-sheet and in a number of surrounding helices. However ITC confirms binding and the NMR ^{15}N-HSQC spectra show a very similar set of results to the wild type suggesting a large number of small changes

rather than drastic ones. It is already known that ligand binding induces a large number of shifts beyond the binding site alone suggesting an inherent flexibility in the N-terminal domain of Hsp90. The large number of shifts observed for both mutants suggests that there is an overall adjustment of the domain and subsequently the binding site which may be linked to the disruption or stabilisation of the lid region. This in turn has an effect on the binding affinity of the nucleotide based ligands to each mutant as described previously. The consequences for using these mutations to look solely at the influence of the lid position over the binding of ADP and AMPPNP is that the results obtained are not based solely on the position of the lid since many other changes are occurring to the binding site. This is reflected in the ΔC_p values observed, as previously described, which cannot be explained by a simple movement of the ATP 'lid' alone. Since the mutations are still influencing the position of the lid it suggests that not only is the lid position important for the binding of nucleotide based ligands but that the position of the lid is also linked to a wider ranging and more subtle series of changes across the ligand binding site that alters binding affinity of the ligand during the binding and hydrolysis cycle.

3.4 Conclusions

There is strong evidence to suggest that the preferred binding state of the ligand to the NT Hsp90 domain is the -3 charge state. ADP shows strongest binding affinity while in this charge state and the transition of AMPPNP from the -3 to the -4 charge state coincides with a drop in binding affinity. The change in binding affinity has been clearly demonstrated by ITC and the presence of a protonation event on the ligand and not on the protein has been confirmed by both ^{1}H and ^{31}P NMR. Values for the pKa of both the bound and free states have also been confirmed as being at pH 6.5 and pH 8 respectively.

The ΔC_p of binding was also determined by ITC for each ligand. Previously predicted values for the ΔC_p were compared to the actual values and variations from this were described in terms of conformational changes associated with the ATP 'lid' region moving between an 'open' and 'closed' conformation and the likelihood of the apo state being in equilibrium between open and closed. The ΔC_p data suggests that ligand binding may lead to a change in equilibrium position of the lid with ADP favouring a 'lid open' conformation while binding of AMPPNP favours a 'lid closed' conformation. Further investigation of the lid region was

undertaken using two mutants, T22I stabilising the 'open' lid conformation and T101I destabilising the 'open' conformation. The nature of the conformational changes within the mutants was also investigated through NMR observing the shifts associated with each mutant in various ligand bound states. These mutants revealed changes in all thermodynamic characteristics and ΔC_p values in a way that supported the overall hypothesis that binding of AMPPNP favoured a 'closed lid' conformation while ADP binding favoured an 'open lid' conformation. Studies involving the mutants also suggested that movement of the lid was not an isolated event but concurrent with a subtle rearrangement of the region around the nucleotide binding site that alters the ligand binding affinity and is also reflected by the change in heat capacity that cannot be explained by the change in buried surface area due to the lid movement alone.

4 NMR Structural Investigation

4.1 Introduction

Within this chapter a detailed analysis by NMR of the N-terminal domain of Hsp90 is presented. Building upon the pre-existing backbone assignment of the N-terminal domain of Hsp90 undertaken by Salek et. al.[15] a series of standard NMR experiments were performed to allow the assignment of the side chains of the domain in the apo, ADP and AMPPNP bound forms. Although crystal structures have been solved for the full length in the presence of both AMPPNP and p23[7] and of the isolated N-terminal domain in the adp bound state[8] it is far from clear how the N-terminal domain of Hsp90 behaves in solution with and without ligands and in the absence of specific co-chaperones. Of particular note is the position of the ATP 'lid'. The lid has been seen in the open conformation in the isolated N-terminal domain crystal structure and with ADP bound while in the full length compact form in the presence of AMPPNP and p23 the lid has been seen closed over the ligand binding site. What is not clear is whether this lid behaviour is dependent upon co-chaperone binding and how much of the capability of conformational change is localised to the N-terminal domain or whether a larger proportion of the chaperone is required to facilitate these movements. The position of the lid region in the apo state in solution is also unclear, although as mentioned in the previous chapter it may occupy a position between open and closed. Studies by NMR can be used to answer some of these questions and give a greater understanding of the movement of this highly dynamic protein. The response of Hsp90 to ADP and AMPPNP ligand binding was observed using chemical shifts from the side chain assignments and using H/D exchange data. A study into the Hydrogen/Deuterium (H/D) exchange parameters of the N-terminal domain of Hsp90 was undertaken monitoring exchange on the backbone amide bond. This was performed in the apo state and in the ADP and AMPPNP ligand bound states to report upon the relative flexibility and accessibility of each amino acid within the protein in each form.

4.2 Sample preparation, data acquisition and processing.

Protein samples of the N-terminal domain of Hsp90 were prepared as described in Chapter 2 using either ^{15}N-ammonium sulphate and ^{12}C-glucose or ^{15}N-ammonium sulphate and ^{13}C-glucose. This resulted in either singly or doubly isotopically labelled proteins suitable for NMR data acquisition.

Data was collected using spectrometers operating at 700 and 800 MHz using experimental parameters described in Chapter 2. Processing of the free induction decay (FID) datasets utilised NMRPipe scripts[58] as described in Chapter 2. Processed data was then analysed using CCPNmr software[59].

Backbone resonances for the N-terminal domain were taken from published data from the group [15] and were used as a basis from which to assign the side chains of the N-terminal domain. HNCA, HNCOCA, HNCACB and HNCOCACB experimental assignments were used to uniquely identify the Cα and Cβ carbon resonances of each side-chain. These resonance assignments were used in conjunction with assigned ^{15}N-edited TOCSY-HSQC (TOWNY-HSQC) data (unpublished work) to facilitate the side chain assignment. The ADP and AMPPNP backbone assignments are not published but were available in house (Salek and Williams personal communication).

Assigning the side chains of a protein involves defining the unique carbon/proton chemical shift associated with each CH group within the side chain. Carbons with a single proton bound to them such as the CαH of most amino acids (bar glycine) or the CγH in Leucine will generate one resonance. Carbons with two protons attached to them, such as in the case of the H-Cβ-H group in Leucine or Glutamate will generate two C-H resonances. The resonances from a CH_2 group may be distinct if the chemical environments of each proton are different. If the chemical environments are very similar, however, these two signals may be degenerate. Methyl groups as found in Leucine, Isoleucine, Valine, Alanine and Methionine will generate only one distinct C-H resonance due to the freedom of rotation around the central carbon. This free rotation means all protons are occupying an equivalent average chemical environment. Side chain amines and aromatic groups beyond the Cβ were not assigned.

4.3 Aliphatic resonance assignment of the side chains of the apo N-terminal domain of Hsp90

Assignment was undertaken using CCPN analysis software[59]. The general method used for side chain assignment is described below using residue Leu50 to illustrate the procedure. Using previously assigned $^{1}H^{15}N$-HSQC and ^{15}N-edited NOESY-HSQC and TOWNY-HSQC spectra, the proton chemical shifts associated with the Cα-H and often the Cβ-H through the connectivity to their own amide N-H bond can be identified. This is shown in Figure 4.1A where the Cα-H resonance can be observed in the TOWNY-HSQC spectrum however no Cβ-H resonance can be seen.

The assigned HNCA and HNCOCA spectra can be used to identify the Cα chemical shift of the amino acid in question. Once identified, the Cα chemical shift from the HNCA can be cross referenced with the Cα-H proton chemical shift identified through the $^{1}H^{15}N$-HSQC/TOWNY-HSQC spectra. This provides chemical shift coordinates for each component of the Cα-H bond. This set of coordinates corresponds to a resonance detected on the constant time ^{13}C-HSQC (CT-^{13}C-HSQC) spectrum recorded for the apo N-terminal domain of Hsp90. This peak on the CT-^{13}C-HSQC spectrum can then be unambiguously assigned (Figure 4.1B).

If a TOWNY-HSQC peak or peaks are visible for the Hβ atom then the process described for locating the Cα-H resonance CHSQC-CT peak can be repeated. The HNCACB and HNCOCACB spectra can be used to identify the carbon chemical shift and the TOWNY/^{15}N-NOESY spectra can be used to identify the proton chemical shift. Often however only a single resonance for the Cβ-H will be visible in the TOWNY-HSQC spectrum where two would be expected, or none at all as is the case with Leu50. When no proton chemical shift is visible from the TOWNY-HSQC data then two alternative experiments can be used to find the carbon/proton linkages between the atoms within a single side chain. Two experiments were used to look at this – an HCCH-TOCSY experiment was used to observe the connectivity of two proton chemical shifts with respect to a single carbon chemical shift. Thus if the chemical shift for one carbon/proton pair is known, such as the Cα/Hα bond, then from this the proton chemical shifts of all other Cx-H nuclei in that side chain can be determined. A CCH-TOCSY experiment was used to observe the connectivity of two carbon chemical shifts with respect to a single proton shift. Thus using the known proton/carbon chemical shifts for the Cα/Hα bond the carbon shifts for all other Cx-H bonds within the side chain can be determined. In each case linkages within the same bond, e.g. Hα to Cα and back to Hα or Cα to Hα and back to Cα result in a self cross-peak occurring on the diagonal (Figure 4.2).

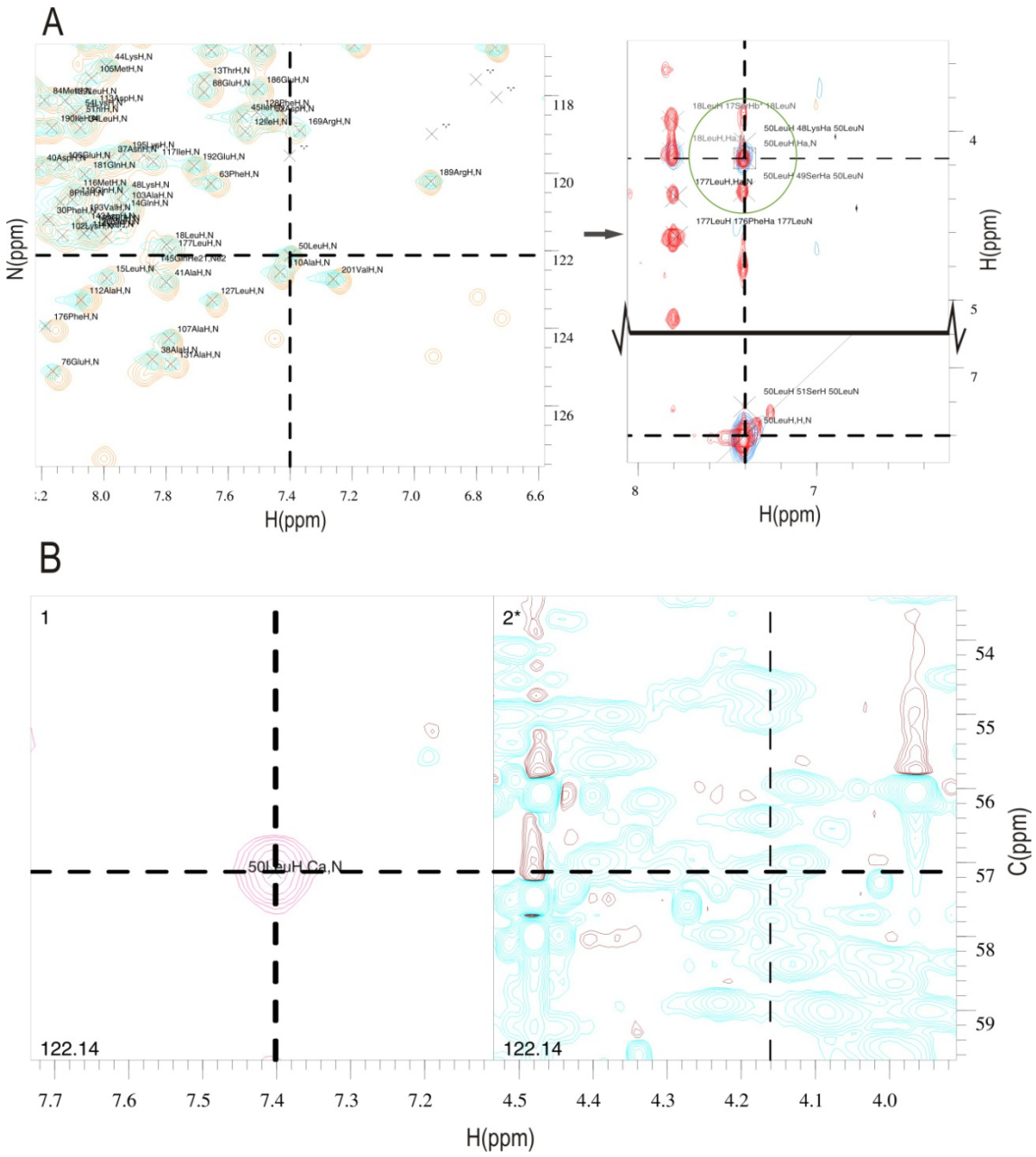

Figure 4.1 The side chain assignment of the CA atom of residue Leu50. A: The ^{15}N-HSQC peak is marked and the associated TOWNY peak corresponding to the HA atom has been identified giving its proton resonance. B: The carbon CA resonance has been identified in the HNCA spectra allowing the intersect to identify the ^{13}C-HSQC peak corresponding to the CA-H group.

The combination of these two techniques is therefore very powerful for determining the proton and carbon chemical shifts of all bonds within the side chain of any given amino acid. The combination of these two techniques does not reveal, however, which proton shift matches to which carbon shift and in order to establish the exact combination of each proton/carbon chemical shift pair for each C-H bond along the side chain the slices through the 3D spectra are observed. A match must be found (compare Figure 4.3A with 4.3B) where the

self peak for the given atom is on the diagonal and cross peaks are observed to the already identified CαHα resonance and to C-H groups further along the chain. Indeed the most certain way of identifying correctly matching C and H shifts is to find matching peak patterns in other 3D slices of the experiment. This procedure can be carried out with both HCCH and CCH-TOCSY experiments to identify exact proton and carbon chemical shifts for each C-H pair along the side chain. Although often this can be inferred from known chemical shift ranges for each atom type it cannot be guaranteed and often the ranges overlap so much as to be impossible to judge. It is also possible that within each spectra, either HCCH-TOCSY or CCH-TOCSY, that there will be excessive overlap of peaks. This makes determining which peaks correspond to the specific CαHα bond under investigation, and which belong to a neighbouring bond with similar carbon and proton chemical shifts, very difficult. In order to resolve some of these issues the various proton/carbon resonance pairs can be compared to the CHSQC-CT to observe whether a cross peak actually exists here. In order to aid assignment of resonance pairs to atoms within a side chain, the resonance values were compared to the expected range of resonances for each group type within each amino acid. E.g. Normally to distinguish the leucine Cβ from the leucine Cγ within a single side chain the presence of two Hβ peaks at a single carbons shift for Cβ, but not the Cγ shift, was used. However if the Hβ peaks were degenerate or only one could be found then the characteristic shift range for a leucine Cβ was used to identify it from the Cγ. The expected ranges for each atom type were taken from the Biological Magnetic Resonance Data Bank (BMRB), http://www.bmrb.wisc.edu/.

Figure 4.2 shows the HCCH and CCH-TOCSY slices from an initial CαHα start point. Panel A shows the CCH-TOCSY experiment followed by possible cross peaks generated from the linkage between the Cα atom and other carbon atoms in the Leu50 side chain marked in blue. The known carbon chemical shift of the Cβ atom is shown marked in black. Panel B shows a similar situation with the HCCH-TOCSY. Here the blue horizontal lines mark possible cross peaks from any given hydrogen atom on the side chain to the Hα through the Cα atom.

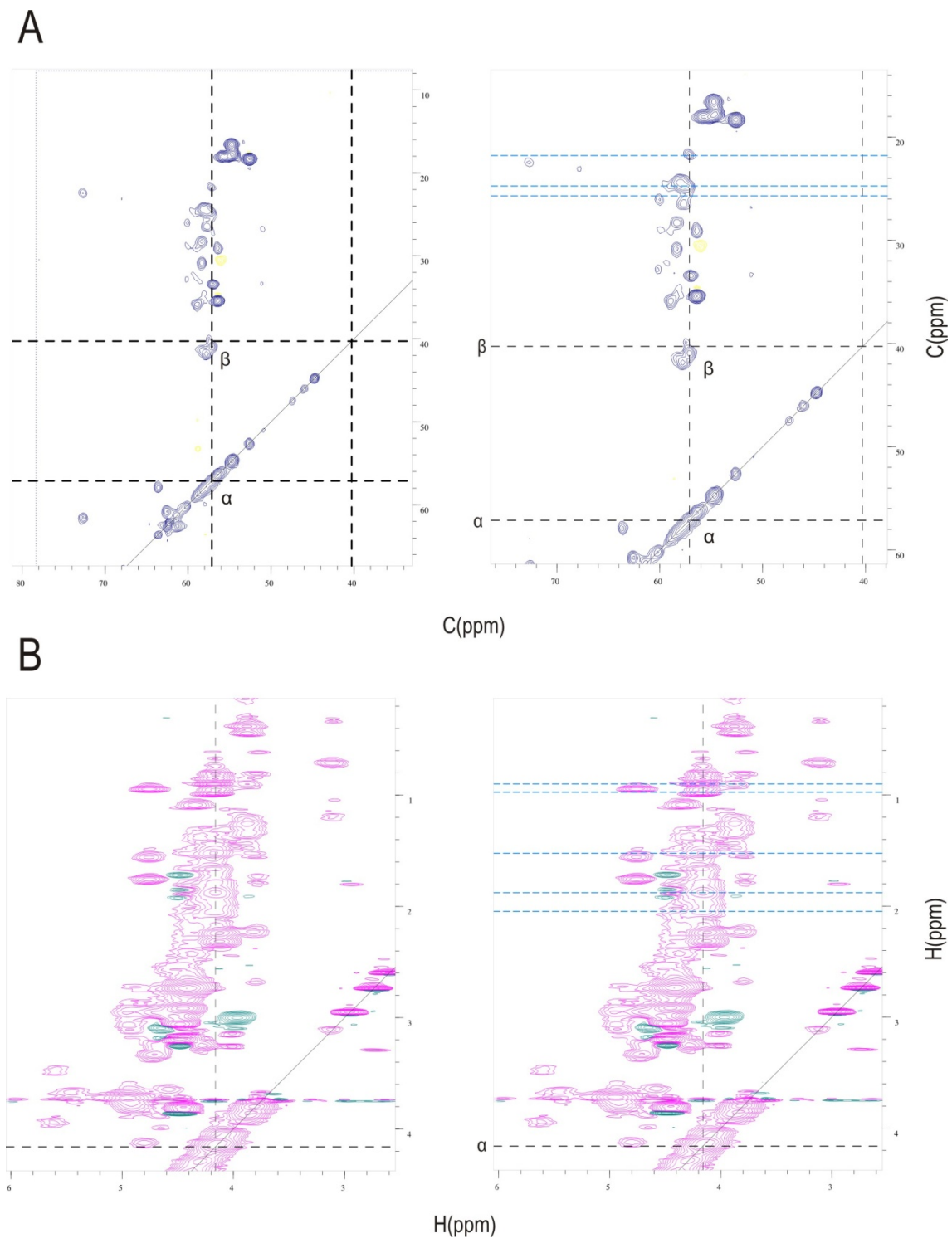

Figure 4.2 Identifying the CH resonances along the side chain. A: The CCH-TOCSY spectrum shown here identifies the Cα-Hα peak marked on the diagonal. The second upper line marks the known Cβ chemical shift obtained from the HNCACB experiment. In the right hand panel possible carbon chemical shifts for the remaining carbon atoms are marked in blue. B: The HCCH-TOCSY spectrum shown here identifies the Cα-Hα peak on the diagonal. Here the proton chemical shift is obtained from the ^{13}C-HSQC spectrum. No Hβ proton chemical shift is known but the right hand panel marks in blue possible proton chemical shifts for each of the C-H groups in the side chain.

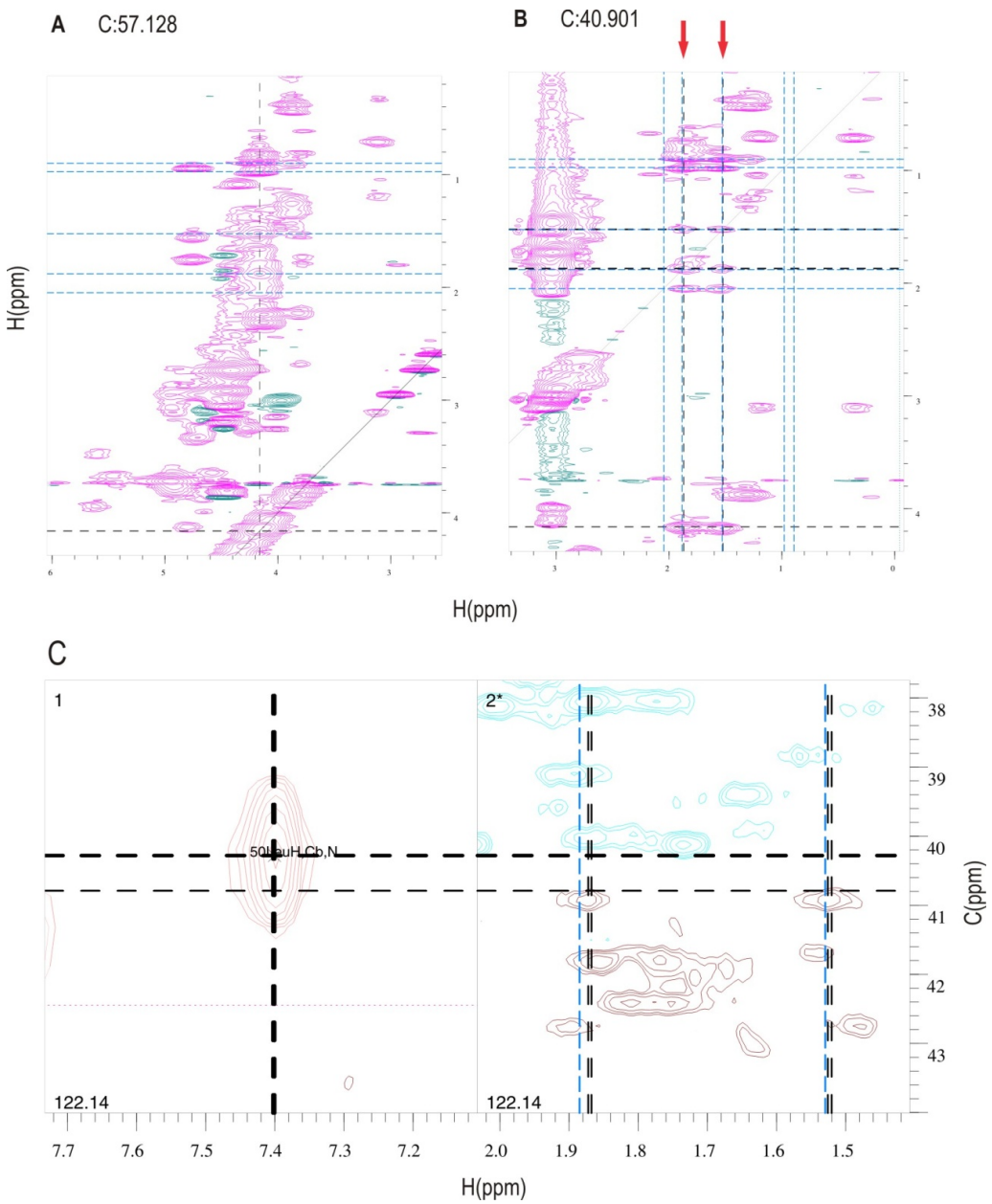

Figure 4.3 Identifying the carbon resonance from the HCCH-TOCSY spectrum. A: Marked in blue are the possible proton shifts corresponding to C-H groups along the side chain as determined from the cross-peaks to the Cα-H resonance marked on the diagonal . B: Marked in black are two resonances that show cross-peaks to the carbons identified previously thus confirming that the peaks in A do correspond to protons in the same side chain. The carbon 'slice' at which this match occurs corresponds to the carbon chemical shift of that atom, in this case the Cβ. C: Each diagonal peak is marked from the HCCH-TOCSY experiment to identify a corresponding ^{13}C-HSQC peak for each Cβ-H pair. In this case the carbon chemical shift identified can be cross-checked against the known Cβ carbon chemical shift from the HNCACB spectrum.

Figure 4.3 shows a case where two cross peaks on the diagonal are observed. These are marked in Figure 4.3B. Both diagonal peaks at this carbon slice have a cross-peak that matches that seen for (Cα-H)Hα. This matching set of resonances adds to the evidence that these resonance belong to the same side chain. Both diagonal peaks show the same pattern of cross-peaks as that seen for the Cα. Specifically this distinctive pattern of two peaks with

different proton resonances but at the same carbon resonance are characteristic of a H-C-H arrangement i.e. as observed in the Cβ of this Leucine where each proton bound to the same carbon inhabits a slightly different environment. Once the correct carbon resonance has been identified through matching of proton resonances the diagonal peaks marked can then be used to locate the corresponding peaks in the CT-^{13}C-HSQC spectrum. This is demonstrated in Panel C where the known Cβ carbon chemical shift from the HNCACB spectrum supports the Cβ chemical shift determined via the HCCH-TOCSY spectrum.

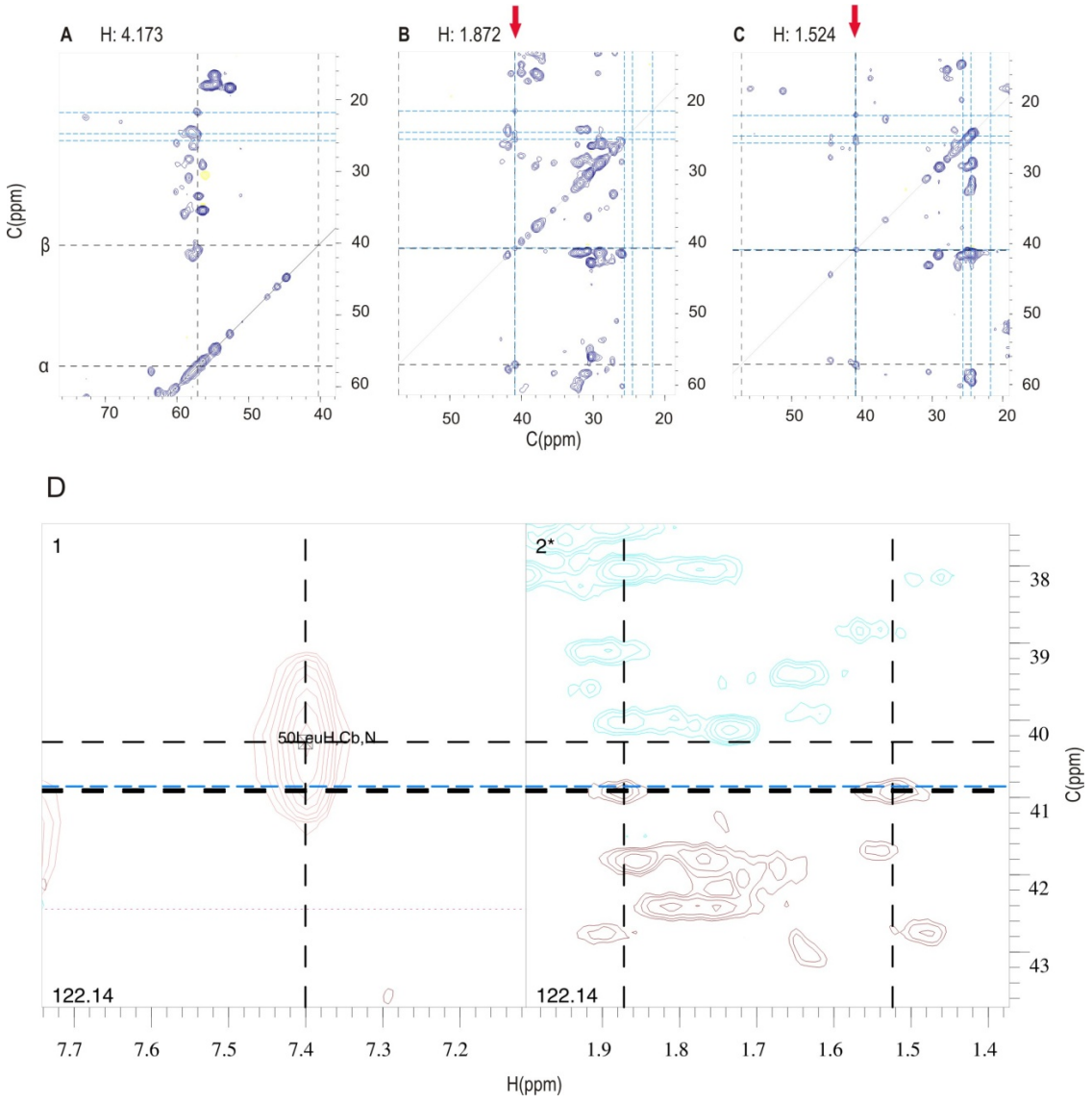

Figure 4.4 Identifying the proton resonances from the CCH-TOCSY experiment. A: Proton resonances are identified from cross-peaks back to the Cα-H group. B: A proton slice is identified where a diagonal peak has the correct pattern of cross-peaks marked in blue to belong to the same side chain. C: A second proton slice is identified where the diagonal peak has the correct pattern of cross-peaks to belong to the same side chain. This is expected since there are two separate protons associated with the CB atom. D: Each identified diagonal peak from B and C is marked to identify two ^{13}C-HSQC peaks. These peaks can be checked against the known carbon resonance from the HNCACB spectrum. The ^{13}C-HSQC peaks also match those identified by the HCCH-TOCSY experiment.

In an analogous situation to the HCCH-TOCSY experiment, the CCH-TOCSY experiment shows cross-peaks which give the carbon chemical shifts within the side-chain. Moving through the proton slices of the CCH-TOCSY spectrum, new diagonal peaks are found with cross-peaks that match those seen for the initial CαHα group. Such matches identify the relevant connected proton resonance. In Figure 4.4 panel A, a cross-section is taken at the proton chemical shift corresponding to the CαHα. Four distinct cross-peaks have been identified and marked with a horizontal line in blue. Figure 4.4 panel B shows a slice in the CCH-TOCSY spectrum where a diagonal peak matches one of the previous cross-peaks and all other cross-peaks also match. The proton resonance at which this slice occurs defines the proton chemical shift for this C-H group. Figure 4.4 panel C shows another slice at which the same situation occurs. This defines the second proton chemical shift for the second H bonded to the Cβ atom. Panel D then shows these proton/carbon chemical shift coordinates on the CT-^{13}C-HSQC spectrum and how these relate to the known Cβ carbon chemical shift from the HNCACB spectrum.

A comparison of panel C from Figure 4.3 and panel D from Figure 4.4 show that the same two peaks are identified using each method. This gives some confidence of the correct assignment of these peaks.

The complimentarity of the methods as described allows the detection of both proton and carbon resonances for the entire side-chain beginning with the CαHα alone. The redundancy of these methods, while best used in conjunction, also allows the use of only one set of data if the overlap in the other is too great to resolve peaks accurately in any region. This can be seen to some extent in Figures 4.5, 4.6 and 4.7 where the regions in the HCCH-TOCSY where in the CγHγ, Cδ1Hδ1 and Cδ2Hδ2 resonances are identified more clearly through the CCH-TOCSY spectrum than from the HCCH-TOCSY spectrum.

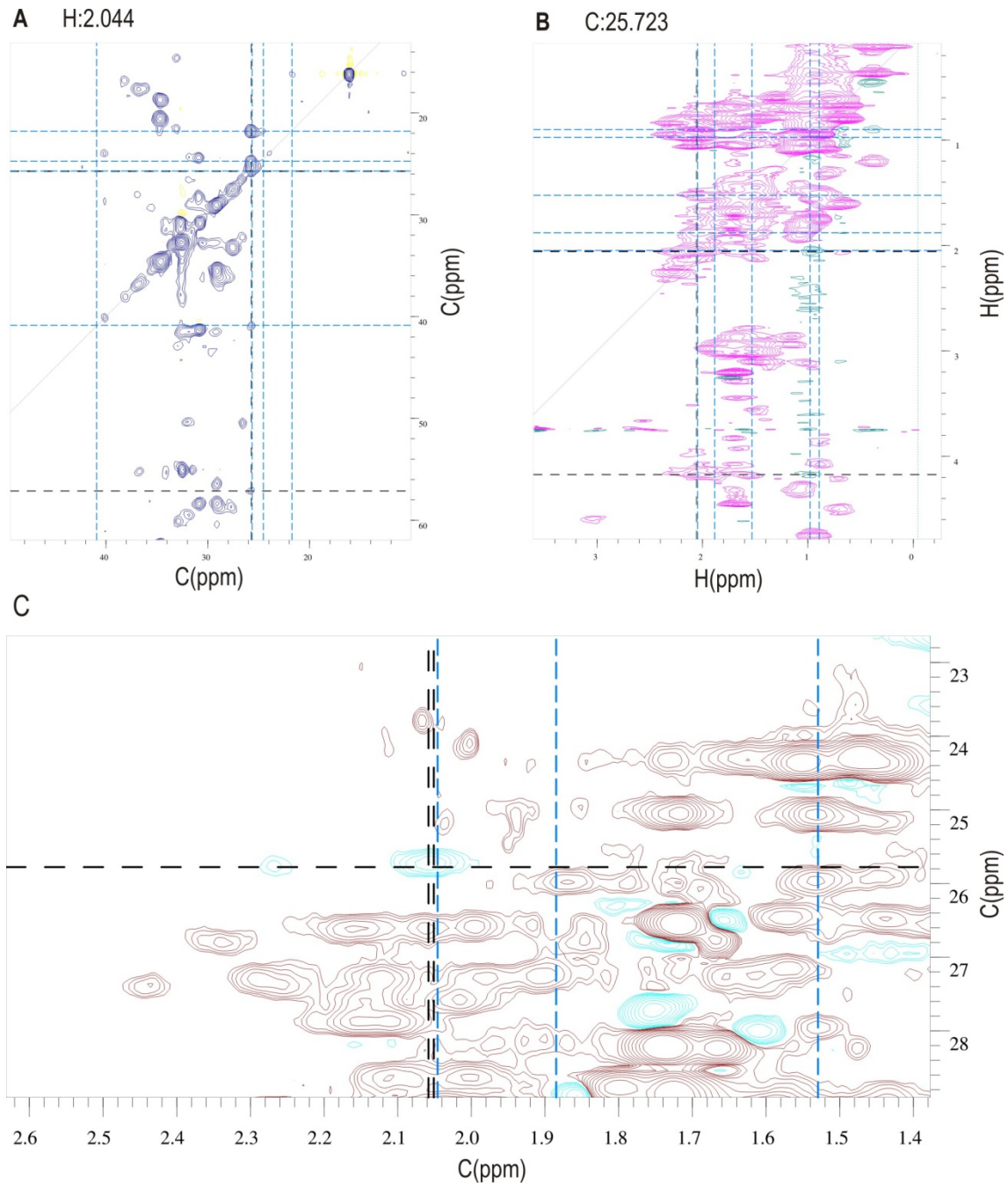

Figure 4.5 Identifying the Cγ-H resonance using both the CCH and HCCH-TOCSY spectra. A: A proton slice is identified in the CCH-TOCSY experiment where the diagonal peak shows the correct cross-peak pattern to belong to the side chain in question marked in black. B: A carbon slice is identified in the HCCH-TOCSY experiment where the diagonal peak shows the correct cross-peak pattern to belong to the side chain in question. C: When marked, both diagonal peaks from A and B correspond to the same ^{13}C-HSQC peak. Once identified the chemical shift range of this peak can be used to identify it as the Cγ-H group of Leu50.

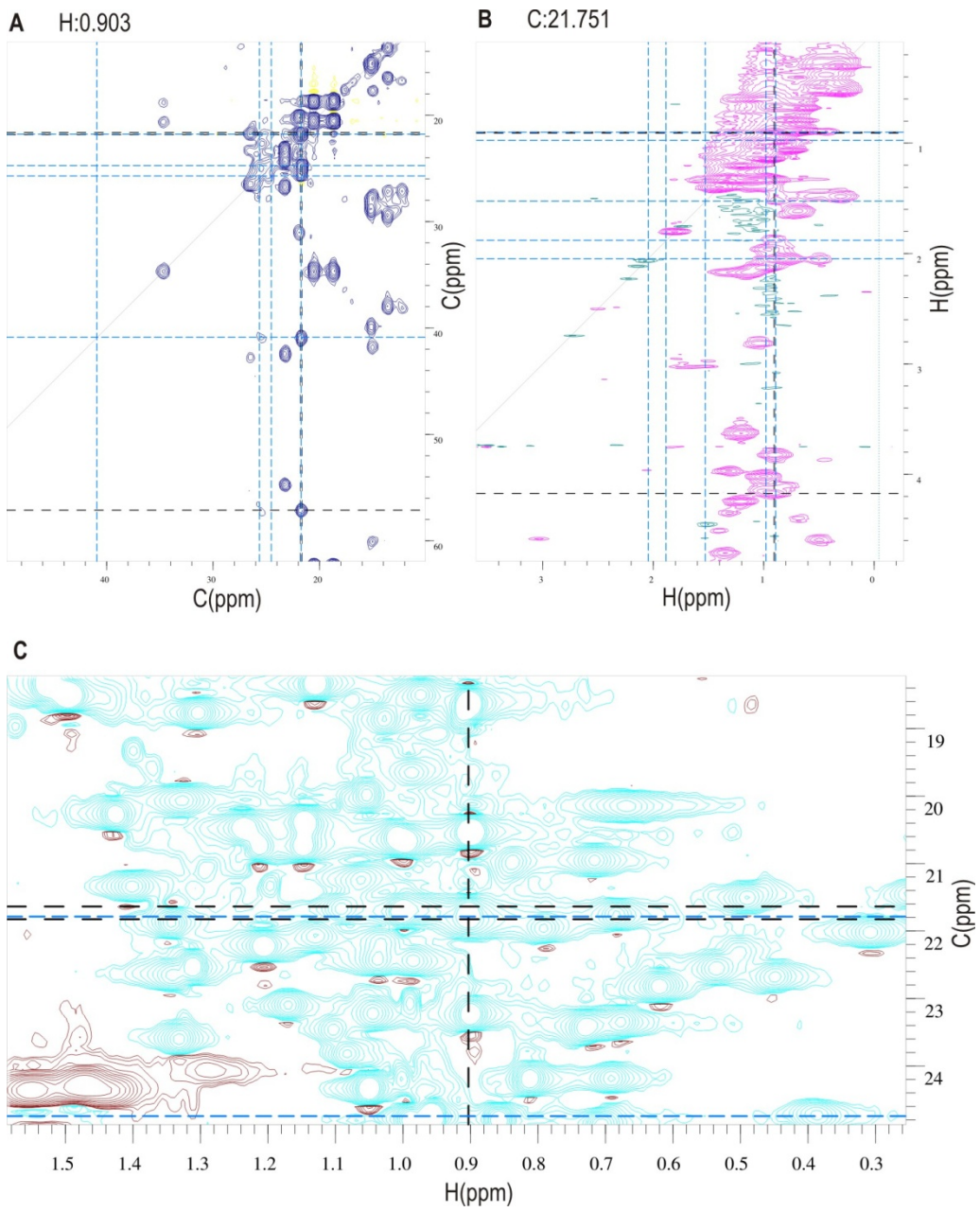

Figure 4.6 Identifying a Cδ1-H resonance using both the CCH and HCCH TOCSY spectra. A: A proton slice is identified in the CCH-TOCSY experiment where the diagonal peak shows the correct cross-peak pattern to belong to the side chain in question marked in black. B: A carbon slice is identified in the HCCH-TOCSY experiment where the diagonal peak shows the correct cross-peak pattern to belong to the side chain in question. C: When marked, both diagonal peaks from A and B correspond to the same ^{13}C-HSQC peak. Once identified the chemical shift range of this peak can be used to identify it as the Cδ1-H group of Leu50.

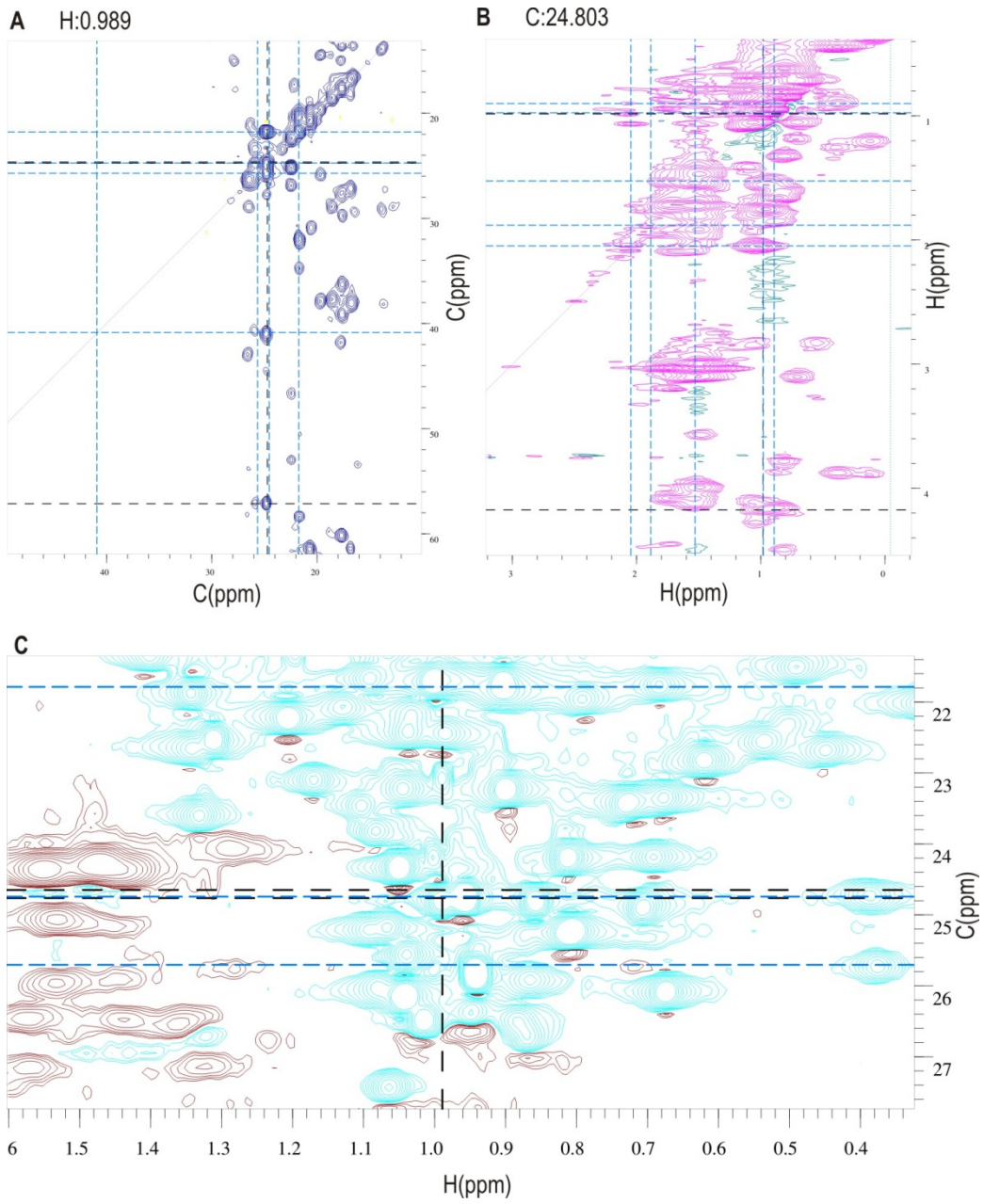

Figure 4.7 Identifying a Cδ2-H resonance using both the CCH and HCCH TOCSY spectra. A: A proton slice is identified in the CCH-TOCSY experiment where the diagonal peak shows the correct cross-peak pattern to belong to the side chain in question marked in black. B: A carbon slice is identified in the HCCH-TOCSY experiment where the diagonal peak shows the correct cross-peak pattern to belong to the side chain in question. C: When marked, both diagonal peaks from A and B correspond to the same ^{13}C-HSQC peak. Once identified the chemical shift range of this peak can be used to identify it as the Cδ2-H group of Leu50.

Systematic assignment of all aliphatic regions of all residues visible in the NHSQC was undertaken. A summary of all Apo assignment data is tabulated in Appendix A. A summary of the assigned data is shown in Table 4.1.

Assigned	Apo	
	H	C
% Side Chain protons	74%	
% Side Chain non-protons		60%
%H/C α	90%	95%
%H/C β	81%	94%
%H/C γ	80%	64%
%H/C δ	63%	55%
%H/C ε	27%	25%

Table 4.1A summary of the degree of assignment of the resonances associated with the side chains of the N-terminal domain of Hsp90. The % assigned for proton and carbon resonances is shown for the apo states.

4.4 Assignment of the side chains of ADP and AMPPNP bound Hsp90

An overlay of the CT-^{13}C-HSQC spectra for the apo, ADP and AMPPNP bound forms of the N-terminal domain of Hsp90 reveal an overall very similar peak distribution. As observed for the NHSQC spectra, the CT-^{13}C-HSQC spectra show some peaks which do not shift in response to a change in ligand bound state suggesting no change in chemical environment. However, a significant number do shift implying a change in their chemical environment upon ligand binding (Figures 4.8 and 4.9). It is already known that ligand binding to the N-terminal domain of Hsp90 causes movement of the backbone and so movement of the side chains is not unexpected. Observations of which side chains move may allow a better picture of the conformational changes occurring in response to ligand binding to be formed.

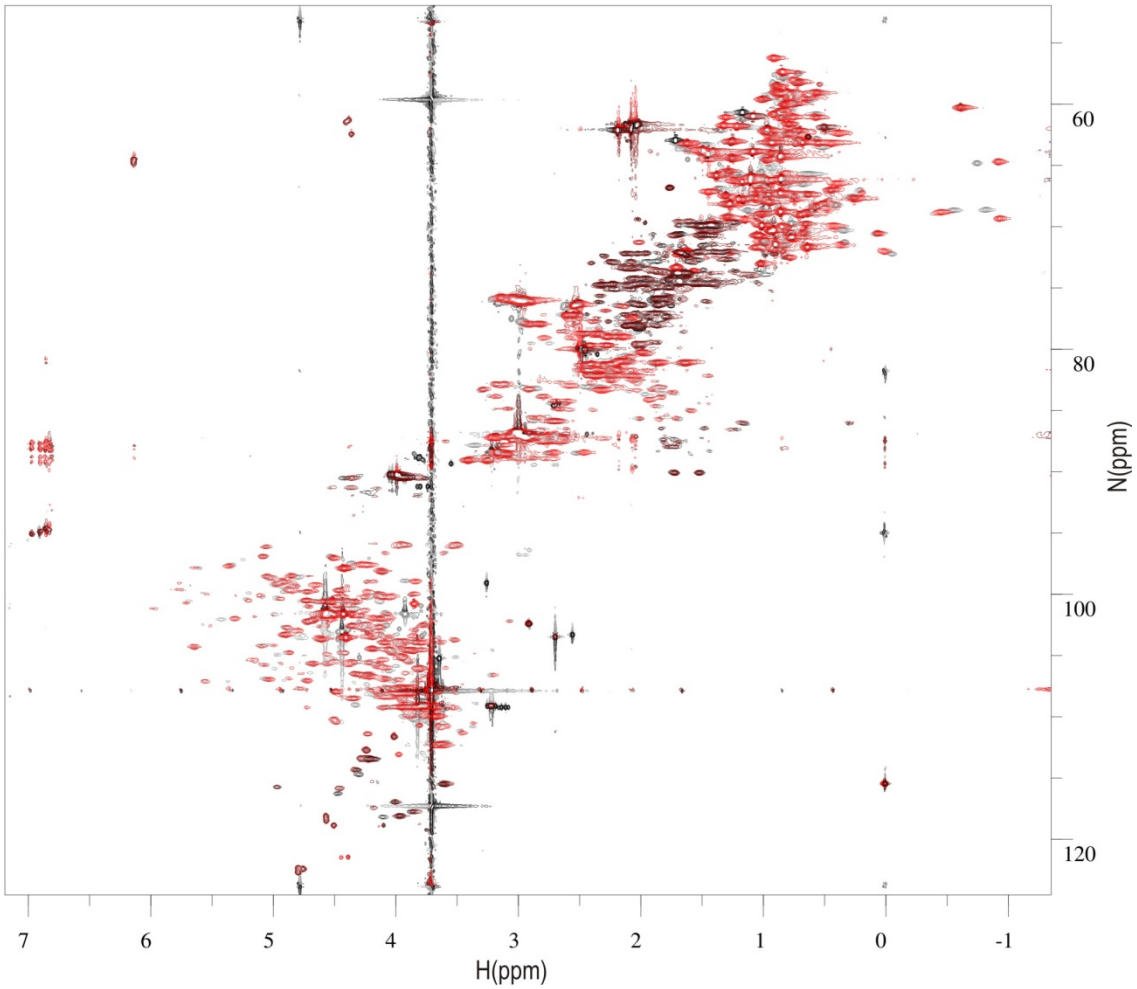

Figure 4.8 An overlay of the CT-^{13}C-HSQC spectra collected for the Apo N-terminal domain of Hsp90 (black) and the ADP bound N-terminal domain of Hsp90 (red) showing overall similarity but with some notable differences.

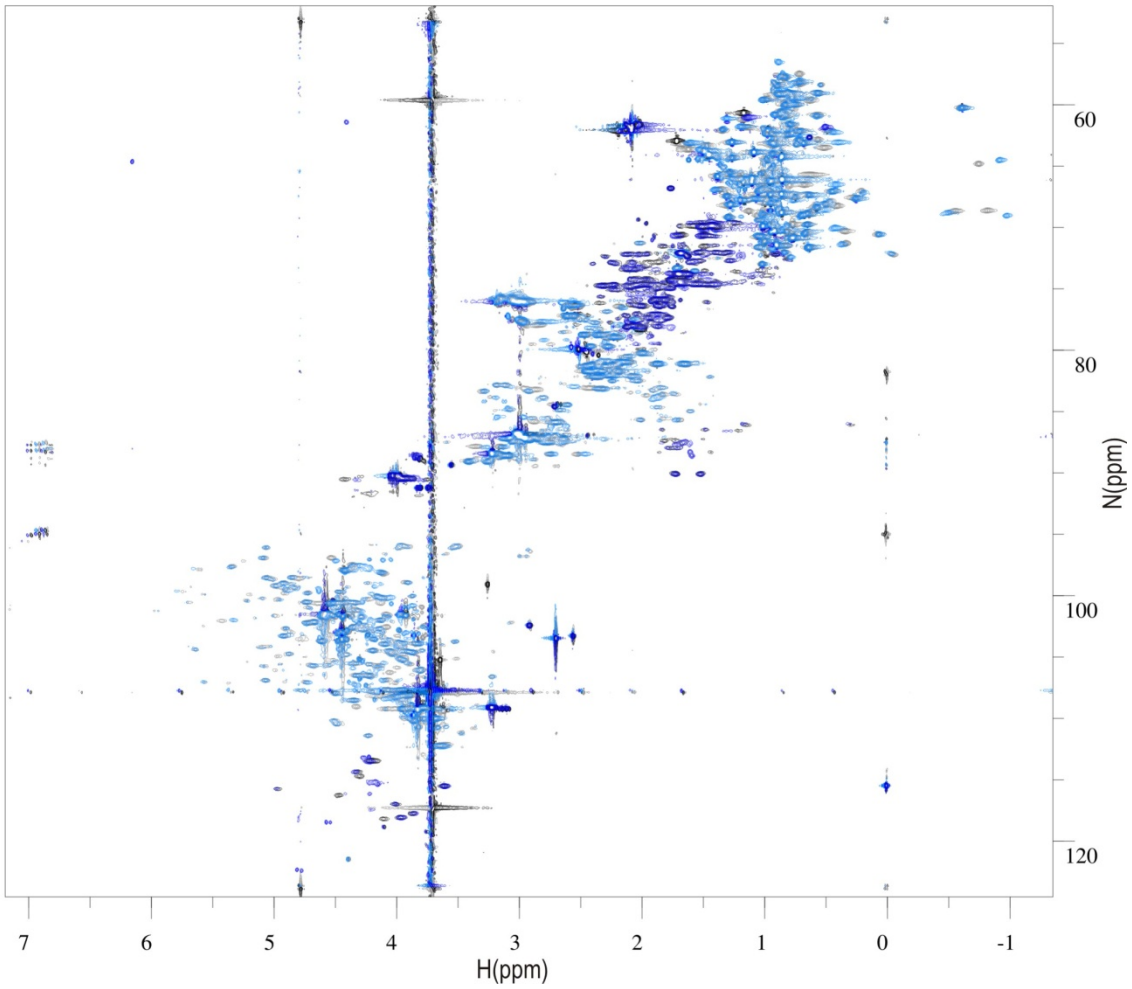

Figure 4.9 An overlay of the CT-^{13}C-HSQC spectra collected for the Apo N-terminal domain of Hsp90 (black) and the AMPPNP bound N-terminal domain of Hsp90 (blue) showing overall similarity but with some notable differences.

A systematic review of all amino acids allows the transfer of peak assignments from the apo dataset to either the ADP or AMPPNP bound dataset. The high similarity between the spectra of the apo and ligand bound domain allows direct transfer of assignments in cases where no movement has occurred. All the assignments for any given side chain are considered together and reference to both HCCH and CCH-TOCSY spectra is used to confirm that the cross-peak pattern is consistent throughout. This is seen for Val163 in Figures 4.10, 4.11 and 4.12.

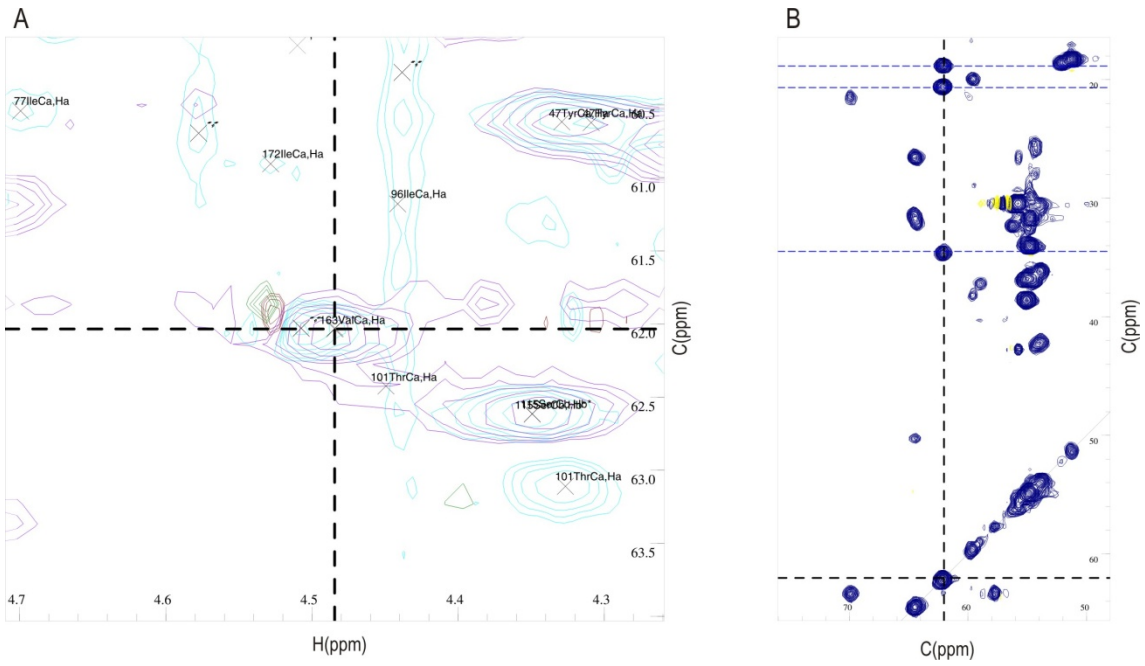

Figure 4.10 A: The identified apo Cα-H peak of Val163 overlays exactly with a peak recorded for the ADP ^{13}C-HSQC constant time experiment. B: Confirmation that the peak in the ADP spectrum is consistent with it belonging to residues Val163 was obtained by inspection of the corresponding CCH-TOCSY spectrum. The pattern of cross-peaks identified (marked in blue) is consistent with the known values of Val163.

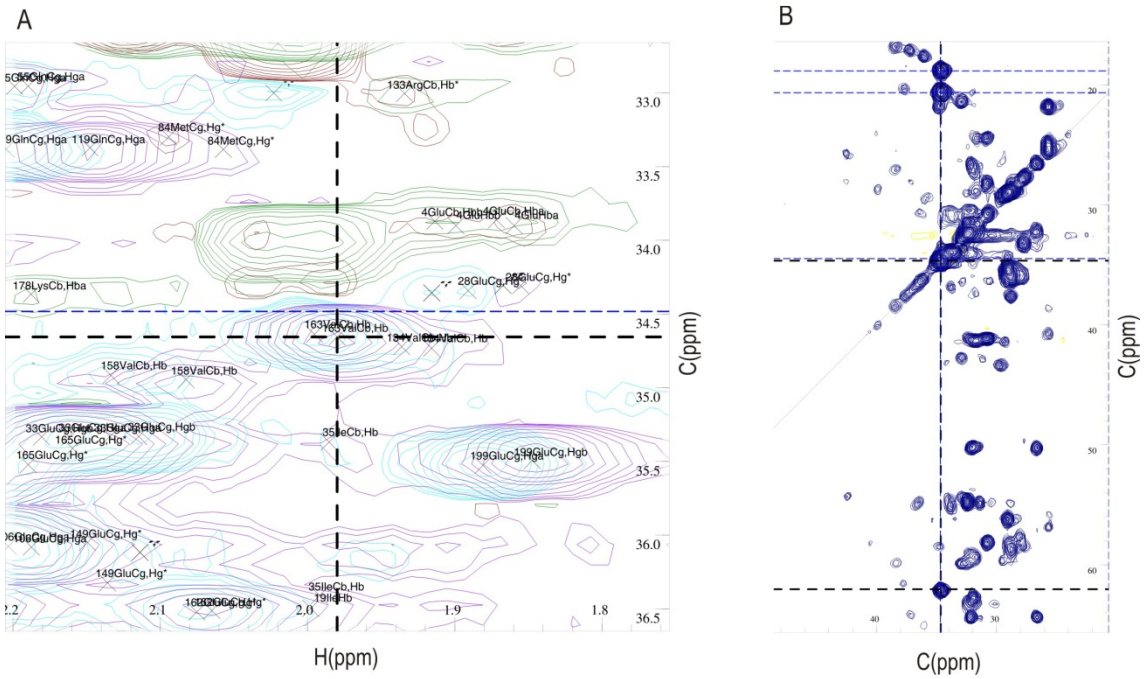

Figure 4.11 A: The identified apo Cβ-H peak of Val163 overlays exactly with a peak recorded for the ADP ^{13}C-HSQC constant time experiment. B: Confirmation that the peak in the ADP spectrum is consistent with it belonging to residues Val163 was obtained by inspection of the corresponding CCH-TOCSY spectrum. The pattern of cross-peaks identified (marked in blue) is consistent with the known values of Val163.

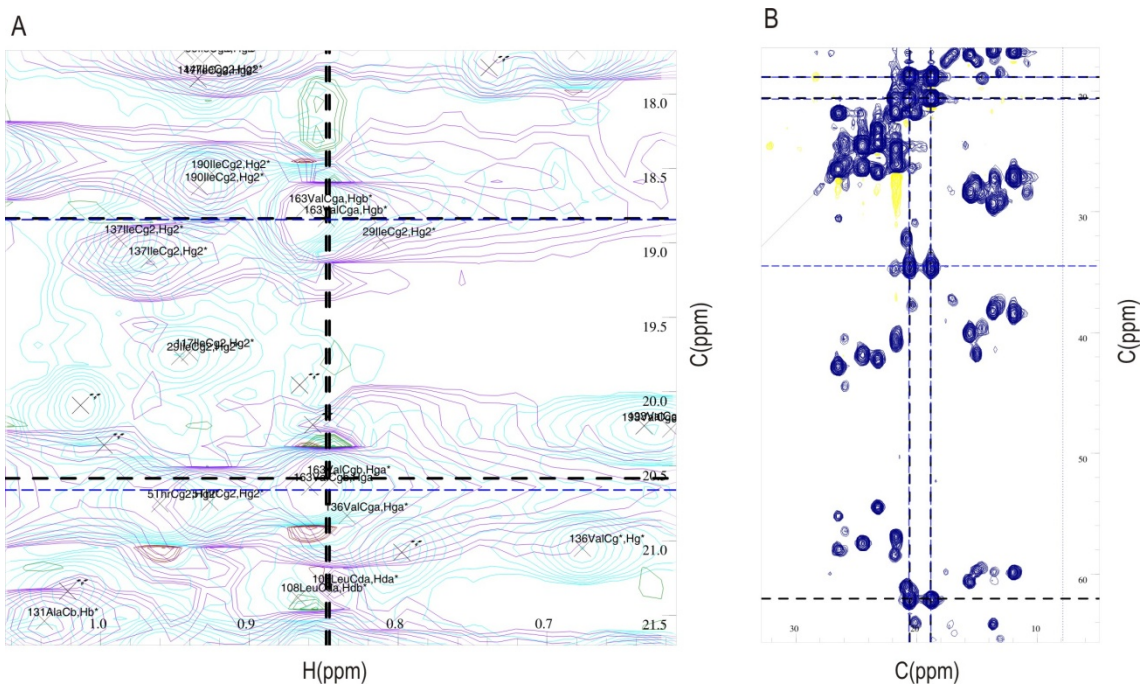

Figure 4.12 A: The identified apo Cγ1-H and Cγ2-H peaks of Val163 overlay exactly with the peaks recorded for the ADP ^{13}C-HSQC constant time experiment. B: Confirmation that the peaks in the ADP spectrum are consistent with them belonging to residues Val163 was obtained by inspection of corresponding CCH-TOCSY spectrum. The pattern of cross-peaks identified (marked in blue) is consistent with the known values of Val163. In this case both methyl groups have very similar proton resonances but differing carbon resonances.

Where some movement of the peak has occurred, the position of the new peak can be identified in a number of ways depending upon the situation. The entire side chain is considered together to allow matching of cross-peak patterns in the HCCH and CCH-TOCSY spectra. If the peak shift is small then the most likely closest peak can be confirmed or ruled out by comparing their cross peaks in the HCCH and CCH-TOCSY spectra to the pattern from the apo dataset. Additional information on the Cα and Cβ carbon chemical shifts was obtained from HNCA and HNCACB spectra for the AMPPNP dataset. The ADP dataset lacked any HNCA and HNCACB spectra and was therefore assigned by comparison to both the apo and the AMPPNP CHSQC-CT, HCCH and CCH-TOCSY spectra. In the case of Thr95 in the ADP bound state as displayed in Figure 4.13 the movements are relatively small. The apo peak is marked with a '*' while the cross hairs are centred on the most likely candidate for the displaced peak in Panel A. Panels B and C below it display the CCH and HCCH-TOCSY spectra respectively corresponding to the proposed 'new' peak position for Thr95. The alignment of the cross peaks on the horizontal markers in each case suggests that the 'new' peak is the correct one. This was repeated for all carbon atoms within the side chain in a similar fashion.

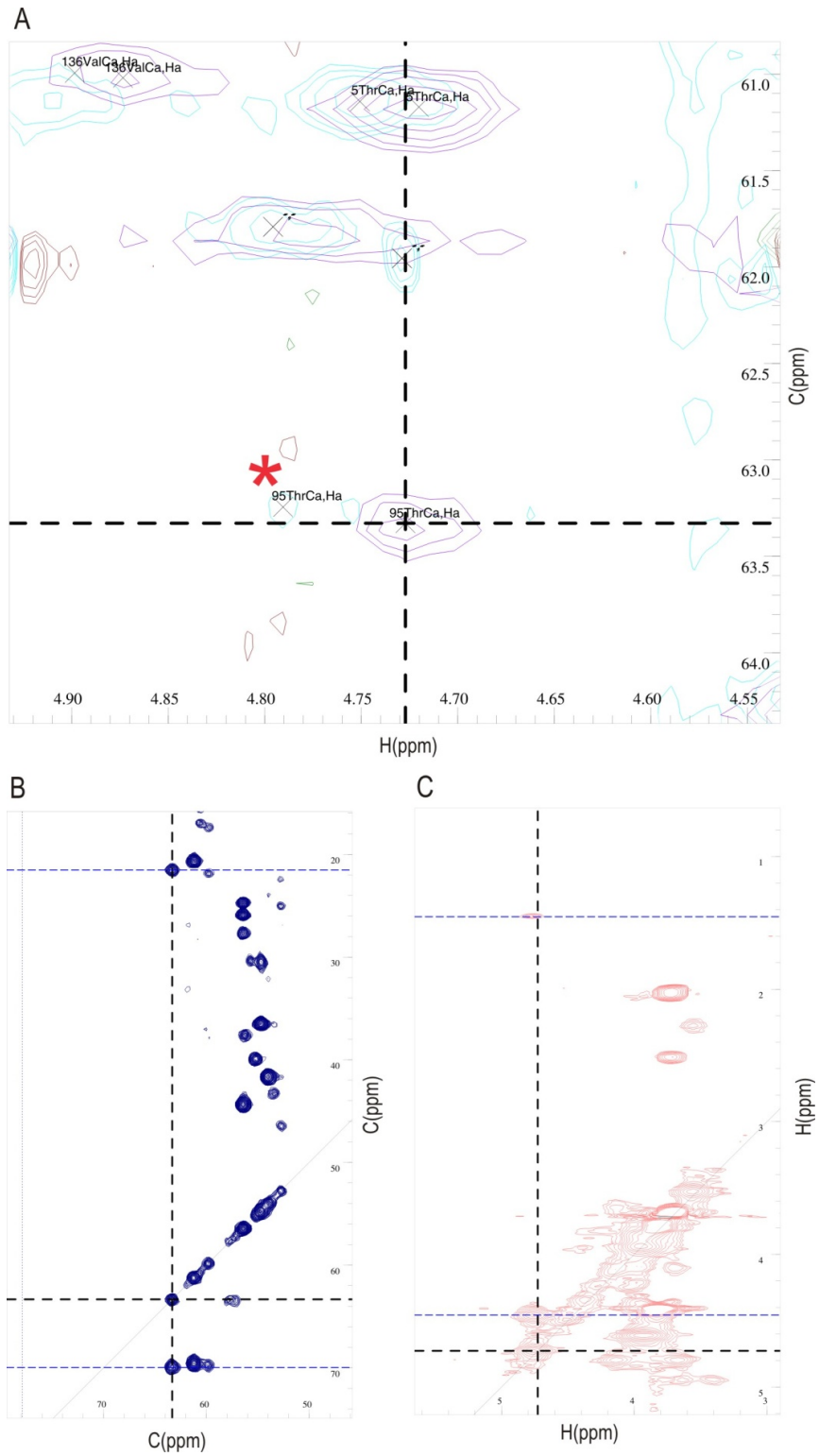

Figure 4.13 A: The identified apo CA-H of Thr95 does not overlay exactly with the peak recorded for the ADP ^{13}C-HSQC constant time experiment. A: The apo peak is starred (*) and the closest candidate for the shifted peak in the ADP spectrum is marked with a cross-hair in black. B: The corresponding cross-peak pattern in the CCH-TOCSY experiment matches that expected for Thr95. C: The corresponding cross-peak pattern in the HCCH-TOCSY experiment matches that expected for Thr95. Any deviation from the marked lines might indicate proton shifts in the other side chain atoms however the number of peaks is characteristic of a Thr residue.

A summary of the side chain assignments for the apo, ADP and AMPPNP bound states is shown in Table 4.2. A table of the assignments for the ADP and AMPPNP bound states can be found in Appendices B and C respectively.

Assigned	**Apo**		**ADP**		**AMPPNP**	
	H	C	H	C	H	C
% Side Chain protons	74%		73%		71%	
% Side Chain non-protons		60%		57%		50%
%H/C α	90%	95%	85%	85%	81%	71%
%H/C β	81%	94%	81%	81%	79%	66%
%H/C γ	80%	64%	81%	65%	78%	62%
%H/C δ	63%	55%	29%	55%	61%	53%
%H/C ε	27%	25%	25%	25%	25%	25%

Table 4.2 A summary of the degree of assignment of the resonances associated with the side chains of the N-terminal domain of Hsp90. The % assigned for proton and carbon resonances is shown for each of the apo and ligand bound states.

Figure 4.14 shows the ^{13}C-HSQC of the apo state of the N-terminal domain of Hsp90. In order to show details of the final assignment, key areas have been highlighted by the red boxes shown. These designated areas refer to the labelled panels in Figures 4.15 – 4.19. Figures 4.15 – 4.19 show the assigned ^{13}C-HSQC peaks for the N-terminal domain in the apo state. These figures are representative of the apo assignment but not exhaustive. For a full list of assignments and a complete diagram in the apo, ADP and AMPPNP bound states please see the supplementary data CD.

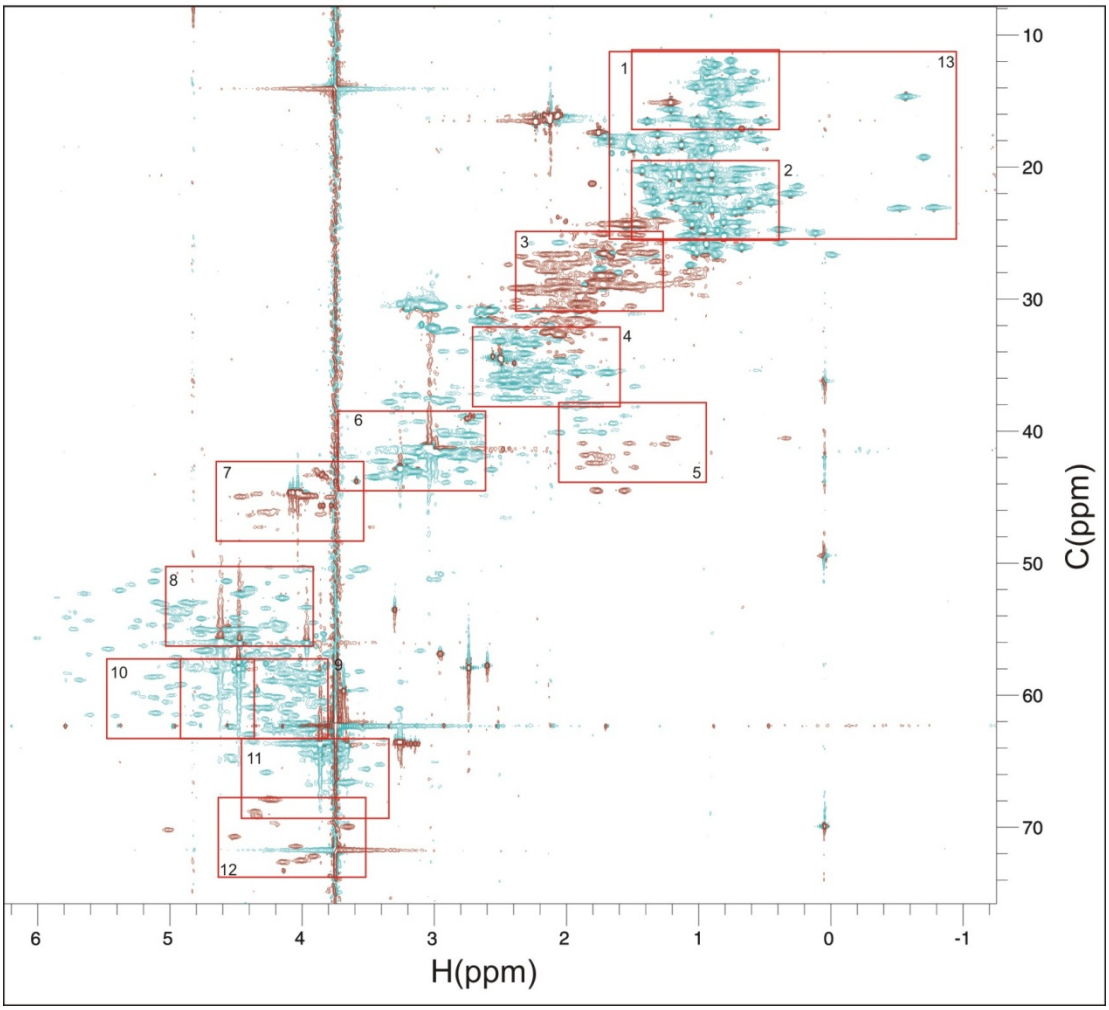

Figure 4.14 Diagram of the CT-^{13}C-HSQC spectrum of the N-terminal domain of Hsp90 in the apo state. The red boxes relate to diagrams 4.15 – 4.16 which show a labelled assignment of the appropriate area.

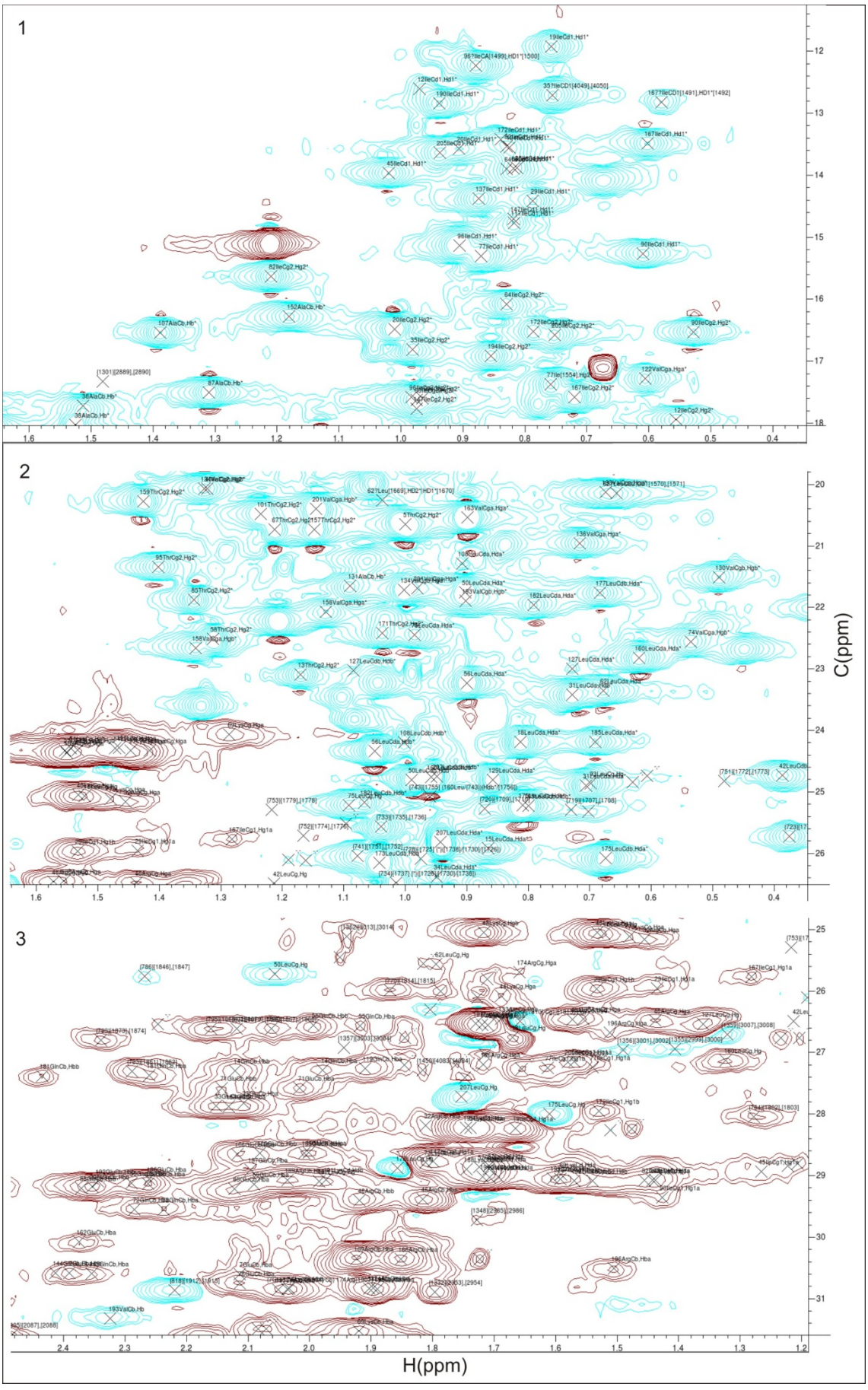

Figure 4.15 Assigned ^{13}C-HSQC spectrum for the N-terminal domain of Hsp90 in the apo state. Refer to figure 4.14 for location information for each of the detailed figures shown here.

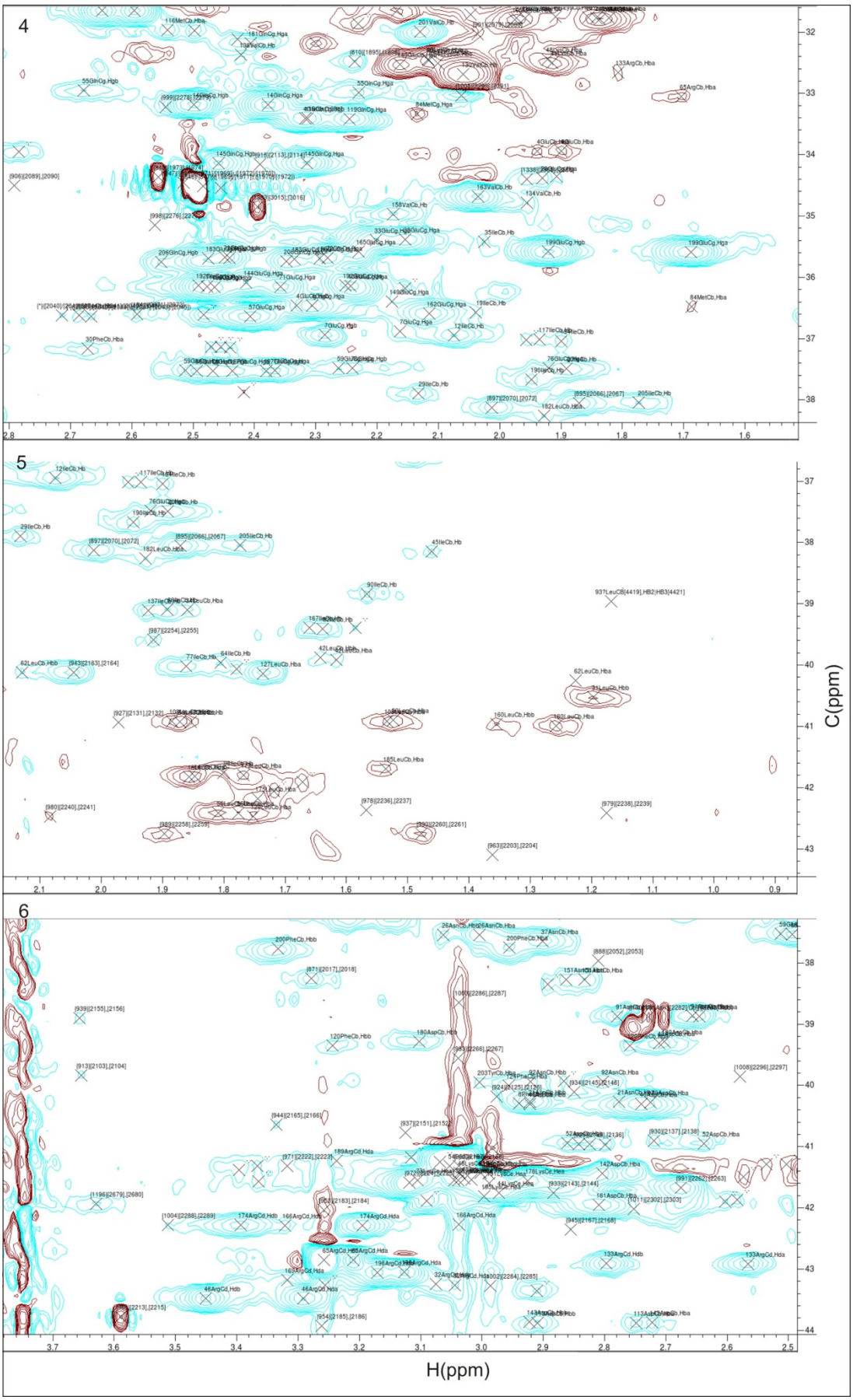

Figure 4.16 Assigned ^{13}C-HSQC spectrum for the N-terminal domain of Hsp90 in the apo state. Refer to figure 4.14 for location information for each of the detailed figures shown here.

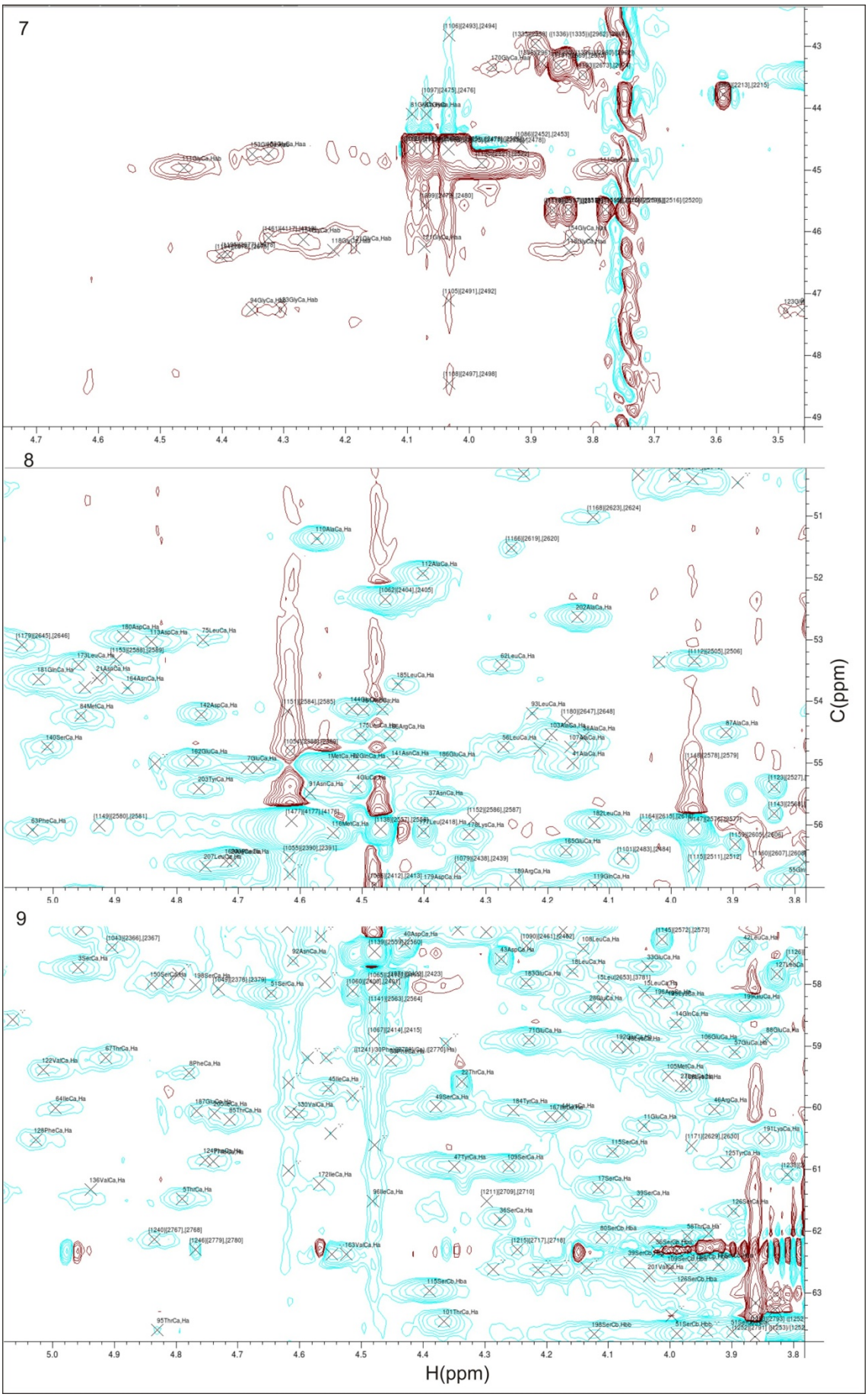

Figure 4.17 Assigned ^{13}C-HSQC spectrum for the N-terminal domain of Hsp90 in the apo state. Refer to figure 4.14 for location information for each of the detailed figures shown here.

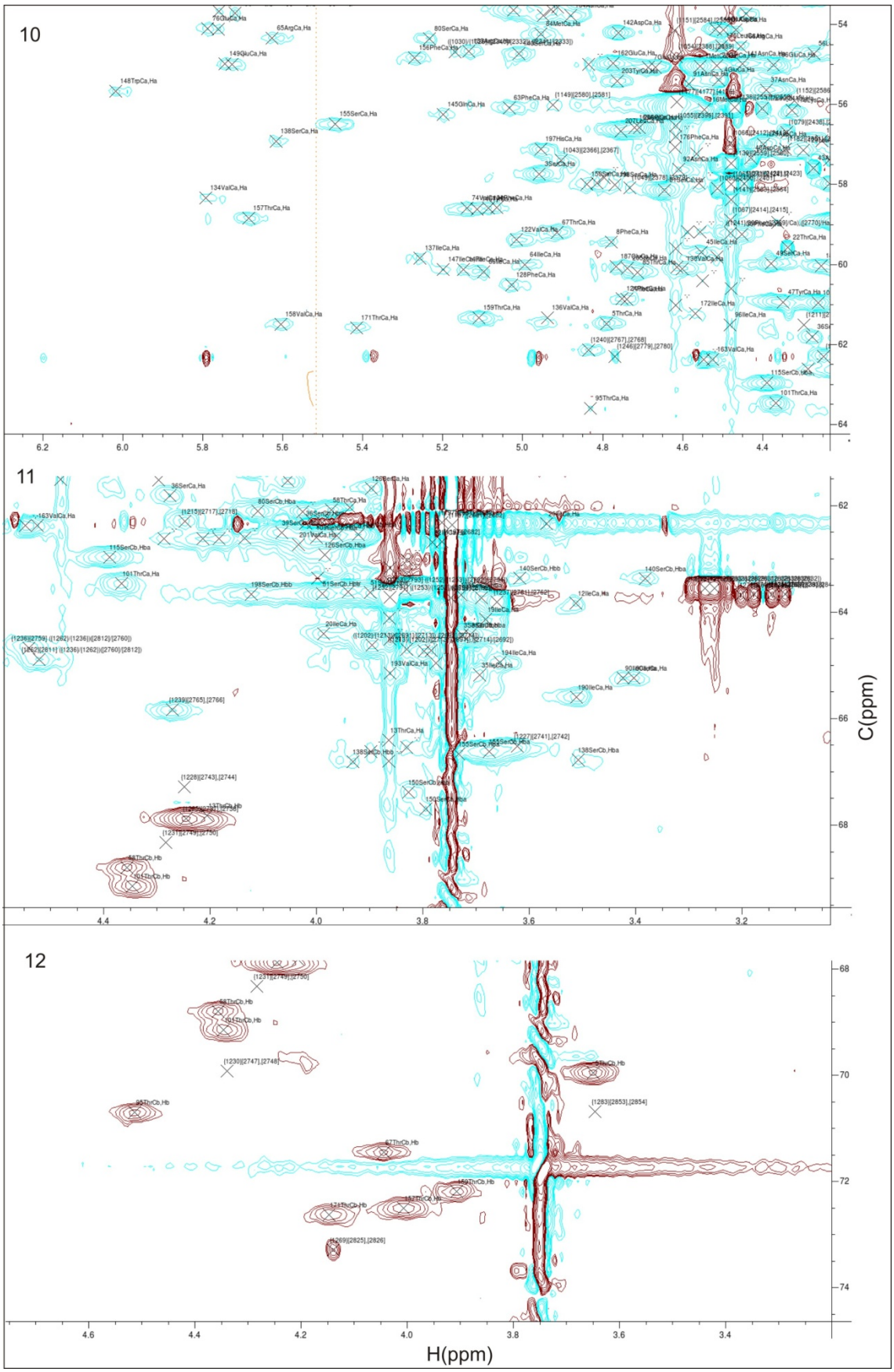

Figure 4.18 Assigned ^{13}C-HSQC spectrum for the N-terminal domain of Hsp90 in the apo state. Refer to figure 4.14 for location information for each of the detailed figures shown here.

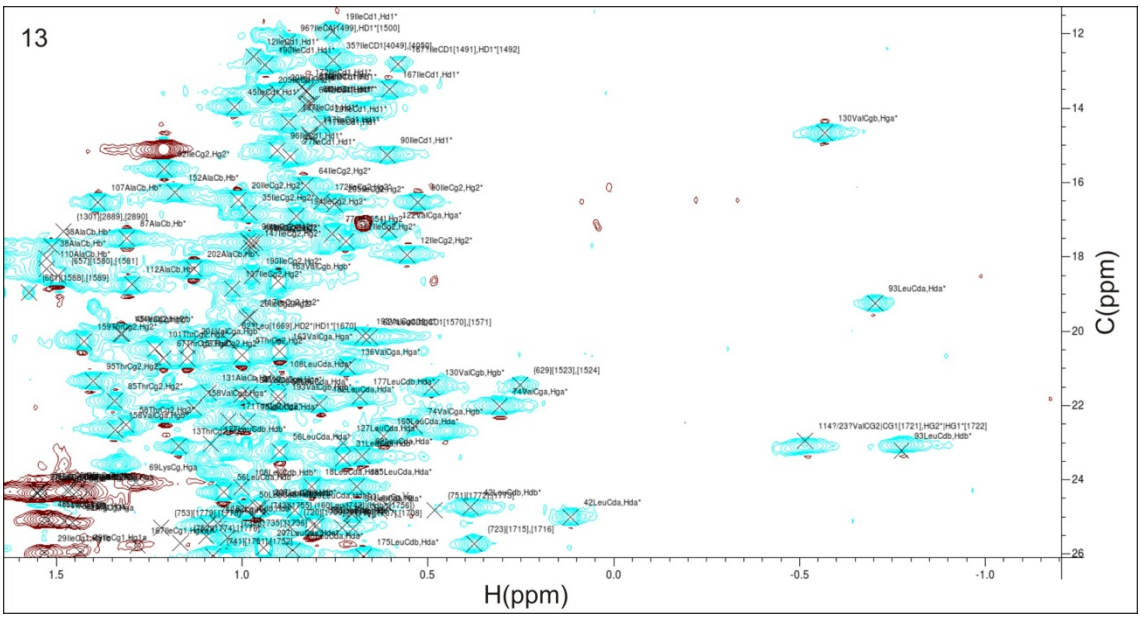

Figure 4.19 Assigned ^{13}C-HSQC spectrum for the N-terminal domain of Hsp90 in the apo state. Refer to figure 4.14 for location information the detailed figure shown here.

4.5 Using the CHSQC spectra

The assigned CHSQC spectra for the apo state, the ADP state and the AMPPNP state were compared and peaks that showed chemical shift differences in the different ligand bound states were identified. The peak shifts could be divided into two categories; those where the shifts were small and those where the shifts were large. The side chains show a far greater sensitivity than the backbone amide groups to changes in their local environment which may indicate conformational changes within the protein reflected in their changes in chemical shift upon ligand binding. This is expected as rearrangement of residue side chains would be vitally important for the functional conformation of the protein but would not necessarily be reflected by movement of the amide resonances depending on the flexibility and size of the side chain involved. Initially all identified changes in chemical shift induced by ligand binding were identified for the ADP and AMPPNP bound state. These shifts were then mapped onto the crystal structure for the ADP bound N-terminal domain (Figure 4.20). The combined shift was calculated in a similar manner to the combined proton/nitrogen shifts (see equation 3.2) using the following equation:

Combined proton/carbon shift = Proton shift + (Carbon shift / 9) (4.1)

Shifts above 0.01 were considered to show a small shift while values above 0.05 were considered to be a large shift.

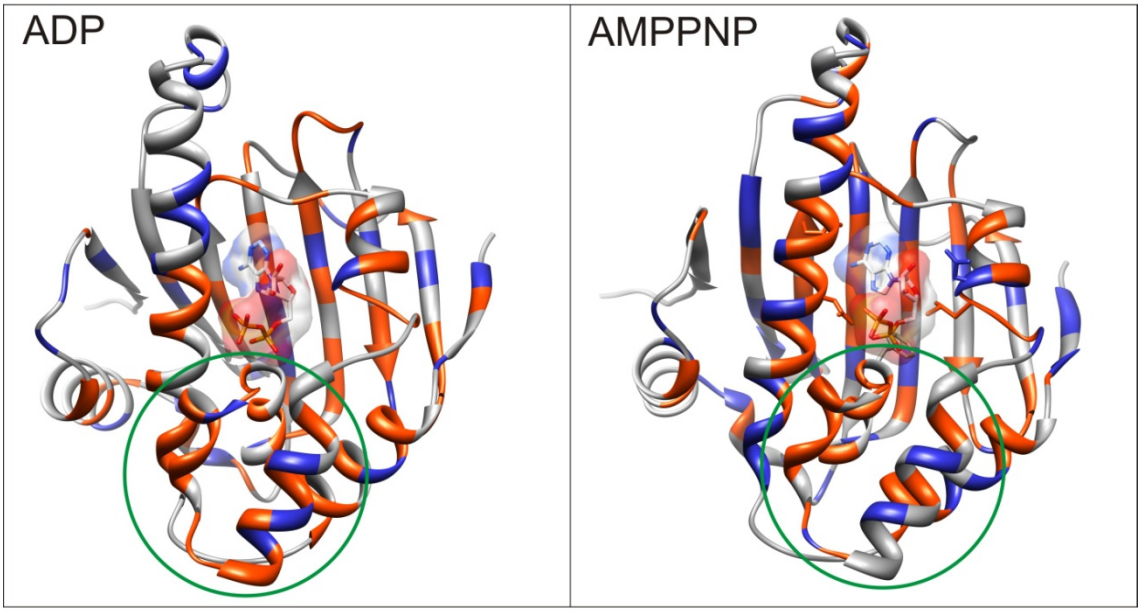

Figure 4.20 Comparison of all identified side-chain chemical shift changes induced by ligand binding in the N-terminal domain of Hsp90. Residues were identified using the ^{13}C-HSQC spectra and plotted onto the known ADP bound crystal structure. Left: Shifts induced upon ADP binding. Right: Shifts induced upon AMPPNP binding. In each case large changes in chemical shift are shown in orange while small changes in chemical shift are shown in blue. The ATP 'lid' is circled in green. PDB of the ADP bound state (1AMW) used for diagrams.

From Figure 4.20 it can be seen that a large number of shifts can be observed across the entire protein in both ligand bound states. More chemical shift changes can be observed in the long helix in the AMPPNP bound state than in the ADP bound state. In contrast more shifts can be seen in the ATP 'lid' in the ADP bound state than in the AMPPNP bound state. A similar number can be seen in each ligand bound state in the β-sheet at the back of the binding pocket. Larger shifts (in orange) appear to be mostly, but not exclusively, closer to the ligand than smaller shifts (shown in blue). The overall pattern of peak shifts implies a great deal of flexibility within the N-terminal domain, however, from Figure 4.20 it is hard to identify ligand specific influences over the protein.

The bigger shifts are likely to be caused by a more significant change in environment and thus are of interest when thinking about how ligand binding influences the conformation of the N-terminal domain. In order to more clearly look at ligand induced changes to the protein, the large shifts only were first considered (Figure 4.21) followed by focusing on the large shifts induced that were unique to each ligand bound state (Figure 4.22).

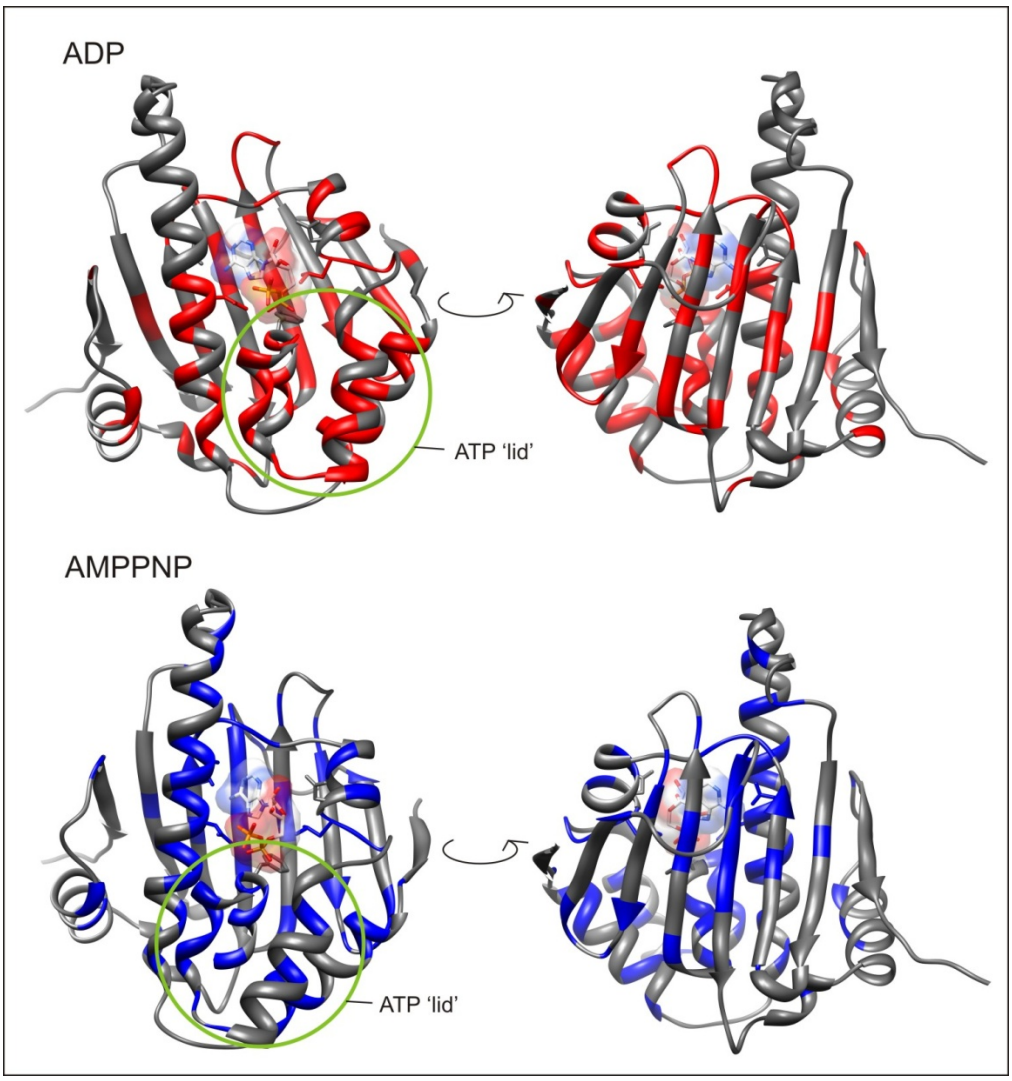

Figure 4.21 Comparison of the side-chain chemical shift changes induced by ligand binding in the N-terminal domain of Hsp90. Residues were identified using the ^{13}C-HSQC spectra and plotted onto the known ADP bound crystal structure. Comparisons were made between the apo state and the ADP bound state (red) and between the apo state and the AMPPNP bound state (blue). PDB of the ADP bound state (1AMW) used for diagrams.

Residues where a majority of resonances in a side chain showed a significant chemical shift were plotted onto the known crystal structure. From Figure 4.21 it is clear that the residues which are substantially shifted by the binding of either ADP or AMPPNP are widely dispersed, most are localised to the back of the binding pocket within the β-sheet and to the flanking helices surrounding the ligand binding pocket. There are also some notable shifts within the lid as shown in Figure 4.21 circled in green. A large number of chemical shift changes occur that are common to both the AMPPNP and ADP bound state, suggesting that many of the changes occurring are due to accommodating any ligand binding.

A more detailed picture of the specific changes that occur upon either ADP or AMPPNP binding can be identified by looking at the shifts that are seen in the presence of one ligand but not the other. These shifts are summarised in Figure 4.22 and Table 4.3.

AMPPNP	Phe8	Ile45	Gly83	Tyr146	
	Glu33	Lys48	Gly118	Arg166	
	Leu34	Gln55	Tyr125	Gly170	
	Asp40	Glu59	Leu129	Leu173	
	Ala41	Lys73	Ile137	Arg174	
	Leu42	Asp79	Gln145	Ala202	
ADP	Thr5	Glu76	Ser109	Ser138	Phe156
	Leu15	Ser80	Ala110	Asn141	Glu165
	Ile29	Met84	Ala112	Asp142	Phe176
	Arg32	Ile90	Phe128	Asp143	Gln181
	Ser36	Phe104	Ala131	Glu149	Glu187
	Ile66	Ala107	Val134	Gly153	Tyr203

Table 4.3 A summary of the uniquely shifted residues identified upon the binding of AMPPNP and ADP to the N-terminal domain of Hsp90.

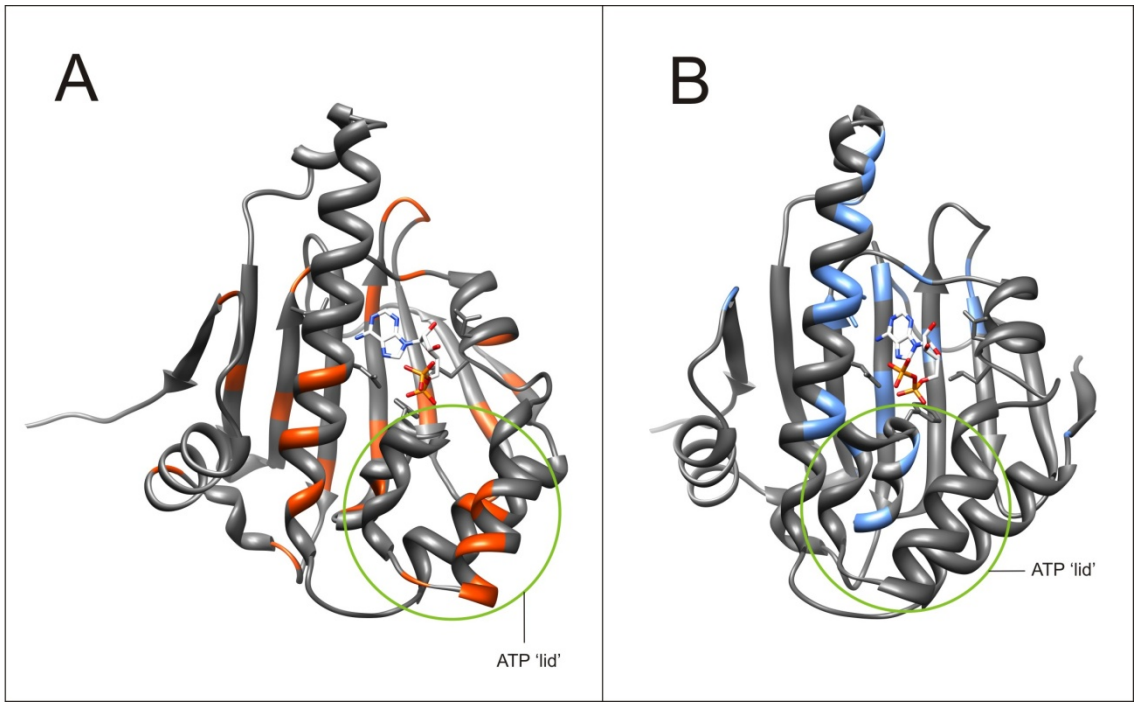

Figure 4.22 Unique shifted residues associated with ligand binding identified by comparing the CHSQC spectrum of the apo state with the spectra of the ADP and AMPNP bound states as plotted on the crystal structure. A: The unique chemical shifts induced by ADP binding. B: The unique shifts induced by AMPPNP binding.

A comparison of panel A and B of Figure 4.22 reveals some distinct differences between the binding of ADP and AMPPNP to the N-terminal domain of Hsp90. The binding of ADP uniquely shifted residues predominantly in the lower section of the long helix, the ATP 'lid' region, the flanking helix just behind the lid and the lower section of the β-sheet and one or two shifts at the top of the β-sheet and in the connecting loops. The binding of AMPPNP

shows uniquely shifted residues predominantly in the long helix, at the top of the β-sheet , one residue in the ATP 'lid' and a few residues in the helix directly following the ATP lid. The differences between the two ligands suggests that ADP causes disruption to the lower portion of the domain while AMPPNP interacts more with the upper portion of the domain. The movement within the β-sheet suggests that ADP may move deeper into the bottom back of the pocket while AMPPNP is then orientated more towards the top of the pocket. This is consistent with the chemical shift differences observed in Chapter 3 that suggest that the β-sheet is sensitive to the ligand position.

The residues which move uniquely in the ATP 'lid' region in the ADP bound protein and in the helix preceding the long helix are consistent with the lid being in an 'open' state when bound to ADP as is shown in the crystal structure used for Figure 4.22. The chemical shift changes induced by ligand binding may suggest that ADP leads to a 'lid open' conformation as the movement apart of these two regions as the lid moved, would alter their chemical environment. The chemical shift changes within the lid seen in Figure 4.20 indicate that upon ligand binding, either ADP or AMPPNP, the ATP 'lid' moves suggesting that the 'ground-state' of the lid is not close to either ligand bound state. The unique changes in chemical shift in the ATP 'lid' region in the AMPPNP bound protein are limited to Gly118. No unique shifts are observed in the first helix of the lid in contrast with the ADP bound state.

This may suggest that ADP causes a significant change in environment of the first helix by a tight association with the main body of the protein, as seen by the unique changes in chemical shift seen in the helix that precedes the long helix. AMPPNP in contrast only shows unique shifts in Gly118 within the 'lid' region. These unique changes in chemical shift are consistent with the apo state of the 'lid' being neither open nor closed and the binding of the ligand moving it from one state to another. The mutual changes in chemical shift also support this as the large numbers of shifts across the lid suggest that it is highly flexible in all states.

4.6 H/D exchange experiments

The use of hydrogen/ deuterium exchange experiments to monitor the accessibility of backbone amide groups is well documented [73-76]. Under normal conditions the proton on the backbone amide will freely exchange with the surrounding solvent. If the amide is protected, either due to its location within the folded structure of a protein or due to specific

non-covalent interactions such involvement in a hydrogen bond, then the proton exchange with the solvent will be limited. Thus changes in proton accessibility under different conditions can inform on conformational changes caused by that particular set of conditions.

In a ^{15}N-HSQC experiment the detected signal is that of backbone amide (NH) group of each amino acid. Under normal circumstances this signal is a composite of all protein molecules present in the sample. When deuterated solvent is introduced into the sample, such as by the addition of 50% D_2O, then amide proton exchange in the solvent will result in a mixed population of protonated and deuterated amide groups. Deuterated amide groups do not contribute to the overall amide signal detected by NMR thus as more amide groups exchange hydrogen for deuterium the signal intensity will decrease. Once an equilibrium with the solvent has been achieved then signal intensity decrease will cease.

As previously mentioned some amide bonds will be more shielded from exchange than others. These groups will decrease less rapidly and will take longer to achieve equilibrium with the solvent. In this series of experiments a 300 µL sample of the N-terminal domain of Hsp90 in the apo state at a concentration of 600 µM in 50 mM Tris was diluted with 300 µL of 50 mM Tris dissolved in D_2O. All experiments were undertaken at pH8. A ^{15}N-HSQC spectrum was recorded every 15 min for the first 10.5 h, then every half hour for 11.5 h then every hour for the final 25 h. The process described for determining the peak intensity decay for the apo N-terminal domain of Hsp90 was repeated for samples of the protein pre-incubated with ten-fold excess ADP or AMPPNP.

Peak heights were determined using NMRPipe. All spectra were initially processed identically using NMRPipe. A pseudo 3d spectrum was then constructed using each individual spectrum from the time course experiment as a spectrum slice with the NMRPipe script 'series.com'. Once processed, each peak was selected and overlapping peaks were identified within the peak list and labelled as belonging to the same cluster. The height of each peak in the pseudo 3d data series was then determined using the NMRPipe script autoFit.tcl. This script generated a 'synthetic' spectrum and a 'difference' spectrum for each 'slice' of the pseudo 3D data. From the synthetic spectrum the peak height was determined for each peak within the peak list. From the decay of a peak height across the pseudo 3d slices the rate of decrease for each peak was then determined. The 'difference' spectrum contains the original data minus the 'synthetic' data and thus acts as a check on the quality of the synthetic spectrum. Due to data handling limitations within the NMRPipe software the analysis of each data set was undertaken in three independent sections comprised of approximately 30 spectra each. Each set was then combined allowing for scaling factors between the sets. Allowance

was also made for the increase in intensity due to the increase in the number of scans at later time points.

4.7 Fast exchange or no exchange

This method of measuring H/D exchange allows determination of rates for amides with a medium to slow exchange rate. Some peaks will show no discernable change in intensity over the time course of the experiment. These peaks are either in very fast or very slow exchange. It is necessary to determine whether a peak fully exchanges before the first experiment or whether no exchange occurs over the time course of the experiment. In order to determine whether a peak is in very fast or very slow exchange its intensity compared to a peak that is known to have a medium rate of exchange was found. The ratios of the target peak to the peak in medium exchange were determined in an unquenched sample. This was repeated using five peaks in medium exchange. This set of five ratio values were then compared to the same ratios determined in the quenched sample. Where the difference between these ratios was small, the peak was determined to be in slow exchange. Where the ratios were very different this indicated that the peak was in very rapid exchange and thus reached equilibrium with the bulk solution before the first spectrum was recorded.

For each ligand bound state, five residues that showed clear proton exchange were selected. For the apo state residues Leu31, Asp40, Ala41, Phe63 and Asn91 were selected. For the ADP bound state residues Glu33, Se36, Phe63, Met116 and Lys191 were selected. For the AMPPNP bound state residues Ser35, Phe63, Asn91, Arg133 and Ile190 were selected. All peaks selected as 'reference peaks' were chosen for their high initial intensity close to the unquenched sample values and their subsequent rapid yet measureable decrease in intensity suggesting that they are neither in very fast or very slow exchange.

For every peak in a control ^{15}N-HSQC spectrum containing no D_2O its peak height was determined using CCPN software. The average ratio of 'reference peak' / 'peak height' was calculated for the five reference peaks. For every peak in the first H/D exchange spectrum the ratio of the reference peak to the peak height was also determined using CCPN software.

A comparison of these two reference values was then used to determine whether a peak was in very fast or very slow exchange. The use of ratio values obtained from each

spectrum ensured that only relative values between two peaks were being considered thus negating the need to adjust for differences in overall intensity between the two spectra. If a peak was in very slow exchange then the peak height ratio would remain close to its unquenched value. If a peak was in very rapid exchange then the peak height ratio in the first exchange spectrum would be far higher than in the unquenched spectrum. Thus any peak that showed a significant ratio increase between the control and first dataset was inferred to be in very rapid exchange. This ratio comparison was used on the apo, ADP and AMPPNP bound states of the N-terminal domain of Hsp90. This is seen in Figures 4.23, 4.24 and 4.25.

Peaks deemed to be in very fast exchange for the apo N-terminal domain of Hsp90 were Asn21, Asn26, Leu93, Thr95, Ile96, Gly118, Val122 and Lys178. Peaks deemed to be in very fast exchange for the ADP bound N-terminal domain of Hsp90 were Phe8, Ala10, Glu11, Lys27, Glu28, Ile29, Leu160, Glu162 and Arg169. Peaks deemed to be in very fast exchange for the AMPPNP bound N-terminal domain of Hsp90 were Arg32, Asn92, Ala017, Asp113, Gly154, Leu160, Arg169 and Trp148.

A comparison of the decay rate (intensity unit delay s^{-1}) for each amide in each state was undertaken. Where a peak for an amino acid was visible in one or two but not the remaining datasets the value for that peak in the missing set was set to a nominal negative value. Since a negative decay rate is impossible this value merely highlights that no peak was present in subsequent graphical analysis. Where rapid proton exchange had been identified by ratio comparison the 'measured' decay rate was very small as all proton exchange had already occurred before the first measurement. To identify these residues the rate was replaced with a value of '$3x10^{-5}$' in each case. This value was not chosen for its accuracy but due to it exceeding all other measurable rates and thus allowing easy identification of a 'rapid decay rate' in subsequent graphical analysis.

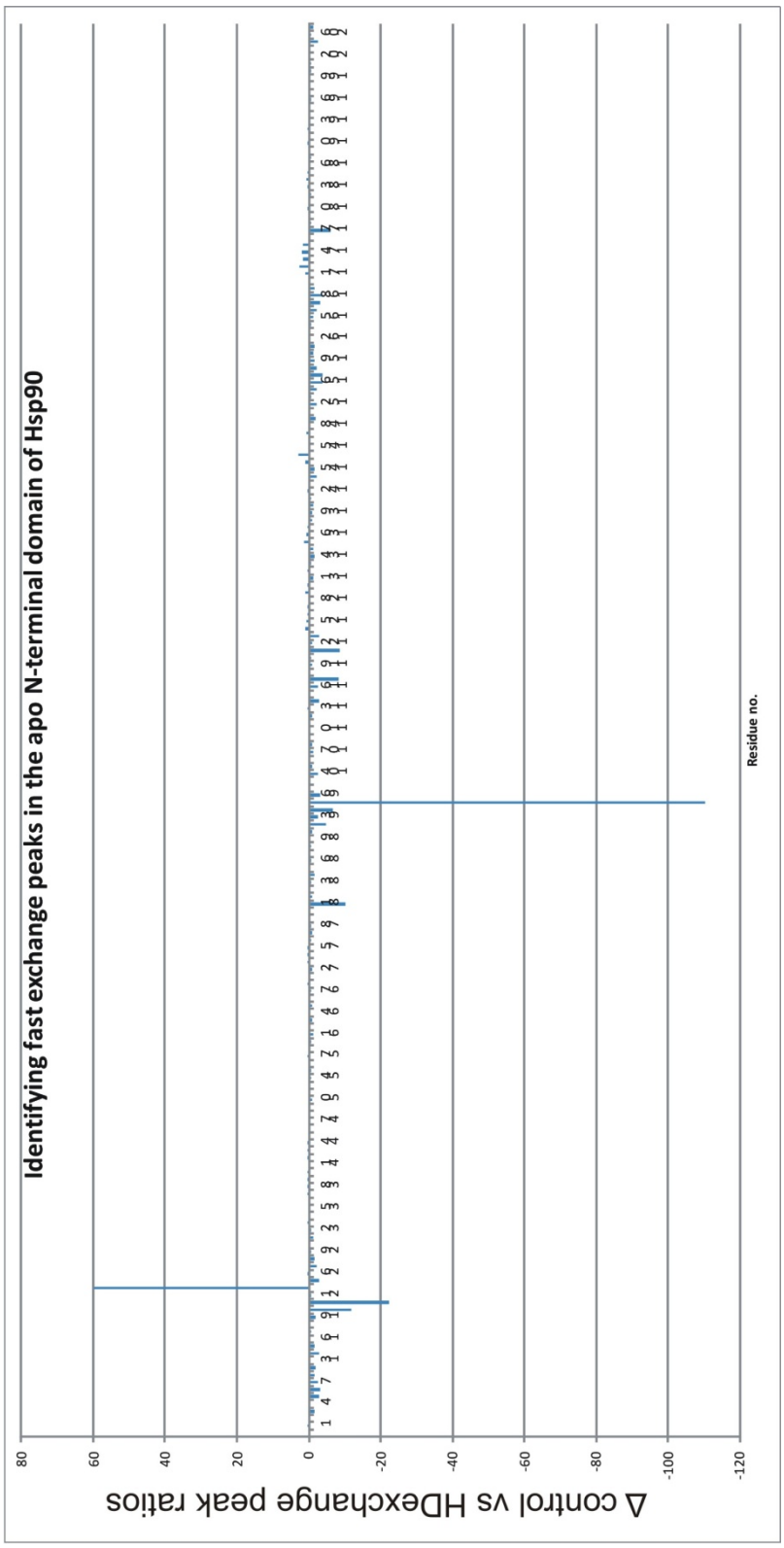

Figure 4.23 Using the apo N-terminal domain of Hsp90, the ratio of peak heights for each residue was determined against five 'reference peaks' in an unquenched and a D_2O quenched sample. The difference in signal between the quenched and unquenched samples was then plotted. Those with a large difference in ratios indicated that the peak was in very rapid exchange.

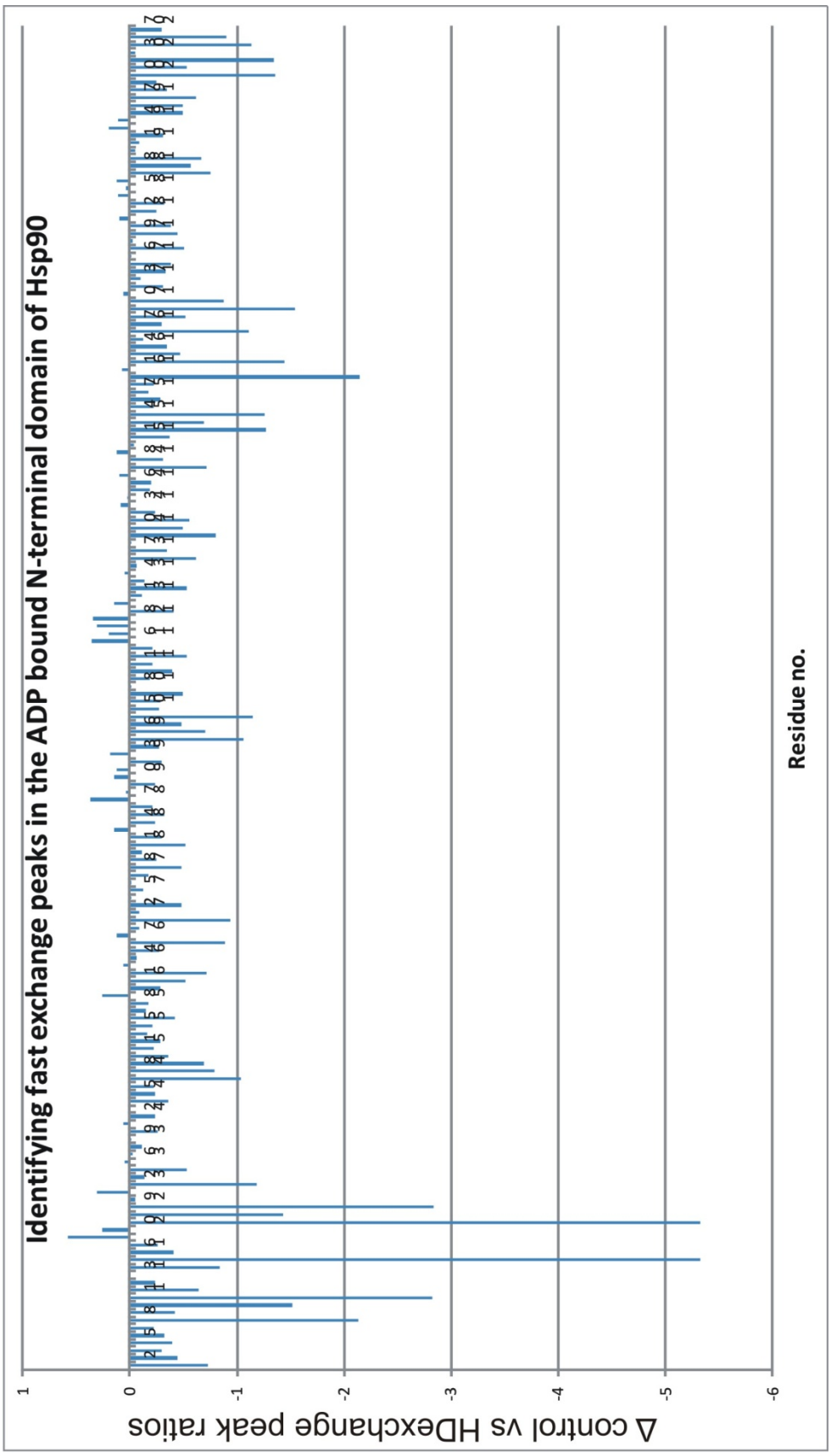

Figure 4.24 Using the ADP bound N-terminal domain of Hsp90, the ratio of peak heights for each residue was determined against five 'reference peaks' in an unquenched and a D_2O quenched sample. The difference in signal between the quenched and unquenched samples was then plotted. Those with a large difference in ratios indicated that the peak was in very rapid exchange.

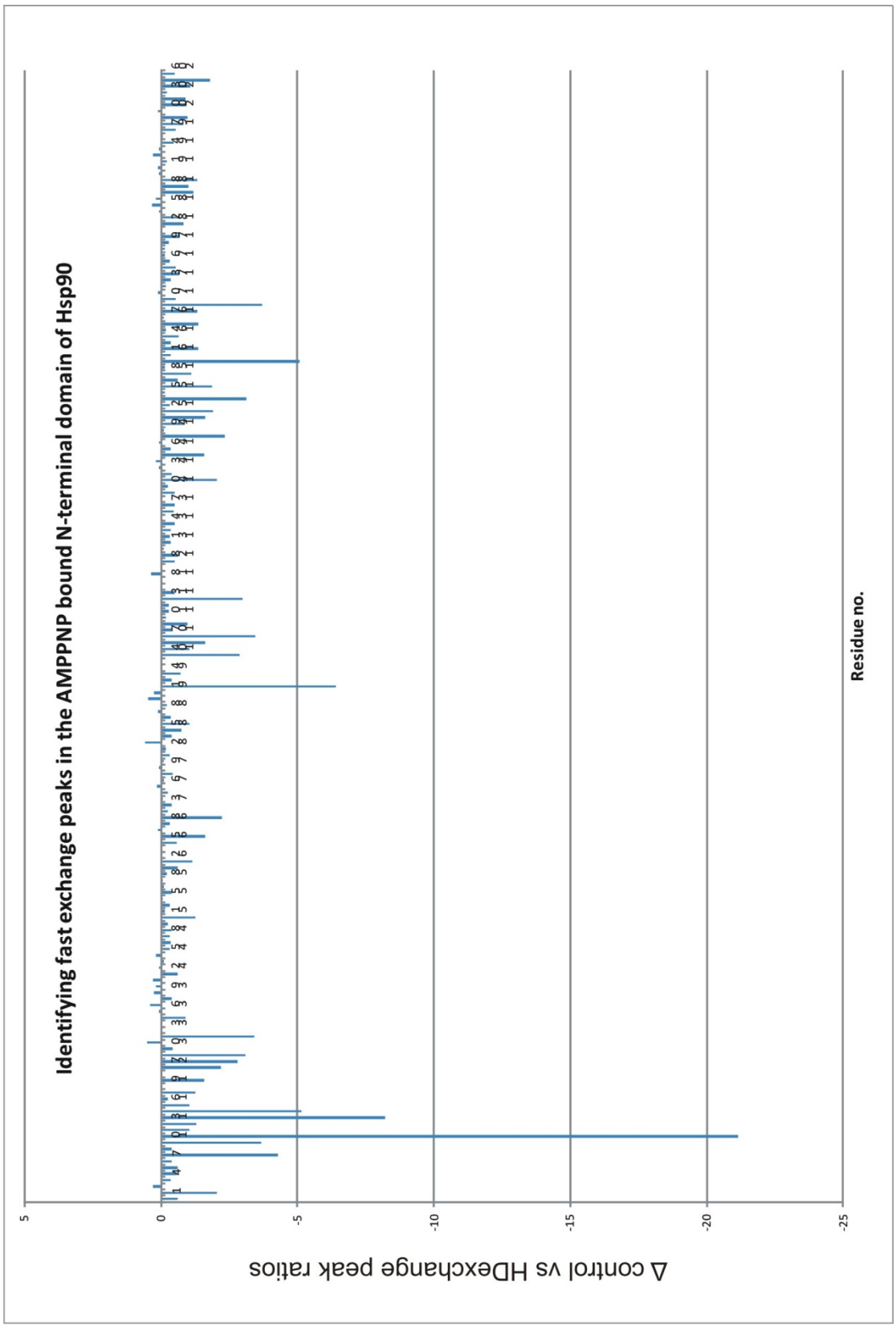

Figure 4.25 Using the AMPPNP bound N-terminal domain of Hsp90, the ratio of peak heights for each residue was determined against five 'reference peaks' in an unquenched and a D_2O quenched sample. The difference in signal between the quenched and unquenched samples was then plotted. Those with a large difference in ratios indicated that the peak was in very rapid exchange.

4.8 A comparison of the proton exchange rates for the apo, ADP and AMPPNP bound states of the N-terminal domain of Hsp90

The decay rate of an amide proton after quenching with D_2O is dependent upon its accessibility to the solvent and whether it is involved in any hydrogen bonding networks such as present in both α-helical and β-sheet secondary structures. Conformational changes including disruption to secondary structure can both influence the rate of proton exchange. Thus the difference in the decay rate between the apo, ADP and AMPPNP bound states is a potentially good method of monitoring/inferring structural changes induced by ligand binding and indentifying different responses to each ligand.

Residues 1 – 21:

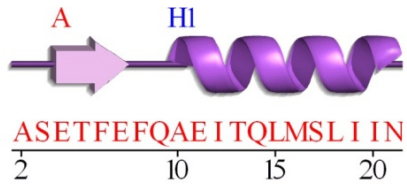

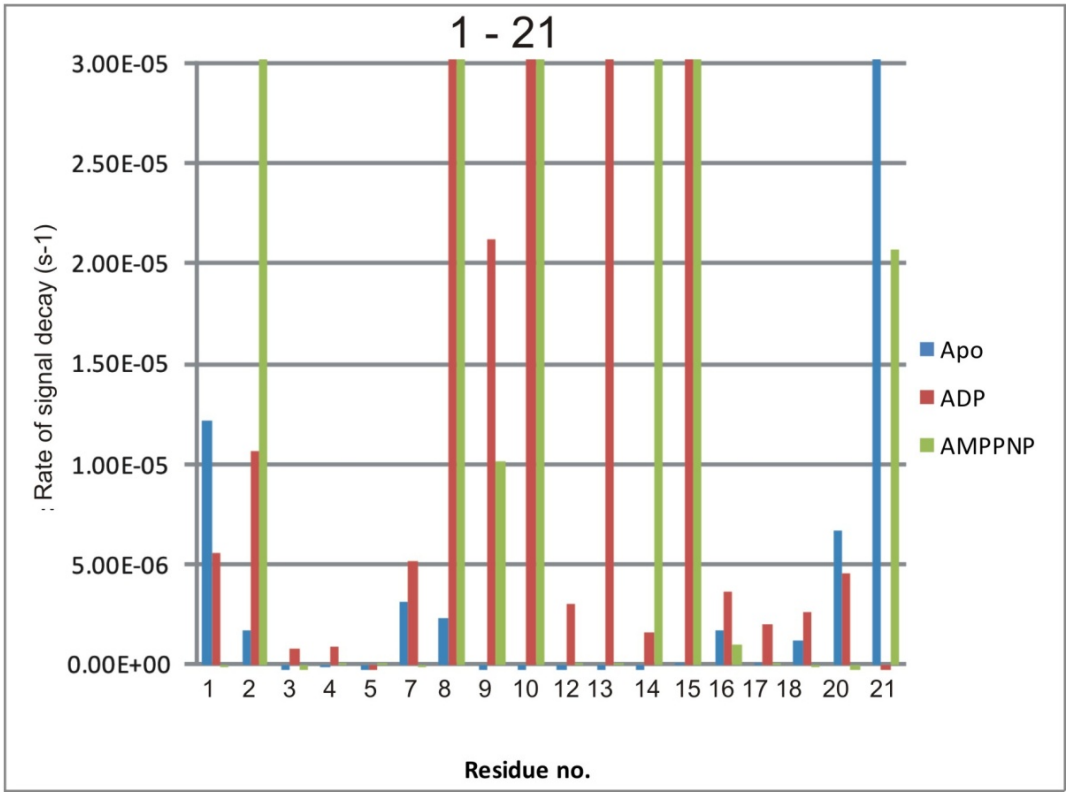

Figure 4.26 Decay rate of each amino acid residue amide proton intensity from residue 1 - 21 in intensity units S^{-1} for each of the three states – apo (blue), ADP bound (red) and AMPPNP bound (green). Negative bars represent a lack of data for that construct at that residue. Values of $3x10^{-5}$ represent residues that exchange very rapidly before the first data point is measured.

The initial 21 amino acids correspond to the first strand and helix of the N-terminal domain of Hsp90. The β strand shows a high degree of protection in all ligand bound states with the exceptions of residues 2, 8 and 15 which show very rapid exchange in the two ligand bound forms in contrast to the apo state.

The first half of the α-helix shows a considerable increase in exchange rate in the ligand bound states (Figure 4.26). ADP and AMPPNP induce a high exchange rate in Thr13 and Gln14 respectively. These two amino acids are located on the α-helix with the amide bond facing towards the main bulk of the protein. The difference between the two ligands suggests a slightly different position of the helix caused by each to allow solvent exposure of the relevant amide protons to the solvent. Residue Leu15 shows an equal change in exposure/exchange for both ligands. The latter half of the helix however shows a degree of protection against proton exchange in all states. This may indicate a degree of uncoiling of the first two turns of the helix induced by the binding of ADP and AMPPNP but a retention of the secondary structure towards the end of the helix. Following the helix the loop from residue 21 again has increased exchange as anticipated for an unstructured region. These results are consistent with increased flexibility in the first strand/helix induced by ligand binding and may be linked to the 'strand swap' event that occurs in the full length protein.

Residues 26 – 51:

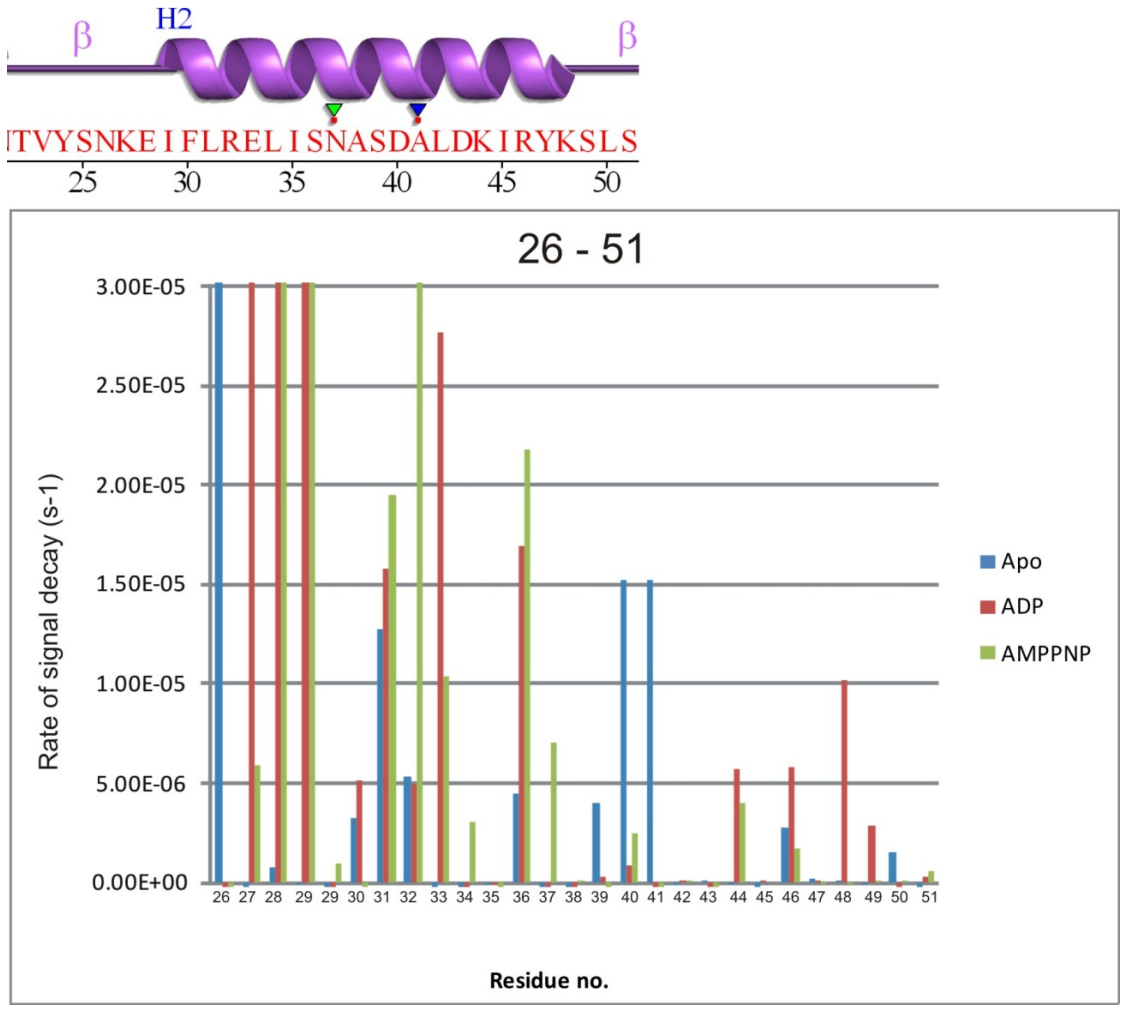

Figure 4.27 Decay rate of each amino acid residue amide proton intensity from residue 26 - 51 in intensity units S^{-1} for each of the three states – apo (blue), ADP bound (red) and AMPPNP bound (green). Negative bars represent a lack of data for that construct at that residue. Values of $3x10^{-5}$ represent residues that exchange very rapidly before the first data point is measured.

No data was available for residues 22 – 25 in any of the datasets due to the inability to resolve peak overlap. Residues 26 – 29 corresponds to a coiled section of α-helical structure just prior to the start of the long α-helix (Figure 2.27). This suggests that ligand binding destabilises this structure compared to the apo state thus increasing the accessibility and rate of exchange. The long α-helix runs from residues 29 – 48. The first four residues (29 – 33) show some accessibility followed by a region of fairly low accessibility suggesting strong secondary structure. The exception is residue Ser36 which shows considerably more accessibility in the ligand bound states than the apo state. Ser36 points towards the strand/helix formed by the first 21 residues which show increased flexibility in the ligand bound states. If these two regions interact then destabilising of one could lead to destabilising of the other. Asp40 and Ala41 show increased protection in the ligand bound states compared to the apo state. These

two residues form part of the long helix directly opposite the ligand binding site thus interaction with the ligand via the water network may lead to stabilisation of this region, preventing proton exchange. The latter half of the long helix shows a low exchange rate under all conditions with a slight increased rate in the ADP bound state.

Residues 52 – 79:

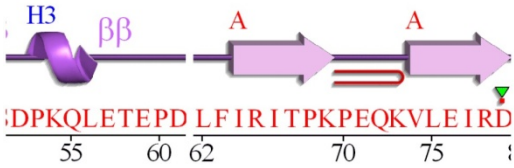

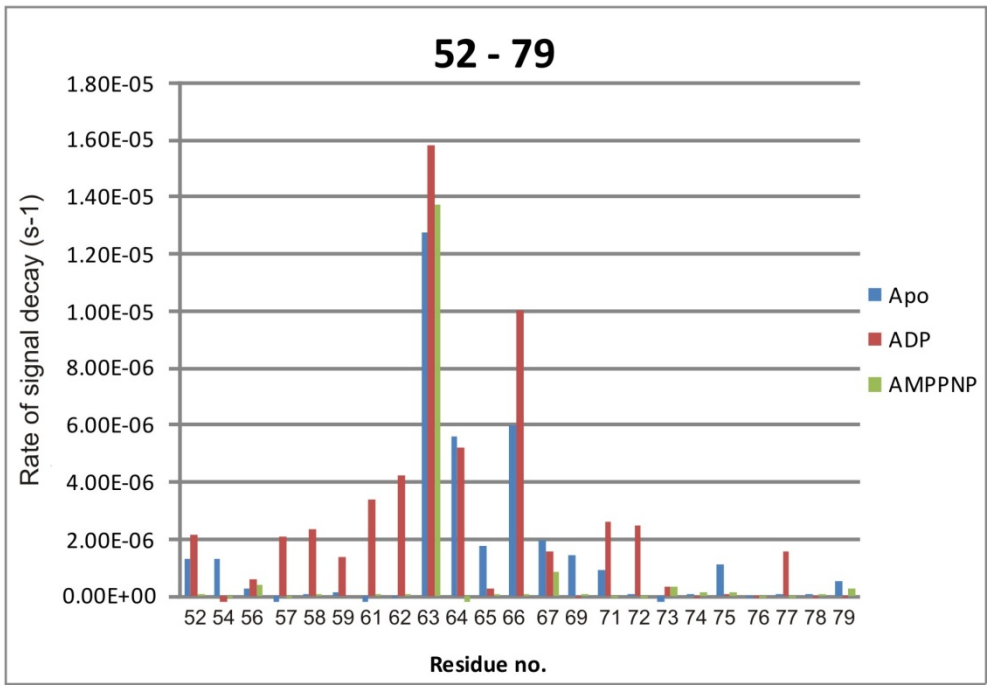

Figure 4.28 Decay rate of each amino acid residue amide proton intensity from residue 52 - 79 in intensity units S^{-1} for each of the three states – apo (blue), ADP bound (red) and AMPPNP bound (green). Negative bars represent a lack of data for that construct at that residue.

Residues 52 – 56 from a short helix showing low exchange in all states (Figure 4.28). Residues 57 – 62 form an exposed loop region that shows a low accessibility in the apo state and AMPPNP bound state but a higher exchange and thus greater flexibility in the ADP bound state. Phe63 shows a roughly equal exchange rate between all three states, it is positioned on the N-terminal end of the first beta strand and is fairly exposed to solvent. Residues 64 – 72 comprise a β-strand that forms part of the binding pocket for the ligand. Exchange is seen in the apo and ADP bound state but not the AMPPNP bound state. This suggests that the AMPPNP bound state leads to a rearrangement of the strand or reduced flexibility that decreases solvent exposure of the amide protons in this region. AMPPNP binding may promote

a stronger association with the C-terminal β-strand that otherwise might be somewhat flexible at the extreme terminus of the protein. It has already been suggested in chapter 3 that in the AMPPNP bound state there is a distinct arrangement of the ligand within the pocket caused by the protonation of the terminal phosphate, this could lead to an increased stability within this region of the binding site. Residues 73 – 79 form a β-strand that is central to the β-sheet of the N-terminal domain. This region shows a low proton exchange rate for all states as is anticipated for a secondary structure region that is not disrupted by ligand binding.

Residues 80 – 98:

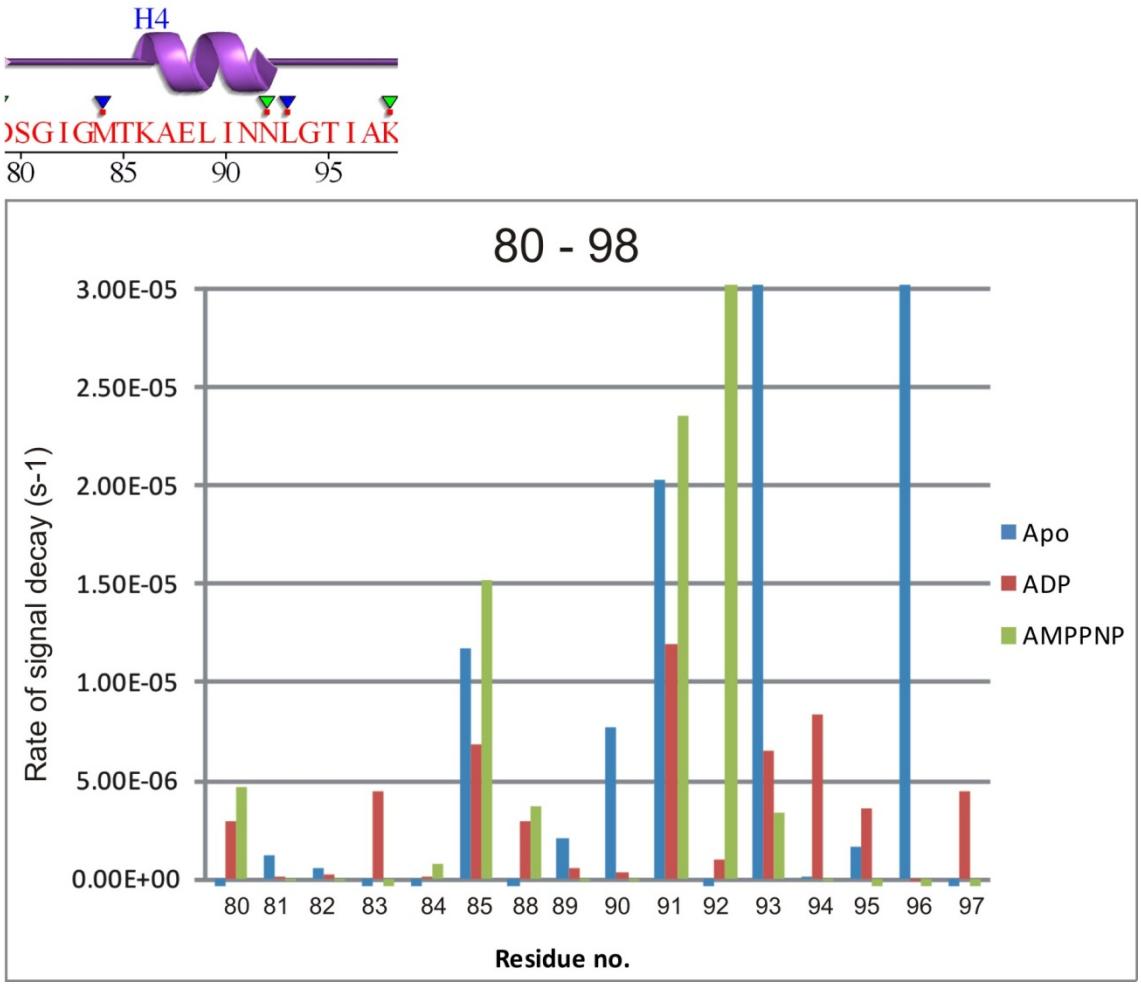

Figure 4.29 Decay rate of each amino acid residue amide proton intensity from residue 80 - 98 in intensity units S^{-1} for each of the three states – apo (blue), ADP bound (red) and AMPPNP bound (green). Negative bars represent a lack of data for that construct at that residue. Values of $3x10^{-5}$ represent residues that exchange very rapidly before the first data point is measured.

Residues 80 to 98 comprises a loop, a short helix and then a loop leading into the ATP 'lid'. The initial loop region from 80 – 85 shows a high degree of proton protection in all states, despite the lack of secondary structure (Figure 4.29) however given its location in the interior of the protein it is likely more shielded from exchange. Residues 86 – 93 form a small two turn

helix that flanks the binding site. This region is most stabilised in the ADP bound state and destabilised by the apo and AMPPNP bound states. Residues 93 to 97 show most exchange in the ADP bound state with the exception of residue 96 which shows most exchange in the apo state. This is close to the hinge lid suggesting that the presence of ADP and AMPPNP stabilise this region in different ways with the ADP bound state being most exposed. The high exchange of residue 96 in the apo state suggests that it is accessible until ligand is bound.

Residues 103 – 130:

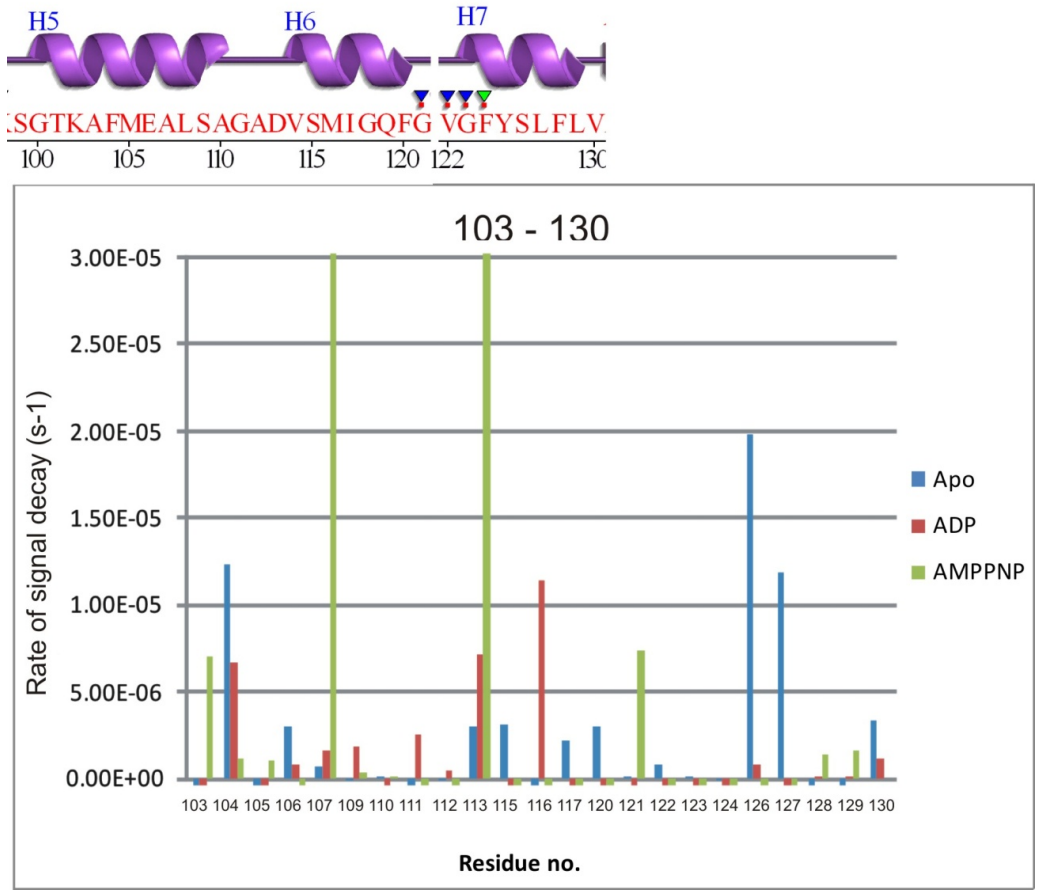

Figure 4.30 Decay rate of each amino acid residue amide proton intensity from residue 103 - 130 in intensity units S^{-1} for each of the three states – apo (blue), ADP bound (red) and AMPPNP bound (green). Negative bars represent a lack of data for that construct at that residue. Values of $3x10^{-5}$ represent residues that exchange very rapidly before the first data point is measured.

Residues 99 – 123 comprises the ATP 'lid' as detailed earlier. In the apo state and the ADP bound state the exchange rate is relatively slow across the lid suggesting that the addition of ADP has a minimal effect on the accessibility or protection of the lid backbone residue protons (Figure 4.30). In the AMPPNP bound state two residues show a dramatic increase in proton exchange rate. These residues, Ala107 and Asp113, are located at the tip of the ATP 'lid' region. Residues 124 – 130, form a short helix following the ATP 'lid'. They show slightly more accessibility in the apo bound state than in either of the ligand bound states at residues 126 and 127. These two residues form part of an α-helix in the ADP bound crystal structure.

Their accessibility in the apo state suggests that ligand binding is required to stabilise this section of secondary structure.

Residues 131 – 161:

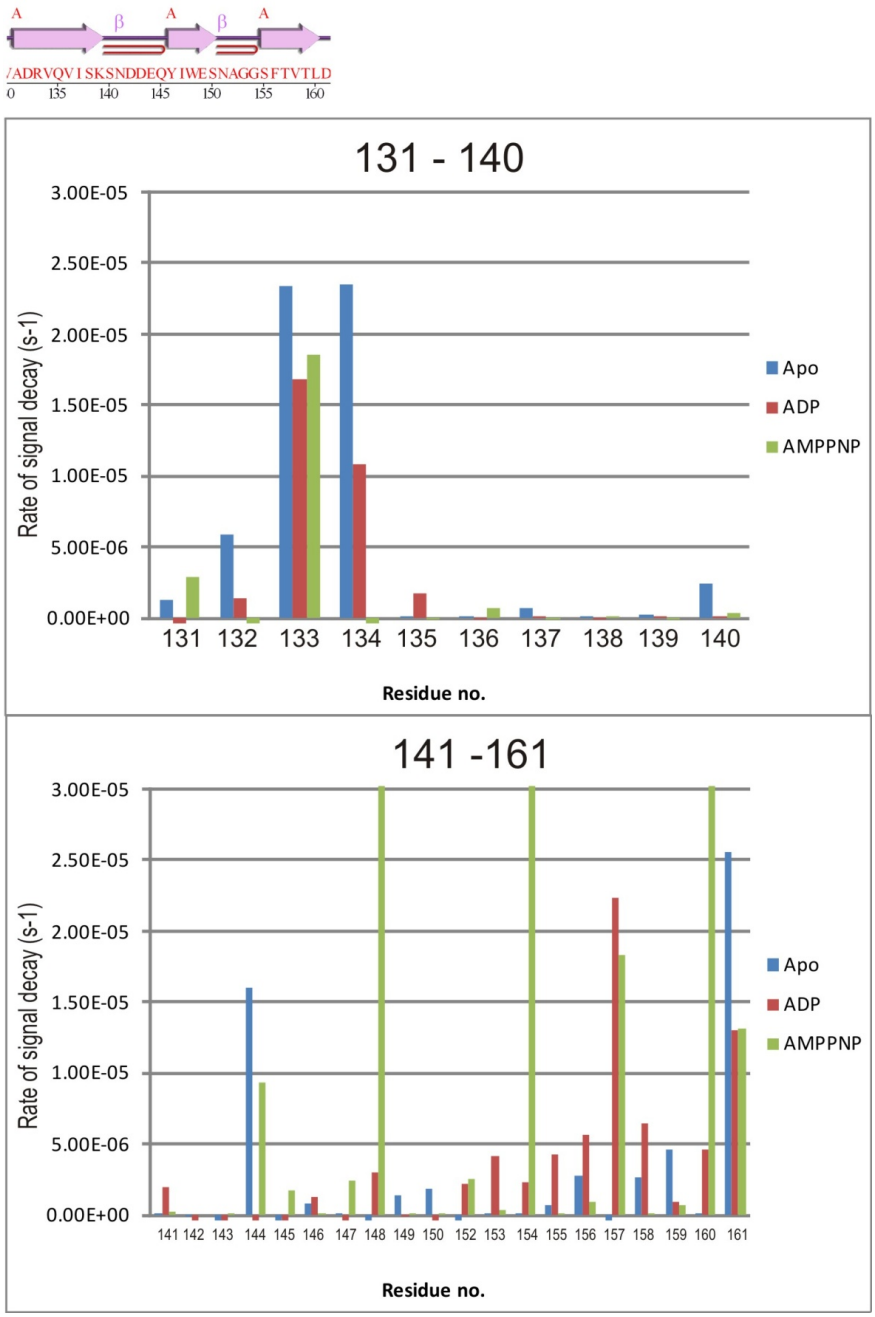

Figure 4.31 Decay rate of each amino acid residue amide proton intensity from residue 131 - 161 in intensity units S^{-1} for each of the three states – apo (blue), ADP bound (red) and AMPPNP bound (green). Negative bars represent a lack of data for that construct at that residue. Values of $3x10^{-5}$ represent residues that exchange very rapidly before the first data point is measured.

Residues 131 – 161 form three strands of the β-sheet that comprises the back of the binding pocket. Much of this section has limited or slow proton exchange with some notable exceptions (Figure 4.31). Residues Arg133 and Val134 are located at the end of the β-sheet and are only flanked on one side by a strand of equal length, they show a high rate of proton exchange in all three states with the exception of Val134 AMPPNP bound where not data was available. Residues 135 – 143 show high stability and low proton exchange corresponding to the first of the β-strands in the sheet and the beginning of the loop connector. Residue 144 shows high exchange corresponding to its location on the outside of the loop. No data is available for the ADP bound state. This is followed by a region of high protection corresponding to the second β strand from 145 – 153. The notable exception here is the high accessibility of residue Trp148 in the AMPPNP but not the ADP bound state with no data available for the apo state. The side chain of Trp148 points in towards the binding pocket. AMPPNP binding may cause a rearrangement of the binding pocket compared to the binding of ADP; this might interact with the Trp side chain leading to it influencing the amide proton on the reverse side of the β-sheet.

Residue Gly154, at the start of a beta strand, shows a large difference in accessibility between AMPPNP bound and the other two states yet curiously Gly153 shows no such behaviour despite both being part of the same loop region. Thr157 shows a high degree of accessibility compared to its neighbouring residues, however it is located in the β strand directly opposite Trp148. This proximity may indicate that any effect upon Trp148 might disrupt the hydrogen bond between the two residues thus making Thr157 more accessible to proton exchange or may indicate a more direct response to ligand binding. ADP presumably causes less disruption in this area compared to AMPPNP only influencing the amide of Thr157 but not managing to influence Trp148.

Leu160 is located at the end of a beta strand exposed to the bulk solvent but only shows a high degree of proton accessibility in the AMPPNP bound state suggesting that the β-sheet hydrogen bond network is disrupted in this bound state only. This matches the trend for AMPPNP to induce chemical shift changes at the top of the binding pocket as seen earlier in this chapter. The neighbouring residue, Asp161, is part of a loop region extending from the β-strand and is slightly less accessible in both ligand bound forms compared to the apo state.

Residues 162 – 186:

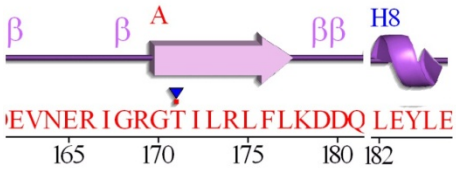

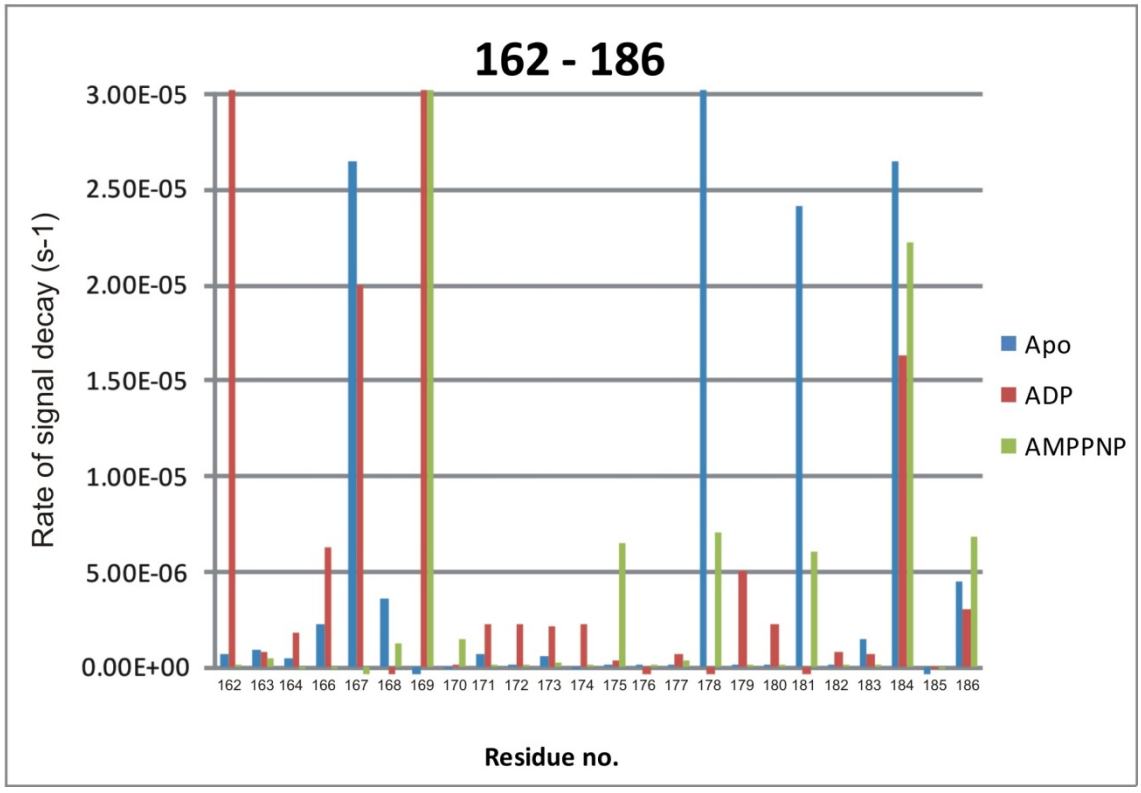

4.32 Decay rate of each amino acid residue amide proton intensity from residue 162 – 186 in intensity units S^{-1} for each of the three states – apo (blue), ADP bound (red) and AMPPNP bound (green). Negative bars represent a lack of data for that construct at that residue. Values of $3x10^{-5}$ represent residues that exchange very rapidly before the first data point is measured.

Residues 162 – 169 form a loop between two beta strands exposed to the solvent. This accessibility however is not reflected in the apo and AMPPNP bound state which shows a very limited exchange until the end of the loop region where rapid exchange is then observed. This may indicate some degree of association between the early portion of the loop and the β-sheet. ADP however seems to lead to a high rate of exchange suggesting that this loop is more flexible in the ADP bound state (Figure 4.32). Residue Arg169 shows a high accessibility in both ligand bound states with no data available for the apo state. The β-strand then shows a low exchange rate in all states with marginally faster exchange in the presence of ADP. Lys178 marks the end of the β strand and the start of the loop region containing one helix turn reflected by the increase in H/D exchange. A high exchange rate is also seen for Gln181 just prior to the helix turn. Residues 182, 183 and 185 show a high degree of protection as expected due to their involvement in an α-helix. Residues 184 and 186 show a decreased

degree of protection in all states which is unexpected due to the hydrogen bonding network provided by the α-helix turn.

Residues 187 – 207:

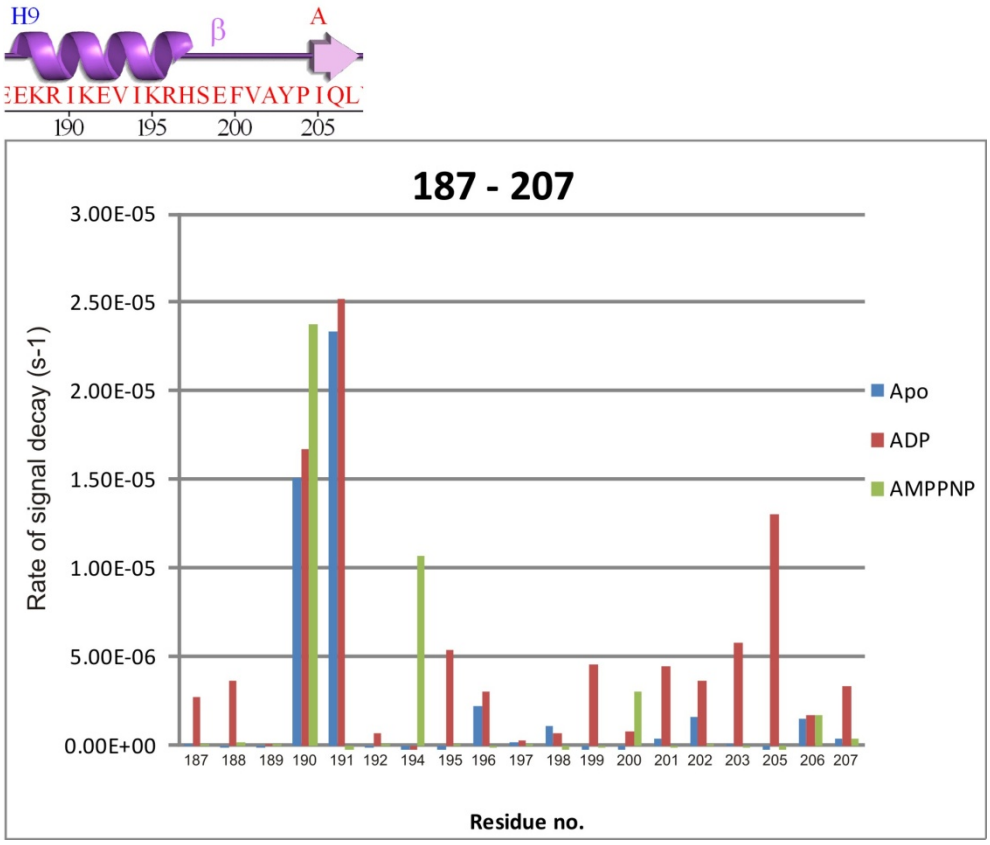

Figure 4.33 Decay rate of each amino acid residue amide proton intensity from residue 187 - 207 in intensity units S^{-1} for each of the three states – apo (blue), ADP bound (red) and AMPPNP bound (green). Negative bars represent a lack of data for that construct at that residue. Values of $3x10^{-5}$ represent residues that exchange very rapidly before the first data point is measured.

The final short α-helix is formed of residues 187 – 196. The first three residues show very low proton exchange with slightly higher accessibility in the ADP bound state (Figure 4.33). In strong contrast, residues 190 and 191 show a very high rate of proton exchange in all states despite their location in the middle of an α-helix, although no data is available for the AMPPNP bound state of 191. Residues 192 – 196 then show a relatively high level of protection, however, some exchange is still occurring suggesting that this helix is not as highly stabilise as others that are located more centrally within the N-terminal domain. Residues 199 to 207 comprise the extreme C-terminal β strand which shows a high degree of protection in the apo and AMPPNP bound states most likely due to the hydrogen bonds formed with the neighbouring β strand as part of the binding pocket β-sheet. Protection of alternate amide groups as might be expected in a β-strand structure is not seen. In contrast in the ADP bound state this strand shows a far higher accessibility suggesting an increased level of flexibility. This region appears to be highly variable in its accessibility. This is reflected by the side-chain

chemical shift changes observed in this region earlier in this chapter suggesting that it responds flexibly to ligand binding.

Figure 4.34 highlights the amino acids where the binding of ligand, either ADP or AMPPNP, leads to a change in H/D exchange pattern observed compared to the apo state. Figure 4.34A shows the residues where both ligands cause a similar change in exchange and possible exposure compared to the apo state, either increasing or decreasing its accessibility to H/D exchange. From this figure it is clear to see that there are a few key areas that show changes and that these areas are mostly located around the edge of the binding site. These regions are likely associated with the general response of the domain to ligand binding reflecting the way the protein accommodates the ligand within the binding site. It would be generally expected that in the ligand bound state the rate of protein unfolding would be slower and the protein more stable thus leading to a lowered exchange rate. Therefore increased exchange rates observed in the ligand bound state are particularly interesting.

Conformational flexibility of the back-bone, as reflected by the change in chemical shift resonances, has been observed upon ligand binding and exploited in Chapter 3. It was additionally seen in the first half of this chapter that changes in chemical shift of the side-chains were observed for a great number of residues across the domain. Although some of these shifts were very small, they occurred in response to both ADP and AMPPNP ligand binding. This suggests an inherent flexibility in response to ligand binding even within stable secondary structural elements. Small chemical shift changes would not necessarily indicate a change in gross conformation, and thus not be as informative on the gross conformational changes induced by ligand binding, but may suggest sufficient flexibility in the protein overall to facilitate the increased H/D exchange observed.

The first strand and helix, comprising the first 20 amino acids, shows an increase in accessibility. This region is involved in the strand swap event and so it seems likely that ligand binding may cause the N-terminal domain to adopt a conformation whereby this ‘strand swap’ event is favoured even in the absence of a second N-terminal domain with which to dimerise. This increased flexibility may denote a decrease in the strength of the secondary structure elements that keep the N-terminal strand and helix associated with the main body of the protein.

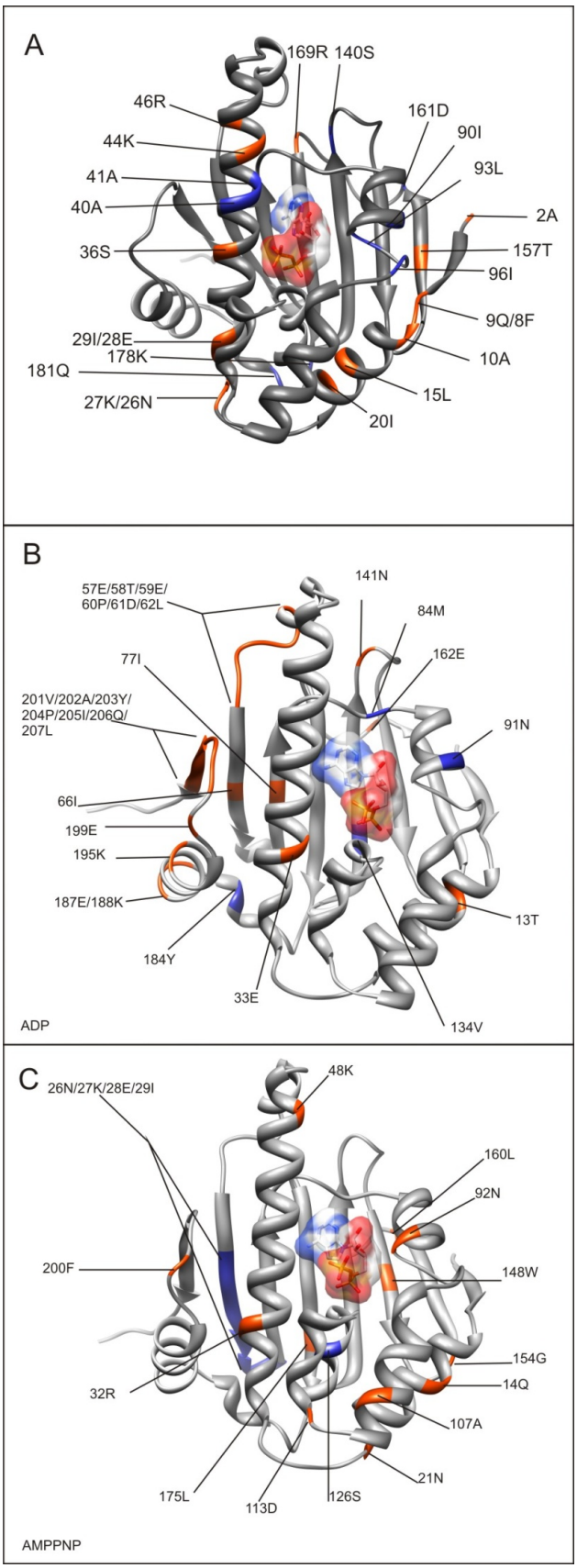

Figure 4.34 Changes in the H/D exchange pattern on the N-terminal domain of Hsp90 induced by ligand binding plotted onto the crystal structure. Orange residues show an increased exchange while blue residues show a decreased exchange. A: The changes in H/D exchange pattern caused by both the binding of ADP and AMPPNP. B: The unique changes in H/D exchange pattern caused by the binding of ADP. C: The unique changes in H/D exchange pattern caused by the binding of AMPPNP.

The long helix shows two regions of increased exchange at the top and bottom of the helix and a region of increased protection in the middle close to the ligand. The region of increased stability involves residues Ala40 and Ala41 which are known to be involved in an extend water network that interact with the adenine group of the ligand through van der waals forces (see Chapter 1). The regions of increased exchange involve residues that are not directly involved in ligand binding. The involvement of Ala41 with the binding of the ligand may lead to a distortion of this long helix leading to a weakening of the α-helical structure towards the ends of the helix and the exposure of the amide groups of these residues to the solvent. Ala41 also showed a change in chemical shift upon binding of AMPPNP as described in the first half of this chapter. Residues Ile90 (which also showed a chemical shift change in its side chain resonances in the ^{13}C-HSQC upon ADP binding) and Leu93 show an increased protection from exchange. Between these two residues, Asn92 is involved with a direct link to the ribose group of the ligand and is one of the few direct contacts with it. This direct contact may lead to a stabilising of the region and thus increased protection for Ile90 and Leu93. The influence of Asn92 may also be felt by Ile96 explaining the increase in protection of this residue as well.

There are three residues in the β-sheet at the back of the binding pocket that show an increase in exchange; Ala2, Thr157 and 169R. None of these residues are involved in the binding of the ligand either directly or indirectly however they are all located either at the end of a β-strand (Ala2 and Arg169) or at the very edge of the β-sheet (Thr157). The side chain of Phe156 is known to show a chemical shift change in the presence of ADP and this movement of the aromatic group could influence the accessibility of the Thr157 amide even if its own amide remains stable. It is has already been detailed in Chapter 3, and earlier in this chapter, that the binding of ligand causes a series of chemical shifts detected by NMR that map to this β-sheet. This suggests that ligand binding causes a rearrangement of the back of the binding pocket, the increase in exchange at the periphery of the β-sheet reflecting perhaps a decrease in the stability of the edge of it caused by movement in the middle where the ligand sits.

The unique shifts associated with the binding of ADP to the N-terminal domain of Hsp90 can be mapped to two main regions (Figure 4.34B). The first location is the extreme C-terminus of the domain and the preceding helix. The second location involves the β-sheet involving residues Ile66 and Ile77 which are also close to the C-terminal region and the loop that connects the long helix to the β-sheet from residues 57-62. It is known that residues Ile66 and Glu76 both show a chemical shift change in the ^{13}C-HSQC spectra as detailed earlier. It is also known that Gln181, Glu187 and Tyr203 all show chemical shift changes in the ^{13}C-HSQC

spectra. These residues are all close to or on the expected interface between the N-terminal and middle domains of the Hsp90 molecule. The increase in exchange here, and the chemical shift change seen in the ^{13}C-HSQC, suggests an increased flexibility in this region or a destabilisation of structure. It is known that during the chaperone cycle the binding of ATP is associated with an association of the N-terminal and middle domains. The data here suggests that the interface is disrupted in the presence of ADP perhaps indicating a role in the dissociation of the domains and the resetting of the cycle. Asn91 shows a decrease in exchange that may again be due to the stabilising influence of Asn92 directly bound to the ligand. Thr13 is located on one of the helices that flank the nucleotide binding site and which also shows additional exchange in panel A. This suggests that ligand binding influences the whole helix causing a weakening of the proton protection and so allowing increased H/D exchange. Thr13 shows one way in which ADP differs slightly in the degree of disruption to the helix compared to AMPPNP. Thr13, Gln14 and Leu15 are all part of the same helix after the first strand. Both Thr13 and Gln14 may be influenced by Leu15 which is known to show a chemical shift change upon ADP binding. The binding of ligand may influence the middle of the β-sheet thus placing the periphery of the sheet under strain that allows increased solvent accessibility. The reverse of this is seen in the final residues Val134 where increased protection is observed. Val134 is located within the middle of the β-sheet and displays a chemical shift change in the ^{13}C-HSQC upon ADP binding; if ligand binding leads to a rearrangement of this region, previously indicated by NMR shifts, then this could lead to a stabilisation of the structure and thus increased protection for the amide proton from exchange.

Figure 4.34C shows the unique changes in H/D exchange associated with the binding of AMPPNP to the N-terminal domain of Hsp90. The pattern of exchange accessibility is distinctly different to that of the ADP bound state. Again residues at either end of the long helix (Lys48 and Arg32) show increased accessibility suggesting that the helix is under strain thus weakening the hydrogen bonding network at the ends. Chemical shift changes in the side-chains of residues Glu33, Leu34, Asp40, Ala41, Leu42, Ile45 and Lys48 under AMPPNP bound conditions support the exchange data observed for this helix. Residue Phe200 also shows an increased accessibility however the large degree of accessibility seen in this region in the presence of ADP is not reflected in the presence of AMPPNP. This suggests that the AMPPNP does not lead to any destabilisation in this region. This fits with the idea that the binding of ligand before hydrolysis promotes the association of the N-terminal and middle domains and thus a destabilisation of the interface is not required. Indeed the region from Asn26 – Ile29 shows an increase in protection in this strand of the β-sheet suggesting an increased stability in this region. Trp148 and Leu175 are located in the middle of the β-sheet and show an increased accessibility suggesting a disruption of the β-sheet hydrogen bonding network that

leads to the amide bond protection. Arg174 shows a chemical shift change upon AMPPNP binding which might explain the increased accessibility observed for Leu175. Such a disruption could be caused by a movement of the AMPPNP ligand against the back of the binding pocket as has already been suggested by NMR data in Chapter 3 where shifts are observed across the β-sheet in response to pH in the AMPPNP bound state and in both ligand bound states of the T22I and T101I earlier in that chapter.

Three residues of note that show an increase in accessibility are Ala107, Asp113 and Asn92. As previously mentioned, Asn92 is bound directly to the adenine base of the ligand upon binding and may be implicated in the stabilisation of this binding site flanking helix. The increased accessibility of the amide group in the AMPPNP bound state only, coupled with the decreased accessibility of the surrounding helix, suggests a more specific influence upon Asn92 that is ligand dependent. Residues Ala107 and Asp113 are only influenced in the AMPPNP state and are the only residues within the ATP 'lid' region that show any shift at all. The crystal structure here is shown in the 'lid open' position however in the 'lid closed' position Asn107 and Asp113 would fold up and end up in very close proximity to Asn92. If the binding of AMPPNP lead to the stabilisation of the 'closed' state, the close proximity of these residues could lead to a disruption in the secondary structure thus leading to an increase in proton exchange. This could be consistent with the idea that in the isolated N-terminal domain of Hsp90, the binding of AMPPNP leads to the stabilisation of the ATP 'lid' in the closed state while ADP does not.

5 Thermodynamics of the extended molecule of Hsp90. Nucleotide ligands binding to the N551 and full length constructs

5.1 Introduction

The thermodynamics of binding of ligands ADP, AMPPNP, adenosine and adenine to the isolated N-terminal domain has already been reported in Chapter 3. However, as was discussed in Chapter 1, the presence of the middle domain is known to have an influence over ATP hydrolysis due to the requirement of Arg380 on the catalytic loop of the middle domain for efficient terminal phosphate cleavage. It is known that the conformational changes induced by ligand binding and hydrolysis within the N-terminal domain of Hsp90 must, in some way, be propagated to the rest of the chaperone molecule. It is also known that during the conformational cycle of Hsp90, the N-terminal and middle domains move closer to one another and that there is a structural rearrangement, including the reorientation of the catalytic loop of the middle domain containing Arg380. This series of changes causes the γ-phosphate of the AMPPNP ligand to be positioned so as to contact the catalytic residue Arg380 as shown in the full-length crystal structure [7]. This contact has also been demonstrated as being significant for full ATPase activity as detailed in Chapter 1. There have, however, been no previous studies as to whether this influence of the middle domain on the kinetics of the reaction also extends to the thermodynamics of initial binding.

In order to study the influence of the middle domain over the N-terminal domain and ligand binding, a construct containing both the N-terminal and middle domains was used. The N551 construct, comprising of the first 551 amino-acid residues of Hsp90, is shown in Figure 5.1. Key features shown in Figure 5.1 include the N-terminal helix and strand involved in the strand-swap event, the ATP 'lid' closed over the ligand binding site, residue Arg380 from the middle domain catalytic loop and the two ends of the long linker that joins the two domains although that proved too flexible to resolve in the crystal structure.

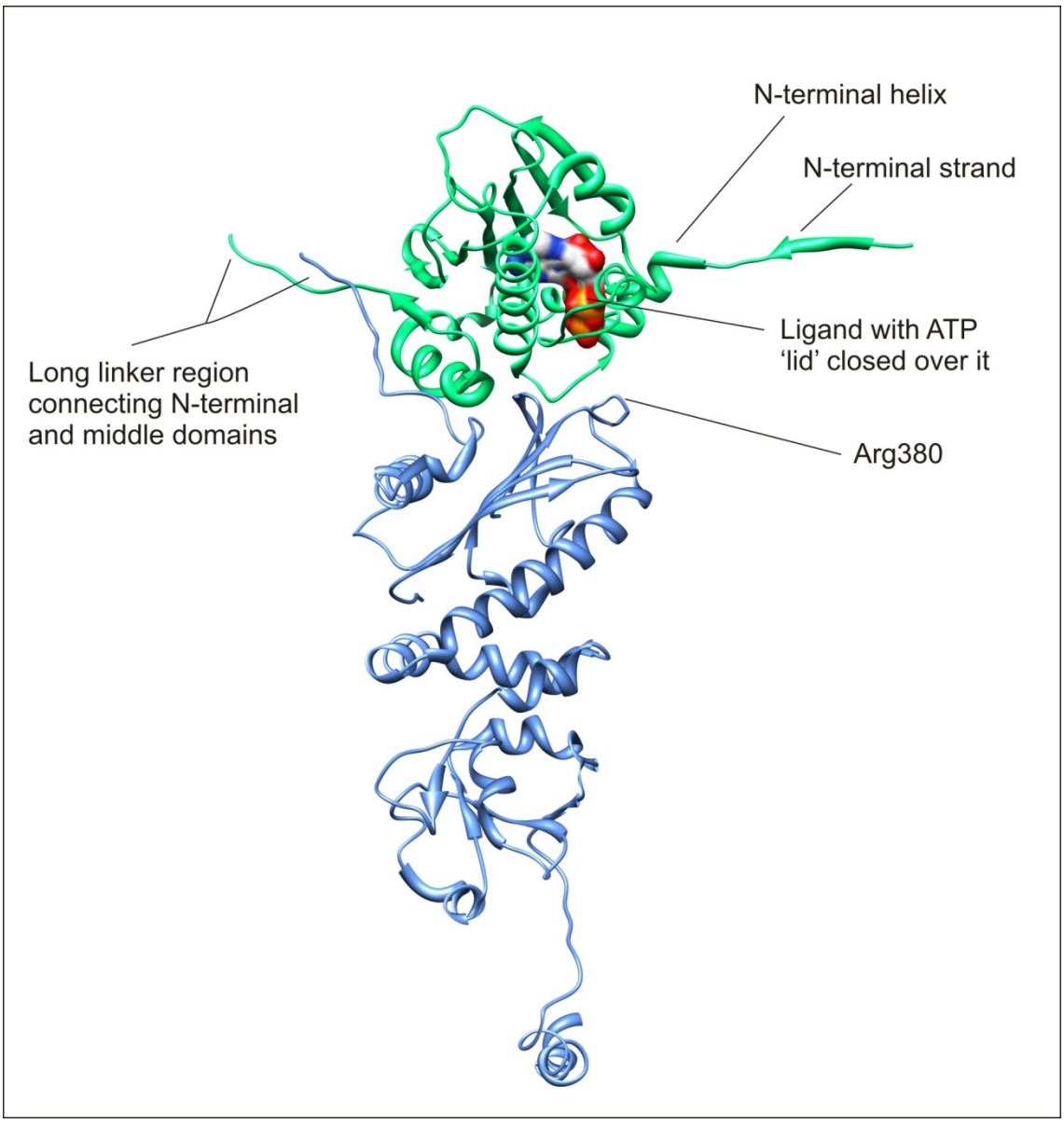

Figure 5.1 The N551 construct illustrated from the full length crystal resolved by Ali et al. [7] The N-terminal domain is shown in green while the middle domain is shown in blue. Key features are labelled. Diagram taken from PDB file 2CG9.

The N551 construct is 50kDa in size and is thus at the limit of what is possible to study by conventional NMR techniques. As the protein being studied increases in size, the rate of tumbling decreases leading to significant peak broadening. This peak broadening leads to a decrease in achievable resolution in the data and of signal intensity. These losses of signal and resolution makes the study of large proteins far harder by solution state NMR than that of smaller ones.

Within this chapter the thermodynamics of the N551 construct were studied using ITC under ADP, AMPPNP and adenosine bound conditions. The ΔC_p was recorded across a temperature range of 10 – 25°C. The thermodynamics was then compared to the isolated N-

terminal domain of Hsp90. Thermodynamic analysis of the full-length Hsp90 chaperone was also undertaken by ITC under ADP, AMPPNP and adenosine bound conditions. The ΔC_p was recorded across a temperature range of 10 – 25°C.

Due to the high expression of the N551 construct and subsequently high yields of pure protein, the use of TROSY NMR was possible. This allowed optimisation of sample preparation conditions and a comparison of the different ligand bound states of the N551 construct. The N-terminal domain spectra overlaid well with the N551 spectra and this allowed exploitation of the N-terminal backbone assignments to look at the N-terminal domain peaks identified within the N551 construct, and associated shifts induced by ligand binding.

5.2 The thermodynamics of binding of ADP, AMPPNP and adenosine to N551 show marked differences from those of binding to the N-terminal domain

Titrations were undertaken between the N551 construct of Hsp90 and the ligands ADP, AMPPNP and adenosine in 20 mM Tris at pH8 across a temperature range from 10°C – 25°C. Protein concentration was 50μM in the cell with ligand concentrations of 1 mM for ADP, 1.5 mM for AMPPNP and 1.5 mM for adenosine in the syringe.

Protein: N551		**Ligand:** ADP		**pH:** 8	**ΔC_p:** -1.52 kJ mol^{-1} K^{-1}		
Temp (C)	Stoichiometry (N)	K_d (µM)	Error (µM)	ΔH (KJ mol-1)	Error (+/-)	TΔS (kJ mol-1)	ΔG (kJ mol-1)
10	1.02 ± 0.01	4.03	±0.19	-93.93	±0.76	-64.61	-29.32
10	1.01 ± 0.01	5.62	± 0.63	-76.65	± 1.78	-48.19	-28.46
15	1.05 ± 0.01	6.92	±0.23	-96.69	±0.69	-68.15	-28.54
15	1.09 ± 0.01	5.26	± 0.31	-75.19	± 0.86	-46.04	-29.14
20	1.01 ± 0.01	10.46	±0.34	-97.027	±0.82	-69.08	-27.95
20	1.04 ± 0.03	13.12	± 1.40	-90.00	± 3.20	-62.55	-27.44
25	1.06 ± 0.01	23.11	±0.64	-122.56	±1.44	-95.77	-26.49
25	1.06 ± 0.05	27.70	± 3.42	-103.60	±6.79	-77.59	-26.00

Table 5.1 Summary of binding data for the ITC experiments of ADP binding to the N551 construct of Hsp90. Titrations undertaken in 20 mM Tris, 5 mM Mg^{2+}, pH 8.

From Table 5.1 it is clear to see that the temperature-dependence of binding of ADP to the N551 construct shows a similar trend to that of the N-terminal domain of Hsp90. The K_d increases with temperature, with weaker binding arising from a more favourable enthalpy change at higher temperature outweighed by a less favourable entropy change. In comparison to the N-terminal domain binding parameters however, it is clear to see that the K_d is smaller in the presence of the middle domain than in its absence. The difference at low temperatures is around a factor of two (4.03μM compared to 8.76μM); however, as temperature increases the difference does as well until at 25°C there is a factor of four (27.7μM compared to 115.75μM) separating the binding affinities of the two constructs of Hsp90.

Protein: N551 **Ligand:** AMPPNP **pH:** 8 **ΔC_p:** -0.28 kJ mol^{-1} K^{-1}							
Temp (C)	Stoichiometry (N)	K_d (μM)	Error (μM)	ΔH (KJ mol-1)	Error (+/-)	TΔS (kJ mol-1)	ΔG (kJ mol-1)
10	0.93 ± 0.02	45.05	±1.83	-44.60	1.07	-20.22	-23.56
15	1.05 ± 0.02	70.42	±2.67	-45.44	1.25	-22.55	-22.91
20	1.07 ± 0.03	110.0	±4.65	-46.11	1.64	-23.67	-22.22
25	1.11 ± 0.04	121.36	±5.55	-41.00	1.91	-18.59	-22.35
30	0.96 ± 0.09	181.00	±11.53	-53.848	5.96	-32.14	-21.71

Table 5.2 Summary of binding data for the ITC experiments of AMPPNP binding to the N551 construct of Hsp90. 20 mM Tris, 5 mM Mg2+, pH 8.

It is found that the binding constants for AMPPNP when bound to the N551 construct of Hsp90 shows marginally smaller binding than the same ligand binding to the N-terminal domain of Hsp90 alone (Table 5.2). The difference between the two affinities is only 10μM, but within the same order of magnitude, at both 10°C and 20°C with a consistently more favourable enthalpy values by around 10kJ mol^{-1} and a consistently more favourable entropy value of around -10kJ mol^{-1} K^{-1} at each temperature.

Protein: N551 **Ligand:** Adenosine **pH:** 8 **ΔC_p:** -9.70 kJ mol^{-1} K^{-1}							
Temp (C)	Stoichiometry (N)	K_d (μM)	Error (μM)	ΔH (KJ mol-1)	Error (+/-)	TΔS (kJ mol-1)	ΔG (kJ mol-1)
10	1.06 ± 0.12	68.82	±3.81	-55.16	7.11	-35.58	-22.58
15	1.01 ± 019	108.89	±4.95	-87.11	17.06	-65.26	-21.85
20	1.00 ± 0.35	154.82	±6.02	-155.14	55.52	-133.69	-21.45

Table 5.3 Summary of binding data for the ITC experiments of adenosine binding to the N551 construct of Hsp90. 20 mM Tris, 5 mM Mg2+, pH 8.

It can be seen that the binding affinity for adenosine binding to the N551 construct is comparable to that for the N-terminal domain at 10 and 15°C temperatures (Table 5.3). As the temperature was increased to 20°C the binding affinity increased with both constructs.

However, binding to the N551 construct was higher than to the N-terminal domain alone. The change in entropy shows similar values between binding to the N-terminal domain and the N551 construct at 10°C. As temperature increases, both constructs show an increasingly negative change in enthalpy term; however, the binding of adenosine to N551 is significantly more enthalpically favourable than binding to the N-terminal domain at the same temperature.

Figure 5.2 shows a comparison of the thermodynamic parameters of binding for the N-terminal to all ligands (top) compared to the N551 construct (bottom) at 15°C. From this figure it is very clear to see that the presence of the middle domain changes the enthalpy/entropy profiles of adenosine and AMPPNP the most with less influence over the binding of ADP. Adenosine shows an increase in magnitude of both entropy and enthalpy but also a difference in their proportions leading to less difference between the two values. AMPPNP binding shows an increase in the entropy with respect to the enthalpy leaving a similar Gibbs free energy overall in comparison to the N-terminal domain.

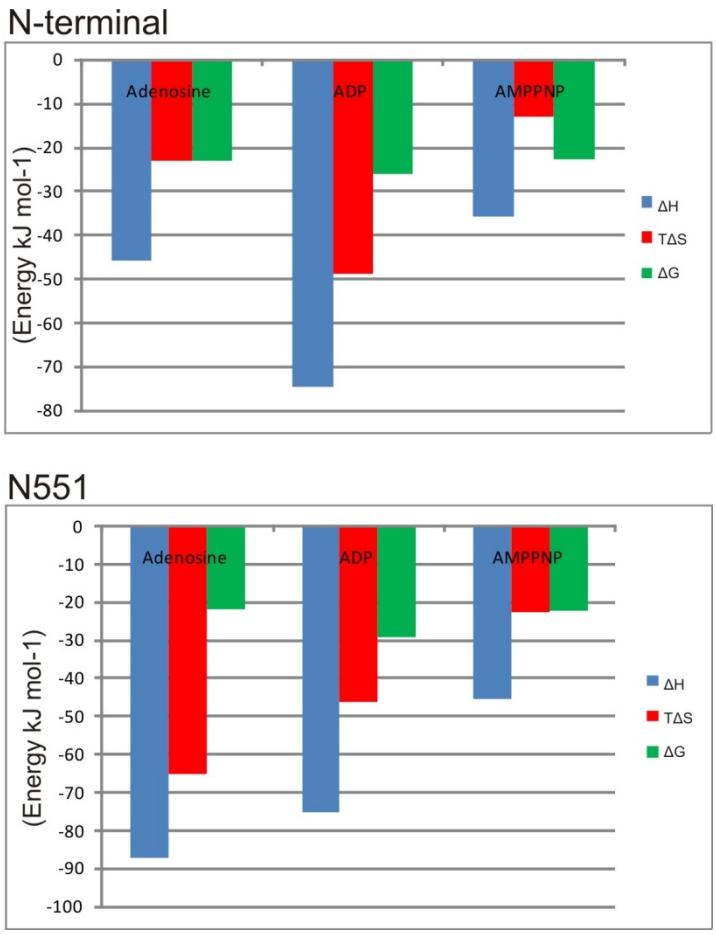

Figure 5.2 Comparison of the ΔH, TΔS and ΔG values for the N-terminal domain under adenosine, ADP and AMPPNP bound conditions against the N551 construct bound to the same ligands. 20 mM Tris, 5 mM Mg2+, pH 8, 15°C.

The heat capacities of binding of ADP, AMPPNP and adenosine to the N551 construct:

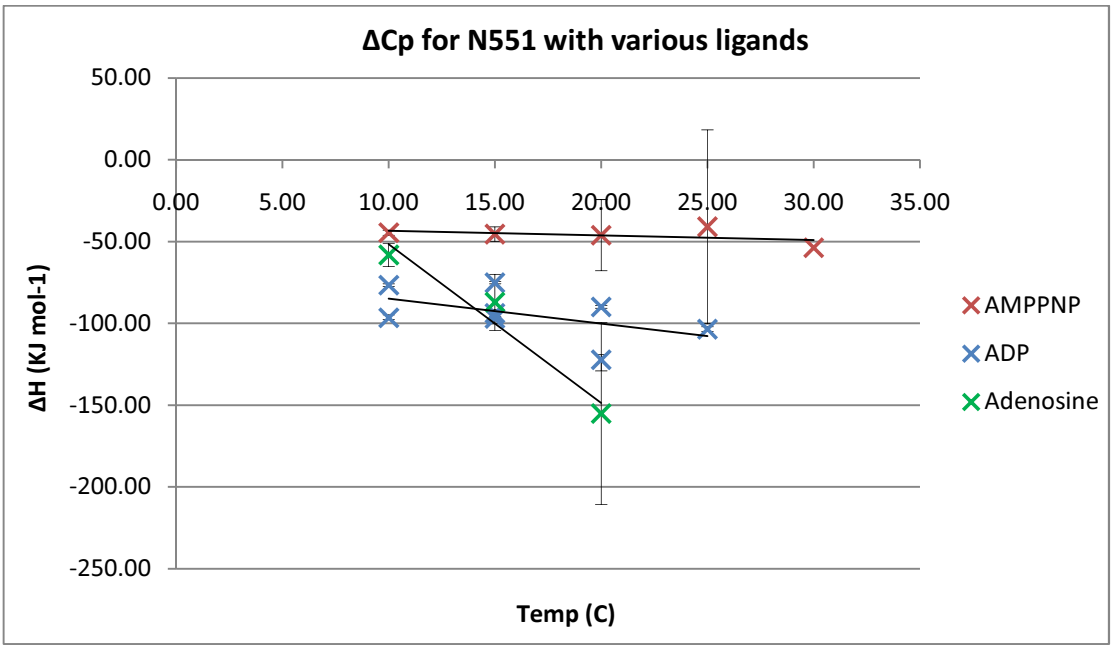

Figure 5.3 ΔC_p plot of ADP, AMPPNP and adenine binding to the N551 construct of Hsp90. 20 mM Tris, 5 mM Mg2+, pH 8.

Figure 5.3 shows the plots used to determine the ΔC_p values. A comparison of the heat capacity data for the N-terminal domain of Hsp90 and the N551 construct yields the following results shown in Table 5.4.

Ligand	N-terminal domain (J mol^{-1} K^{-1})	N551 construct (J mol^{-1} K^{-1})
AMPPNP	+286	-280 ±60
ADP	-900	-1500 ±140
Adenosine	+600	-9700 ±2700

Table 5.4 Comparison of the ΔC_p values calculated for various ligands binding to the N-terminal domain of Hsp90 compared to the N551 construct as determined by ITC at pH 8 in 20 mM Tris, 5 mM Mg^{2+}.

From Table 5.4 it is clear that there are some significant differences between the ΔC_p values determined for the same ligand with the different protein constructs. In the case of ADP, the result is an increase in magnitude of the ΔC_p with the N551 construct compared to the N-terminal domain; however, both ΔC_p values are negative. In the case of the ligands AMPPNP and adenosine there is a change in sign between the ΔC_p values determined for the N551 construct compared to the N-terminal domain from positive to strongly negative. The implications of this will be discussed later.

5.3 The binding of ADP, AMPPNP, adenosine and adenine to the full length Hsp90 molecular chaperone molecule

ITC titrations between the full length Hsp90 molecular chaperone and the ligands ADP, AMPPNP, adenosine and adenine were undertaken across the temperature range 10 – 25°C. An initial concentration of 30μM protein in the calorimeter cell was used in each case. The ligands were used at the following initial concentrations in the syringe: ADP at 1 mM, AMPPNP at 1.5 mM, adenosine at 1.5 mM and adenine at 1.5 mM. Using the full length protein the chaperone is assumed to form a dimer via the C-terminal domain. The presence of a stoichiometry of 1 in all experiments suggests that the binding to the two N-terminal domains of the dimer is sufficiently independent and that the ligand can bind as easily to one as to the other.

Protein: Hsp90		**Ligand:** ADP		**pH:** 8		**ΔC_p:** -1.53 kJ mol^{-1} K^{-1}		
Temp (C)	Stoichiometry (N)	error	K_d (μM)	Error (μM)	ΔH (KJ mol-1)	Error (+/-)	TΔS (kJ mol-1)	ΔG
10	1.05	0.01	1.75	±0.12	-78.58	1.25	-47.39	-31.19
15	1.07	0.01	4.13	±0.22	-85.10	1.07	-55.46	-29.64
20	1.1	0.02	6.49	±0.41	-87.86	1.65	-58.75	-29.13
25	1.04	0.07	13.25	±1.27	-116.27	10.21	-88.32	-27.95
30	1.04	0.05	15.20	±1.05	-101.17	6.28	-73.19	-27.98

Table 5.5 Summary of binding data for the ITC experiments of ADP binding to the full length Hsp90 molecular chaperone molecule. 20 mM Tris, 5 mM Mg2+, pH 8.

The binding of ADP to the full length Hsp90 molecule shows no increase of binding affinity compared to the N551 construct (Table 5.6). Again it has four times the affinity as for the N-terminal domain alone. Both enthalpy and entropy terms for the binding of ADP to the full length molecule are more negative than binding to the N-terminal domain of Hsp90 or the N551 construct suggesting that perhaps the addition of the C-terminal domain has an effect on ligand binding thermodynamics. However, the increased complexity of the system, taking into account the high flexibility of the chaperone dimer and therefore the increased number of degrees of freedom of the protein, may account for this.

Protein: Hsp90 **Ligand:** AMPPNP **pH:** 8								
Temp (C)	Stoichiometry (N)	error	K_d (μM)	Error (μM)	ΔH (KJ mol-1)	Error (+/-)	TΔS (kJ mol-1)	ΔG
10	1.02	0.27	67.52	±11.76	-55.69	17.64	-33.09	-22.60
15	1.01	3.15	160.26	±63.45	-196.82	648.94	-176.02	-20.80
20	1.04	0.96	144.93	±111.95	-38.96	48.74	-17.42	-21.54

Table 5.6 Summary of binding data for the ITC experiments of AMPPNP binding to the full length Hsp90 molecular chaperone molecule. 20 mM Tris, 5 mM Mg2+, pH 8.

The binding of AMPPNP to the full length Hsp90 molecule shows a slightly lower affinity than the N551 construct (Table 5.7); however, the affinity is still stronger than for the N-terminal domain alone. The low heats obtained for the ITC experiments and the limited supply of full length protein have led to the large errors in the calculated K_d values at higher temperatures and so an accurate ΔC_p cannot be determined. The ΔH and TΔS terms are both more negative in the full length protein than in the N551 construct. This is, however, to be expected with the increased size of the protein and the large degree of flexibility associated with the chaperone molecule. It should be noted again, the large error at higher temperatures does not allow accurate analysis of the enthalpic and entropic contributions.

Protein: Hsp90 **Ligand:** Adenosine **pH:** 8								
Temp (C)	Stoichiometry (N)	error	K_d (μM)	Error (μM)	ΔH (KJ mol-1)	Error (+/-)	TΔS (kJ mol-1)	ΔG
10	1.07	0.48	71.94	±6.49	-141.38	66.40	-118.94	-22.43
15	1.02	0.11	58.69	±3.62	-43.39	5.19	-20.03	-23.36

Table 5.7 Summary of binding data for the ITC experiments of adenosine binding to the full length Hsp90 molecular chaperone molecule. 20 mM Tris, 5 mM Mg2+, pH 8.

The measurement of the binding of adenosine to the full length Hsp90 molecule was made more difficult by the small heats involved and could only be determined at low temperatures (Table 5.8). From this we can see that the presence of the full length molecule leads to no change in binding affinity at 10°C; however, the binding affinity is increased by a factor of two from 108 μM to 58 μM at 15°C. At 10°C the ΔH and TΔS values are more negative compared to the N551 construct while at 15°C, less negative ΔH and TΔS values are observed. The high error associated with the ΔH and TΔS values at 10°C do not allow for much analysis of the thermodynamic parameters. The smaller error at 15°C perhaps suggests a more reliable set of figures and suggests that in the presence of adenosine, the full length chaperone shows less negative ΔH and TΔS values than with the N551 construct.

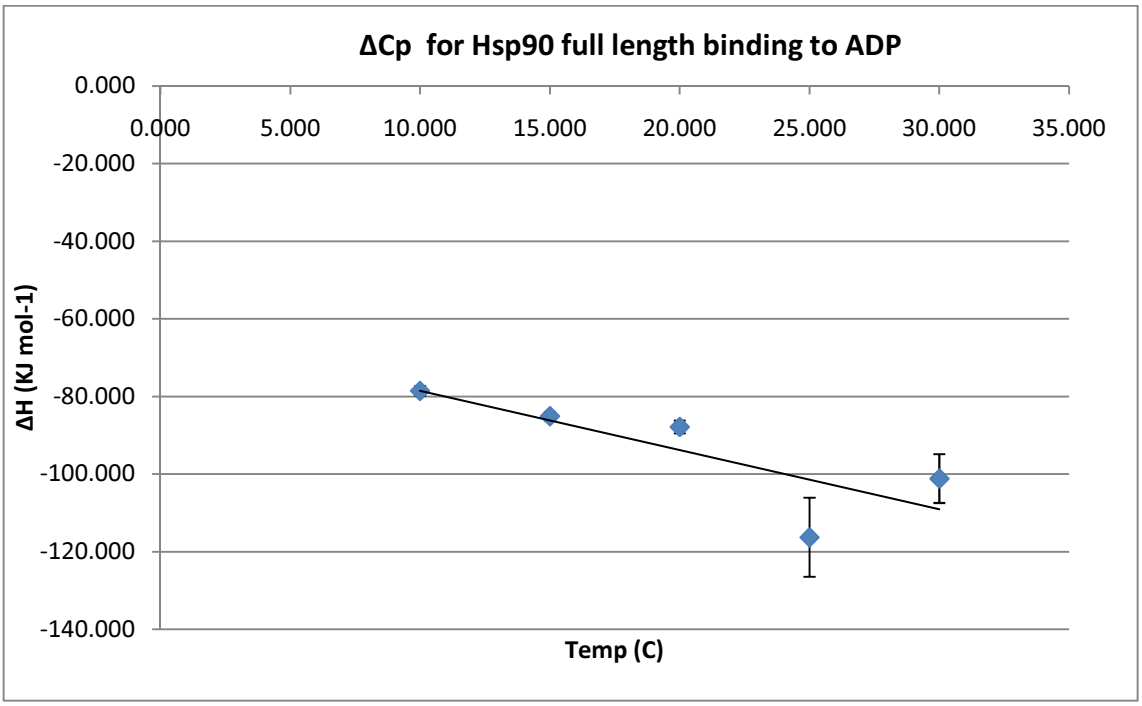

Figure 5.4 ΔC_p plot of ADP binding to the full length Hsp90 molecular chaperone. 20 mM Tris, 5 mM Mg2+ pH 8.

The ΔC_p value for ADP binding to the full length Hsp90 molecule, -1.53 $kJ \cdot mol^{-1} \cdot K^{-1}$, is very similar to that determined for the N551 construct (Figure 5.4). This suggests that the addition of the C-terminal domain of Hsp90 does not lead to any significant changes in the change in exposed surface area that occur on binding nucleotide, and that the difference between the ΔC_p values for the full length protein and the N-terminal domain alone are due to the middle domain and its interactions with the N-terminal domain.

5.4 NMR of the N551 construct of Hsp90

TROSY spectra were collected of the N551 construct at a concentration of 150 µM. Perdeuteration of the sample was required to minimise noise within the spectrum and reduce relaxation through non-amide protons. Surprisingly good spectra were obtained with good peak dispersion suggesting that the two domains were tumbling somewhat independently rather than as one large unit. This is shown in Figure 5.5A.

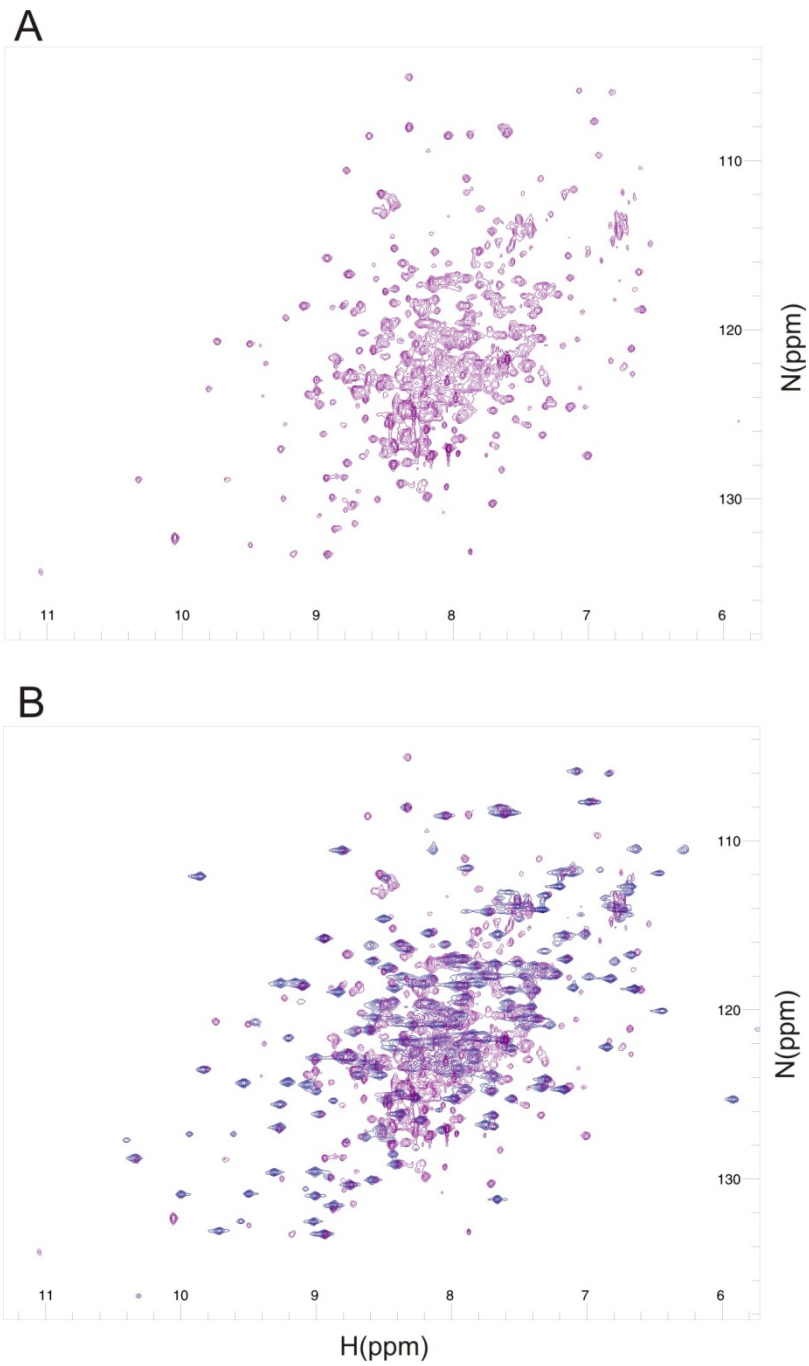

Figure 5.5 A: ^{15}N-TROSY spectra of the apo N551 construct of Hsp90 (purple). 50 mM Tris 50 mM NaCl pH 7.5 25°C 800 MHz. B: ^{15}N-TROSY spectra of the apo N551 construct of Hsp90 overlayed with the ^{15}N-HSQC spectra of the N-terminal domain of Hsp90 (blue).

A comparison of the N551 spectrum with that of the N-terminal domain reveals that many of the N551 peaks overlay exactly and others are sufficiently close to identify as having undergone a small chemical shift (Figure 5.5B). The closeness of the match suggests that the presence of the middle domain has minimal influence over the gross conformation of the N-terminal domain in the apo-state, but does have a subtle effect. The presence of the long flexible loop connecting the N-terminal and middle domains would allow each domain the possibility of independent movement. This distance between the two large globular domains

could allow each one to tumble in an independent fashion, thus reducing the peak broadening effects caused by the increased size of the protein.

5.4.1 Comparison of the N551 domain and the N-terminal domain of Hsp90 and identification of peak shifts

The overlay of the chemical shift changes of the N-terminal domain with the N551 construct mapped onto the crystal structures of the N551 construct (Ali et al.[7]) as seen in Figure 5.6 shows that although the spectrum for the N-terminal domain overlays well, there are some resonances that show a chemical shift change in response to the addition of the middle domain. These shifts were identified using the existing backbone assignments for the N-terminal domain. Shifts within the central region of the spectrum were not considered as they overlapped too much, with resonances arising from the middle domain and are thus impossible to identify unambiguously. The presence of a small number of strong peaks in this central region in all bound states in the mutant protein, suggests the formation of some unstructured regions however the exact nature and identity of this possible local unfolding is not clear.

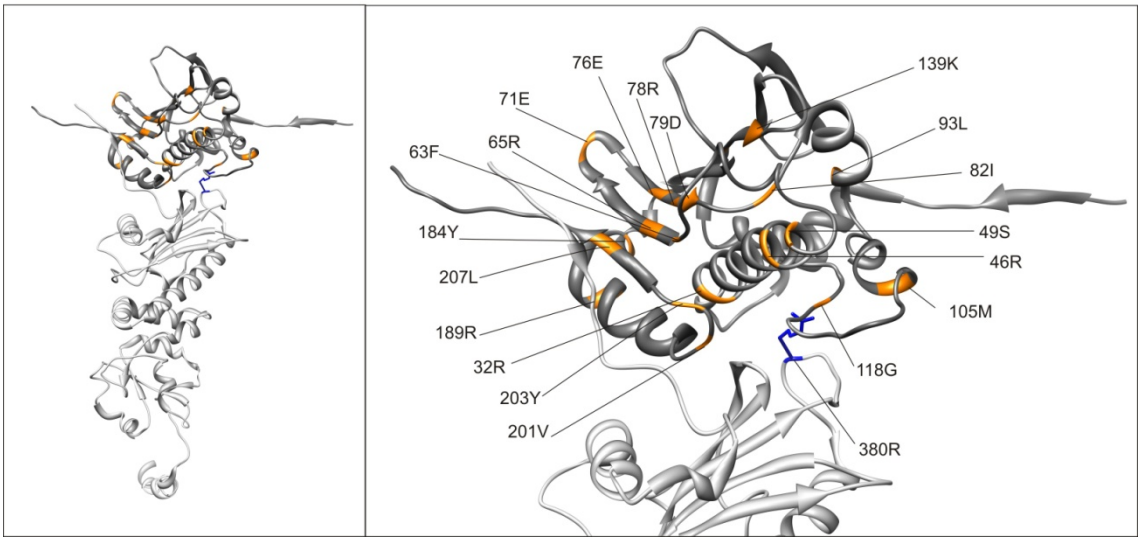

Figure 5.6 Residues in the N-terminal domain of apo-state N551 construct which show different chemical shifts compared to the isolated apo N-terminal domain. Residues showing a chemical shift change are shown in orange. The N-terminal domain of the N551 construct is shown in dark grey. The middle domain of the N551 construct is shown in light grey. An expanded view is shown and labelled in the right hand panel. The catalytic residue (Arg380) from the catalytic loop of the middle domain is shown in blue for reference. Diagram taken from PDB file 2CG9.

From Figure 5.6 it is clear that the shifts can be divided into two categories. The first includes residues Arg32, Arg46, Ser49, Met105, Gly118, Val201 and Tyr203. These shifts are all

close to the interface between the N-terminal and middle domains, suggesting that the two domains do interact, at least transiently, with one another in the apo state. A transient association is suggested on the basis that permanent association would lead to significant peak broadening in the NMR spectra recorded that was not observed. The second set of shifts includes residues Phe63, Arg65, Glu71, Glu76, Arg78, Asp79, Ile82, Leu93, Lys139, Tyr 184 and Leu207. These shifts all map either to the back β-sheet of the binding pocket or to the far end of the long helix close to the binding pocket. These regions are not in direct contact with the middle domain suggesting that the association at the known domain interface leads to a series of small structural changes within the binding pocket.

5.4.2 Comparison of the N551 domain and the N-terminal domain of Hsp90 and identification of peak shifts in the AMPPNP bound state

A TROSY spectrum was recorded of the N551 construct bound to AMPPNP (Figure 5.7). A comparison to the N-terminal spectrum bound to AMPPNP was undertaken.

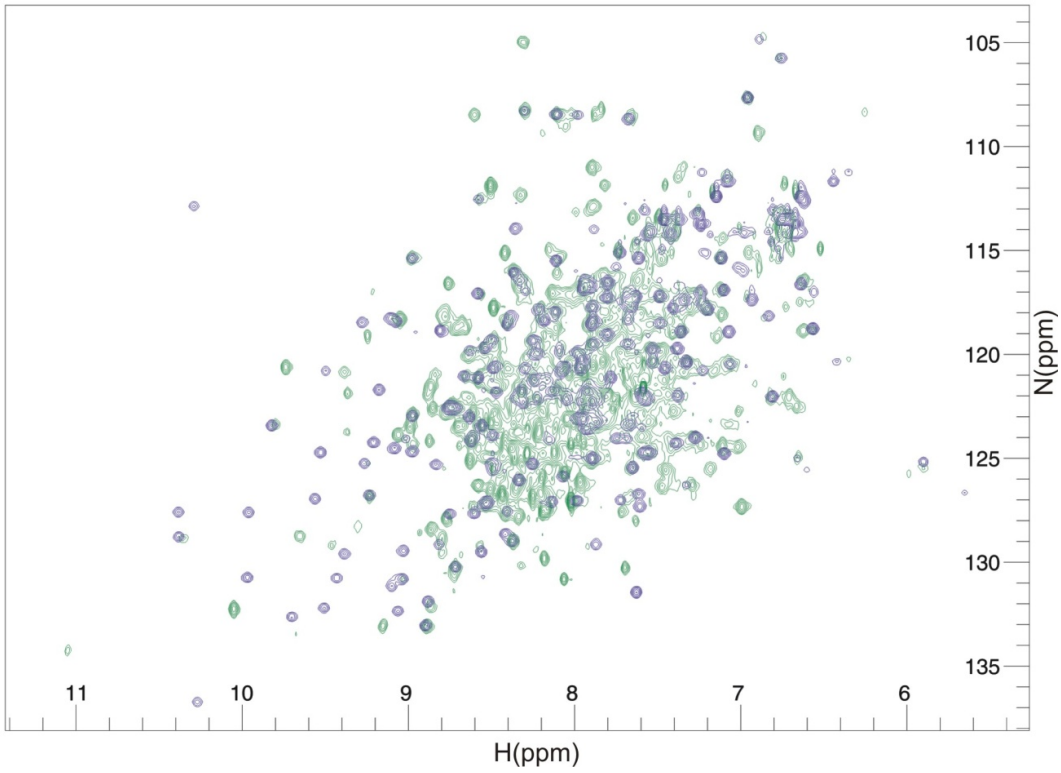

Figure 5.7 ^{15}N-TROSY spectrum of the N551 construct bound to AMPPNP (green) overlaid with a ^{15}N-HSQC spectrum of the N-terminal domain alone bound to AMPPNP (blue). ^{15}N-TROSY recorded in 50 mM Tris, 50 mM NaCl, 5 mM $MgCl^{2+}$ at pH 7.5, 700 MHz.

Shifts were identified where the N-terminal domain spectrum differed from the N551 spectrum and these were plotted onto the crystal structure (Figure 5.8).

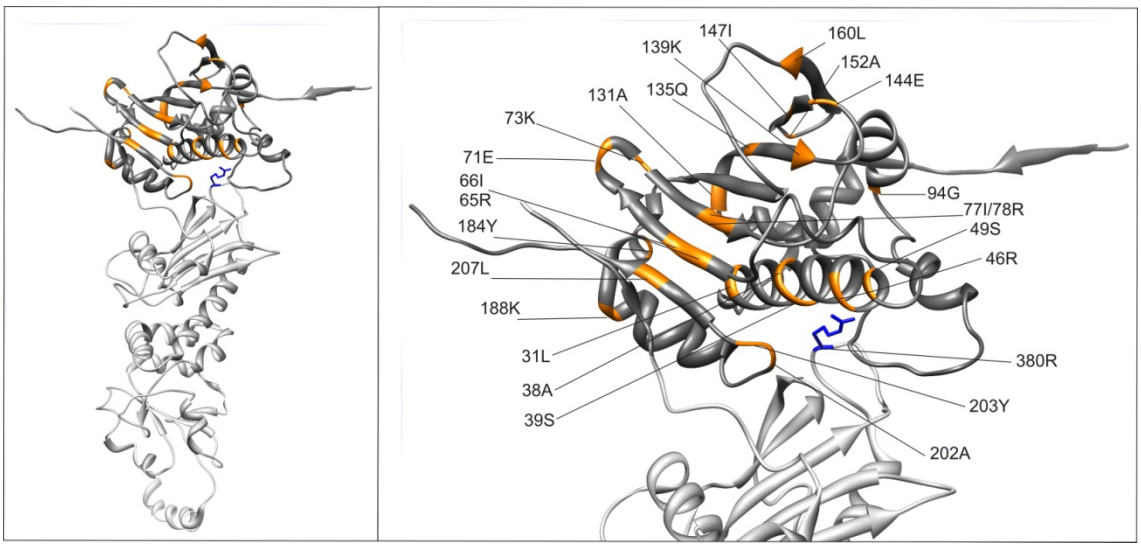

Figure 5.8 Shifts in residues in the N-terminal domain of the N551 construct compared to the isolated N-terminal domain in the AMPPNP bound state. Residues with a chemical shift change are shown in orange. The N-terminal domain of the N551 construct is shown in dark grey. The middle domain of the N551 construct is shown in light grey. An expanded view is shown and labelled in the right hand panel. Catalytic residue Arg380 from the catalytic loop of the middle domain is shown in blue for reference. Diagram taken from the PDB file 2CG9.

The chemical shift differences observed for the N551 construct compared to the N-terminal domain of Hsp90, both in the AMPPNP-bound state, revealed a similar pattern to that observed for the apo state. The presence of peak shifts at the domain interface suggests that the two domains, at least transiently, associate with one another as the peak broadening does not suggest a permanent association. More residues were significantly shifted in the AMPPNP-bound state than for the apo state but these shifts mostly mapped to the same regions observed before. Leu160, Ala152 and Gln144 show shifts in a region previously undisturbed at the far end of the β-sheet indicating some link to the binding of AMPPNP. It has already been noted that the presence of the middle domain has an influence over the β-sheet (Figure 5.8) and as this region is at the top of the β-sheet and close to the edge of the binding pocket. A different response to ligand binding than that seen in the N-terminal domain alone is not unreasonable and may indicate an explanation for the increased binding affinity observed for AMPPNP binding to the N551 construct compared to the N-terminal domain alone.

5.4.3 Comparison of the N551 domain and the N-terminal domain of Hsp90 and identification of peak shifts in the ADP bound state

A TROSY spectrum was recorded of the N551 construct bound to ADP (Figure 5.9). A comparison to the N-terminal spectrum bound to ADP was undertaken.

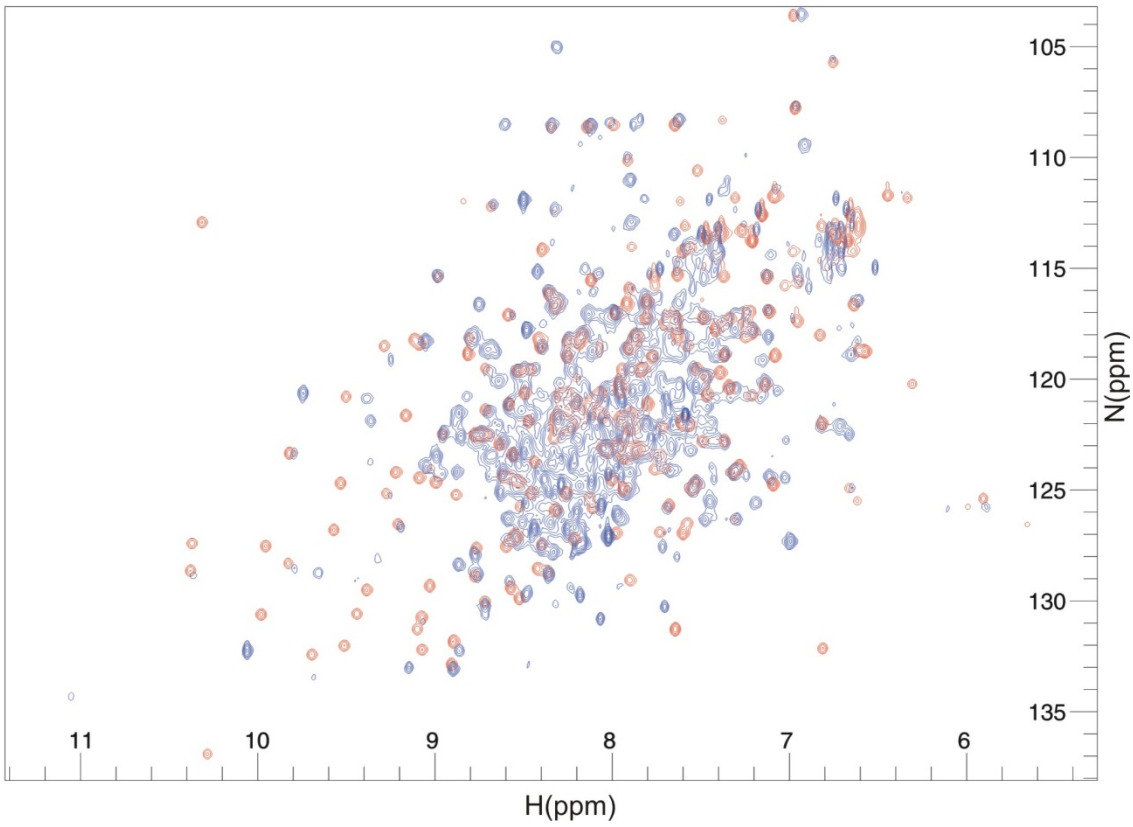

Figure 5.9 ^{15}N-TROSY spectrum of the N551 construct bound to ADP (blue) overlaid with an HSQC spectrum of the N-terminal domain alone bound to ADP (red). ^{15}N-TROSY recorded in 50 mM Tris, 50 mM NaCl, 5 mM $MgCl^{2+}$ at pH 7.5, 700MHz.

Shifts were identified where the N-terminal domain spectrum differed from the N551 spectrum and these were plotted onto the crystal structure (Figure 5.10).

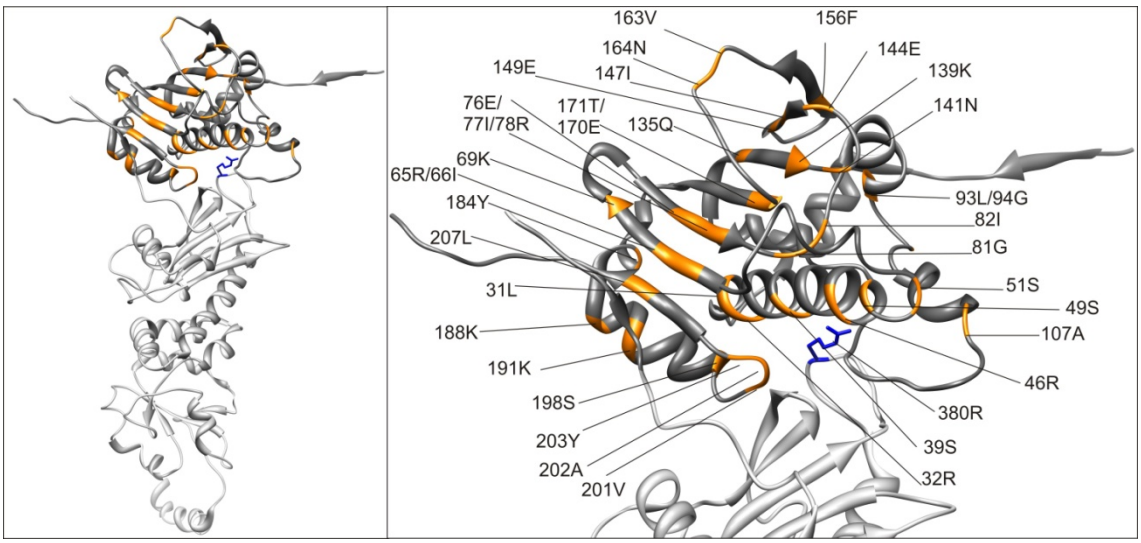

Figure 5.10 Shifts in residues in the N-terminal domain of the N551 construct compared to the isolated N-terminal domain in the ADP bound state. Residues with a chemical shift change are shown in orange. The N-terminal domain of the N551 construct is shown in dark grey. The middle domain of the N551 construct is shown in light grey. An expanded view is shown and labelled in the right hand panel. Catalytic residue Arg380 from the catalytic loop of the middle domain is shown in blue for reference. Diagram taken from PDB file 2CG9.

From the plotted data it can be seen that there is far more variation between the two constructs in the ADP bound state than was evident in the apo state. Once more the peak shifts mostly map to two distinct regions; the interface with the middle domain and the β-sheet at the back of the binding pocket. Again the presence of peak shifts at the domain interface suggests that the two domains, are transiently associated with one another as the peak broadening does not suggest a permanent association. There are, however, more shifts in the β-sheet and along the long helix that flanks the binding site than were observed for the N551 construct in the apo state. The ADP bound state shows more shifts overall than in the AMPPNP bound state with slightly more shifts located in the β-sheet and long α-helix. The exception to this peak distribution pattern is a small number of shifts seen in the loop regions that connect the β strands together to form the sheet, such as Gly81, Ile82, Asn141, Gln144, Phe156, Val163 and Asn164.

The pattern of peak shifts when N551 is bound to ADP suggests that the presence of the middle domain influences the way ADP binds to the N-terminal domain. The ITC has already shown that ligand binding is enhanced by the presence of the middle domain. The chemical shifts observed indicate that binding enhancement involves small conformational changes across the binding site within the N-terminal domain and are not limited to the N-terminal domain/ middle domain interface. The presence of shifts across the back of the binding pocket in the β-sheet may suggest that this region is important for the strong binding

of ligand and that the presence of the middle domain may help in orientating the β-sheet correctly.

5.4.4 Missing peaks are observed when the N551 domain spectra are compared to the N-terminal domain spectra

An overlay of the spectra for the N551 construct and N-terminal domain reveals that some peaks are missing in the spectrum for the N551 construct when compared to the spectrum for the N-terminal domain (Figure 5.11) such as Asn21, Gly81, Val74, Ser138, Asn141, Ile172, Leu173 and Arg174. The perdeuteration of the protein, necessary for increased resolution as previously mentioned, requires that backbone amide deuterium atoms exchange with protons within the buffer prior to recording the TROSY spectrum. Incomplete back exchange of the backbone amide protons would lead to those residues not being detected on the TROSY spectrum. Incomplete back-exchange can arise from increased protection of the amide proton, either through its location in the centre of a globular domain, or through its involvement in secondary structural elements that provide protection via the formation of hydrogen bonds, such as in stable α-helices or β-sheets.

In order to recover these backbone TROSY peaks the protections of the amide deuterons must be relaxed either by allowing solvent access to the centre of the globular domain or by disrupting the secondary structural elements. This can be achieved by partial unfolding of the protein to disrupt the overall tertiary structure and the secondary structural elements that were previously protecting the amide/proton bond and allowing proton/deuteron exchange.

Partial unfolding can be achieved by dialysis into a high concentration of guanidinium chloride (GndCl), a known denaturing agent, followed by dialysis back into a suitable refolding buffer with no GndCl present. The process of fully unfolding and refolding a protein can be detrimental to the final folded protein structure; however, the more complete the unfolding the more complete the proton back exchange can be.

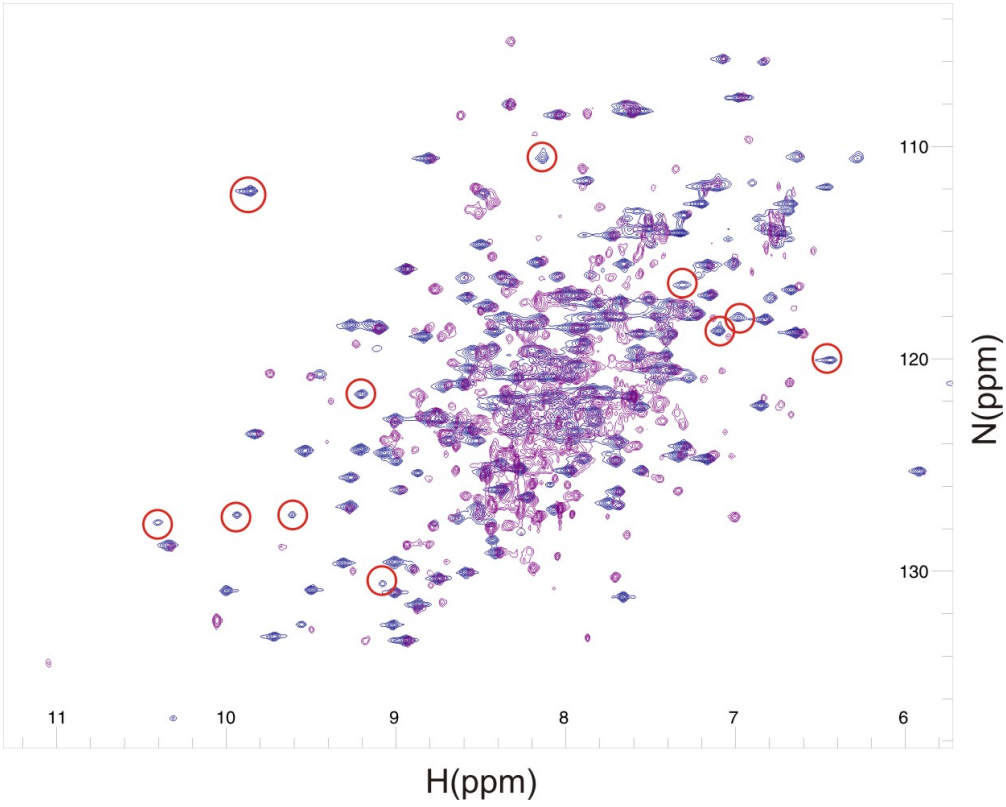

Figure 5.11 The apo ^{15}N-TROSY spectrum for the N551 construct (purple) overlaid with an ^{15}N-HSQC spectra of the N-terminal domain alone in the apo state (blue). Note some peaks present in the N-terminal spectrum but not in the N551 spectrum circled in red. Spectra recorded in 20 mM Tris, 5 mM Mg^{2+} pH 8, 700MHz.

Protein folding was monitored by circular dichroism (CD) spectroscopy to monitor the presence of α-helical and β-sheet content in the native folded state, a partially unfolded state in the presence of different concentrations of guanidinium chloride and the refolded state after dialysis out of various concentrations of guanidinium chloride.

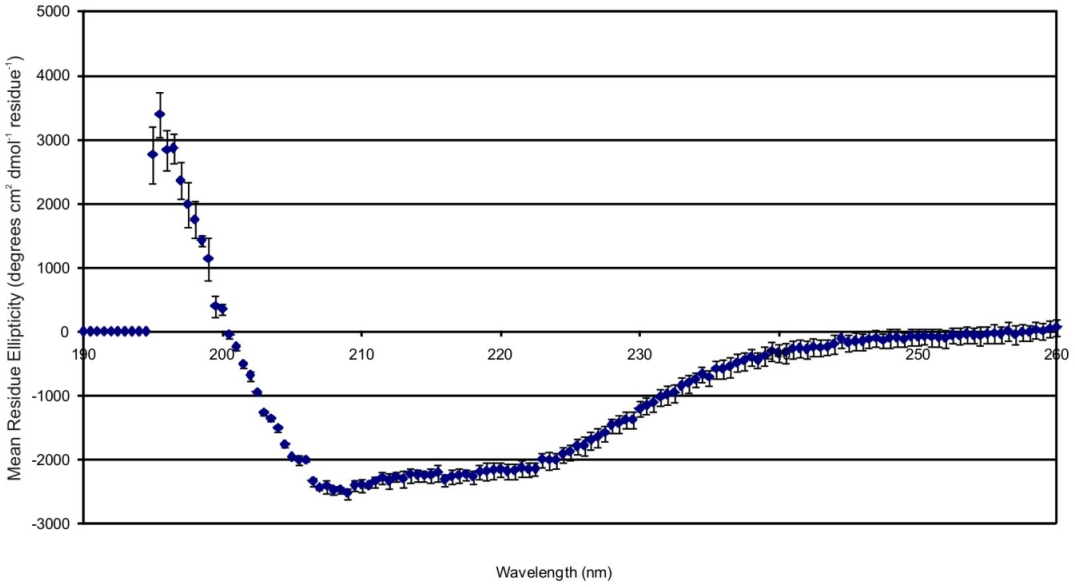

Figure 5.12 CD spectroscopy trace of the N551 construct of Hsp90 at 25°C. Data recorded from 260 – 195 nm every half nm.

From Figure 5.12 we can see the distinctive double trough trace with minima at 208nm and 222nm characteristic of a protein containing α-helical content. The shallow transition, as opposed to a local maximum between the troughs, is within the region where a minimum caused by β-sheet content would be expected (216nm). Thus the average signal contributed by both α-helical and β-sheet structures leads to a shallow transition between the two minima as is observed. Immediately following purification, and therefore at 0mM GndCl, the protein is fully folded.

Dialysis overnight of the N551 construct into 1M or 2M GndCl was undertaken in order to partially unfold the protein. Partial protein unfolding was confirmed by CD as show in Figure 5.13A and 5.14 A. Full unfolding in 4M GndCl was tried but caused protein precipitation when refolding was attempted.

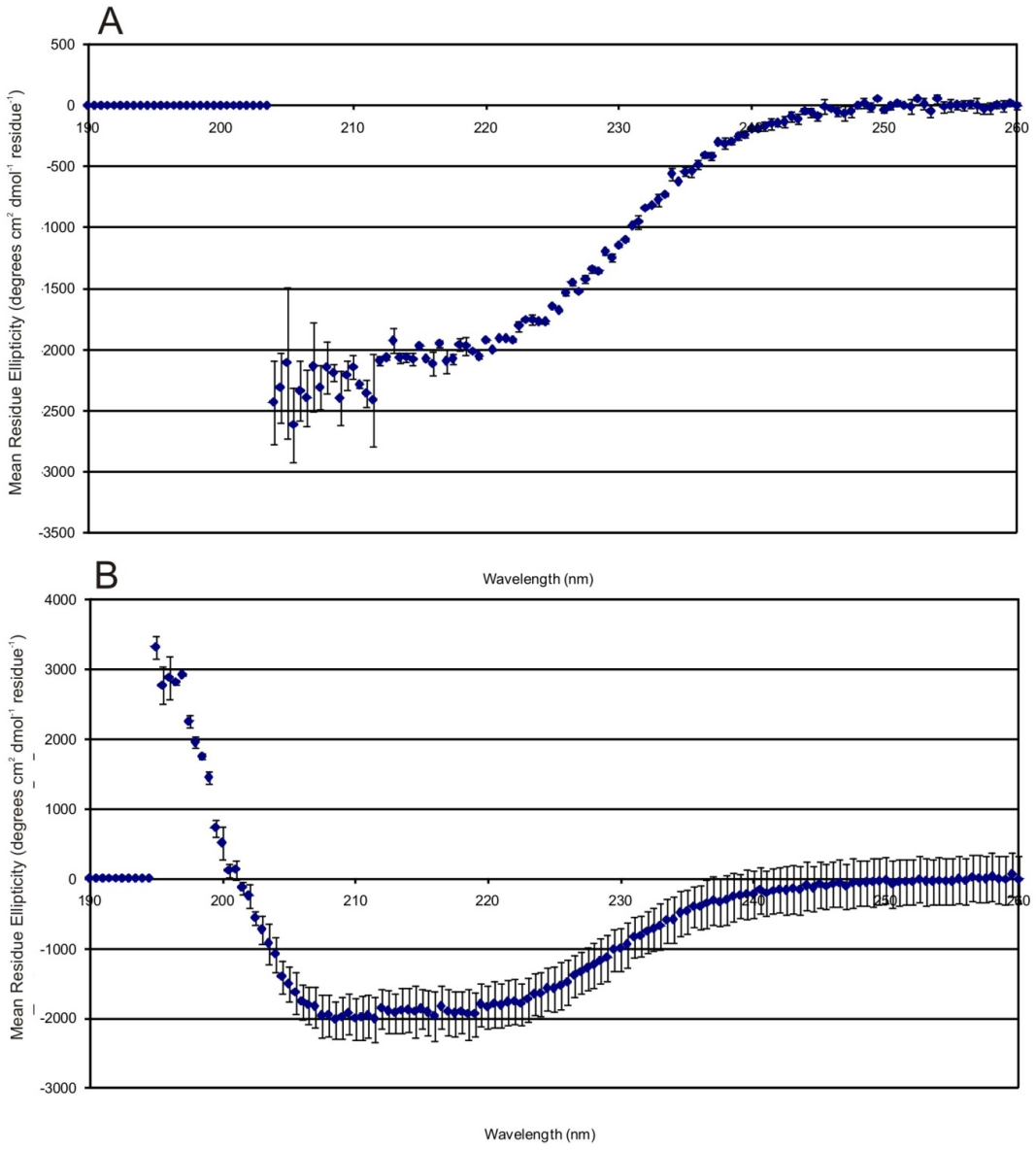

Figure 5.13 CD spectroscopy trace of the N551 construct of Hsp90 at 25°C. Data recorded from 260 – 195 nm every half nm. A. Trace recorded in the presence of 1M GndCl. B. Trace recorded after removal of 1M GndCl by dialysis.

Figure 5.13 A shows the CD trace recorded for the N551 construct in the presence of 1 M GndCl. Figure 5.13 B shows the CD trace recorded for the N551 construct following refolding after 1 M GndCl is dialysed out of solution. When compared to the initial trace (Figure 5.12) two effects can be observed. The first is the disruption by the GndCl of the ability of the CD to detect a signal from the protein without being overwhelmed by the signal generated by the GndCl at low wavelengths. This is seen by the lack of data from 209 – 195 nm due to a signal channel overload. The second is that following removal of GndCl (Figure 5.13 B) the trace resembles that of the original protein (Figure 5.12) suggesting that fully refolded protein has been recovered.

The unfolding/refolding procedure was repeated with 2M GndCl as shown in Figure 5.14.

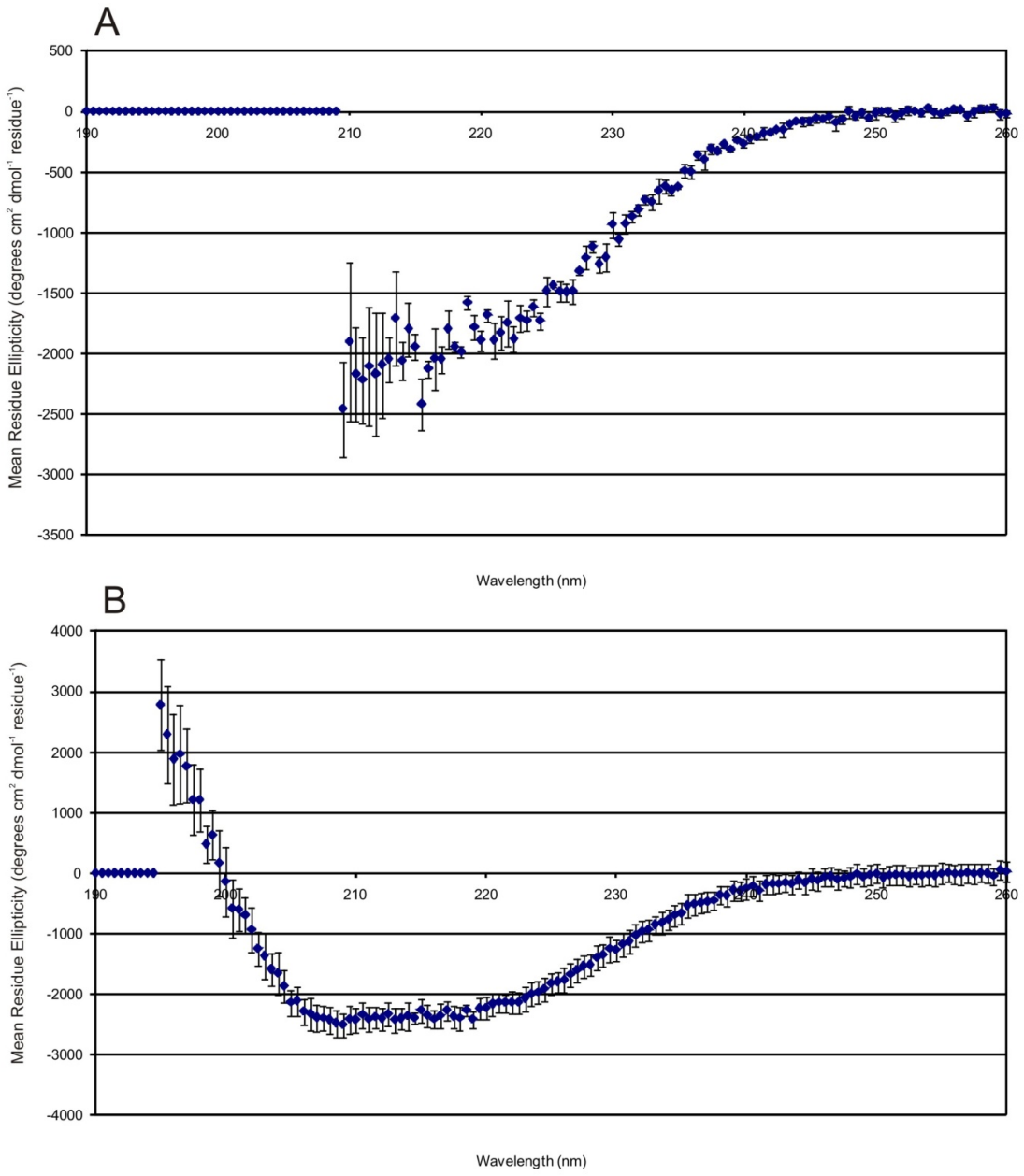

Figure 5.14 CD spectroscopy trace of the N551 construct of Hsp90 at 25°C. Data recorded from 260 - 195nm every half nm. A. Trace recorded in the presence of 2M GndCl. B. Trace recorded after removal of 2M GndCl by dialysis.

From Figure 5.14 a similar effect is seen using 2 M GndCl as in Figure 5.13 using 1 M GndCl. Again a comparison of the refolded trace with the 0 mM GndCl trace (Figure 5.14) shows that refolding does occur. Given that greater unfolding is likely to lead to greater backbone amide exchange and that unfolding is likely to be greater in the presence of 2 M GndCl than 1 M GndCl, 2 M GndCl was chosen for the partial unfolding/refolding of the N551 construct.

Having confirmed that dialysis into 2 M GndCl overnight followed by dialysis into 0 M buffer overnight results in a folded protein, an NMR ^{15}N-TROSY spectrum was recorded. A comparison with the previous ^{15}N-TROSY spectrum was used to determine whether partial unfolding had resulted in the full back exchange of previously missing peaks.

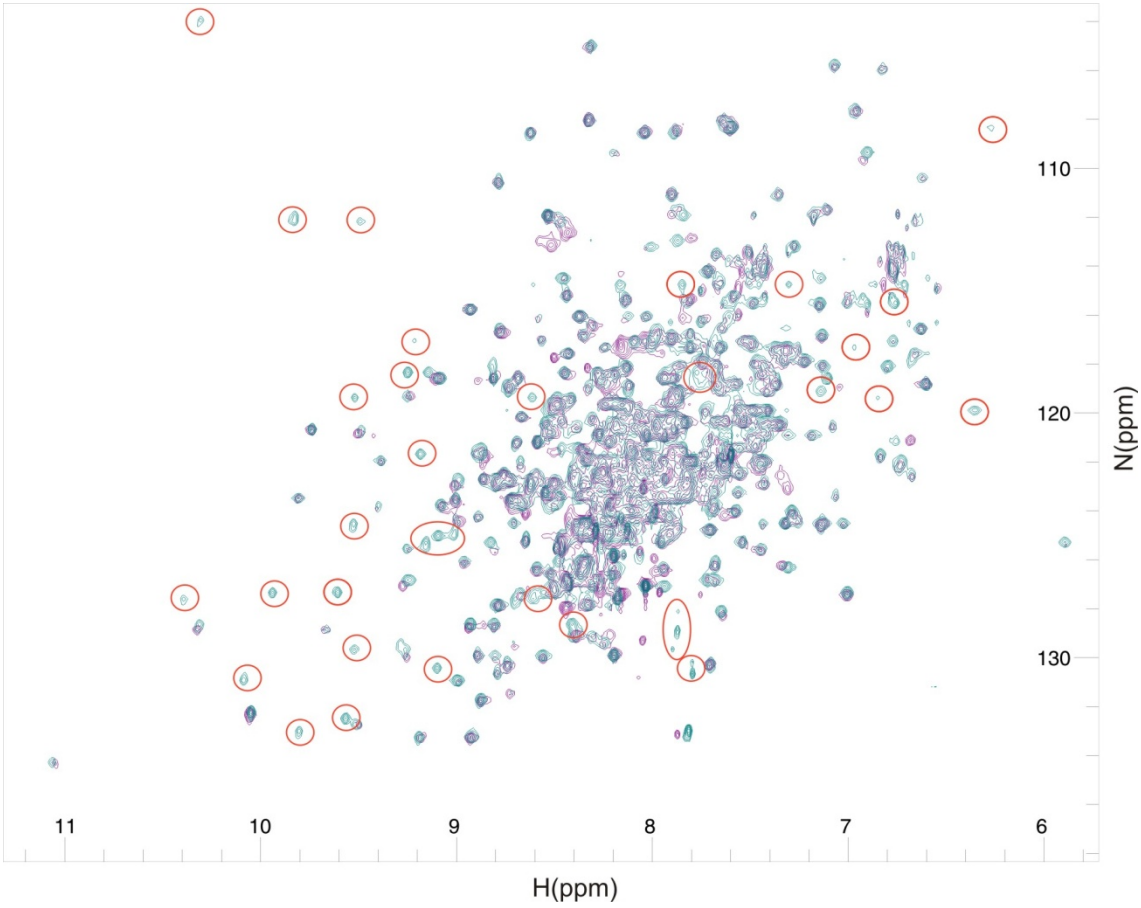

Figure 5.15 Overlaid ^{15}N-TROSY spectra of the N551 construct and the N551 construct following unfolding/refolding by GndCl. Peaks that have been recovered through back exchange following partial unfolding are circled in red. Spectra recorded in 50 mM Tris, 50 mM NaCl, pH 7.5 25°C.

From Figure 5.15 it is clear to see that peaks previously identified as missing from the overlay with the N-terminal domain spectrum have reappeared. These peaks are shown in Figure 5.16 and all map either to the interior of the N-terminal domain or known secondary structural features which might act to prevent amide back exchange under normal conditions. Several other peaks that cannot be attributed to the N-terminal domain have also appeared. These peaks are likely to originate from protected regions within the middle domain.

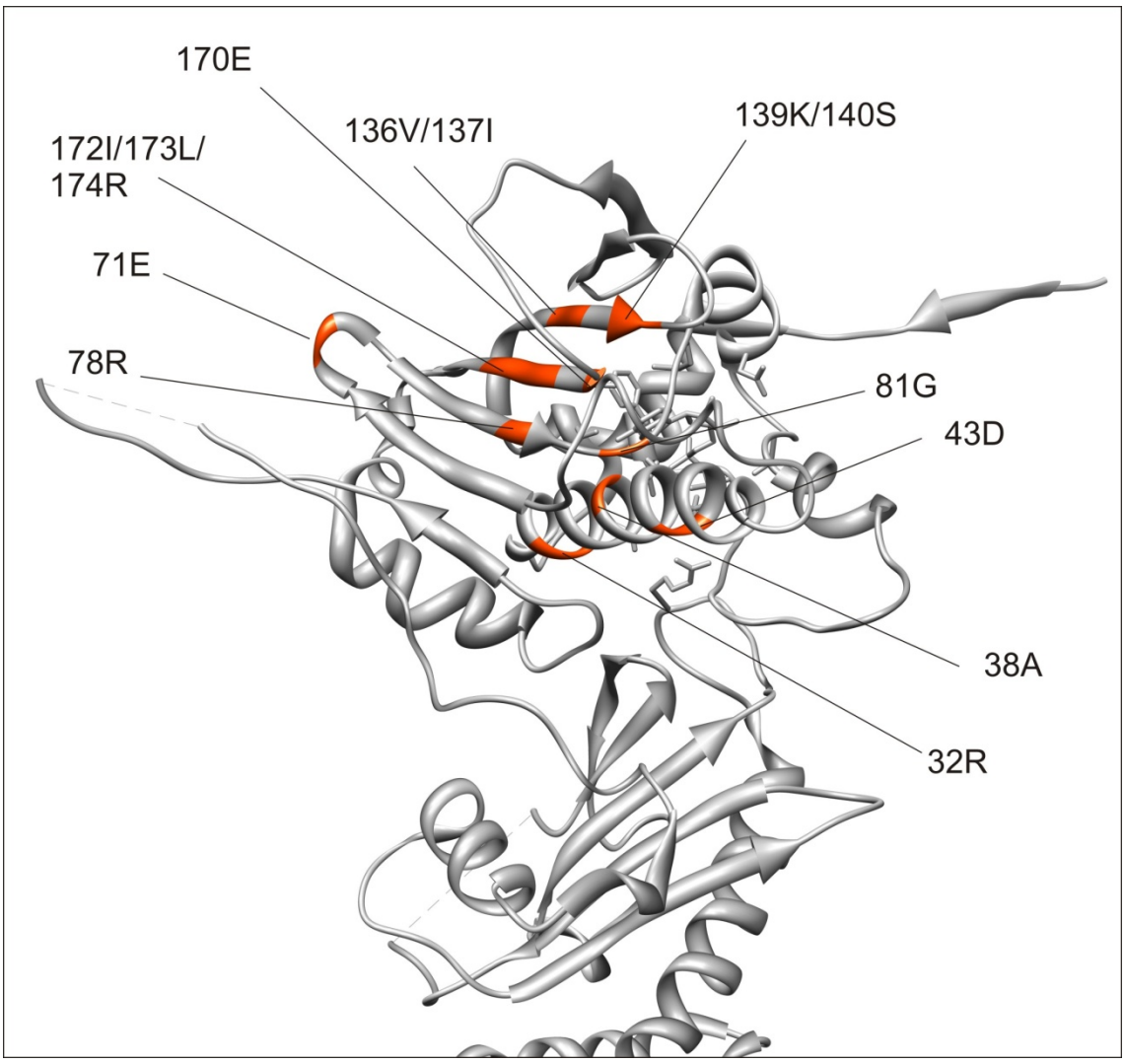

Figure 5.16 A plot of the peaks appearing in the N-terminal domain of the N551 construct after partial unfolding and refolding of the protein. Appearing peaks are plotted onto the ribbon representation of the crystal structure solved by Ali et al.[7]. Diagram taken from PDB file 2CG9

5.5 Discussions on the thermodynamics and conformational changes of the larger constructs of Hsp90

As observed by ITC, the binding of N551 to ADP shows a binding affinity around four times higher than that seen for the N-terminal domain alone. The thermodynamic profile, however, looks very similar, with the enthalpy and entropy values varying only a little between the two different constructs used. Both the N-terminal data and the N551 data show negative ΔC_p values; however, the value for the N551 construct is 600 $J \cdot mol^{-1} \cdot K^{-1}$ more negative than the

N-terminal data alone. The similar enthalpy/entropy profile suggests that the presence of the middle domain enhances the binding affinity of the ligand but without altering the overall gross arrangement of the ligand within the binding pocket. A similar change in ΔC_p is associated with the binding of AMPPNP to the N551 construct with slightly more favourable ΔH and $T\Delta S$ values.

It is known from the crystal structure [7] that the N-terminal domain and the middle domain associate with one another in the AMPPNP ligand bound state. It is possible that this may also occur in the ADP bound state, however, no crystal structure has been solved in this state. The NMR data presented here, however, does suggest that under all ligand bound conditions and in the apo state there is some association between the N-terminal and middle domains. With both ADP and AMPPNP, the ΔC_p value for binding to the N551 construct is 600 $J \cdot mol^{-1} \cdot K^{-1}$ more negative than that observed for the N-terminal domain alone consistent with a common reason behind this decrease in ΔC_p in both ligand bound states.

As has been previously detailed, the ΔC_p can be influenced by a number of potential contributions, including the association of two protein surfaces, a change in the hydration of a protein and the associated displacement of water molecules or a conformational change such as local un/folding. The association of the N-terminal domain and middle domain leads to the burial of a large amount of surface area which will have an influence on the ΔC_p. The burial of surface area due to domain association can be computed from the known structure of full-length Hsp90.

The surface area of the interface between the N-terminal domain and the middle domain of Hsp90 was calculated using NACCESS software[77] and the pdb file 2CG9. This pdb file contains two Hsp90 strands in a dimer and two p23 monomers. The pdb file was altered to contain a single Hsp90 strand including just the N-terminal and middle domains (residues 1 – 551 - NM) and excluding the C-terminal domain. This file was then used to create two further pdb files containing either just the N-terminal domain (residues 1 – 207 - N) or just the middle domain (residues 208 – 551 - M). The N-terminal domain was bound to ADP and coordinated to magnesium, neither of which were removed from the file.

NACCESS was used with the default settings of a 1.4 Å probe together with the default van der Waals radii file. An analysis of the total surface area of the NM, N and M files was performed. Additionally this was broken down into non-polar and polar components. The surface area difference between the values for N+M and NM revealed the surface area of the interface between the N-terminal and Middle domains of the chaperone protein. This is summarised in Table 5.5.

Construct	Total surface area (Å)	Non-polar surface area (Å)	All polar surface area (Å)
N	11789.6	7081.3	4708.3
M	18838.3	10719.3	8199.3
NM	28114.1	16325.4	11786.7
Difference: NM-(N+M)	-2516.1	-1475.2	-1040.9

Table 5.8 A comparison of the accessible surface areas of the N-terminal domain (N), the middle domain (M) and the N551 construct (NM).

Using equation (3.3) the expected ΔC_p value due to the burial of surface area between the two domains was calculated as -1.37 $kJ \cdot mol^{-1} \cdot K^{-1}$. This is twice the difference observed in the ΔC_p between the N-terminal domain and the N551 construct binding to the nucleotide ligands.

This value of -1.37 $kJ \cdot mol^{-1} \cdot K^{-1}$ is twice as large as that expected from the previously determined ΔC_p values for both ADP and AMPPNP binding to the N551 construct. To explain this discrepancy it must be considered that some process, in addition to the association of the domains, is opposing the contribution to the ΔC_p that is made by the burial of surface area. This process is probably the same for both ADP and AMPPNP binding suggesting that it is not a part of the chaperone cycle that is driven by specific ligand binding or hydrolysis.

Whatever is influencing the ΔC_p value occurs upon ligand binding in the transition from the free to the bound state. The NMR ^{15}N-TROSY data collected already supports the association of the N-terminal domain with the middle domain; however, the spectra also reveal an influence upon the β-sheet at the back of the binding pocket. This is most likely not due to direct interactions with the middle domain, judging by the crystal structures previously mentioned [7]. It is possible, that whatever is occurring in this region of the N-terminal domain may account for the ΔC_p discrepancy between that predicted and observed.

The ^{15}N-TROSY data do suggest one alternative possibility for the ΔC_p discrepancy observed. Looking in detail at the central region of the spectra one would expect to see several sharp peaks corresponding to the unstructured long linker between the two domains. As this loop is believed to be unstructured one would expect the peaks arising from it to be identical in all states. A diagram showing the central region of the overlaid ^{15}N-TROSY spectra in the apo, ADP and AMPPNP bound states is shown in Figure 5.17. The contour levels have been greatly increased so as to only show very intense peaks that are most likely to arise from the unstructured loop region and are less likely to arise from the unassigned middle domain. It is

known that the long linker is not essential for function, as detailed in the introduction. However it cannot be explicitly seen in the crystal structure[7] and has not been assigned by NMR. The fact that the loop is not essential does not preclude some minor involvement in the chaperone cycle that has previously not been detectable.

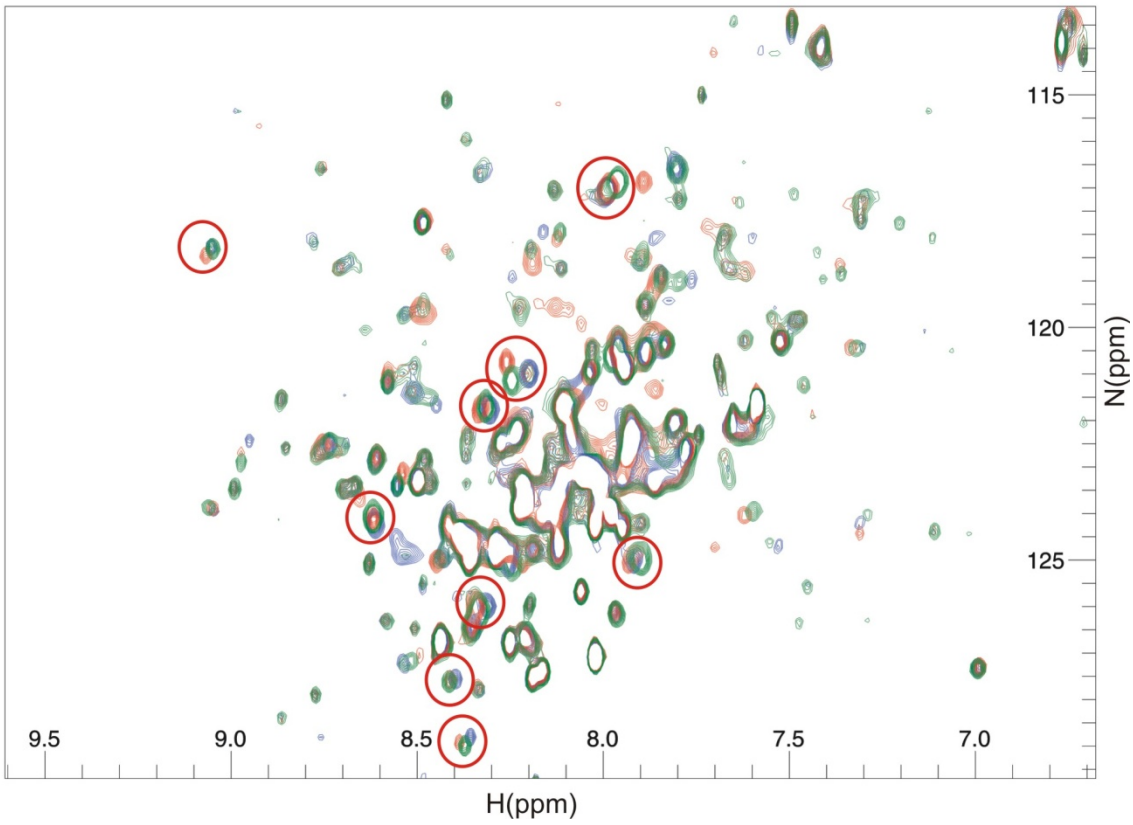

Figure 5.17 An overlay of the TROSY spectra for the apo (red), ADP (blue) and AMPPNP (green) states of the N551 construct. Spectra recorded in 50 mM Tris, 50 mM NaCl, 5 mM Mg^{2+}, pH 7.5. Circled in red are intense peaks that show shifts between the three different states but that do not match to any known N-terminal peak.

The circled peaks do not match any assigned N-terminal domain peak and show differences between the ligand bound states, yet are also very intense, suggesting they are from an unstructured region of protein. This may indicate that the flexible loop in some way responds to the binding of ligand in a specific fashion. Using equation 5.1 it can be predicted that the exposure of 448 Å of non-polar surface area or the burial of 1025 Å of polar surface area would result in a +600 $J \cdot mol^{-1} \cdot K^{-1}$ ΔC_p change. Using the estimate that one amino acid has an accessibly surface area of 100 Å[78] this either leads to the burial of 4 polar amino acids or the exposure of 10 apolar amino acids or to suitable combinations therein to add up to a total ΔC_p predicted value of -600 $J \cdot mol^{-1} \cdot K^{-1}$. If the linker were to form any sort of secondary structure in the apo state that was disrupted by the binding of ligand, or, alternatively, if the binding of ligand induced the formation of secondary structure, or even simply association of part of the linker with either of the structured domains, this would lead to a change in the

buried surface area and also a change to the ΔC_p. Alternatively, if the linker were to associate with the back of the β-sheet in the N-terminal domain in the apo state and that this was disrupted by a change in ligand bound state, this could also lead to a change in the buried surface area and also a change to the ΔC_p.

From Figure 5.17, 9 peaks have been identified that could belong to the long linker but which also show differences between the ligand bound states. This number is within the range that could explain the ΔC_p discrepancy described earlier and is roughly the correct number to account for the number of shifts observed in the ligand bound state in the β-sheet. One thing to note is that intense peaks are always unstructured and flexible and so the circled peaks indicate an effect of ligand binding upon some residues in the long linker region. If secondary structure was formed or lost, a change in peak intensity would also be expected but currently such peaks are not easily identifiable. As such the peaks involved in any linker region role may not be limited to the circled peaks. With current data it is not possible to determine which residues are involved in any secondary structure formation or association with either of the domains present in the construct. However, the existence of intense peaks from a potentially unstructured region of the protein that show specific changes upon ligand binding, potentially suggests a previously unknown role for the long linker region.

The ITC titrations between the N551 construct and the nucleotide based ligands ADP, AMPPNP and adenosine have revealed that the presence of the middle domain increases the binding affinity for all ligands compared to the N-terminal domain alone. This effect is most prominently observed with ADP. The use of the full length protein shows no significant change in binding affinities of the ligands compared to the N551 domain, suggesting that the addition of the C-terminal domain, and therefore the ability to dimerise, does not significantly alter the binding properties of the nucleotide to the N-terminal domain and that the N-terminal domain and middle domain contribute most towards defining the binding thermodynamics of the nucleotide.

NMR spectra have been obtained for the apo, ADP and AMPPNP bound states. The quality of the spectra and the lack of peak broadening suggest that the two domains do not permanently associate with one another under any ligand bound state. An analysis of the peak shifts observed in the N551 construct in comparison to the known peak positions of the N-terminal domain suggest two things. The first is that there is some contact at the domain/domain interface, as shifts are observed in this region. The second is that the presence of the middle domain leads to changes in the β-sheet at the back of the binding pocket. These changes in the binding pocket may give some indication as to how the binding affinity for the ligands is increased, and that it is due to altered interaction with this region of the binding

pocket that leads to increased binding affinity. What is not clear, however, is how the middle domain influences this region of the N-terminal domain.

The presence of the middle domain also has a dramatic influence on the ΔC_p recorded for all ligands. The effect on the ΔC_p for ADP and AMPPNP is the same, suggesting a common process; however, the burial of surface area alone does not correctly account for the change in heat capacity observed. Here it is tentatively suggested that the discrepancy between observed and predicted ΔC_p values could be attributed to the long linker between the N-terminal domain and middle domain. This is based upon the intense peaks, most likely corresponding to a mostly unstructured region in the central portion of the spectrum showing specific differentiation between ligand bound states. This suggests that the linker may have a previously unforeseen influence upon ligand binding, either by the formation of some ordered structure, or by an association with the N-terminal domain.

6 Discussion

In the course of this thesis the response of the molecular chaperone Hsp90 to ligand binding has been studied in detail. The thermodynamics of nucleotide-based ligand binding have been investigated and the conformational changes induced by ligand binding within the N-terminal domain have been studied. Additionally the influence of the middle domain and the presence of the full length protein upon ligand binding was investigated. Throughout the course of these studies it has become increasingly obvious that Hsp90 is a highly dynamic protein that can respond specifically to the binding of ligands that differ by only one phosphate group and that this difference in response is shown both in the thermodynamics of ligand binding and in the conformational changes observed.

The molecular chaperone Hsp90 is driven by ATP binding and hydrolysis as already described in Chapter 1. The binding site has been studied in some detail both here and elsewhere; however many of the previous studies undertaken at atomic resolution focus on the static structure and have only touched upon the dynamic changes in structure induced by nucleotide ligand binding. The two known crystal structures [7;8] show two distinct conformations of the N-terminal domain of Hsp90 in two different ligand-bound states; however, these two structures were obtained under very different circumstances. One is in the ADP bound state in the isolated N-terminal domain while the other is in the AMPPNP bound state but with the full length protein and in the presence of p23. Distinct differences can be seen between these two states, however, dissecting the influence of elements other than the nucleotide is not trivial. In the isolated N-terminal domain with ADP bound the 'ATP lid' is seen in the open position and the first twenty amino acids are in a strand and helix that are close into the main structure. In contrast in the AMPPNP-bound structure 'ATP lid' is seen in the closed position over the ligand. Whether this is induced by the different ligand binding, by the presence of p23 or by the presence of the remainder of the protein and its dimer partner is unclear. Additionally the N-terminal strand and helix are seen to associate with the N-terminal domain of the other half of the dimer, but again whether this is due to the presence of the different ligand or due to the presence of the other elements mentioned is unclear.

6.1 The thermodynamics of ligand binding

Investigation of the effects of ligand binding were assessed by ITC measurement. This was done in a systematic way by binding the adenine ring system and effectively building out the adenosine fragment to adenosine, ADP and finally ATP/AMPPNP. Binding of adenine to the isolated N-terminal domain revealed that much of the binding affinity arose from the adenine ring system that, from the crystal structure, appears to sit on the β-sheet at the back of the binding pocket. The addition of the ribose group to form adenosine and the addition of the first two phosphate groups was then observed to increase the affinity to a small degree, but to within the same order of magnitude as that achieved by the adenine ring alone. The presence of the third phosphate group led to a decrease in binding affinity back to a level that was equivalent to that of the adenine base alone. The binding of the adenine ring to the binding pocket is mostly mediated by water molecules with van der Waals bonds between the ring and Met84 providing the only direct contact. The addition of the ribose ring leads to an additional direct contact between Asn92 and the ring. The first two phosphate groups also add more direct and indirect contacts including those to Phe124, Lys98 and Asn37. The addition of the third phosphate leads to no additional direct contacts in the N-terminal domain. Therefore whatever influences there are upon the binding affinity, therefore must occur through a large number of water intermediates rather than depending solely upon direct bonds. It is this lack of direct bonds that may well be the key to the dynamic response of the protein to the ligand.

It has previously been noticed by Nilapwar [17] et al., that the binding of AMPPNP to the N-terminal domain of Hsp90 is sensitive to pH with a decreasing affinity as pH increases. Here it has been established that ADP is insensitive to pH and that the change in affinity with respect to pH for AMPPNP is due to a single protonation event. This protonation event has been identified by NMR as being due to the protonation state of the γ-phosphate group in AMPPNP. Protonation on the protein was ruled out by ^{15}N-HSQC NMR data and positive identification of protonation on the γ-phosphate was achieved using direct monitoring of the phosphorus atoms by ^{31}P-NMR 1D spectroscopy.

The determination of the heat capacity was also used to great effect in investigating the conformational changes induced by ligand binding through use of the thermodynamic measurements alone. The implications of these heat capacity measurements will be discussed later. One very interesting point to note, which is something rarely seen in protein/ligand binding events, is the difference in sign between the binding of two very similar ligands, ADP

and AMPPNP, to the same binding site, suggesting that each ligand plays a distinct and very important role in the Hsp90 chaperone cycle.

6.2 Assignment of the side chain resonances of the N-terminal domain of Hsp90

The necessity for a side chain assignment of the N-terminal domain is clear since armed with these data a more detailed understanding of the conformational changes of the protein can be achieved and structural determination can be attempted. Knowledge of the side chain assignments allows shifts in response to different conditions, ligand binding, pH or otherwise, to be monitored. Chemical shifts correlated with a known crystal structure has already been shown to be a powerful combination; however, side chain shifts are far more sensitive to side chain protonation events and interactions with the ring currents of aromatic residues than backbone shifts. The side chain assignments here presented will allow a much more detailed study of the dynamics and flexibility of the N-terminal domain of Hsp90 to be undertaken. Comparisons of shifts under different conditions can now be undertaken and a more sensitive response measured through observation of side chain interactions. Movement of the side chain resonances will provide additional information than the chemical shifts observed for backbone resonances alone as side-chain movement often occurs during conformational changes. Having assignments for the side chain resonances also allows for future structural determination through the use of carbon and nitrogen edited NOESY experiments.

Already a comparison of the side chain resonances in the apo, ADP and AMPPNP bound state has been undertaken in Chapter 4, revealing a more detailed look at the regions of the protein which respond to ligand binding and possible conformational changes that may occur. Details of this are discussed below.

6.3 Conformational changes in the N-terminal domain

The chaperone molecule Hsp90 is an incredibly dynamic protein and goes through a large series of conformational changes during ligand binding and hydrolysis. As previously detailed, the large scale conformational changes can be identified by the crystal structures. However, elucidating the detailed and dynamic behaviour of the protein in solution is key to understanding the overall function of Hsp90 and how it is driven. The response of the N-terminal domain of Hsp90 to different ligands has been observed by NMR within this thesis. As detailed previously, particular interest was taken of the first 20 amino acids and the likely position of the ATP 'lid' region in any given state. It was also interesting to note the changes in conformation in regions of the protein not linked to large conformational changes, as indicated by chemical shifts in the NMR spectra, particularly in the flanking helices around the entrance to the binding site and across the β-sheet at the back of the binding site.

6.3.1 The ATP Lid

The movement of the lid from an 'open' to 'closed' position is not disputed here, however the impetus for the change from one state to the other is not clear. The movement of the lid marks one of the most dramatic known conformational changes within the N-terminal domain. Chapter 3 details the use of ITC to compare the recorded heat capacity change upon binding of ADP and AMPPNP to the N-terminal domain. Given the knowledge of the two potential positions (open or closed) predictions of the expected heat capacity change could be made and compared to the recorded values. This is possibly due to the dominant influence of the change in surface area buried upon the heat capacity change. A comparison of the predicted and actual heat capacity changes lead to the interpretation that as anticipated ADP led to the lid adopting an 'open' conformation while AMPPNP led to a 'closed' position. What became clear was that the assumed position of the apo was not as close to the 'closed' position as was initially anticipated. The data presented here is consistent with the apo state of the lid being in equilibrium between the open and closed forms described.

H/D exchange information was used to probe the flexibility of each amino acid and from these data it can be seen that the accessibility of the lid is different in each case as detailed in Chapter 4. The results agree with previous information to suggest that ADP leads to a 'lid open' conformation and that AMPPNP leads to a 'lid closed' conformation.

The side chain assignments can be used to probe with greater sensitivity the conformational changes that occur in different ligand bound states of the N-terminal domain. Here unique shifts are observed in the ADP-bound state within part of the lid and within a section of the protein that is close to the lid but only when the lid is in the open state. In the AMPPNP bound state, unique shifts are observed in a position of the long helix that would come into contact with the lid only if it were in a closed state.

Overall all evidence seems to point to a dynamic movement of the 'ATP lid' between an open and closed position in the apo state with the binding of ADP or AMPPNP moving it to the expected open or closed positions respectively. This confirms that binding of ligand alone is sufficient to cause specific movement of the 'lid' region and that the presence of the middle domain or the partner N-terminal domain is not required for lid movement, nor is the presence of any co-chaperones such as p23.

6.3.2 The N-terminal helix and strand

The first 20 amino acids of the N-terminal domain of Hsp90 consist of a β-strand and an α-helix that are involved in a strand swap event during the chaperone cycle with the N-terminal domain of the opposite monomer. Observation of the side chain chemical shifts of the AMPPNP and ADP-bound states of the N-terminal domain show some chemical shifts in this region suggesting that the environment of the side chains has changed. Of the shifts observed, more residues are affected in the AMPPNP bound state than in the ADP bound state. The strand swap event is associated with the start of the chaperone cycle and so a greater degree of movement seen in the AMPPNP bound state, also mimicking the start of the cycle, may indicate a loosening of the association of the N-terminal strand and helix with the main body of the protein induced by ligand binding. The smaller number of shifts observed in the ADP bound state suggests that the environment of the helix and strand has changed a little but not as significantly as in the AMPPNP bound state. This pattern of shifts is reflected in the H/D exchange data where the first 20 amino acids show a far greater accessibility to H/D exchange in each of the ligand bound states than in the apo state. However the AMPPNP bound state contains more residues that exchange than the ADP bound state.

Whether a full dissociation occurs without the presence of the second N-terminal domain, or whether the association with the main body of the protein is simply weakened, is unclear. From this information it can be seen that both ligands induce chemical shifts that suggest a weakening of the association of the N-terminal strand with the main body of the

protein. AMPPNP mimics ligand bound state at the start of the chaperone cycle and the large number of chemical shifts in the region may suggest that the ligand either induces the strand swap or favours it significantly. The ADP bound state mimics the end of the chaperone cycle and the decrease in observed chemical shifts in this region suggests that the ligand, while not favouring a fully associated form, does not favour the 'strand swapped' state as much as at the beginning of the cycle. This may be an indication that the ADP bound state is involved in resetting the cycle.

6.3.3 The β-sheet at the back of the binding pocket

In all of the 2D NMR experiments observing chemical shift changes, one feature seen was the presence of shifts located in the β-sheet. These shifts appear to show some differentiation depending on which ligand is bound to the protein yet the contact with this region is with a group, the adenine ring, that is common to all the ligands observed.

This suggests that the position of the adenosine group of the ligand within the binding site is flexible and determined by the interaction of the phosphate groups with the protein. It has already been established that the majority of the binding affinity is provided by the adenine ring yet it is also clear from this that the position of the adenine ring varies depending on the ligand. The contacts between the adenine ring and the protein are mostly water mediated with the exception of van der Waals forces between the ring and Met84 and a direct contact with Asp79. The movement of the ligand as reflected by the shifts on the β-sheet, does not correspond to a dramatic drop in affinity suggesting that the water molecules that line the binding site buffer the ability of the ligand to bind to a certain extent, while still allowing for small variation such as that observed between ADP and AMPPNP at physiological pH. This buffering effect may allow conformational changes in the protein while still permitting the binding of the ligand under physiological conditions.

It could be theorised that small differences in the ligand, such as the presence of a third phosphate group in AMPPNP, might interact with the mouth of ligand binding site as supported by chemical shifts of resonances in these regions. However this interaction propagates through the ligand causing a shift in the positioning of the adenine ring of the ligand with a subsequent influence over the binding pocket via the β-sheet that is greater than would be anticipated based on just the difference in interaction at the terminal phosphate site. This propagation of movement may indicate a path by which the binding of two such similar

ligands as ADP and AMPPNP can induce such drastically different conformational changes within the N-terminal domain of Hsp90.

6.4 The influence of the middle and C-terminal domains

While previous work has shown the importance of the middle domain and the dimer for ATPase activity, the thermodynamics of binding had not been investigated before. The addition of the middle domain to form the N551 construct leads to an increase in affinity for both ADP and AMPPNP binding although the greatest influence is observed with ADP binding. This is despite the presence of the Arg380 residue in the catalytic loop of the middle domain which contacts the γ-phosphate. This suggests that Arg380 is involved primarily with efficient hydrolysis of ATP and does not contribute significantly to the binding affinity of the ligand. It was observed in Chapter 4 that the interface between the N-terminal domain and the middle domain became more accessible with a greater level of H/D exchange observed. This might indicate that ADP facilitates a conformation that interacts favourably with the middle domain and leads to the stabilisation of a structure where ADP binding is enhanced.

The binding of adenosine to the N551 construct shows a decreased binding affinity when compared to the N-terminal domain alone. Although the adenine ring of adenosine contributes most towards the binding affinity it has already been noted that it is the presence of the phosphate groups that differentiates the conformational changes induced by the different ligands. In the smaller construct it might be easier for the adenine to exert sufficient influence over the domain to provide good binding contacts without the aid of the phosphate groups in the larger ligand. In the larger protein construct it might be less favourable for the small adenosine molecule to exert its influence over the entire protein to allow it to bind as tightly as in the N-terminal domain alone.

The full length Hsp90 chaperone showed a similar binding affinity for ADP as the N551 construct, while the binding of AMPPNP was slightly weaker than for the N551 construct. This suggests that the C-terminal domain has very little influence over the binding of ligand and is consistent with a weak transient N-terminal dimerisation.

The NMR undertaken on the N551 construct shows much promise with good dispersion seen despite the size of the protein. The precise overlay with the N-terminal domain spectra

has allowed the identification of a number of the N551 peaks, and subsequently observed chemical shift differences between the N551 and N-terminal constructs. Shifts are observed for both ligands across the β-sheet at the back of the binding pocket. This influence over the β-sheet may indicate a path by which the middle domain has influence over the binding of ligand as previously described.

The heat capacity data from the N551 construct shows that both the binding of ADP and AMPPNP are around 600J·mol^{-1}·K^{-1} more negative than anticipated from predicted surface area burial calculations. This suggests that the presence of the middle domain leads to a common event that occurs upon ADP and AMPPNP ligand binding leading to a ΔC_p of 600J·mol^{-1}·K^{-1}. The NMR shows some very strong peaks that cannot be attributed to the N-terminal domain and due to their intensity may well belong to the unstructured, long linker between the two domains. However, most interesting to note is that these peaks, in a supposedly unstructured region, show ligand-induced specific chemical shifts. This suggests that there is some specific interaction or structure that is ligand-dependent and the formation or unfolding of which may explain the decrease in the change in heat capacity observed with both ligands. The linker region has previously been shown to be unnecessary for protein function. Any interaction is then clearly not essential. Evidence presented here may indicate a role for this region, albeit a nonessential one, where previously nothing of import was thought to occur. Certainly this shows the importance of dynamic studies of the protein by NMR to identify such areas of interest where crystallography cannot resolve them due to the inherent flexibility of the region.

6.5 Future Work

The study of Hsp90 is ongoing and this thesis suggests a number of avenues for future research. The solution state structure of the N-terminal domain has yet to be solved by NMR. It has been demonstrated that the apo state, the ADP bound state and the AMPPNP bound state are all subtly different and that these changes are due to the ligand alone rather than the influence of any co-chaperones or client proteins. Ascertaining the levels of conformational change due to ligand binding will be very important for future studies regarding Hsp90 inhibition and its function within client protein activation and co-chaperone interaction. The position of the 'ATP lid' has yet to be definitively confirmed and the data here presented

suggests that the exact conformation of the β-sheet may have a significant role in determining ligand induced conformational change.

The change in heat capacity data suggests that the two ligands induce different conformational changes within the protein. However they also suggest that the apo state is also flexible and, with particular regard to the position of the ATP 'lid', in a state of equilibrium between the open and closed forms. A growing body of evidence [5;9;22;40] suggests that Hsp90 moves through the cycle, not through a series of practically irreversible steps, but by favouring the forward equilibrium of each step. This makes solving the solution state structure of all three states important in order to ascertain how they relate to one another and to determine more detail about the equilibrium between the states.

This thesis has also shown the feasibility of undertaking NMR spectroscopy on the 50 kDa N551 construct comprising the N-terminal and middle domains. Good dispersion was observed in the ^{15}N-TROSY spectra for the apo and both ligand bound states. Since good overlap was seen between the N551 and the N-terminal spectra many peaks in the larger construct could be identified. Further optimisation of the conditions used, potential selective labelling strategies and use of the information already acquired for the N-terminal domain alone could allow the backbone assignment of the larger construct. This in turn would provide a way of directly studying the N-terminal domain and middle domain interactions under different conditions.

Overall this thesis highlights the immense degree of flexibility within the N-terminal domain and its ability to respond specifically to two nucleotide based ligands that differ by one phosphate group only. The conformational changes induced by ligand binding mostly appear to cause small changes in position however these changes are numerous enough that cumulatively they could cause the far greater and wide ranging changes observed in many of the crystal and EM structures. The one large conformational change observed is in the 'ATP lid' which here has been seen to move in response to ligand binding alone, but the influence of this, beyond the isolated N-terminal domain, is still a matter for discussion. The role of Hsp90 in the cell is one of great complexity and involves the interplay of many different components from co-chaperone and client binding to ligand binding and hydrolysis. The dissection of the influence of each of these elements is key to understanding the overall mechanism of Hsp90 action. With the work presented here our knowledge of the influence of the ligand over the protein has been greatly expanded.

Bibliography

Reference List

1. Chang HJ, Lindquist S: **Conservation of Hsp90 Macromolecular Complexes in *Saccharomyces cerevisiae***. *Journal of Biological Chemistry* 1994, **269:**24983-24988.

2. Picard D, Khursheed B, Garabedian MJ, Fortin MG, Lindquist S, Yamamoto KR: **Reduced levels of Hsp90 compromise steroid receptor action in vivo.** *Nature* 1990, **348:**166-168.

3. Pearl LH, Prodromou C: **Structure and mechanism of the Hsp90 molecular chaperone machinery**. *Annual Review of Biochemistry* 2006, **75:**271-294.

4. Dollins DE, Warren JJ, Immormino RM, Gewirth DT: **Structures of GRP94-Nucleotide Complexes Reveal Mechanistic Differences between the hsp90 Chaperones**. *Molecular Cell* 2007, **28:**41-56.

5. Hessling M, Richter K, Buchner J: **Dissection of the ATP-induced conformational cycle of the molecular chaperone Hsp90**. *NATURE STRUCTURAL & MOLECULAR BIOLOGY* 2009, **16:**287-293.

6. Shiau AK, Harris SF, Southworth DR, Agard DA: **Structural analysis of E-coli hsp90 reveals dramatic nucleotide-dependent conformational rearrangements**. *Cell* 2006, **127:**329-340.

7. Ali MMU, Roe SM, Vaughan CK, Meyer P, Panaretou B, Piper PW, Prodromou C, Pearl LH: **Crystal structure of an Hsp90-nucleotide-p23/Sba1 closed chaperone complex**. *Nature* 2006, **440:**1013-1017.

8. Prodromou C, Roe SM, OBrien R, Ladbury JE, Piper PW, Pearl LH: **Identification and structural characterization of the ATP/ADP-binding site in the Hsp90 molecular chaperone**. *Cell* 1997, **90:**65-75.

9. Mickler M, Hessling M, Ratzke C, Buchner J, Hugel T: **The large conformational changes of Hsp90 are only weakly coupled to ATP hydrolysis.** *NATURE STRUCTURAL & MOLECULAR BIOLOGY* 2009, **16:**281-286.

10. Richter K, Moser S, Hagn F, Friedrich R, Hainzl O, Heller M, Schlee S, Kessler H, Reinstein J, Buchner J: **Intrinsic inhibition of the Hsp90 ATPase activity**. *Journal of Biological Chemistry* 2006, **281:**11301-11311.

11. Harris SF, Shiau AK, Agard DA: **The crystal structure of the carboxy-terminal dimerization domain of htpG, the Escherichia coli Hsp90, reveals a potential substrate binding site**. *Structure* 2004, **12:**1087-1097.

12. Meyer P, Prodromou C, Hu B, Vaughan C, Roe SM, Panaretou B, Piper PW, Pearl LH: **Structureal and Functional Analysis of the Middle Segment of Hsp90: implications for ATP hydrolysis and Client Protein and Cochaperone Interactions**. *Molecular Cell* 2003, **11:**647-658.

13. Richter K, Muschler P, Hainzl O, Buchner J: **Coordinated ATP hydrolysis by the Hsp90 dimer**. *Journal of Biological Chemistry* 2001, **276:**33689-33696.

14. Martinez-Yamout MA. Localization of sites of interaction between p23 and Hsp90 in solution. Edited by Venkitakrishnan RP, Preece NE, Kroon G, Wright PE, Dyson HJ. J Biol Chem. 281(20):14457-64. 2006.

15. Salek RM, Williams MA, Prodromou C, Pearl LH, Ladbury JE: **Letter to the editor: Backbone resonance assignments of the 25kD N-terminal ATPase domain from the Hsp90 chaperone**. *Journal of Biomolecular Nmr* 2002, **23:**327-328.

16. Rudiger S, Freund SMV, Veprintsev DB, Fersht AR: **CRINEPT-TROSY NMR reveals p53 core domain bound in an unfolded form to the chaperone Hsp90**. *Proceedings of the National Academy of Sciences of the United States of America* 2002, **99:**11085-11090.

17. Nilapwar S, Williams E, Fu C, Prodromou C, Pearl LH, Williams MA, Ladbury JE. Structural-Thermodynamic Relationships of Interactions in the N-Terminal ATP-Binding Domain of Hsp90. Journal of Molecular Biology 392, 923-936. 2009.

18. Sreeramulu S, Jonker HRA, Langer T, Richter C, Lancaster CRD, Schwalbe H: **The Human Cdc37-Hsp90 Complex Studied by Heteronuclear NMR Spectroscopy.** *Journal of Biological Chemistry* 2009, **284:**3885-3896.

19. Dehner A, Furrer J, Richter K, Schuster I, Buchner J, Kessler H: **NMR chemical shift perturbation study of the N-terminal domain of Hsp90 upon binding of ADR AMP-PNP, geldanamycin, and radicicol**. *Chembiochem* 2003, **4:**870-877.

20. Siligardi G, Hu B, Panaretou B, Piper PW, Pearl LH, Prodromou C: **Co-chaperone regulation of conformational switching in the Hsp90 ATPase cycle**. *Journal of Biological Chemistry* 2004, **279:**51989-51998.

21. Roe SM, Prodromou C, O'Brien R, Ladbury JE, Piper PW, Pearl LH: **Structural basis for inhibition of the Hsp90 molecular chaperone by the antitumor antibiotics radicicol and geldanamycin**. *Journal of Medicinal Chemistry* 1999, **42:**260-266.

22. Neckers L, Tsutsumi S, Mollapour M: **Visualising the twists and turns of a molecular chaperone**. *NATURE STRUCTURAL & MOLECULAR BIOLOGY* 2009, **16:**235-236.

23. Prodromou C, Panaretou B, Chohan S, Siligardi G, O'Brien R, Ladbury JE, Roe SM, Piper PW, Pearl LH: **The ATPase cycle of Hsp90 drives a molecular 'clamp' via transient dimerization of the N-terminal domains**. *Embo Journal* 2000, **19:**4383-4392.

24. Queitsch C, Sangster TA, Lindquist S: **Hsp90 as a capacitor of phenotypic variation**. *Nature* 2002, **417:**618-624.

25. Scheibel T, Weikl T, Rimerman R, Smith D, Lindquist S, Buchner J: **Contribution of N- and C-terminal domains to the function of Hsp90 in *Saccharomyces cerevisiae***. *Molecular Microbiology* 1999, **34:**701-713.

26. Rutherford SL, Lindquist S: **Hsp90 as a capacitor for morphological evolution**. *Nature* 1998, **396:**336-342.

27. Nathan DF, Lindquist S: **Mutational Analysis of Hsp90 Function: Interactions with a Steriod Receptor and a Protein Kinase**. *Molecular and Cellular Biologoy* 1995, **15:**3917-3925.

28. Nemoto T, Ono T, Tanaka K: **Substrate-binding characteristics of proteins in the 90 kDa heat shock protein family**. *Biochemical Journal* 2001, **354:**663-670.

29. Maruya M, Sameshima M, Nemoto T, Yahara I: **Monomer Arrangement in Hsp90 Dimer as Determined by Decoration with N and C-Terminal Region Specific Antibodies.** *Journal of Molecular Biology* 1999, **285:**903-907.

30. Jakob U, Scheibel T, Bose S, Reinstein J, Buchner J: **Assessment of the ATP binding properties of Hsp90**. *Journal of Biological Chemistry* 1996, **271:**10035-10041.

31. Sangster TA, Lindquist S, Queitsch C: **Under cover: causes, effects and implications of Hsp90-mediated genetic capacitance**. *BioEssays* 2004, **26:**348-362.

32. Pearl LH, Prodromou C, Workman P: **The Hsp90 molecular chaperone: an open and shut case for treatment**. *Biochemical Journal* 2008, **410:**439-453.

33. Richter K, Buchner J: **Hsp90: Chaperoning signal transduction**. *Journal of Cellular Physiology* 2001, **188:**281-290.

34. Panaretou B, Siligardi G, Meyer P, Maloney A, Sullivan JK, Singh S, Millson SH, Clarke PA, Naaby-Hansen S, Stein R, Cramer R, Mollapour M, Workman P, Piper PW, Pearl LH, Prodromou C: **Activation of the ATPase activity of Hsp90 by the stress-regulated cochaperone Aha1**. *Molecular Cell* 2002, **10:**1307-1318.

35. Weikl T, Muschler P, Richter K, Veit T, Reinstein J, Buchner J: **C-terminal regions of Hsp90 are important for trapping the nucleotide during the ATPase cycle**. *Journal of Molecular Biology* 2000, **303:**583-592.

36. Dunbrak RLJr, Gerloff DL, Bower M, Chen X, Lichtarge O, Cohen FE: **Meeting review: the second meeting on the critical assessment of techniques for protein structure predition (CASP2)**. *Folding and Design* 1997, **1:**27-42.

37. Phillips JJ, Yao Z, Zhang W, McLaughlin S, Laue ED, Robinson CV, Jackson SE: **Conformational Dynamics of the Molecular Chaperone Hsp90 in Complexes with a Co-chaperone and Anticancer Drugs**. *Journal of Molecular Biology* 2007, **372:**1189-1203.

38. Richter K, Reinstein J, Buchner J: **N-terminal residues regulate the catalytic efficiency of the Hsp90 ATPase cycle**. *Journal of Biological Chemistry* 2002, **277:**44905-44910.

39. Retzlaff M, Stahl M, Eberl HC, Lagleder S, Beck J, Kessler H, Buchner J: **Hsp90 is regulated by a switch point in the C-terminal domain**. *Embo Journal* 2009, **10:**1147-1153.

40. Bron P, Giudice E, Rolland J, Buey RM, Barbier P, Diaz JF, Peyrot V, Thomas D, Garnier C: **Apo-Hsp90 coexists in two open conformational states in solution**. *Biology of the Cell* 2008, **100:**413-425.

41. Meyer P, Prodromou C, Liao CY, Hu B, Roe SM, Vaughan CK, Vlasic I, Panaretou B, Piper PW, Pearl LH: **Structural basis for recruitment of the ATPase activator Aha1 to the Hsp90 chaperone machinery**. *Embo Journal* 2004, **23:**511-519.

42. Roe SM, Ali MMU, Meyer P, Vaughan CK, Panaretou B, Piper PW, Prodromou C, Pearl LH: **The mechanism of Hsp90 regulation by the protein kinase-specific cochaperone p50(cdc37)**. *Cell* 2004, **116:**87-98.

43. Chang HJ, Nathan DF, Lindquist S: **In Vivo Analysis of the Hsp90 Cochaperone Sti1 (p60)**. *Molecular and Cellular Biologoy* 1997, **17:**318-325.

44. Sambrook J, Russell D: *Molecular Cloning: A Laboratory Manual*, edn 3rd Edition. Cold Spring Harbour Laboratory Press; 2001.

45. Marley J, Lu M, Bracken C: **A method for efficient isotopic labeling of recombinant proteins**. *Journal of Biomolecular Nmr* 2001, **20:**71-75.

46. Ladbury JE, Chowdhry BZ: *Biocalorimetry: applications of calorimetry in the biological sciences.*, edn 1. John Wiley & Sons (Sd); 1998.

47. Gomez J, Hilser VJ, Xie D, Freire E: **The Heat Capacity of Proteins**. *Proteins, Structure, Function and Genetics* 1995, **22:**404-412.

48. Privalov PL, Makhatadze GI: **Contribution of Hydration and Non-Covalent Interactions to the Heat Capacity Effect on Protein Unfolding**. *Journal of Molecular Biology* 1991, **224:**715-723.

49. Ha J, Spolar RS, Record T: **Role of the Hydrophobic Effect in Stability of Site-specific Protein-DNA Complexes**. *Journal of Molecular Biology* 1989, **209:**801-816.

50. Cooper A. Heat does not come in different colours: entropy-enthalpy compensation, free energy windows, quantum confinement, pressure perturbation calorimetry, solvation and the multiple causes of heat capacity efects in biomolecular ineractions. Edited by Johnson CM, Lakey J.H., Nollmann M. Biophysical Chemistry 93, 215-230. 2001.

51. Spolar RS, Record T: **Coupling of Local Folding ot Site-Specific Binding of Proteins to DNA**. *Science* 1994, **263:**777-784.

52. Ladbury JE, Wright JG, Sturtevant JM, Sigler PB: **A thermodynamic study of the trp repressor-operator interaction**. *Journal of Molecular Biology* 1994, **238:**669-681.

53. Luque I, Mayorga OL, Freire E: **Structure-Based Thermodynamic Scale of a-Helix Propensities in Amino Acids**. *Biochemistry* 1996, **35:**13681-13688.

54. Bergqvist S, Williams MA, O'Brien R, Ladbury JE: **Heat Capacity Effects of Water Molecules and Ions at a Protein-DNA interface**. *Journal of Molecular Biology* 2004, **336:**829-842.

55. Morton C, Ladbury JE: **Water mediated protein-DNA interactions: The relationship of themodynmaics to structural detail.** *Protein Science* 1996, **5:**2115-2118.

56. Bradshaw JM, Waksman G: **Calorimetric Investigation of Proton Linkage by Monitoring both the Enthalpy and Association Constant of Binding: Application to the Interaction of the Src SH2 Domain with a High-Affinity Tyrosyl Phosphopeptide**. *Biochemistry* 1998, **37:**15400-15407.

57. Baker BM, Murphy KP. Evaluation of Linked Protoination Effects in Protein Binding Reactions Using Isotermal Titration Calorimetry. Biophysical Journal 71, 2049-2055.

58. Delaglio F, Grzesiek S, Vuister GW, Zhu G, Pfeifer J, Bax A: **NMRPipe: a multidimensional spectral processing system based on UNIX pipes**. *Journal of Biomolecular Nmr* 1995, **6:**277-293.

59. Vranken WF, Boucher W, Stevens TJ, Fogh RH, Pajon A, Llinas M, Ulrich EL, Markley JL, Ionides J, Laue ED: **The CCPN data model for NMR spectroscopy:Development of a software pipeline**. *Proteins, Structure, Function and Genetics* 2004, **59:**687-696.

60. Keeler J: *Understanding NMR Spectroscopy*, edn 1st edition. Wiley; 2005.

61. Rattle H: *An NMR Primer for Life Scientists*, edn 1st edition. Partnership Press; 1995.

62. Claridge TDW: *High-Resolution NMR Techniques in Organic Chemistry*, edn 1st edition. Pergamon; 1999.

63. Olsson TSG, Williams MA, Pitt WR, Ladbury JE: **The Thermodynamics of Protein-Ligand Interaction and Solvation: Insights for Ligand Design**. *Journal of Molecular Biology* 2008, **384:**1002-1017.

64. Brian M.Baker, Kessler H. Evaluation of Linked Protoination Effects in Protein Binding Reactions Using Isotermal Titration Calorimetry. Biophysical Journal 71, 2049-2055.

65. J.Michael Bradshaw, Gabriel Waksman: **Calorimetric Investigation of Proton Linkage by Monitoring both the Enthalpy and Association Constant of Binding: Application to the Interaction of the Src SH2 Domain with a High-Affinity Tyrosyl Phosphopeptide**. *Biochemistry* 1998, **37:**15400-15407.

66. Alan Cooper. Heat does not come in different colours: entropy-enthalpy compensation, free energy windows, quantum confinement, pressure perturbation calorimetry, solvation and the multiple causes of heat capacity efects in biomolecular ineractions. Edited by Christopher M Johnson, Jeremy H.Lakey, Marcelo Nollmann. Biophysical Chemistry 93, 215-230. 2001.

67. Boukhalfa H, Lewis JG, Crumbliss AL: **Beryllium(II) binding to ATP and ADP: Potentiometric determination fo the thermodynamic constants and implications for in vivo toxicity**. *BioMetals* 2004, **17:**105-109.

68. Mildred Cohn, Thomas R Hughes Jr.: **Nuclear Magnetic Resonance Spectra of Adenosine Di- and Triphosphate. II. Effect of complexing with divalent metal ions**. *Journal of Biological Chemistry* 1962, **237:**176-181.

69. Mildred Cohn, Thomas R Hughes Jr.: **Phosphorus Magnetic Resonance Spectra of Adenosine Di- and Trisphosphate I. Effect of pH.** *Journal of Biological Chemistry* 1960, **235:**3250-3253.

70. Richter K, Buchner J: **Hsp90: Twist and fold**. *Cell* 2006, **127:**251-253.

71. Ruth S.Spolar, M.Thomas Record Jr.: **Coupling of Local Folding ot Site-Specific Binding of Proteins to DNA**. *Science* 1994, **263:**777-784.

72. Irene Luque, Obdulio L.Mayorga, Ernesto Freire: **Structure-Based Thermodynamic Scale of a-Helix Propensities in Amino Acids**. *Biochemistry* 1996, **35:**13681-13688.

73. Casares S, Sadqi M, Lopez-Mayorga JC, Martinez FC: **Structural cooperativity in the SH3 domain studied by site-directed mutagenesis and amide hydrogen exchange**. *FEBS letters* 2003, **539:**125-130.

74. Hilser VJ, Lee C, Hong Pan J: **Binding site in Escherichia coli dihydrofolate reductase communicate by modulating the conformational ensamble**. *Proceedings of the National Academy of Sciences of the United States of America* 2000, **97:**12020-12025.

75. Polshakov VI, Birdsall B, Feeney J: **Effects of Co-operative Ligand Binding on Protein Amide NH Hydrogen Exchange**. *Journal of Molecular Biology* 2006, **356:**886-903.

76. Loh SN, Prehoda KE, Wang J, Markley JL: **Hydrogen Exchange in Unligated and Ligated Staphylococcal Nuclease**. *Biochemistry* 1993, **32:**11022-11028.

77. Hubbard SJ, Thornton JM. 'NACCESS' computer program Department of Biocheistry and Molecular Biology, University College London. 1993.

78. Simpson R: *Proteins and proteomics*, edn 1. Cold Spring Harbour Laboratory Press; 2003.

Supplementary Data CD

Containing:

ITC raw data and processed origin files

Assigned side-chain CHSQC data for the apo, ADP and AMPPNP N-terminal domain of Hsp90 in CCPN format.

PDF version of this thesis.

PDF containing the side-chain assignment data for the apo, ADP bound and AMPPNP bound N-terminal domain of Hsp90.